

**Effect of hypertrophic and dilated cardiomyopathies
associated mutations in troponin I on cardiac thin
filament dynamics.**

**Thesis submitted for the degree of Doctor of Philosophy at the
University of Leicester**

By

Sameeh Abdulkareem Al-Sarayreh

Department of Biochemistry

College of Medicine, Biological Sciences and Psychology

University of Leicester

June 2011

*As we learn more we
realize how little we know*

To my uncle Hamed soul.....

Abstract

Effect of hypertrophic and dilated cardiomyopathies associated mutations in troponin I on cardiac thin filament dynamics

By Sameeh Abdulkareem Al-Sarayreh

Troponin I mutations have been linked to genetic hypertrophic and dilated cardiomyopathies. We aimed to understand, at the molecular level, how six HCM mutations (R21C, Q130R, R145G, G203S, and K206Q) and one DCM mutation (A2V) in troponin I affect its structure and function. Circular dichroism, co-sedimentation with actin and ATPase assays demonstrated that these mutations had little or no effect on the folding or the thermal stability of the troponin complex. Isothermal calorimetry, fluorescence spectroscopy, and transient kinetics were used to assess the effect of these mutations on the function of troponin I. We found that: 1) all TnI mutations increased the affinity of the troponin complex for actin in the presence of Ca^{2+} and increased the Ca^{2+} affinity of troponin within thin filaments. This suggests an uncoupling between Ca^{2+} binding and actin binding. 2) The size of the cooperative unit n was not affected by troponin I mutations. 3) A2V, R21C, Q130R, A157V, G203S, and K206Q mutations did not affect the proportion of thin filaments in the blocked state (at low Ca^{2+}). In contrast R145G mutation dramatically reduced the amount of thin filaments switched to the blocked state. This effect was also observed using electron microscopy and helical reconstruction. 4) A2V, R21C, Q130R, R145G, G203S, and K206Q did not affect the observed rate constant of Ca^{2+} dissociation from troponin and thin filaments. In contrast troponin I A157V showed a decrease in the Ca^{2+} dissociation rate constant. 5) Finally, we found that calcium alone is sufficient to fully activate the cardiac thin filament while skeletal muscle thin filaments complete activation required both Ca^{2+} and myosin heads. Overall these results provide insight into the mechanism by which troponin I mutations affect contractility in hypertrophic and dilated cardiomyopathy. These findings could have important clinical consequences.

ACKNOWLEDGMENTS

First and foremost, I am thankful to Almighty ALLAH for all his bounties and blessings, for giving me the ability to make this happens. I would like to express my gratitude to my sponsor "Mu'tah University" for funding this project.

This thesis arose in part out of four years of research that has been done since I came to the University of Leicester in 2007. During this time, I have worked with great people whose contribution to this work deserves a special mention. It is my pleasure to convey my gratitude to all of them.

In the first place I would like to record my gratitude to Dr Mohammed El-Mezgueldi for his excellent supervision from the very early stage of this research. His unflinching encouragement and support are much appreciated. I am also grateful for his helpful comments and critical reading of this thesis.

I gratefully acknowledge my PhD committee members Prof Clive Bagshaw and Dr Mark Pfuhl for their advice and encouragement. Thanks to Dr Cyril Dominguez for advice on the use of the circular dichroism machine and to Dr Jung (South Korea) for performing the EM experiment.

Many thanks for Prof Mike Geeves and Dr Peter Moody for reading this thesis and giving me their valuable comments.

I am very grateful for providing the cDNAs encoding wild-type TnT, TnI and TnC by Dr C. Redwood (University of Oxford, UK), Dr N.Brand (Imperial college, UK) and Prof K.Jacquet (Clinic of the Ruhr-University of Bochum, Germany). I would like to express my gratitude to Dr Xiaowen Yang and Andrew Prescott at the Protein and Expression Laboratory (PROTEX) for carrying out the mutagenesis.

Special thanks to my colleagues and friends, Dr Jaswir Basran, Dr Andrea Gumiero, Dr Zimna Wazeer, Dr Sami al-Harbi, Naif Bin Jomah, and Abdulwahab Binjomah for supporting and encouragement.

My parents deserve a special mention for their unwavering support and prayers. My Father has shown me the joy of intellectual pursuit ever since I was a child. My Mother's affection and love are immensely inspiring. Aheda, Ahed, Raed, Nisreen, Fares, Mohammed, Renata, and Ahmad thanks for being supportive and caring siblings. I wish to express my love and gratitude to all my brothers and sisters in law, and to all my nieces and nephews for their love.

My time at Leicester was made enjoyable in large part due to the many friends and groups that became part of my life. Special thanks to Dr Mohammad Taye, Anan Younes, Jihad Alhasanat, Mohammad Kharabsheh, Firas Kabbara, and Anjum Saqib.

Last, but by no means least, I thank my friends in Jordan, Great Britain, America and elsewhere for their support and encouragement. They continually called and emailed to offer their help and support, and thus encouraged me to continue to the end.

Sameeh Al-Sarayreh

Leicester/ England

June 2011

Abbreviations

ADP	Adenosine diphosphate
AP	Atrial Pressure
ATP	Adenosine TriPhosphate
AV	Atrioventricular Valves
CD	Circular Dichroism
cTnC	cardiac Troponin C
cTnI	cardiac Troponin I
cTnT	cardiac Troponin T
DCM	Dilated Cardiomyopathy
DNA	Deoxyribonucleic Acid
DTT	Dithiothreitol
EDTA	Ethylene diamine tetra-acetic acid
EGTA	Ethylene glycol tetraacetic acid
F-actin	filamentous actin
fsTnI	fast skeletal Troponin I
G-actin	Globular actin
HCM	Hypertrophic Cardiomyopathy
IAANS	2-[4'-(iodoacetamido)anilino]naphthalene-6-sulfonic acid
IPTG	IsoPropyl-beta-d-ThioGalactopyranoside
ITC	Isothermal titration calorimetry
K_B	equilibrium constant between blocked and closed states
K_T	equilibrium constant between closed and open states
LAP	Left Atrial Pressure
LB	Luria-Bertani
LV	Left Ventricle
LVP	Left Ventricular Pressure
MEG	7-methylguanosine
MDCC	N-[2-(1-maleimidyl)ethyl]-7-(diethylamino) coumarin-3-carboxamide
MOPS	3-(n-Morpholino)Propanesulfonic Acid
n	size of the cooperative unit
n_H	Hill's coefficient
NMR	Nuclear Magnetic Resonance
PBP	phosphate binding protein
PCR	Polymerase Chain Reaction
PIA	N-(1-pyrenyl)-iodoacetamide
Pi	inorganic phosphate
PIPES	Piperazine-1,4-Bis-2-Ethanesulfonic Acid

PKA	Protein Kinase A
PKC	Protein Kinase C
PMSF	Phenylmethanesulfonyl Fluoride
PNPase	purine nucleoside phosphorylase
RyR	Ryanodine Receptors
S1	Myosin subfragment 1
SDS	Sodium Dodecyl Sulfate
SR	Sarcoplasmic Reticulum
ssTnI	slow skeletal troponin I
TAE	Tri Acetate EDTA
TCA	Trichloroacetic acid
Tm	Tropomyosin
Tn	Troponin

Units/Symbols

A	Absorption
Å	Angström ($1 \text{ Å} = 1 \times 10^{-10} \text{ m}$)
bp	base pairs
g	gram
h	hour
kb	kilobase
kDa	kilo dalton
l	litre
M	molar
min	minute
mV	milliVolt
°C	degrees Celsius
OD	optical density
rpm	revolutions per minute
s	second
v/v	volume to volume
w/v	weight per volume
ϵ	Absorption coefficient
λ	wavelength

Table of Contents

Abstract	III
Acknowledgement	IV
Abbreviations	VI
Table of contents	VIII
List of figures	XII
List of tables	XVII
<u>Chapter 1: Introduction</u>	1
1.1 Human cardiac structure and physiology	2
1.1.1 Structure of the normal heart	2
1.1.2 The cardiac cycle	3
1.1.3 Calcium homeostasis in cardiac myocytes	4
1.1.4 Cardiac physiology in exercises	6
1.2 Heart Disease	7
1.3 Inherited heart disease classification	8
1.3.1 Hypertrophic Cardiomyopathy (HCM)	9
Definition of HCM	9
Clinical phenotype presentation	10
Etiology	10
Pathophysiological mechanisms	11
1.3.2 Dilated Cardiomyopathy (DCM)	12
Definition of DCM	12
Clinical presentation	13
Etiology	13
Pathophysiological mechanisms	14
HCM and DCM mutations classes	15
1.4 Structure of the Sarcomere	15
1.4.1 Myosin	16
1.4.2 Actin	19
1.4.3 Tropomyosin	22
1.4.4 The troponin complex	24
1.4.4.a Troponin C: The calcium binding subunit	24
1.4.4.b Troponin I: The key regulatory protein	26
1.4.4.c Troponin T: The tropomyosin binding protein	29
1.4.4.d Structure of the whole troponin complex	31
1.5 Regulation of muscle contraction	33
1.5.1 Mechanism of regulation	34
1.5.1.1 Thin filament acts as a cooperative allosteric system	35
1.5.1.2 The role of tropomyosin in regulation	37
1.5.1.3 The role of troponin in regulation	39
1.6 Troponin I Dysfunction	42
1.6.1 Functional Studies	45
1.6.2 Transgenic animal models for TnI mutations	48

1.7	Research Programme	51
	<u>Chapter 2 : Materials and Methods</u>	54
2.1	Preparation of recombinant Proteins	55
2.1.1	Preparation and expression of recombinant human cardiac troponin	55
2.1.2	Plasmid Mini Preps	56
2.1.3	Transformation	56
2.1.4	Glycerol Stocks	57
2.1.5	Reconstitution of troponin complexes	57
2.1.6	IAANScys35ser-cTnC and IAANScys84ser-cTnC preparation and purification-	58
2.2	Fluorescent phosphate binding protein (MDCC-PBP) preparation and purification	60
2.3	Protein purification from tissues	63
2.3.1	Cardiac muscle proteins purification	64
2.3.1.1	Cardiac myosin preparation	64
2.3.1.2	Cardiac myosin subfragment-1 (S1) preparation	65
2.3.2	Sheep cardiac muscle acetone powder preparation	67
2.3.2.1	Preparation of cardiac F-actin	67
2.3.2.2	Preparation of <i>N</i> -(1-pyrenyl)-iodoacetamide-labelled cardiac F-actin	69
2.3.2.3	Cardiac Troponin Preparation	70
2.3.2.4	Purification of cardiac tropomyosin	71
2.3.2.5	Preparation of <i>N</i> -(1-pyrenyl)iodoacetamide -labelled tropomyosin	72
2.4	Skeletal muscle proteins purification	73
2.5	General Methods	73
2.5.1	Determination of Protein Concentration	73
2.5.2	Polyacrylamide Gel Electrophoresis	74
2.5.3	Agarose Gel Electrophoresis	75
2.5.4	Co-sedimentation Assay	75
2.6	Determination of Actomyosin Mg^{2+} ATPase Activity	76
2.7	Circular Dichroism	77
2.8	Isothermal titration calorimetry (ITC) experiment	77
2.9	Enzyme kinetics	78
2.9.1	Transient State Kinetic Measurements	78
2.9.1.1	Myosin subfragment-1 (S1) Binding to PIA-actin thin filament switch between blocked and closed states	79
2.9.1.2	ATP Induced S1 dissociation from Actin Thin Filament – Switch between open to closed state	79
2.9.1.3	Phosphate release experiment	80
2.9.1.4	Calcium Dissociation Kinetics Measurements	81
2.10	Steady State Kinetic Measurements	82
2.10.1	Calcium Binding Measurements	82

Chapter 3: Structural and functional characterization of cardiomyopathy associated troponin I mutants 84

3.1	Introduction	85
3.2	Results	87
3.2.1	Cloning and Expression of TnI Mutations	87
3.2.2	Reconstitution of Troponin Complex	89
3.2.3	Circular Dichroism of TnI Mutations	91
3.2.4	Effect of TnI HCM and DCM mutations on the ability of the troponin complex to regulates the actomyosin ATPase in a Ca ²⁺ dependent manner	94
3.2.4.a	Effect of increasing troponin concentration on maximal inhibition and activation of the actomyosin ATPase:	95
3.2.4.b	Effect of TnI mutations on the cooperative activation of actin-Tm-Tn-myosin ATPase by myosin heads.	98
3.2.4.c	Effect of TnI mutations on the Ca ²⁺ sensitivity of the actin-Tm-Tn activation of S1 myosin head ATPase.	100
3.2.5	Binding of troponin complexes containing WT and TnI mutants into thin filament.	102
3.2.5.1	Co-sedimentation of TnI WT and mutants with thin filament	102
3.2.5.2	Binding of troponin complexes to actin.Tm thin filaments by using ITC assay	104
3.3	Discussion	108

Chapter 4: Effects of cTnI mutations on the affinity and kinetics of Ca²⁺ binding to and release from troponin 112

4.1	Introduction	113
4.2	Results	115
4.2.1	Effect of TnI mutation on calcium binding properties	115
4.2.1.1	Fluorescence Properties of IAANS-Cys 35/84 Labelled TnC	115
4.2.1.2	Effect of TnI Mutations on Ca ²⁺ Affinity of the Tn Complex	116
4.2.1.3	Effect of TnI mutations on the Ca ²⁺ Affinity of Thin Filaments	120
4.2.1.4	Effect of TnI mutations on the Ca ²⁺ Affinity of Thin Filaments in the presence of rigor myosin heads	123
4.2.2	Effect of TnI mutations on the kinetics of Ca ²⁺ dissociation	126
4.2.2.1	Ca ²⁺ dissociation kinetics of cTnI mutations using TnC ^{IAANSC35}	126
4.2.2.2	Ca ²⁺ dissociation kinetics of cTnI mutations using TnC ^{IAANSC84}	132
4.2.2.3	Ca ²⁺ dissociation kinetics of cTnI mutations using Quin-2	138
4.3	Discussion	143

Chapter 5: Effect of cTnI mutations on thin filaments dynamics 146

5.1	Introduction	147
5.2	Results	149
5.2.1	Effect of TnI mutations on K _B	149

5.2.1.1	Calcium dependence of K_B	155
5.2.1.2	Electron microscopy and helical reconstruction of thin filaments containing TnIR145G	157
5.2.2	Effect of TnI mutations on K_T	159
5.2.3	Effect of TnI mutations on the size of cooperative unit	165
5.3	Discussion	174
<u>Chapter 6: A comparative study of skeletal muscle and cardiac muscle thin filaments activation of the actomyosin ATPase</u>		177
6.1	Introduction	178
6.2	Results	180
6.2.1	The dual effect of the regulatory proteins on the acto-S1	180
6.2.2	Kinetics of phosphate release	181
6.2.3	The equilibrium constant between blocked and closed states	186
6.2.4	The size of cooperative unit	188
6.3	Discussion	190
<u>Chapter 7: General Discussion</u>		192
7.1	Introduction	193
7.2	Main Findings in the Thesis	194
7.2.1	Common effects between the TnI mutations	195
7.2.2	Functional consequences of TnI mutations	196
7.2.3	Mutation specific effects	198
7.2.3.1	TnI R145G	198
7.2.3.2	TnI A157V	201
7.2.4	Comparison of Cardiac and skeletal muscle thin filament activation	203
7.3	Mechanism of pathogenesis	205
7.4	Limitations of study	207
7.5	Conclusion	208
	Appendices	209
	References	214

List of Figures

Chapter 1

Figure 1.1	Anatomy of the heart	2
Figure 1.2	The cardiac cycle	4
Figure 1.3	Calcium cycling and signalling in cardiac myocyte	6
Figure 1.4	Effect of heart rate on the diastolic period available for filling	7
Figure 1.5	Major types of ventricular remodelling	8
Figure 1.6	Illustrations of normal heart, hypertrophic and dilated cardiomyopathies	9
Figure 1.7	Regular and parallel alignment of muscle cells in a normal heart and irregular disorganised alignment of muscle cells or myocardial disarray found in some parts of the heart in HCM	10
Figure 1.8	Structure of cardiac muscle sarcomere	16
Figure 1.9	Ribbon representation of myosin II subfragment-1	18
Figure 1.10	Structure of actin	21
Figure 1.11	Structure of tropomyosin	24
Figure 1.12	Crystal structure of TnC	26
Figure 1.13	Human cardiac troponin I amino acid sequence	27
Figure 1.14	Effects of PKA phosphorylation on cTnI structure	29
Figure 1.15	TnT structural and functional domains	30
Figure 1.16	The x-ray structure of calcium saturated structure of the core domain of human cardiac troponin	31
Figure 1.17	A schematic representation of the interaction between the troponin complex and the rest of the thin filament	33
Figure 1.18	Normalized force versus pCa	34
Figure 1.19	Contractile cycles for a single cross-bridge	35
Figure 1.20	The three states model	37
Figure 1.21	Model for the interaction between actin and tropomyosin	39
Figure 1.22	Exon organisation and TnI HCM localisation in human cardiac troponin I	42

Chapter 2

Figure 2.1	Expression vector of hcTnI and hcTnC (pLEICS-05)	56
Figure 2.2	The purification of cTnC by using Q-sepharose column.	60
Figure 2.3	The purification of MDCC-PBP by using Q-sepharose column	63
Figure 2.4	Purification of cardiac myosin subfragment-1(S1) by using Q-sepharose column	66
Figure 2.5	The purification of actin by using gel filtration column	68
Figure 2.6	The purification of cardiac tropomyosin by using DEAE column	72

Chapter 3

Figure 3.1	Agarose gel of the PCR products of HCTnI mutants obtained by the overlap extension method.	87
------------	--	----

Figure 3.2	15% SDS-polyacrylamide gel electrophoresis	88
Figure 3.3	The reconstitution and purification of troponin complex by using gel filtration chromatography	91
Figure 3.4	Circular Dichroism spectra of TnI WT and HCM and DCM mutants reconstituted in troponin complexes	93
Figure 3.5	Thermal denaturation of TnI WT and HCM and DCM mutants reconstituted in troponin complexes	94
Figure 3.6	Effect of increasing TnI mutants concentration on Actin-Tm activated Myosin-S1 ATPase in the presence and absence of calcium.	97
Figure 3.7	Bar chart of the maximal activation or inhibition obtained with each mutation.	97
Figure 3.8	Effect of TnI mutations on the S1 dependence of the actomyosin ATPase	99
Figure 3.9	Effect of TnI mutations on Ca ²⁺ dependent Actin.Tm activated S1 ATPase activity	101
Figure 3.10	15% SDS-PAGE for of WT and TnI mutations cosedimented to Actin-Tm	103
Figure 3.11	Microcalorimetric titration of actin.tropomyosin with troponin complexes (wild type and A2V) in the presence of 50μM CaCl ₂ .	105
Figure 3.12	Microcalorimetric titration of actin.tropomyosin with troponin complexes (R21C and Q130R) in the presence of 50μM CaCl ₂	105
Figure 3.13	Microcalorimetric titration of actin.tropomyosin with troponin complexes (R145G and A157V) in the presence of 50μM CaCl ₂ .	106
Figure 3.14	Microcalorimetric titration of actin.tropomyosin with troponin complexes (G203S and K206Q) in the presence of 50μM CaCl ₂	106

Chapter 4

Figure 4.1	Emission spectra of (A) IAANS attached to Cys-35 of cTnC ^{C84S} and (B) Cys-84 of cTnC ^{C35S} in various regulatory complexes	116
Figure 4.2	Ca ²⁺ binding to the cTn complex with TnI mutations given by IAANS-Cys35-TnC	118
Figure 4.3	Representative data for the Ca ²⁺ binding to the cTn complex with TnI mutations given by IAANS-Cys35-TnC	118
Figure 4.4	Ca ²⁺ binding to the thin filament reconstituted with TnI mutations given by IAANS-Cys84-TnC	121
Figure 4.5	Representative data for the Ca ²⁺ binding to the thin filament reconstituted with TnI mutations given by IAANS-Cys35-TnC	121
Figure 4.6	Ca ²⁺ binding to the thin filament reconstituted with TnI mutations in the presence of myosin heads given by IAANS-Cys84-TnC	124
Figure 4.7	Representative data for the Ca ²⁺ binding to the thin filament reconstituted with TnI mutations in the presence of myosin heads given by IAANS-Cys35-TnC	124
Figure 4.8	Ca ²⁺ dissociation fluorescence given by TnC ^{IAANSC35} reconstituted in Tn complex	128

Figure 4.9	Ca ²⁺ dissociation normalised fluorescence given by TnC ^{IAANSC35} reconstituted in Tn complex	128
Figure 4.10	Ca ²⁺ dissociation fluorescence given by TnC ^{IAANSC35} reconstituted in thin filament	129
Figure 4.11	Ca ²⁺ dissociation normalised fluorescence given by TnC ^{IAANSC35} reconstituted in thin filament	129
Figure 4.12	Ca ²⁺ dissociation fluorescence given by TnC ^{IAANSC35} reconstituted in thin filament + rigor myosin heads	130
Figure 4.13	Ca ²⁺ dissociation normalised fluorescence given by TnC ^{IAANSC35} reconstituted in thin filament + rigor myosin heads	130
Figure 4.14	Ca ²⁺ dissociation fluorescence given by TnC ^{IAANSC84} reconstituted in Tn complex	134
Figure 4.15	Ca ²⁺ dissociation normalised fluorescence given by TnC ^{IAANSC84} reconstituted in Tn complex	134
Figure 4.16	Ca ²⁺ dissociation fluorescence given by TnC ^{IAANSC84} reconstituted in thin filament	135
Figure 4.17	Ca ²⁺ dissociation normalised fluorescence given by TnC ^{IAANSC84} reconstituted in thin filament	135
Figure 4.18	Ca ²⁺ dissociation fluorescence given by TnC ^{IAANSC84} reconstituted in thin filament + rigor myosin heads	136
Figure 4.19	Ca ²⁺ dissociation normalised fluorescence given by TnC ^{IAANSC84} reconstituted in thin filament + rigor myosin heads	136
Figure 4.20	Ca ²⁺ dissociation fluorescence given by Quin-2 of reconstituted Tn complex	139
Figure 4.21	Ca ²⁺ dissociation normalised fluorescence given by Quin-2 of reconstituted troponin complex	139
Figure 4.22	Ca ²⁺ dissociation fluorescence given by Quin-2 of thin filament	140
Figure 4.23	Ca ²⁺ dissociation normalised fluorescence given by Quin-2 of thin filament	140
Figure 4.24	Ca ²⁺ dissociation fluorescence given by Quin-2 of thin filament + rigor myosin heads	141
Figure 4.25	Ca ²⁺ dissociation normalised fluorescence given by Quin-2 of thin filament + rigor myosin heads	141

Chapter 5

Figure 5.1	Binding of S1 to PIA-actin and to actin.Tm.Tn WT in the presence and absence of calcium	151
Figure 5.2	Binding of S1 to PIA-actin in the presence and absence of calcium for TnI mutations in the N-terminal TnC binding region	151
Figure 5.3	Binding of S1 to PIA-actin in the presence and absence of calcium for TnI mutation in TnT binding region	152
Figure 5.4	Binding of S1 to PIA-actin in the presence and absence of calcium for TnI mutations in inhibitory region	152
Figure 5.5	Binding of S1 to PIA-actin in the presence and absence of calcium for TnI mutations in C-terminal TnC binding region	153
Figure 5.6	The blocked state population in the absence of calcium for TnI	154

	WT and HCM and DCM mutations.	
Figure 5.7	Binding of S1 to PIA-actin.Tm.Tn WT	155
Figure 5.8	The equilibrium constant K_B as a function of pCa	156
Figure 5.9	Surface views of actin and thin filament reconstructions showing the position of tropomyosin	158
Figure 5.10	Dependence of the rates of phosphate release from acto(TmTn)myosinS1-ADP-Pi on thin filament concentration and calcium and rigor S1 bound to the thin filament	161
Figure 5.11	Dependence of the rates of phosphate release from acto(TmTn)myosinS1-ADP-Pi on thin filament concentration and calcium and rigor S1 bound to the thin filament. Troponin I mutations in the N-terminal TnC binding region	161
Figure 5.12	Dependence of the rates of phosphate release from acto(TmTn)myosinS1-ADP-Pi on thin filament concentration and calcium and rigor S1 bound to the thin filament. Troponin I mutations in the TnT binding region	162
Figure 5.13	Dependence of the rates of phosphate release from acto(TmTn)myosinS1-ADP-Pi on thin filament concentration and calcium and rigor S1 bound to the thin filament. Troponin I mutations in the inhibitory region	162
Figure 5.14	Dependence of the rates of phosphate release from acto(TmTn)myosinS1-ADP-Pi on thin filament concentration and calcium and rigor S1 bound to the thin filament. Troponin I mutations in the C-terminal TnC binding region	163
Figure 5.15	Fluorescence emission spectra of PIA-labelled Tm (Tm*)	166
Figure 5.16	Fluorescence emission spectra of PIA-labelled Tm (Tm*) in the presence of troponin complex	166
Figure 5.17	Kinetics of ATP induced dissociation of S1 from Actin.Tm* and Actin.Tm*.Tn thin filament (wild type).	168
Figure 5.18	Kinetics of ATP induced dissociation of S1 from TnI mutations in the N-terminal TnC binding region	170
Figure 5.19	Kinetics of ATP induced dissociation of S1 from TnI mutation in TnT binding region	171
Figure 5.20	Kinetics of ATP induced dissociation of S1 from TnI mutation in inhibitory region	171
Figure 5.21	Kinetics of ATP induced dissociation of S1 from TnI mutation in C-terminal TnC binding region	172

Chapter 6

Figure 6.1	The dual effect of the regulatory proteins on the acto-S1	181
Figure 6.2	The effect of ATP concentration on the rates of phosphate release from acto(TmTn)myosinS1-ADP-Pi in the presence of calcium	183
Figure 6.3	Dependence of the rates of phosphate release from acto(TmTn)myosinS1-ADP-Pi on thin filament concentration and calcium and rigor S1 bound to the thin filament	184

Figure 6.4	Binding of S1 to PIA-actin and to actin.Tm.Tn in the presence and absence of calcium for both cardiac and skeletal systems	187
Figure 6.5	The equilibrium constant K_B as a function of pCa for cardiac and skeletal systems	187
Figure 6.6	Kinetics of ATP induced dissociation of S1 from Actin.Tm*.Tn thin filament (cardiac and skeletal systems)	189

Chapter 7

Figure 7.1	Exon organisation and TnI HCM localisation in human cardiac troponin I.	195
Figure 7.2	Locations of TnIQ130R and TnIA157V in troponin structure.	195

List of Tables

Table 1.1	Diseases Genes in HCM and DCM	12
Table 1.2	Troponin I mutations associated with HCM and DCM.	44
Table 2.1	Extinction coefficients	73
Table 2.2	Ca ²⁺ - EGTA buffer for calcium titration experiment	83
Table 3.1	The maximal activation and inhibition obtained by wild type and TnI mutants	98
Table 3.2	The effect of cTnI mutations on the Ca ²⁺ binding dependent of actin-activated acto-S1 ATPase activity	102
Table 3.3	Binding parameters for complexation between troponin complexes and actin.Tm thin filaments	107
Table 4.1	Summary of the effect of TnI mutations on the calcium binding properties of Tn complex by using TnC ^{IAANSC84S}	119
Table 4.2	Summary of the effect of TnI mutations on the calcium binding properties of regulated thin filament by using TnC ^{IAANSC35S}	122
Table 4.3	Summary of the effect of TnI mutations on the calcium binding properties of regulated thin filament in the presence of myosin heads by using TnC ^{IAANSC35S}	125
Table 4.4	Summary of the effect of cTnI mutations on the Ca ²⁺ dissociation rate constant obtained by using TnC ^{IAANSC35} probe.	131
Table 4.5	Summary of the effect of cTnI mutations on the Ca ²⁺ dissociation rate constant obtained by using TnC ^{IAANSC84} probe.	137
Table 4.6	Summary of the effect of cTnI mutations on the Ca ²⁺ dissociation rate constant obtained by using Quin-2.	142
Table 5.1	The effect of cTnI mutations on the thin filament switching parameter K _B	154
Table 5.2	Calcium dependence of K _B	156
Table 5.3	The effect of cTnI mutations on the equilibrium constant K _T	164
Table 5.4	Summary of the effect of TnI mutations on the size of cooperative unit n	173
Table 6.1	Maximum rate constant and dissociation constant for cardiac and skeletal system	185
Table 7.1	Summary of general findings in this thesis	202

CHAPTER 1

Introduction

1.1 Human cardiac structure and physiology

1.1.1 Structure of the normal heart

The heart is a four-chambered organ consisting of right and left halves. Two of the chambers, the left and right atria, are entry-points into the heart, while the other two chambers, the left and right ventricles, are responsible for contractions that send the blood through the circulation. The heart is a three-dimensional hollow complex structure with mechanical properties that are nonlinear, time varying and spatially inhomogeneous, figure 1.1. Inferior and superior vena cavae bring the deoxygenated blood from the body to the right atrium then the blood enters to the right ventricle (RV) through the tricuspid valve. The right ventricle pumps the blood (through the pulmonary valve) via the pulmonary artery to reach to the lungs then to be re-oxygenated. The re-oxygenated blood is then carried back to the left atrium through the pulmonary veins. Once the left atrium is filled, the blood is pushed into the left ventricle (LV) through the mitral valve. The left ventricle then pumps the blood via the aortic valve to the aorta and then to the rest of the body.

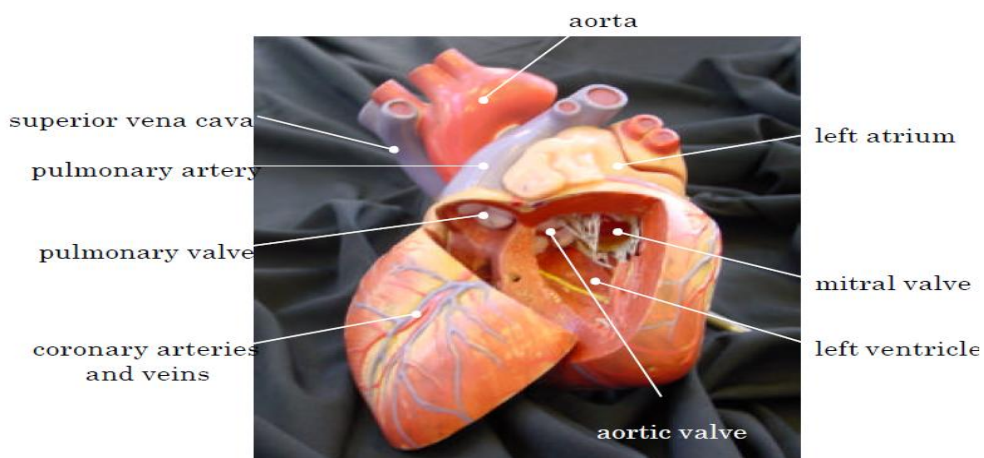


Figure 1.1 Anatomy of the heart. Arteries are marked in red and veins are marked in blue (Masood and Yang 2001).

1.1.2 The cardiac cycle

Contraction of the heart is controlled by electrical impulses that travel through its pacemaker cells. The impulse starts at the Sino-atrial (SA) node (cardiac pacemaker); the SA node is located in the wall of the right atrium near the entrance of the superior vena cava. 50 ms is the time needed for the impulse to travel from SA node to the atrio-ventricular (AV) node. Because of the slow conduction through the AV node (about 100 ms), the atria would start contracting before the ventricles. The impulse then keeps travelling through the Bundle of His (atrial bundle), in the interventricular septum to the Purkinje fibers, which then spread throughout the ventricles. The electrical impulse leads to membrane depolarisation and activation of Ca^{2+} release in the cytoplasm of the cardiomyocyte. The liberated Ca^{2+} diffuses to the myofilaments, binds the Ca^{2+} sensor troponin C and activates the subsequent mechanical event of the heart.

The ventricular (cardiac) cycle consists of three major events: LV contraction, LV relaxation and LV filling. The cardiac cycle is illustrated in figure 1.2. Contraction triggered by calcium leads to the build up of the LV pressure. Since the mitral and aortic valves are closed, the contraction takes place under isovolumic conditions. When LV reaches a greater pressure than the aortic one, then the aortic valve opens and triggers a rapid ejection. As LV pressure falls, the aortic valve closes and the LV goes into isovolumic relaxation. Finally, when LV reaches a lower pressure than the atrial one, then the mitral valve opens and filling begins again.

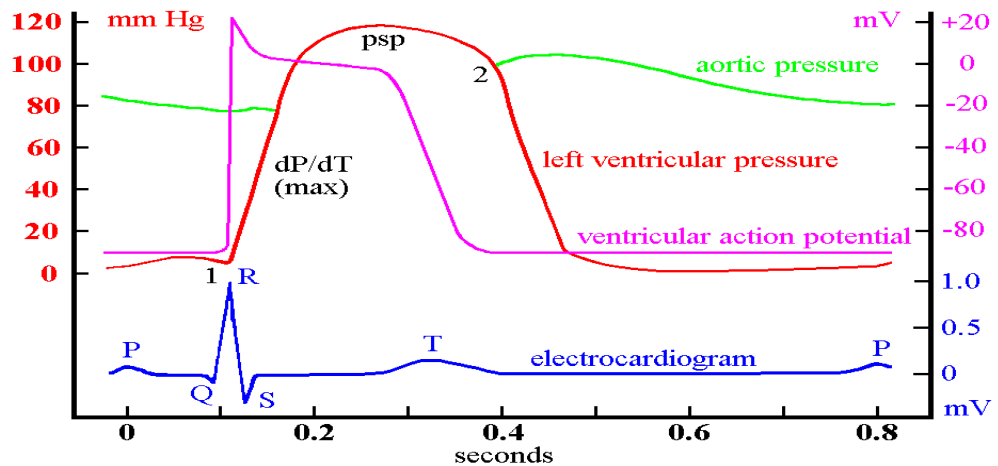


Figure 1.2 The cardiac cycle. The echocardiogram trace (with its various phases P, Q, R, S, and T) is shown as a blue line, in mV, during one cardiac cycle. The ventricular action potential is shown as a purple line. The red line, a trace of the ventricular pressure (dP/dT), rises rapidly after the mitral valve closes until the aortic valve opens to allow rapid ejection of the blood into the aorta. The aortic pressure represented as a green line which rises in systole and then decreases slowly as flow slows due to ventricular pressure decreasing (Masood and Yang 2001).

1.1.3 Calcium Homeostasis in cardiac myocytes

In cardiac myocyte, the transition from a relaxed state at low calcium concentration to the contraction occurs because a small quantity of calcium enters the sarcolemma and induces much calcium release from the sarcoplasmic reticulum (SR) (Barry and Bridge 1993). This process starts with the depolarization of the cell membrane that influences the opening of the voltage-gated sodium and calcium channels.

Excitation-contraction coupling (E-C coupling) is a crucial process in which electrical impulses are translated to mechanical activities in the muscle fibres (Bers 2008). Although sodium influx via the sodium channel can lead to calcium entering through the sodium-calcium exchanger in a reverse mode, but calcium influx through L-type calcium channel is the main step in E-C coupling. When calcium enters the cell, it binds to the calcium release channels of the SR (ryanodine receptors (RyRs)), and by

activating these channels, a much larger release of calcium from the internal stores within the SR would occur by a process called calcium-induced calcium release (CICR) (Fu and Yang 2006). As the calcium concentration increases, the sodium-calcium exchanger begins a sodium-in/calcium-out mode. The small relatively calcium influx across the sarcolemma thought to trigger the SR calcium releasing, while most of the calcium causing contraction during the E-C coupling is calcium released from the SR. The calcium released from the SR would initiate the contraction by binding to troponin C (TnC). When calcium binds to TnC, myosin heads would bind to actin after a conformational change within the thin filament.

The calcium homeostasis should not be altered; hence the amount of calcium that enters the cytosol of cardiac myocytes must be extruded from the cytosol. The reuptake of calcium into the SR is mediated by the SR calcium ATPase. The 'reuptake calcium' into the SR is bound to the calcium binding protein (calsequestrin) that is located in the junctional SR. Calcium extrusion from the cytosol is mediated by the sodium –calcium exchanger. For every 2+ charge entering the cell as calcium, a 3+ charge leaves the cell as sodium and vice versa ($3\text{Na}^+ : 1\text{Ca}^{2+}$ ratio). It has been shown that a minor fraction of the calcium is removed from cytosol using the sarcolemmal calcium ATPase and mitochondrial transporters (Bers 2008).

Overall, there are two basic principles that maintain the steady state contraction of cardiac physiological function: i) there is a balance between the amount of calcium that enters the cell via calcium channel and the amount of calcium that is extruded by the sodium–calcium exchanger, and ii) calcium amount released by SR is equal to the calcium uptake by the SR calcium pump ATPase (Fu and Yang 2006). The whole process

(figure 1.3) can be altered in different diseases and the changes resulted by these diseases would cause crucial alterations in contraction and relaxation of the heart (Bers 2008; Hasenfuss et al., 1992).

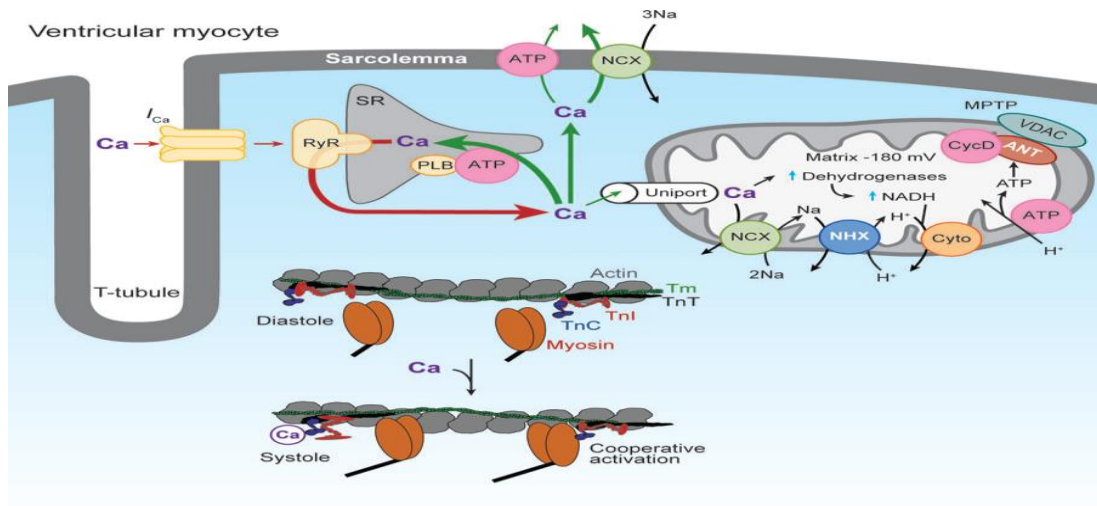


Figure 1.3 Calcium cycling and signalling in cardiac myocyte (Bers 2008).

1.1.4 Cardiac physiology in exercises

The cardiac response to exercise is complex and involves changes in contractility, heart rate, preload, and after load. At rest the heart rate is about 60 beat per min while during exercise the heart rate increases substantially (up to 200 beats per min). This leads to a shortening of all phases of the heart cycle (1 beat per 0.33 sec). These phases however do not all shorten to an equal degree. The ventricular systole shortens to 0.2 sec, and that will leave 0.13 sec for the diastolic refilling, figure 1.4.

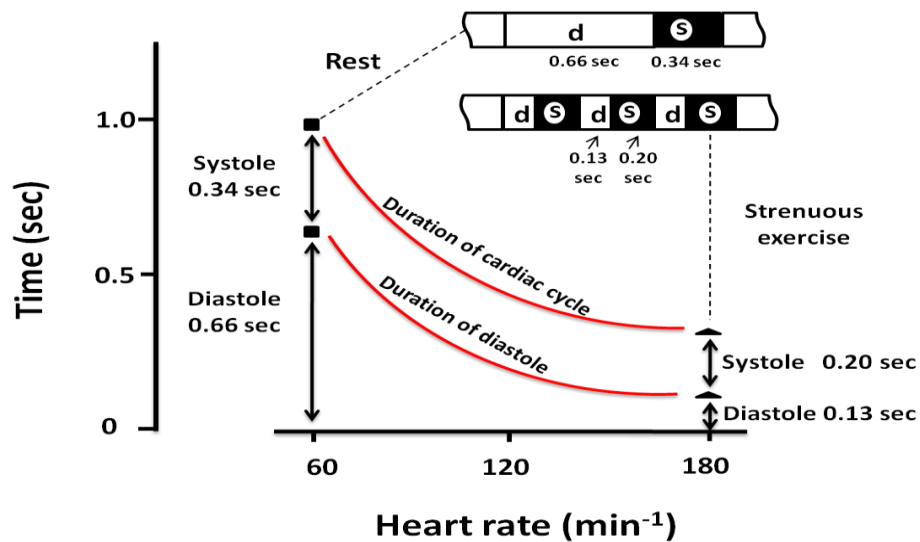


Figure 1.4 Effect of heart rate on the diastolic period available for filling. As heart rate increases, diastole is more curtailed than systole. d is diastole and s is systole (adapted from Levick 2003).

1.2 Heart disease

Cardiac failure and dysfunction can be caused by many factors that would stress the myocardium (Ashrafian and Watkins 2007). Genetic diseases (condition caused by abnormalities in genes or chromosomes), ischemia (restriction in blood supply due to factors in the blood vessels with resultant damage of tissues), myocardial infarction (interruption of blood supply to a part of the heart that leads the heart cells to die), and hypertension (medical condition in which the systematic arterial blood pressure is elevated) are all factors that can stop the heart from working efficiently (Ashrafian and Watkins 2007). Because of these stress factors, the heart can undergo changes in its structure caused by chronic alterations in loading conditions (Opie et al., 2006). This structural changes process is called "remodelling".

Clinically, cardiac remodelling is manifested as a change in shape, size and function of the heart produced by cardiac injury or load. Remodelling can be described as adaptive (physiological) or maladaptive (pathological) (Dorn and Robbins 2003).

There are three major types of ventricular remodelling: (1) concentric modelling where the thickness of the cardiomyocyte is increased as a result of the pressure load increasing (2) eccentric hypertrophy when the volume load influence myocyte lengthening and (3) myocardial infarction when the left ventricle volume increases by both pressure and volume loads, figure 1.5 (Opie et al., 2006).

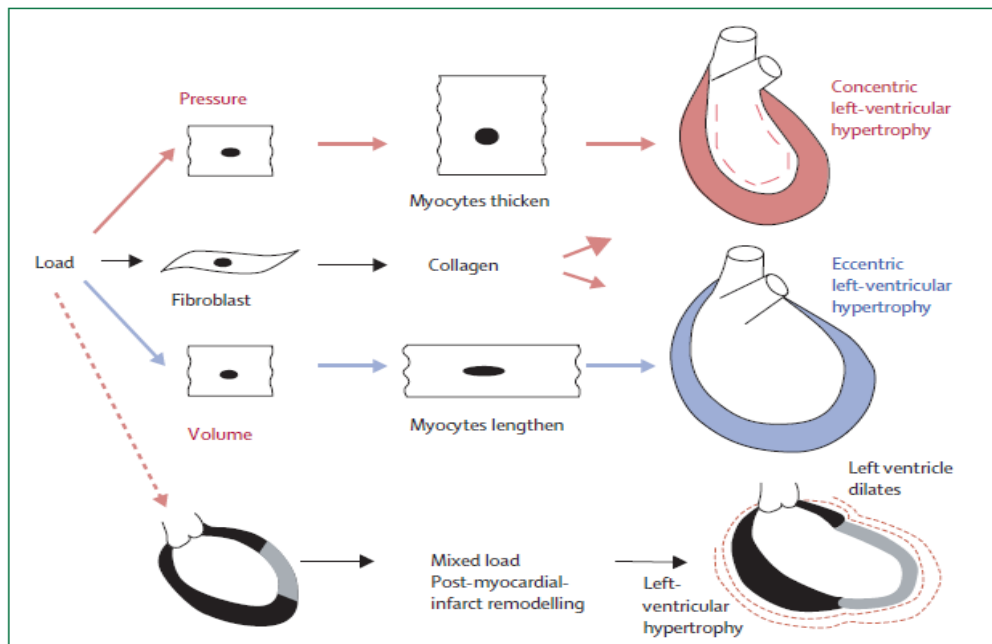


Figure 1.5 Major types of ventricular remodelling (Opie et al., 2006).

1.3 Inherited heart disease classification

Four major classes of cardiomyopathies have been classified (Towbin and Bowles 2002): hypertrophic (HCM), dilated (DCM), restrictive (RCM), and arrhythmogenic right ventricular cardiomyopathies. HCM and DCM are diseases of perturbed sarcomeric

function, figure 1.6 (Ashrafian and Watkins 2007). RCM is the rarest class, while arrhythmogenic right ventricular is a very complex disorder characterized by loss of myocytes and replacement by fatty and fibrous tissues (Towbin and Bowles 2002).

These cardiomyopathies are associated with cardiac failure and dysfunction that can lead to cardiovascular morbidity and mortality. Defining the genotype-phenotype relationship might provide a crucial clue to understand the disease and help to find the proper treatment (Arad et al., 2002). Here we are interested to investigate the troponin I mutations related to hypertrophic cardiomyopathies (HCM) and dilated cardiomyopathies (DCM).

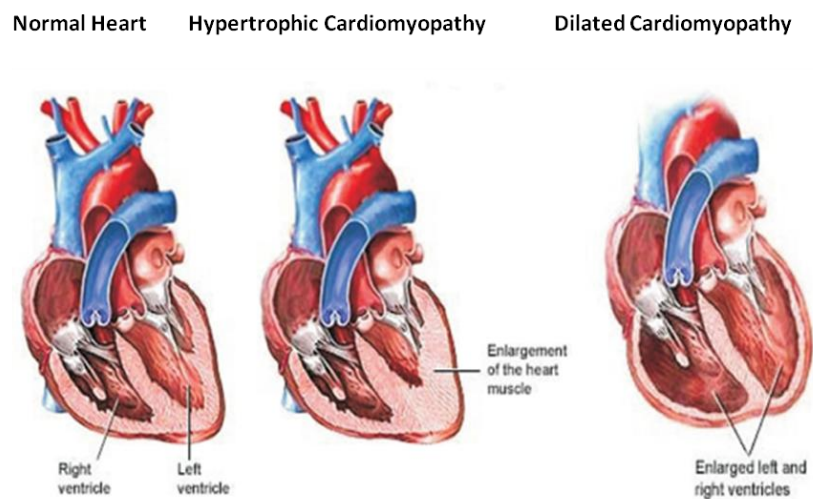


Figure 1.6 Illustrations of normal heart, hypertrophic and dilated cardiomyopathies
www.nlm.nih.gov/medlineplus/ency/imagepages/18141.htm
www.nlm.nih.gov/medlineplus/ency/imagepages/18136.htm

1.3.1 Hypertrophic cardiomyopathy (HCM)

Definition of HCM

Hypertrophic cardiomyopathy is a cardiac disorder that can be characterized by left ventricular hypertrophy accompanied by myofibrillar disarray, figure 1.7 (Arad et al.,

2002; Seidman and Seidman 2001; Teare 1958; Kimura et al., 1997). The prevalence of HCM is 0.2 % in the population (1:500 individuals) (Tardiff 2005; Richard et al., 2003). HCM is an autosomal dominant disorder. This disease is the major cause of sudden cardiac death in the young (Harada and Morimoto 2004). The clinical phenotype of HCM ranges from a lack of cardiovascular symptoms to sudden death (Tardiff 2005) and these phenotypes are affected by additional factors including modifier genes, epigenetic, single nucleotide polymorphism or environmental effects.

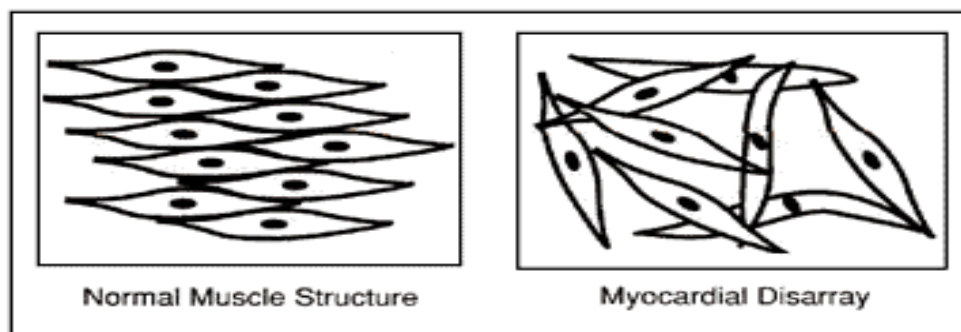


Figure 1.7 Regular, parallel alignment of muscle cells in a normal heart and irregular disorganised alignment of muscle cells or myocardial disarray found in some parts of the heart in HCM (Cardiomyopathy association www.cardiomyopathy.org/index.php)

Clinical phenotype presentation

The overall clinical phenotype of HCM patients is broad and ranges from a complete lack of cardiovascular symptoms to shortness of breath (dyspnea), chest pain (angina), or cardiac sudden death (Tardiff 2005; Vikstrom and Leinwand 1996; McKenna and Camm 1989).

Etiology

HCM is an autosomal dominantly inherited disorder that is characterized by increased left ventricular mass in the absence of other diseases. Genetic studies have established

that HCM is linked to more than 400 mutations in 10 different sarcomeric genes (Richard et al., 2003), table 1.1. The genes encode proteins which are components of either thick or thin filament of the sarcomere. Mutations in thick filament proteins are located in the beta myosin heavy chain (Geisterfer-Lowrance et al., 1990) and cardiac essential and regulatory myosin light chains (Poetter et al., 1996). Mutations in thin filament proteins have been found in alpha tropomyosin (Thierfelder et al., 1994; Watkins et al., 1995), cardiac actin (Mogensen et al., 1999), cardiac troponin T (Thierfelder et al., 1994; Watkins et al., 1995; Moolman et al., 1997; Ho et al., 2000), cardiac troponin I (Kimura et al., 1997), and cardiac troponin C. In addition a large number of mutations have been linked to myosin binding protein C (Bonne et al., 1995; Watkins et al., 1995) and titin (Sato et al., 1999).

Pathophysiological mechanisms

Different mechanisms have been suggested in which sarcomeric mutations would lead to hypertrophic cardiomyopathy (Seidman and Seidman 2001). The amount of functional protein could be reduced (haploinsufficiency) by dominant gene mutations that inactivate an allele. The production of such non functional protein would produce an imbalance in stoichiometry of thick to thin filament components leading to sarcomeric functional and structural changes (Bonne et al., 1998). Alternatively, dominant gene mutations would produce a mutant protein which will be incorporated in the sarcomere and acts as a poison peptide interfering with normal protein function (dominant negative) (Bonne et al., 1998; Vikstrom and Leinwand 1996).

A major effort has been devoted to unravel the mechanism by which these mutations cause the disease. Early functional studies have shown that cardiac sarcomeric

mutations alter the function of the sarcomere and reduce the amount of force generated by cardiomyocyte (Bonne et al., 1998). This was suggested to lead to adaptive mechanisms resulting in a compensatory mechanism.

Alternatively it has been suggested that HCM mutations could increase the cost of force production (less force per ATP) and as a result this increase in energy consumption will result in putting more energy demand on the myocyte which can not be met (Redwood et al., 1999; Crilley et al., 2003).

Table 1.1 Diseases Genes in HCM and DCM

<http://www.hgmd.cf.ac.uk/ac/search.php>

Gene	Chromosomal Loci	Protein	HCM Mutations Number	DCM Mutations Number
MYH7	14q12	β-myosin heavy chain	196	13
TPM1	15q22	α-tropomyosin	11	2
ACTC	15q14	α-cardiac actin	7	2
TNNT2	1q32	Troponin T	34	13
TNNI3	19q13.4	Troponin I	29	1
TNNC1	3p21-p14	Troponin C	5	2
MYBPC3	11p11	Myosin Binding Protein C	164	3
MYL2	12q23-q24	Regulatory Myosin Light Chain	10	-
MYL3	3p21	Essential Myosin Light Chain	5	-

1.3.2 Dilated cardiomyopathy (DCM)

Definition of DCM

Dilated cardiomyopathy can be defined as a heart disease which is characterized by ventricular dilation and impaired contraction of left or both ventricles (Harada and Morimoto 2004; Chang and Potter 2005; Franz et al., 2001; Towbin and Bowles 2002), figure 1.6. DCM diagnosis is based on finding increased cardiac diastolic and systolic dimensions with diminished function of the contractile. Substantial distortions of cell architecture or myocyte disarray are not features of DCM (Seidman and Seidman 2001). DCM is considered as a major cause for morbidity and mortality among cardiovascular diseases that can lead to heart transplantation (Mestroni et al., 1999). DCM is a common disease affecting about 36.5 out of 100,000 people. Although toxic, metabolic, ischemic, or infectious causes are recognized, familial DCM accounts for up to 35% of the cases (Franz et al., 2001; Kamisago et al., 2000). Mutations associated with dilated cardiomyopathy have been found in the proteins of the sarcomere, sarcolemma, and the cytoskeleton (Chang and Potter 2005).

Clinical presentation

The overall clinical presentation of DCM patients includes some symptoms such as fainting, fatigue, shortness of breath, light headedness, sweating at rest, sudden death, and some times enlarged liver (Towbin and Bowles 2002; Franz et al., 2001).

Etiology

To date, there are no clear genotype-phenotype correlations to allow the prediction of the clinical course of DCM (Chen et al., 2002). Although familial dilated cardiomyopathy FDCM accounts for up to 35% of the DCM cases, the number of

mutations in each identified gene is relatively small. DCM is involved with other diseases such as skeletal myopathy and abnormal mitochondrial function (Ichida et al., 2001; Suomalainen et al., 1992).

Table 1.1 shows the DCM genetic loci that have been identified so far. The genes encode proteins which are components of either thick or thin filament of the sarcomere: (A) beta myosin heavy chain (Kamisago et al., 2000) (B) thin filament proteins, cardiac actin (Olson et al., 1998), alpha tropomyosin (Olson et al., 2001), cTnT (Kamisago et al., 2000; Li et al. 2001; Mogensen et al., 2004), cTnI and cTnC (Mogensen et al., 2004) (C) titin (Gerull et al., 2002) and cardiac myosin binding protein C (Shimizu et al., 2005).

Pathophysiological mechanisms

It has been suggested that defective force transmission in DCM would impair cardiac function and lead to remodelling of the heart (Kamisago et al., 2000). Cytoskeletal proteins (such as desmin and dystrophin) provide intracellular scaffolding which is crucial for force transmission from the sarcomere to the extracellular matrix; in addition it is important for the protection of myocytes from extrinsic mechanical stress. Defects in these cytoskeletal proteins would lead to DCM by reducing force transmission and/or resistance to mechanical stress (Franz et al., 2000; Franz et al., 2001).

Another hypothesis has been proposed, specific mutations in the mitochondrial DNA could lead to DCM, in which these mutations are believed to alter the energy production (Franz et al., 2001).

HCM and DCM mutations classes

There are three different classes of mutations that can lead to either HCM or DCM:

- 1) missense mutations (by changing one DNA nucleotide, one amino acid is replaced by another)
- 2) In-frame deletion mutations (deletion of one specific amino acid)
- 3) Splice-donor-site mutations (formation of truncated mutant by removing the carboxyl terminal amino acids).

1.4 Structure of the Sarcomere

Cardiac myocytes are binucleate, cylindrical shape cells that are enveloped by sarcolemmal membrane (sarcolemma). Myocytes are made up of a large number of fibrils extending along the length of the cell. The muscle fibre is composed of myofibrils that appear in micrographs as an alternating pattern of light and dark bands. The dark band is mainly composed of myosin II that makes up the thick filament, while the light band is mostly composed of actin that forms the thin filament. Myofibrils are composed of repeating contractile units called the sarcomere (Gregorio and Antin 2000). A sarcomere is defined as the segment between two neighbouring Z-lines (figure 1.8). The protein components of the sarcomere are: the Z-disc (alpha actinin), thick filament (myosin), thin filament (actin, troponin complex, and tropomyosin), M line (M protein and myomesin), and titin (Bönnemann and Laing 2004). It also contains myosin-binding protein C, which binds at one end to the thick filament and the other to actin.

Electron microscopic studies of muscle contraction showed that only the light band (I-band) decreases in length, whereas the dark band (A-band) remains unchanged. The thin and the thick filaments do not change in length. This can be explained by the sliding filament model that describes muscle contraction as the sliding of the thick filaments past the thin filaments with no change in the length of either type of filament. Cyclic interactions between the myosin-S1 head and actin are responsible for muscle contraction.

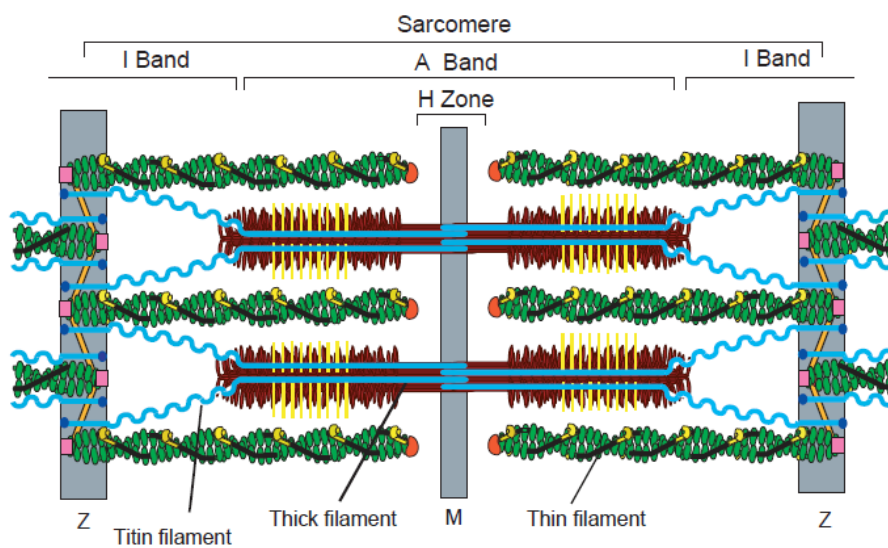


Figure 1.8 Structure of cardiac muscle sarcomere: actin represented in green, myosin in red, tropomyosin in black, troponin in yellow, actinin in gold, and myosin binding protein C in yellow transverse lines (Gregorio and Antin 2000).

1.4.1 Myosin

Myosin is one of the molecular motors machines that can direct the movement along the actin filament by ATP hydrolysis (Howard 1997). These motors are enzymes that transduce the chemical energy into mechanical work (Ruppel and Spudich 1996). So far more than 37 myosin's families have been classified. Most of these myosins are non muscle myosins. Myosin II (or conventional myosin) is the most common class

that you can find in the muscle. There are four subgroups for myosin II: skeletal, cardiac, smooth, and non muscle myosin II. V1, V2, and V3 are the three mammalian cardiac myosin isoforms that have been found in the cardiac muscle (Sugiura 1999). Various studies revealed that V1 has the highest ATPase activity, and it is a homodimer of alpha heavy chains. V3 has the lowest ATPase activity and structurally it is a homodimer of beta heavy chains. Finally V2 is a heterodimer of both alpha and beta heavy chains.

Muscle myosin is a hexamer composed of two major chains: two heavy chains (about 220 kDa) and two pairs of myosin light chains (MLC), a pair of essential light chains (17 kDa each) and a pair of regulatory light chains (20 kDa each) (Kazmierczak et al., 2009). The heavy chain is consisting of three domains: subfragment 1 (S1), subfragment 2 (S2), and light meromyosin (LMM). The carboxyl-terminal region of the heavy chains form an alpha helical coiled coil which makes the tail (Sellers and Knight 2007), while the amino terminal of the heavy chains form the globular heads that contain the actin and nucleotide binding sites. The globular heads can be further divided into three subdomains: the central 50 kDa domain that can be also divided into upper and lower segments, the 25 kDa amino-terminal segment, and the 20 kDa carboxyl-terminal segment, figure 1.8. Each one of the heavy chains has two motifs (essential and regulatory light chains) that lie on the carboxyl-terminal of the globular head domain.

Chicken skeletal myosin subfragment-1 was the first 3-D structure of a motor domain; it was crystallized at a high salt without bound nucleotide. Myosin subfragment 1 is divided into two functionally distinct segments, the lever arm and the catalytic motor domain, with the two separated by the converter region (Rayment et al., 1993b). It has

been found that the chicken skeletal muscle S1 is an asymmetric molecule, this molecule was found to be consisting of a globular catalytic domain that contains the actin and ATP binding sites in addition to an alpha helical regulatory domain that works to connect the catalytic domain to the tail. The actin binding site is located on the same side of the catalytic domain and opposite to the nucleotide binding site. The lever arm is a 85 Å alpha helix. Due to its length and C terminal location, it was proposed that the lever arm plays a role to amplify small conformational changes generated in the core of the motor domain, figure 1.9 (Tyska and Warshaw 2002).

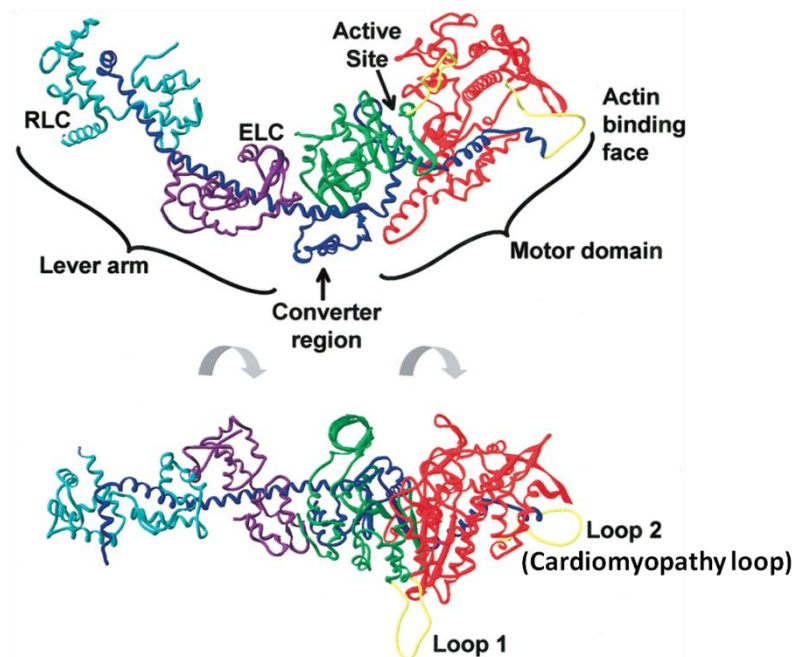


Figure 1.9 Ribbon representation of myosin II subfragment-1: The N-terminal domain (25 kDa) is labelled in green, the lower and upper 50 kDa domains are labelled in red, the C-terminal domain (20 kDa) is labelled in blue, the regulatory light chain (RLC) is labelled in light blue, and the essential light chain (ELC) is labelled in purple. The myosin subfragment-1 is further divided into two distinct segments, the motor domain and the lever arm separated by the converter region. Loops 1 (nucleotide binding region) and 2 (cardiomyopathy loop) are labelled in yellow (Tyska and Warshaw 2002).

1.4.2 Actin

Actin is one of the most conserved and abundant eukaryotic proteins. It was discovered in muscle tissue by Straub (Straub 1942). Actin is a 42 kDa adenine nucleotide-binding protein that made of 375 amino acids, and it is essential for so many cell functions. There are six different genes for actin, and each one of them encodes a different actin isoform. Alpha skeletal, alpha cardiac, alpha smooth and gamma smooth actins are expressed in muscles, while beta cytoskeleton and gamma cytoskeleton are non-muscle expressed actins (Perrin and Ervasti 2010).

Actin is found in two major forms: Globular which is the monomeric form (G-actin) that can spontaneously polymerise into the filamentous form (F-actin) at physiological salt concentration.

The first crystal structure of G-actin has been determined by Kabsch and his collaborators (Kabsch et al., 1990). They have determined the atomic structure of actin from the complex of skeletal G-actin with bovine pancreatic DNase I in the presence of ATP (resolution of 2.8 Å) and ADP (resolution of 3 Å). In this structure, the actin has two domains, large (inner) and small (outer) domains, and they are separated by a cleft that contains a nucleotide and divalent cation bound between these two domains. The two domains are joined by a hinge that allows a limited movement of the cleft with its bound nucleotide. The small domain is further subdivided into subdomain one and subdomain two. Subdomain one contains the S1 binding sites; it also contains the N and C terminals of the actin that have been predicted to be close to each other. The large domain is also further subdivided into subdomains three and four, figure 1.10 A. The atomic structure of the actin monomers was used to construct

a model for the actin filament (Holmes et al., 1990). Recently, a direct visualization of the secondary structures of the F-actin was achieved using electron cryomicroscopy of actin filament at a 6.6 Å resolution; figure 1.10 B (Fujii et al., 2010). In their model, complex domain motions, specific D-loop and terminal conformations are revealed, and all appear to be crucial for dynamic functions of actin (Fujii et al., 2010).

1.4.3 Tropomyosin

Four Tm genes have been identified in the human genome. They have been named as TPM1, TPM2, TPM3, and TPM4, and can generate more than 20 different Tm isoforms (Perry 2001). The striated muscle tropomyosins alpha and beta chains are coded by TPM1 and TPM2 genes respectively. The alpha and beta isoforms are the major components of the skeletal muscle Tm, while in cardiac muscle only the alpha isoform is present (Perry 2001).

The highest resolution crystal structure of full length Tm is only 7 Å (Whitby and Philips 2000; Hitchcock-DeGregori 2008). Cardiac muscle tropomyosin is a parallel, in register, coiled-coil homodimer made of two alpha helical chains made of 284 amino acids. This structure is achieved by a seven residue heptad repeat (residues are designated as a, b, c, d, e, f, and g), figure 1.11. The hydrophobic residues in positions a and d, are packed in a knobs into holes fashion to hold the two tropomyosin chains together. In addition interhelical salt bridges between residues in positions e and g enhance the stability of the coiled coil structure (Hitchcock-DeGregori 2008). Recent studies have however revealed that tropomyosin is not a pure coiled coil alpha helix. Brown and co-workers observed that there is an axial sliding of the two chains in the coiled-coil, where there are clusters of alanine in position d (Brown et al., 2001). These alanine clusters are located near the C terminus of each gene-duplication repeat. A larger hole will be between the small side chains of alanines in the core in this region, while the knob that fits into this hole will be correspondingly smaller, therefore this enables one chain to move a small distance (about 1 Å) relative to the other, (Brown et al., 2001).

Tropomyosin is always found associated with actin. Each tropomyosin spans the length of seven actin monomers. The mechanism of tropomyosin binding to actin is still not fully understood but a number of characteristics of tropomyosin binding to actin have been established: i) The N-terminal acetylation of tropomyosin is very important for strong actin binding affinity; the acetylation of N-terminal methionine residue must be present in both chains of both homo and hetero dimers of tropomyosin (Gimona 2008). ii) The head to tail binding interactions between adjacent tropomyosin molecules strengthen the interaction with actin. iii) The presence of alanine clusters is crucial for the tropomyosin to wind around the actin filaments (Stewart 2001; Li et al., 2010). iv) Seven quasi equivalent regions of tropomyosin have been suggested to interact each with an actin monomer.

In the skeletal and cardiac muscles, the contraction of muscle is controlled by the troponin-tropomyosin switch on the thin filament. Tropomyosin's main troponin partner is the TnT subunit. There are two TnT binding sites on the tropomyosin sequence. The region near residue cys-190 of tropomyosin binds to the C terminal of TnT in a Ca^{2+} sensitive manner. While the head to tail junction (C terminal of one tropomyosin and N terminal of the next tropomyosin) interacts with the N terminus of TnT in a Ca^{2+} insensitive fashion (Li et al., 2002). The role of cardiac tropomyosin is to introduce cooperativity to the thin filament (Lehman et al., 2009), and to induce different thin filament states with different activities.

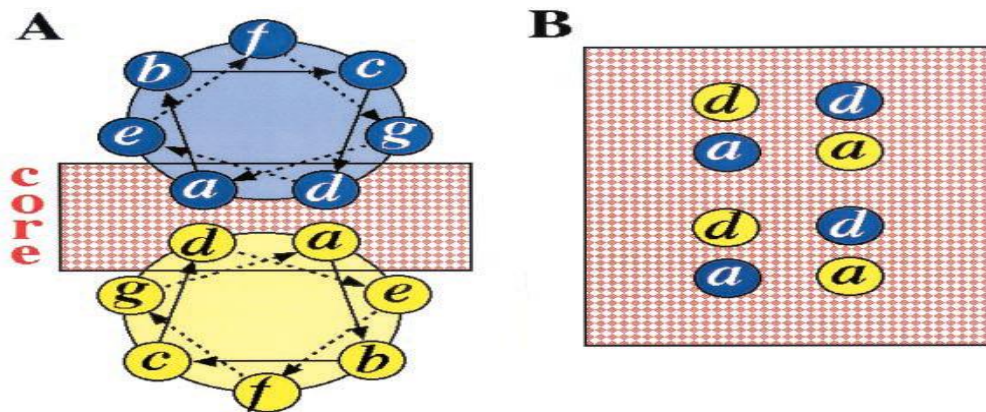


Figure 1.11 Structure of tropomyosin. Interaction between the two alpha-helices in the tropomyosin coiled-coil. (A) End-on view looking from N terminus. The interface between the alpha-helices derives mainly from hydrophobic residues in core positions *a* and *d*. (B) The core interface shows how residues from one chain occupy the spaces between the corresponding residues from the second chain to give “knobs in holes” packing (adapted from Stewart 2001).

1.4.4 The Troponin complex

Troponin is the calcium-based regulator of striated muscle contraction. Troponin is a heterotrimeric complex that is composed of three interacting subunits: Troponin C, which is the calcium sensor subunit (18 kDa), Troponin I which is the inhibitory subunit (24 kDa) and Troponin T which is the tropomyosin binding subunit (37 kDa).

1.4.4.a Troponin C: The calcium binding subunit

Troponin C is a highly acidic protein; it has a high content of aspartate and glutamate residues. Two similar isoforms are expressed in vertebrates: the fast skeletal TnC and the slow skeletal/cardiac TnC (Zot et al., 1987).

Troponin C (TnC) is a 76 Å long, 18 kDa dumbbell-shaped molecule. Structurally TnC is composed of an N-terminal regulatory lobe connected to a C-terminal structural lobe by a single alpha helical linker (Vinogradova et al., 2005). The regulatory lobe contains

five alpha helices, helix N (residues 5-11), helix A (residues 14-27), helix B (residues 41-46), helix C (residues 54-63), and helix D (residues 75-86) (Oleszczuk et al., 2010), also in the N terminal domain there are two calcium binding sites (in cardiac TnC, only site II is able to bind calcium in low affinity while site I is defunct because of amino acid substitutions). The structural lobe contains four alpha helices, helix E (residues 95-105), helix F (residues 116-124), helix G (residues 131-141), and helix H (residues 151-158) (Slupsky and Sykes 1995). The C terminal domain contains two metal binding sites occupied in high affinity by magnesium in the relaxed state and with calcium during contraction. In addition there are two antiparallel beta sheet regions: the antiparallel beta sheet in the N terminal domain, which consists of residues (36-38 and 72-74), and the antiparallel beta sheet in the C terminal domain (residues 112-114 and 148-150). These beta sheets together with the helices form four helix-loop-helix calcium binding sites, figure 1.12 (Slupsky and Sykes 1995).

The D/E linker that connects the regulatory and structural TnC subdomains is crucial for the activity of the troponin complex. This linker is very flexible and has no clear defined structure (Takeda et al., 2003).

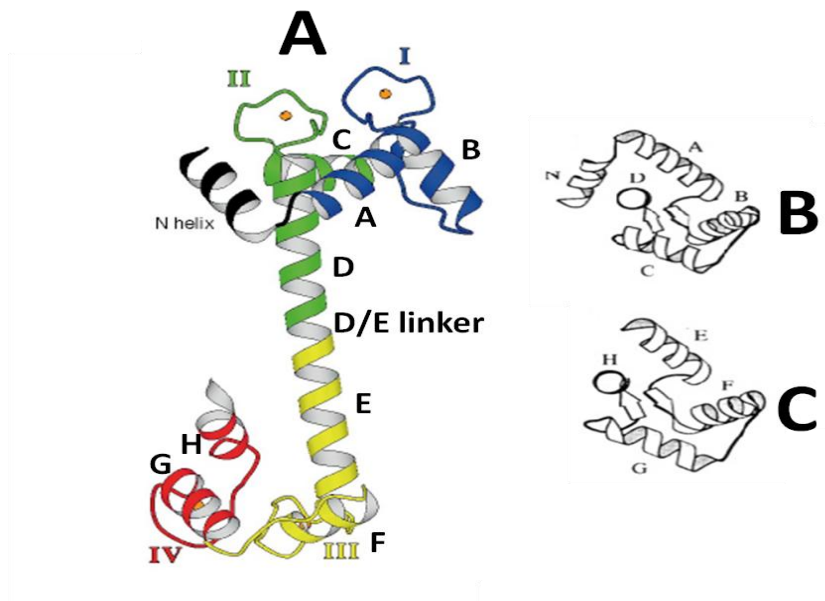


Figure 1.12 Crystal structure of TnC. (A) Helices A-H and N are shown. The N lobe (that contains calcium binding sites I and II) is connected to C lobe (that contains metal binding sites III and IV) by the D/E linker (Houdusse et al., 1997). (B) The N terminal lobe of TnC (residues 5-83), helix D coming out of the page (Slupsky and Sykes 1995). (C) The C terminal lobe of TnC (residues 98-155), helix H coming out of the page (Slupsky and Sykes 1995).

1.4.4.b Troponin I: The key regulatory protein

Troponin I (TnI) is a 24 kDa protein that holds the troponin complex bound to the actin and inhibits the actomyosin ATPase. There are three different isoforms for TnI: cardiac TnI (cTnI), fast skeletal TnI (fsTnI), and slow skeletal TnI (ssTnI). Human cardiac TnI was found to contain eight exons, and this cTnI gene was mapped to segments of chromosome 19 (19q13.4). cTnI (the 210 amino acids protein) differs from other TnI isoforms by having an extra 32 amino acids as an N terminal extension, figure 1.13. The N terminal extension contains three regions: an acidic N terminal part that contains a single turn of a helix (residues 1-11), a polyproline helix (residues 12-18) in the middle, and a C' helix that contains the bisphosphorylation motif (residues 19-30) (Sadayappan et al., 2008). The rest of the TnI molecule can be divided into four

different regions (Solaro et al., 2008). The IT-arm region (which includes two alpha helices interact with TnC and TnT2), the inhibitory region, the molecular switch region, and the C terminal mobile domain. The inhibitory region in the cardiac TnI is flexible and not visible in the crystal structure (Takeda et al., 2003), while it is well ordered in the skeletal troponin crystal structure (Vinogradova et al., 2005).

MADGSSDAAR	EPRPAPAPIR	RRSSNYRAYA
TEPHAKKKSK	ISASRKLQLK	TLLLQIAKQE
LEREAEERRG	EKGRALSTRC	QPLELAGLGF
AELQDLCRQL	HARVDKVDEE	RYDIEAKVTK
NITEIADLTQ	KIFDLRGKFK	RPTLRRVVIS
ADAMMQALLG	ARAKESLDLR	AHLKQVKKED
TEKENREVGD	WRKNIDALSG	MEGRKKKFES

Figure 1.13 Human cardiac troponin I amino acid sequence. The N- Extension is labelled in red.

The crystal structure shows only the IT arm made of two TnI alpha helices (Takeda et al., 2003). The first TnI helix (H1) binds to the C terminal of TnC by multiple polar and Van de Waals interactions, and through its C terminal part to troponin T by hydrogen bonds and hydrophobic interactions. Together with the troponin T H2 helix, the TnI H2 helix forms a coiled-coil like structure. Functionally, the inhibitory region of TnI binds to actin filament in the absence of calcium; this binding prevents actin strong interactions with myosin by inducing a structural change in actin-tropomyosin (Solaro et al., 2008). A second actin binding site is present on TnI and is thought to facilitate the interactions between actin and inhibitory region (Solaro et al., 2008). The calcium binding to the regulatory lobe of TnC facilitates the molecular switch region (H3 (I)) binding to the hydrophobic surface of this lobe and that binding would induce the

inhibitory region detachment from actin (Takeda et al., 2003). H4 (I) found to have no direct interactions with the rest of Troponin complex.

It has been postulated that the TnI phosphorylation may be responsible for the increased rate of relaxation in adrenergically stimulated hearts (Hunkeler et al., 1991). cTnI can be phosphorylated by PKA (Ser-23, and Ser-24 in the N terminal extension), PKC (Ser-42, and Ser-44 in the N domain, and Thr-143 in the inhibitory region), and P²¹ activated kinase (Ser-150) (Solaro et al., 2008). In the absence of phosphorylation, the N terminal extension interacts weakly with the N lobe of TnC by multi weak hydrophobic and electrostatic interactions. Beta adrenergic stimulation would introduce a negatively charges in the N terminal extension of cTnI, through bisphosphorylation at Ser-23 and Ser-24. Bisphosphorylation at Ser-23 and Ser-24, results in more weakening of the interaction between the cardiac N terminal extension of TnI and the regulatory lobe of TnC. The acidic N terminal extension has a crucial role in regulating the myocardial function. Introducing a negatively charges in the C terminal helix of the N terminal extension would stabilize this helix. Ser-23/24 bisphosphorylation induces a bending in the cTnI and that leads to a molecular linkage between the acidic N terminal extension and the basic inhibitory unit through electrostatic interactions (Sadayappan et al., 2008). Therefore the inhibitory region-actin interaction would be weakened (figure 1.14). Ser-23/24 phosphorylation results in reducing the calcium binding affinity for TnC, and that would increase the cross bridge cycling rate. In addition it reduces the myofilament calcium sensitivity (Sadayappan et al., 2008). Bisphosphorylation of Ser-42/44 by PKC induces a reduction in the cross bridge kinetics (Solaro et al., 2008).

TnT is an asymmetric protein with globular C terminal domain. It consists of about 223 to 305 amino acids with a molecular weight in the 30-35 kDa range. The length of the N terminal region in TnT is variable from nearly absent to more than 70 amino acids in mammalian cardiac TnT (Wei and Jin 2010). Its sequence is also variable.

Protein binding studies found that TnT has two functional domains (Wei and Jin 2010). The C terminal domain or TnT2 interacts with the rest of troponin complex and with the middle region of tropomyosin in a calcium sensitive manner. The TnT1 domain includes both the N terminal domain and the middle region of TnT, figure 1.15. The middle region binds to the head–tail junction of tropomyosin while the N terminal region plays a major role in modulating the molecular functions of TnT (Wei and Jin 2010).

TnT is phosphorylated by PKC and this would inhibit the calcium dependent ATPases activity. TnT has two PKC phosphorylation sites: one on the N terminal serine, and the others on the C terminal of TnT (Thr₁₉₇, Ser₂₀₁, Thr₂₀₆, and Thr₂₈₇) (Wei and Jin 2010).

The major role of TnT is to hold all the Tn subunits together and to bind them to the thin filament.

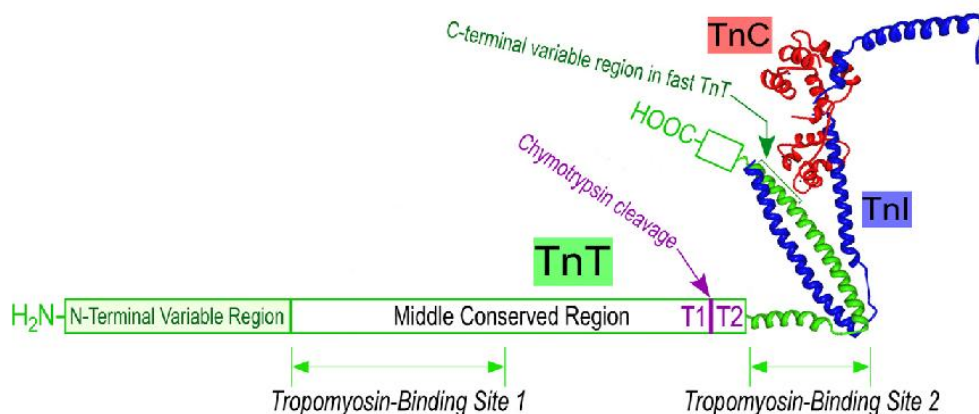


Figure 1.15 TnT structural and functional domains (Wei and Jin 2010).

1.4.4.d Structure of the whole troponin complex

The highest resolution crystal structure of cardiac troponin in the calcium-saturated form was determined by Takeda et al. (Takeda et al., 2003). In previous electron microscopy and low resolution x-ray studies, it has been shown that the troponin complex could be divided into two domains: the TnT1 fragment, and the rest of the troponin molecule (Flicker et al., 1982; White et al., 1987). In order to crystallize the troponin complex, Takeda et al. excluded the TnT1 fragment because it leads to aggregation.

The crystal structure of the cardiac troponin complex has been determined at 3.3 Å resolution (Takeda et al., 2003). This structure has shown that the troponin complex is composed of five subdomains: The regulatory head, the IT arm, C-TnT, TnT1, and TnI_{reg} (residues 137-210). These domains are connected by flexible linkers that make the troponin molecule flexible (figure 1.16).

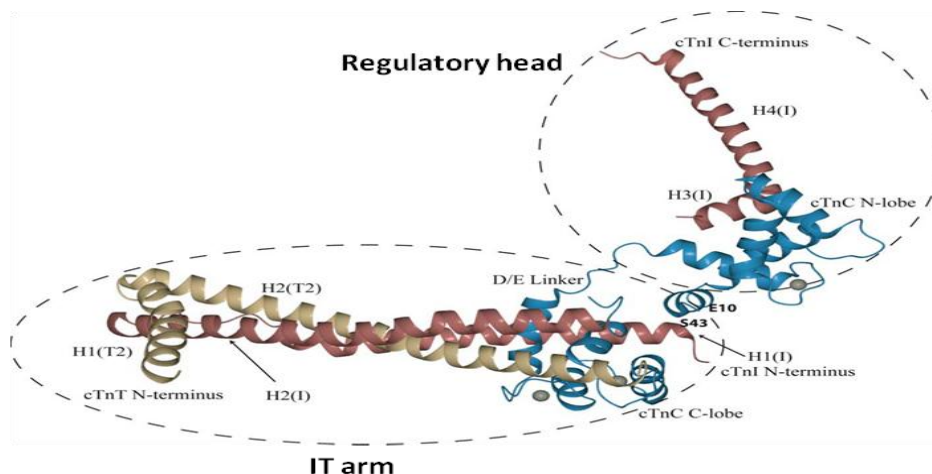


Figure 1.16 The x-ray structure of calcium saturated structure of the core domain of human cardiac troponin as determined by Takeda et al. TnC is coloured in cyan, TnI is coloured in red, and TnT is coloured in yellow. Calcium ions bound to the calcium-binding sites (II-IV) are represented by gray spheres. (Adapted from Li et al., 2004)

TnC contains four EF-hand alpha helix-loop-alpha helix motif divalent metal binding sites. There are nine helices labelled A-H in addition to the N helix.

TnI is composed of four alpha helices (H1 (residues 43-65), H2 (residues 90-135), H3 (residues 150-159), and H4 (residues 164-188)) and the inhibitory region (residues 137-148) (Takeda et al., 2003). There are two TnT helices: the H1 (T2) residues 204-220 and H2 (T2) residues 226-271. H2 (T2) helix together with H2 (I) helix forms a parallel alpha helical coiled coil. The regulatory head is composed of the N lobe of TnC (residues 3-84) and the third alpha helix of TnI or H3 (I) (residues 150-159). The H3 (I) which is also called the TnI switch segment is able to transmit the signal of calcium binding to site II (of the regulatory lobe of TnC) to the other thin filament components. The IT- arm is consisted of the C lobe of TnC, H1 (I), H2 (I), H1 (T2), and H2 (T2). In this arm the TnI (H1, H2) and TnT (H1, and H2) helices wind around each other and hold the C lobe of TnC. In addition, the C-terminus of the H2 (T2) in the coiled coil interacts with the C lobe of TnC. The D/E linker of TnC and the inhibitory region of TnI form together a flexible joint that allow the globular head and the IT arm to rotate relatively to their orientations which is be involved in the regulatory mechanism (Takeda et al., 2003).

Calcium binding to site II in the N lobe of TnC induces the movement of the switch region of TnI H3 (I) toward the open hydrophobic patch of this site through multiple van der Waals contacts, this movement drags the inhibitory unit and the C terminus of TnI and release it from the actin-tropomyosin. The C-terminal of TnI toggles between actin-tropomyosin and the N lobe of TnC in the regulatory head during the contraction relaxation cycle and this motion is controlled by the IT arm (figure 1.17). When cTnI is

released from the actin-tropomyosin, residues within the inhibitory unit switch from beta turn/coil to an extended quasi alpha helical conformation, while the switch segment remains the same alpha helix (H3 (I)) (Robinson et al., 2004).

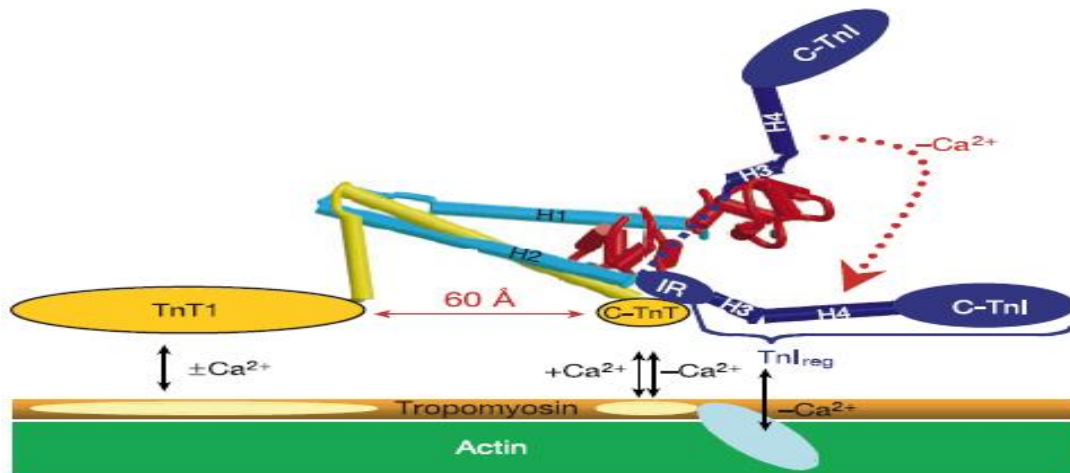


Figure 1.17 A schematic representation of the interaction between the troponin complex and the rest of the thin filament. The black arrows indicate the interaction between actin-tropomyosin and troponin in the presence and absence of calcium (Takeda et al., 2003).

1.5 Regulation of muscle contraction

Muscle contraction is initiated by calcium binding to the N-terminus of troponin C, followed by conformational changes on thin filament that exposes myosin-binding sites on actin which leads to thin filament activation and force generation (Gordon et al. 2000). The relationship between the concentration of Ca^{2+} and various contractile parameters (actomyosin ATPase, force, in vitro motility) has been extensively studied. This relationship is named: Ca^{2+} sensitivity. The Ca^{2+} sensitivity curve has a sigmoidal shape characteristic of cooperative behaviour and suggesting cooperative transition during activation. Two parameters can be derived from this curve: the Hill coefficient (n_H) and the half of the maximal value (pCa_{50}), figure 1.18. When pCa_{50} shifts to left

(increases), then the Ca^{2+} sensitivity is greater, while a shift to the right indicates a decrease in Ca^{2+} sensitivity.

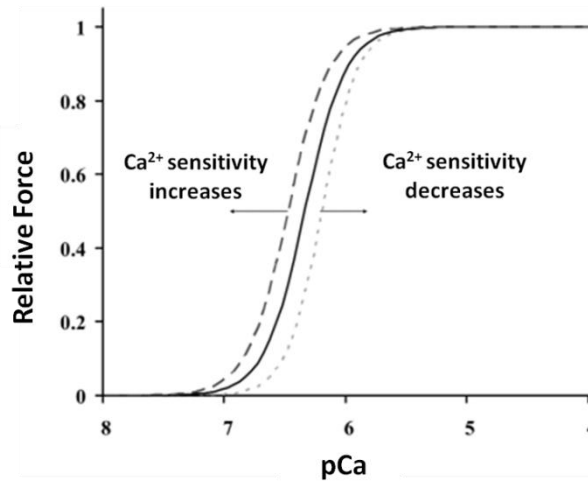


Figure 1.18 Normalized force versus pCa. The middle line represents a neutral condition. A shift to the right represents a decrease in Ca^{2+} sensitivity (lower value of pCa_{50}) and a shift to the left represents an increase in Ca^{2+} sensitivity (higher value of pCa_{50}) (MacIntosh 2003).

1.5.1 Mechanism of regulation

The contraction in striated muscles results from force generating interactions between myosin cross-bridges on the thick filament and actin on the thin filament to form the actomyosin complex, the process is powered by ATP (Geeves and Holmes 1999). When ATP binds to the ATPase site on the myosin head it would rapidly dissociate the actomyosin complex, then myosin will hydrolyse ATP and form a stable myosin head products complex ADP.Pi. Actin recombining with the latter complex will form the actomyosin again and release the ADP.Pi. In this process the actin works as a phosphate release factor while the myosin subfragment 1 is described as a substrate (Geeves and Holmes 1999), figure 1.19.

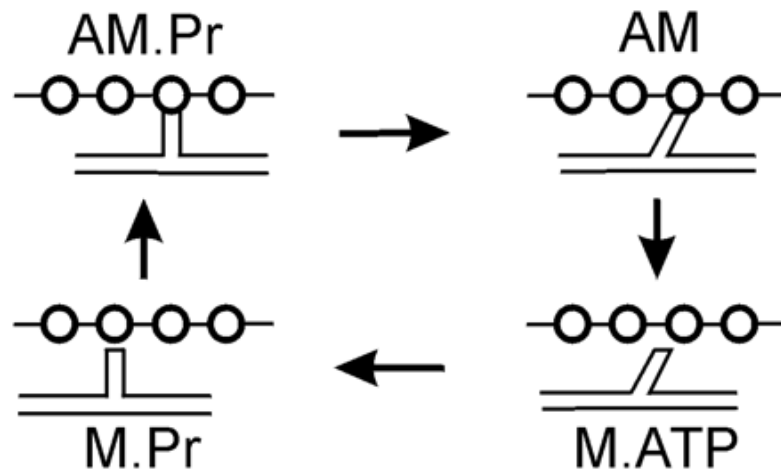


Figure 1.19 Contractile cycles for a single cross-bridge. The Lymn-Taylor alignment of biochemical states with the cross bridge cycle. Actin (A) is represented as open circles bridged by tropomyosin (line); M is the myosin head; Pr is the product (ADP.Pi) (Lymn and Taylor 1971).

1.5.1.1 Thin filament acts as a cooperative allosteric system

Calcium binding to the regulatory troponin complex induces structural changes in the troponin complex itself; these changes would relocate the tropomyosin away from the outer domain of actin, myosin binding sites on actin would be available for interaction with myosin heads (Kobayashi et al., 2008; Stehle et al., 2007). Early studies proposed that each tropomyosin-troponin unit (which includes seven binding sites on actin filament) can be in equilibrium between two states with different S1 binding affinities (Hill et al., 1980). In the OFF state, S1 binds weakly to the thin filament while in the ON state S1 can bind strongly.

However this model was not able to account for the effect of troponin- tropomyosin on the kinetics of S1 binding to actin although it was successfully able to explain the equilibrium binding (Hill et al., 1980).

An alternative three states model has been suggested by Geeves and co-workers (McKillop and Geeves 1993). In this model the thin filament can exist in three distinct states, figure 1.20:

- 1) In the blocked state, the thin filament is unable to bind myosin. This state is obtained in the absence of calcium and achieved by the positioning of the Tn-Tm complex on the outer domain of actin covering the S1 binding sites.
- 2) The closed state is obtained in the presence of calcium. In this state, the troponin-tropomyosin complex moves to the groove (between inner and outer domains of actin) exposing most but not all the S1 binding sites, and hence the S1 is able to bind weakly with actin.
- 3) Finally in the open state, the troponin-tropomyosin complex moves to the inner domain of actin exposing all the S1 binding sites, and the myosin head is able to bind strongly to actin.

Calcium controls the transition from the blocked to the closed state, while the myosin head controls the transition from the closed to the open state.

Transitions between the three different states are cooperative and the number of actin monomers that simultaneously switch from one state to another is defined as the cooperative unit (n) (Geeves and Lehrer 1994). The equilibrium constant between the blocked and the closed states is K_B while the equilibrium constant between the closed and the open states is K_T (Maytum et al., 1999).

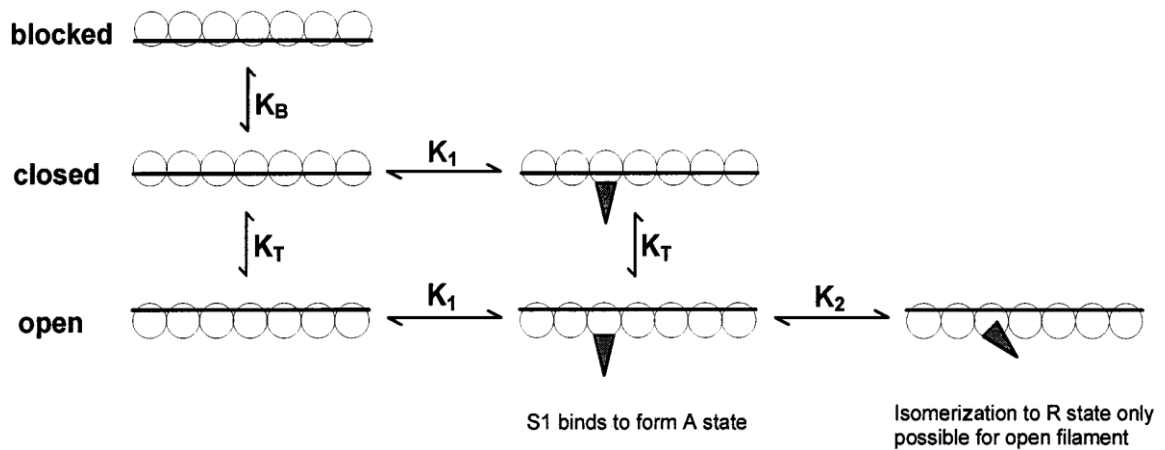


Figure 1.20 The three states model. Actin monomers (open circles) are bridged by tropomyosin (line). The calcium controls the equilibrium between blocked and closed states K_B while strong S1 binding controls the equilibrium between closed and open states K_T . S1 can bind both to closed and open states in equal affinity (A state) shown as (▼), but open state only allows the isomerisation to R state shown as (▲)(Maytum et al., 1999).

1.5.1.2 The role of tropomyosin in regulation

Current models of regulation of muscle contraction suggest that muscle thin filaments behave as a cooperative allosteric system switching between three biochemical states: blocked, closed and open and that the transitions between these states are cooperative (Geeves and Lehrer 1994). The details of this cooperative allosteric mechanism of regulation dictate the physiological behavior of cardiac muscle and its alteration is likely to compromise cardiac performance.

Striated muscle tropomyosin binds actin and troponin and through these interactions, plays a key role in the cooperative allosteric switching of thin filaments and in the modulation of actin-myosin interactions (Wolska and Wieczorek 2003). Biochemical and structural investigations have established that tropomyosin position on the surface of actin is the key difference between the three different states (figure 1.21).

In the blocked state, tropomyosin is positioned on the outer domain of actin blocking the myosin binding sites on actin. In the closed state tropomyosin moves away from the myosin weak binding sites but still covers actin regions involved in the isomerisations of myosin from the weak to the strong binding force generating state. Only in the open state, tropomyosin occupies a position which does not interfere with myosin interaction with actin. These various tropomyosin positions on the actin surface are coordinated by Ca^{2+} modulated interactions between the various troponin subunits and tropomyosin and actin. It is important to note the critical role played by troponin I via its numerous interactions with TnC, actin and Tm in this coordination (Farah and Reinach 1995).

Tropomyosin also plays a pivotal role in the second important feature displayed by Ca^{2+} regulation of thin filament: cooperativity. Cooperativity is the ability of Ca^{2+} binding/dissociation within a single site to impart changes to many actin monomers. Cooperativity is an important determinant of force production and of relaxation during the contractile cycle. Thin filament cooperativity is conferred by tropomyosin ability to cover 7 actin monomers, tropomyosin end to end interaction and the rigidity of the tropomyosin strand. Therefore the structural cooperative unit can be defined as the seven actins bridged by a single tropomyosin, while the functional cooperative unit is the number of actin subunits that can be simultaneously switched between the three states (dependent on end to end interaction and tropomyosin flexibility) (McKillop and Geeves 1993; Geeves and Lehrer 1994). The functional cooperative unit is therefore affected by tropomyosin isoform and by troponin T interaction at the tropomyosin head to tail junction. Cardiac muscle tropomyosins (alpha homodimers) have

increased cooperativity than skeletal muscle tropomyosin (alpha-beta heterodimers) and overexpression of beta-tropomyosin in the heart reduces cooperativity (Wolska et al., 1999). Troponin T binding to tropomyosin increases cooperativity. The degree of cooperativity is quantified by the size of the cooperative unit (n).

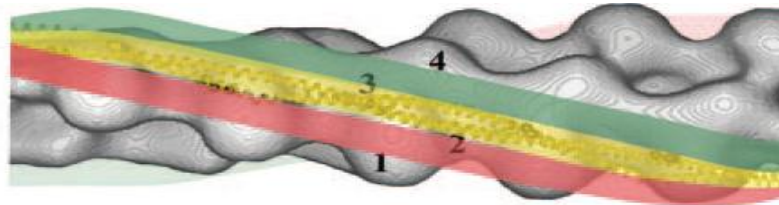


Figure 1.21 Model for the interaction between actin and tropomyosin. The azimuthal positions of tropomyosin, in the blocked (red), Closed (yellow) and open (green) states, on F-actin (gray) according to electron microscopic studies (Brown et al., 2005).

1.5.1.3 The role of troponin in regulation

The calcium binding to the N terminal domain of skTnC leads to a conformational transition from closed to an open state, this transition means a large change in the interhelical angles involving a significant reorientation of helices B and C relative to the helices N, A, and D. Upon Ca^{2+} binding to skeletal TnC, experimental results suggested that the inhibitory region undergoes conformational changes from short helix structure when bound to actin to more elongated structure; this elongated structure interacts with the central helical region of TnC to stabilize the active form of the troponin complex (Vinogradova et al., 2005). The TnT residues 66-99 have been showed to interact with the head to tail binding region of tropomyosin in skeletal Tn.Tm complex (Murakami et al., 2008). In the presence of calcium, TnT has a major role to shift the azimuthal position of tropomyosin toward the inner domain of actin and that would allowed myosin heads to bind to actin (Murakami et al., 2007).

The ability of troponin C to regulate the muscle contraction appears to have slightly different mechanism in skeletal versus cardiac muscles. In skeletal muscle, binding of two calcium ions to the Ca^{2+} -specific regulatory sites of TnC switches the N-lobe from a closed to an open conformation; the hydrophobic pocket of TnC is exposed, releasing the TnI from actin by enabling the interaction between TnI and TnC (Gomes et al., 2002).

In the absence of calcium, the hydrophobic surface of the N terminal of cTnC is buried in the structure and calcium binding alone is not able to switch N terminal of cTnC to the open state. In cTnC, calcium and cTnI₁₄₇₋₁₆₃ are needed to stabilize the open state. In addition the binding affinity of cTnI₁₄₇₋₁₆₃ to cTnC.Ca²⁺ is reduced 13 folds (Li et al., 1999). NMR studies have revealed that the binding of calcium to site II of the N regulatory lobe of cTnC is able to open this site partially but not fully. For further opening, the C-terminal of TnI (switch segment) is needed to bind to the N-terminal of TnC. Then TnC would pull the inhibitory region and the second actin binding site from the actin-tropomyosin surface; therefore it releases the inhibitory action of TnI on the thin filament, and troponin-tropomyosin will move to the grooves between inner and outer domains of actin (Lehman et al., 2000). After all these conformations, the myosin heads could be able to interact with actin filament weakly. This S1 binding moves the troponin-tropomyosin further to the inner domain of actin and that leads to the strong binding of S1 or rigor state R (Kobayashi et al., 2008; Solaro et al., 2008; Gomes et al., 2002; Stehle et al., 2007).

It has been found that the N terminal domain of TnC regulates the muscle contraction and relaxation through the binding and release of Ca^{2+} , while the C terminal domain

anchors the TnC into the troponin complex. Ca^{2+} binding properties of TnC play a major role in determining the level of thin filament activation and force generation in muscle. The thin filament system equilibrates very fast with Ca^{2+} (faster than the mechanical events of contraction and relaxation), therefore it should have fast Ca^{2+} association and dissociation rates (Gordon et al., 2000). Kinetic studies of the association of Ca^{2+} to and its dissociation from TnC suggest that the low affinity sites of skeletal and cardiac TnC can exchange Ca^{2+} rapidly enough to serve as the trigger for contraction (Pan and Solaro 1987). The calcium affinities of the two classes of binding sites in cardiac TnC are essentially the same as the corresponding ones for skeletal TnC (Dong et al., 1996). Calcium binding to TnC leads to a series of conformational arrangements in troponin and tropomyosin which reveals strong myosin binding sites on actin, allowing cross bridges to cycle and muscle contraction. Relaxation occurs as intracellular Ca^{2+} declines, calcium dissociates from TnC, Tm blocks strong myosin binding sites on actin and cross bridges detach (Gordon et al., 2000). A decline in intracellular Ca^{2+} concentration would lead to the dissociation of the switch region of TnI from the hydrophobic patch on the N terminal domain of TnC resulting in muscle relaxation. TnC and actin compete for the binding of TnI; this competition might be the reason behind the decrease in the Ca^{2+} sensitivity and acceleration of the Ca^{2+} dissociation rate occurring upon troponin reconstitution into thin filament (Davis and Tikunova 2008). Myosin binding to actin displaces Tm on actin further than what Ca^{2+} can do alone and increases the affinity of Tm for actin. The rate of myosin head detachment is the primary determinant of muscle relaxation. The rate of muscle contraction is Ca^{2+} dependent (Gordon et al., 2000).

1.6 Troponin I Dysfunction

Kimura et al were the first to report HCM causing mutations in the cardiac troponin I gene (Kimura et al., 1997). While Murphy et al were the first to report the only DCM TnI mutation (A2V) (Murphy et al., 2004). In Kimura's study, they reported six TnI mutations associated with HCM (R145G, R145Q, R162W, G203S, K206Q, and Δ K183). Since then, 29 HCM mutations have been reported, table 1.2. Mutations are distributed throughout the cardiac troponin I sequence, figure 1.22.

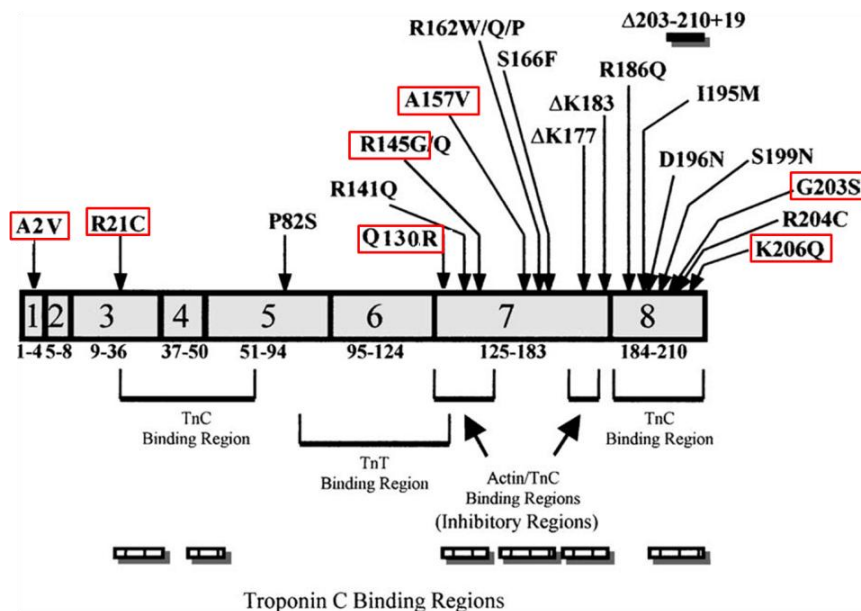


Figure 1.22 Exon organisation and TnI HCM localisation in human cardiac troponin I. TnC, TnT, and actin binding regions are shown. The TnC binding regions are at the bottom of the figure (adapted from Gomes and Potter 2004). Mutants have been studied in this project are labelled in red boxes.

In our study we have chosen six HCM mutations (R21C, Q130R, R145G, A157V, G203S, and K206Q) and the only DCM mutation (A2V) to investigate the effect of these mutations on the dynamics of thin filament switching by using transient kinetics, figure 1.22. However previous studies have focused on steady state parameters, such as

maximal activation and inhibition of ATPase and force and Ca^{2+} sensitivity. Although transient kinetics is more complex and demanding, but it is a good method for unravelling the molecular mechanism of proteins action. . We aimed to use transient kinetics to assess the impact of cTnI mutations on single step reactions that take place during activation or de-activation of myofilament.

These mutations are located within the four functional regions (Gomes and Potter 2004):

- i) N-terminal TnC binding region(residues 1-55)
- ii) TnT binding region (residues 90-135)
- iii) The inhibitory region (residues 128-148)
- iv) C-terminal TnC binding region (residues 191-210)

Troponin I contains high arginine content (11.9%) compared to the average occurrence of this amino acid in all proteins. In addition mutations in Arginine account for about 40% of the missense troponin I HCM mutations.

Table 1.2 Troponin I mutations associated with HCM and DCM.

Functional region of cardiac TnI	Mutation
N-terminal TnC binding region	A2V ¹ , R21C ^{2,3}
TnT binding region	P82S ⁴ , Q130R ⁵
The inhibitory region (residues 128-148)	R141Q ^{6,7,8} , L144P ⁹ , R145G ^{10,11,12,13,14,15,16,17,18} , R145Q ^{8,10,14}
C-terminal TnC binding region	A157V ^{6,8,19} , R162W ^{10,11,12} , R162Q ^{7,8,20,21,22} , R162P ^{6,20,22} , S166F ^{1,7,23} , ΔK177 ⁶ , K183E ⁸ , ΔK183 ^{10,14,24,25,26} , R186Q ^{6,8} , I195M ² , D196N ^{4,6,8} , L198V ⁹ , L198P ²⁰ , S199G ⁸ , S199N ^{8,19} , E202G ⁸ , G203R ⁸ , G203S ^{10,14,16,25} , G203fs ^{6,27,28} , R204C ² , R204H ^{20,22} , K206Q ^{10,14,25}

1.(Murphy et al., 2004) 2.(Barr et al., 2001) 3.(Arad et al., 2002) 4.(Niimura et al., 2002) 5.(Morita 2003) 6.(Richard et al., 2003) 7.(Van Driest et al., 2003) 8.(Mogensen et al., 2004) 9.(Merk et al., 2005) 10.(Kimura et al., 1997) 11.(Takahashi-Yanaga et al., 2000) 12.(Elliot et al., 2000) 13.(Deng et al., 2001) 14.(Takahashi-Yanaga et al., 2001) 15.(Lang et al., 2002) 16.(Burton et al., 2002) 17.(Lindhout et al., 2002) 18.(Lindhout et al., 2005) 19.(Brito and Madeira 2005) 20.(Doolan et al., 2005) 21.(Cheng 2005) 22.(Ingles et al., 2005) 23.(Van Driest et al., 2004) 24.(Kokado et al., 2000) 25.(Kohler et al., 2003) 26.(Konno et al., 2005) 27.(Morner et al., 2000) 28.(Morner et al., 2003).

1.6.1 Functional Studies

The N-terminal TnI R21C mutation caused an increase in the calcium sensitivity but did not affect either the maximal ATPase activity or the ability of TnI to inhibit ATPase activity, also it showed more susceptibility for proteolysis by calpain II compared to the wild type (Gomes et al., 2005). Replacing wild type by R21C in porcine papillary preparation showed enhanced myofilament calcium sensitivity under basal conditions.

In early study, TnIR145G showed reduced intrinsic inhibitory activity of cardiac troponin I without changing the affinity for actin (Takahashi-Yanaga et al., 2001). While R145G and R145Q are the two TnI HCM mutations in the main inhibitory region of TnI (residues 137-148), R145G is the most investigated TnI HCM mutation in in vitro studies. Both R145G and R145Q showed decreased inhibition of the ATPase activity from different studies (Elliot et al., 2000; Takahashi-Yanaga et al., 2000; Takahashi-Yanaga et al., 2001; Lang et al., 2002). The R145G mutation showed an increase in the calcium sensitivity of the myofibrillar ATPase activity (Takahashi-Yanaga et al., 2000).

R145G mutation also exhibited an increase in calcium sensitivity of force and impaired inhibitory effectiveness of troponin I (Lang et al., 2002). Exchange of cardiac troponin I in skinned fiber bundles with mouse TnIR146G mutation (R145G in human) induced enhanced calcium sensitivity and an elevated resting tension (Kobayashi et al., 2004). Deng et al also showed that R145G enhanced the calcium sensitivity of actoS1-ATPase activity independent of the phosphorylation state of cTnI (Deng et al., 2001). TnI containing the R145G mutation showed less force inhibition in skinned trabeculae compared to the wild type (Burton et al., 2002). NMR studies showed that the affinity of inhibitory region contained the R145G mutation was reduced four fold for the C-

terminal of TnC. 2Ca^{2+} (Lindhout et al., 2002). It has been found that R145G and R162W resulted in reduced inhibition of ATPase activity and increased the calcium sensitivity of actin-Tm-activated myosin ATPase regulation (Elliot et al., 2000).

The R162W and ΔK183 mutations showed reduced in the apparent affinity of TnI for actin without changing the intrinsic inhibitory activity (Takahashi-Yanaga et al., 2001). In the same study they found that the mutations R145G, R145Q, R162W, K206Q, and ΔK183 increased the calcium sensitivity of myofibrillar ATPase activity and force generation in skinned muscle fibers (Takahashi-Yanaga et al., 2001).

The HCM R145G, G203S, and K206Q mutations found not to affect their calpain-1-mediated degradation or the phosphorylation-induced protection against proteolysis (Barta et al., 2003). While the skinned trabeculae reconstituted with G203S mutation, troponin showed less calcium activated force and low calcium sensitivity compared to the wild type. Thin filament contained the G203S mutation showed similar results as the wild type in in vitro motility and ATPase assays (Burton et al., 2002).

ΔK183 is clinically the most studied mutation in cTnI and has been shown to be involved in a malignant prognosis (Ward et al., 2004). It has been found that G203S, K206Q, and ΔK183 HCM mutations showed enhanced filament sliding, and that was in agreement with the hypothesis that hypertrophy could result from enhanced contractility as evidenced by increased filament sliding speed at saturating calcium (Köhler et al., 2003). K206Q mutation showed an increased in the calcium sensitivity of the myofibrillar ATPase activity and force generation in contrast to the G203S mutation that did not show a significant increase (Deng et al., 2003).

In most mutations the calcium sensitivity of force development was increased, and in some cases the filament sliding velocity was increased too. The increased in calcium sensitivity would result in a hypercontractile muscle and as a result increase the amount of ATP utilized.

Most of the HCM causing mutations are relatively subtle mutations, typically missense mutations. The mechanism by which mutants in the sarcomeric proteins can cause HCM and DCM is unknown. It has been proposed that mutant sarcomeric proteins exert a dominant negative effect on myocyte function and structure (Oberst et al., 1998), and this is in agreement with previous group findings that support the proposed poison-peptide hypothesis in the pathogenesis of HCM (Watkins et al., 1996). The development of cardiac hypertrophy could be dependent on the dose of mutant sarcomeric protein (Oberst et al., 1998). A sarcomeric protein mutant that might be able to cause a hypertrophy can act as a poison peptide; this altered protein is incorporated in the sarcomere and would lead to structural changes that can develop the compensatory hypertrophy (Daloz et al., 2001). These mutants' peptides can be stably expressed and are able to incorporate into the sarcomere, but they result in abnormalities either in further assembly or in the function of the multimeric array of contractile proteins (Redwood et al., 1999). Studies of 100% mutant protein might not be relevant to the heterozygous disease state; in addition the relative expression and incorporation efficiency of mutant protein in the heart would be varied between different mutations (Redwood et al., 1999). The amount of TnI HCM mutant in human is unlikely to be more than 50% of the total because of the severe effect of these mutations on the contractile system. Low levels of transgenic protein in the presence

of the phenotypic feature of HCM suggest that the mutant protein acts as a dominant negative, small numbers of mutant polypeptides exert a drag on sarcomere function (Vikstrom et al., 1996). Early study using a wild type/TnI R145G mutant mixtures showed that the wild type phenotype was dominant in that calcium sensitivity and inhibition conferred by a 50:50 mixture was more similar to the wild type (Elliott et al., 2000). In another study, a mixture of wild type and R145G mutant gave a markedly biphasic response (wild type and the mutant effects) when the total troponin concentration was partially saturated, the reversal inhibition of R145G became apparent only when more than 50% of the mixture was mutant protein (Burton et al., 2002). Sarcomeric gene analysis identified two novel troponin I mutations (Pro82Ser and Asp196Asn) in HCM patients with elderly-onset disease, both of these mutations are predicted to have dominant-negative activity that might impair the inhibitory and troponin T binding for Pro82ser mutation, and troponin C binding for Asp196Asn mutation (Niimura et al., 2002). One of the consequences of HCM is the interference with sarcomere assembly that leads to the myofibrillar disarray characteristic of affected human hearts (Watkins et al., 1996).

1.6.2 Transgenic animal models for TnI mutations

Different troponin I mutations have been expressed successfully in animals developing phenotypes similar to the clinical disease expression seen in both HCM and DCM patients. The functional effect of TnI R145G mutation was investigated by generating transgenic mice that express TnI R146G (R145G in the human sequence) (James et al., 2000). In this model they observed consistent results with skinned fiber studies where they found a decrease in the maximal force in the R146G transgenic mice. In addition

they proposed that this decrease in maximal force could be accounted for the loss of myocytes they observed in these animals. TnIR146G mice showed cardiomyocyte disarray and interstitial fibrosis and depending on the mutant expression level, suffered premature death. The lines expressing 60% of R146G (the highest amount) had severe myocardial fibrosis and disarray and died young, while the lines expressing lower amount of R146G (40% of total TnI) showed abnormalities only after the physiological stress of pregnancy. They also found that the expression of cTnI R146G in the mouse heart resulted in enhanced systolic function and compromised diastolic function (impaired relaxation).

In Westfall et al, they showed that myofilament pH sensitivity and enhanced calcium sensitivity are crucial for the cardiac dysfunction development by the cTnIR146G HCM mutation. They demonstrated that at certain pH conditions, the enhancement of calcium sensitivity of contraction is lost in the cTnIR146G compared with the ssTnI. In this work, they suggested a diminished ability of cTnIR146G to replace the endogenous cTnI within the sarcomere and the reduced presence of cTnIR146G within the sarcomere is because the reduced ability of this mutation to incorporate in myofilaments relative to the wild type TnI (Westfall et al., 2002).

Another group studied the cTnIR146G mutation; the inhibitory domain mutation was modelled by using the transgenic expression in the rabbit ventricle. The transgenic rabbits in this study that showed 40% of replacement level did not survive past the perinatal period. The capacity of myocyte to express and incorporate TnIR146G into the sarcomere was impaired compared to the wild type and that can be explained by the mutant protein instability or reduced ability of the mutant to incorporate into the

myofilaments. The 50% replacement was found not to be compatible with life. In this model the myocyte data showed no enhancement of calcium responsiveness contrary to the expected steady state skinned fiber experiments (Sanbe et al., 2005).

The transgenic murine hearts carrying the $\Delta K183$ showed no effect on the maximum rate of force development, but impaired the relaxation kinetics and increase passive force. Transgenic myofibrils showed higher forces at low and high calcium concentrations and it also increased the calcium sensitivity of contraction (Iorga et al., 2008).

Mice with the cTnIG203S gene mutation developed all phenotypic features of human FHC (Tsoutsman et al., 2006). Mice from all TnIG203S transgenic lines demonstrated normal life and developed FHC at different rates correlated with the amount of mutant protein expression. Histological analysis demonstrated interstitial fibrosis and myofibril disarray in hearts extracted from cTnIG203S mice, and these analyses indicated some increase in the myocyte size consistent with cellular hypertrophy. They suggested that mutation in cTnI at one location can alter the structure and folding of the entire protein and that would lead to direct consequences on sarcomere function and calcium cycle. In this study, they found that cTnIG203S lead to reduced protein-protein interactions with TnC and TnT although this mutation is located in a region has not been reported before as a binding domain for either TnC or TnT. The calcium cycle was abnormal in adult cardiomyocyte extracted from cTnIG203S mice, this study findings support the concept that changes in calcium cycling and homeostasis could be a crucial early event for pathogenesis

Another group created a transgenic mouse model expressing cTnIG203S and developed all the characteristic phenotype features of FHC. The FHC mice demonstrated an abnormal response to exercise. Non transgenic and WT swum mice developed a normal physiological response to exercise (including improved cardiac contractility, and reduced heart rate) while cTnIG203S mice lacked this adaptive response (Nguyen et al., 2007).

The first study that presented the differential proteomic analysis of cardiomyopathic tissue from a genetically engineered mouse with cTnIG203S showed the importance of tissue proteomic profiling for mapping proteins, which can be critical in cardiac dysfunction and progression to heart failure in HCM (Lam et al., 2010). They suggested that the major protein alterations relevant to HCM pathogenesis can be grouped into three main categories; proteins involved in energy production, calcium handling and muscle structure and contraction. The various molecular functions and biological processes of these proteins suggest that the manifestation of HCM is likely the consequence of the combined functional impairment resulting from these multiple alterations rather than a single key protein.

1.7 Research Programme

Troponin I plays a fundamental role in the regulation of cardiac muscle contraction. Its multiple interactions are crucial for the Ca^{2+} dependent activation and de-activation of thin filaments. In the absence of Ca^{2+} , TnI-actin interaction is critical for muscle relaxation. The rapid rise in Ca^{2+} concentration in the myoplasm promotes TnI-TnC interaction and weakens TnI-actin interactions.

Several acquired cardiac diseases including ischemia, stunning and heart failure have been linked to alterations in cTnI. Moreover, recent genetic studies have shown that genetic cardiomyopathies (hypertrophic, dilated, and restrictive) are caused by mutations in the cTnI gene. Consequently, unravelling how alterations in cTnI structure, function, and role in activation and relaxation of cardiac thin filaments are critical for understanding of the onset and progression of the diseases. Since the discovery of the first HCM linked mutations in cTnI, a huge effort has been devoted to the study of the biochemical and functional defect caused by these mutations. All of these studies used steady state methods such as in vitro motility, Ca^{2+} sensitivity, actomyosin ATPase, and fibre mechanics. These investigations have uncovered a number of changes in steady state parameters such as maximal activation and inhibition of ATPase, the Hill coefficient and the pCa_{50} of the Ca^{2+} dependence of filament sliding velocity, and ATPase and tension. However, steady state parameters are composite parameters and linking the observed changes to molecular mechanics underlying the development and progression of the disease has been challenging. In this thesis we aimed to use transient kinetics to assess the impact of cTnI mutations on single step reactions that take place during activation or de-activation of myofilament. We studied six HCM mutations and the only DCM mutation (A2V) that were previously characterised by steady state methods. These mutations are located in the four TnI functional regions:

- i) N-terminal TnC binding region (A2V and R21C)
- ii) TnT binding region (Q130R)
- iii) The inhibitory region (R145G)

iv) C-terminal TnC binding region (A157V, G203S, and K206Q)

We investigated the effect of TnI mutations on the size of cooperativity unit (n), on the proportion of thin filaments in the blocked state (K_B), on the equilibrium constant between open and closed states (K_T), on the Ca^{2+} affinity of troponin and thin filaments, and on the rate of Ca^{2+} dissociation.

The overall goal of this project is to understand, at the molecular level, how mutations in TnI that cause cardiomyopathies alter the regulation of the cardiac contractile cycle.

CHAPTER 2

Materials and Methods

2.1 Preparation of recombinant Proteins

2.1.1 Preparation, and expression of recombinant human cardiac troponin

Wild-type TnI, TnT and TnC cDNAs were obtained as a gift from Dr. N.Brand (Imperial college, UK) Dr. C. Redwood (University of Oxford, UK), and Prof. K. Jacquet (Clinic of the Ruhr-University of Bochum, Germany) respectively. The human cardiac troponin I mutants (Q130R, R145G, A157V, G203S, A2V, R21C, and K206Q) and human cardiac troponin C mutants (C35S, and C84S) were formed by overlapping PCR using HcTnI cDNA and HcTnC cDNA respectively. The products were cloned into bacterial expression vector (PLEICS-05), figure 2.1. Overlap extension PCR was carried out by Dr. Xiaowen Yang at the University of Leicester. The TnI and TnC constructs were over expressed in *Escherichia coli* strain BL21 (DE3) plys (Studier et al., 1990). The HcTnI and HcTnC clones were verified by sequencing prior to expression and reconstitution (PNAFL, University of Leicester). Human cardiac troponin T (Redwood et al., 2000), and troponin C (Al-Hillawi et al., 1994) were expressed as described previously.

The expressions of the new recombinant proteins have been checked, cells were grown in LB broth medium at 37 °C, the induction was achieved by the addition of IPTG (isopropyl-1-thio-β-D-galactopyranoside) to the medium of growing cells when the absorption of the culture at 600 nm reached 0.6-0.8 (exponential growth phase). The protein expression was monitored by SDS-PAGE.

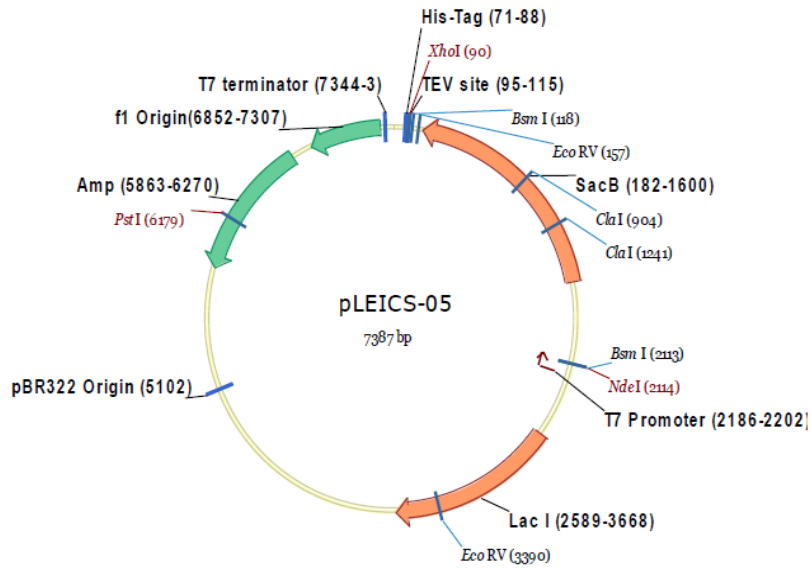


Figure 2.1 Expression vector of hcTnl and hcTnC (pLEICS-05)

2.1.2 Plasmid Mini Preps

Troponin subunits and Tnl and TnC mutants were purified from JM109 competent cells using a Wizard® Plus Miniprep kit (Promega). Cells from 5-10 ml overnight culture were pelleted in a micro-centrifuge by spinning down for 5 minutes at 13,000 rpm at room temperature. The supernatant was discarded and the pellet was then re-suspended in the various buffers as described in the protocol provided in the kit. The DNA was stored at -80 °C.

2.1.3 Transformation

Competent cells BL21(DE3)pLysS were used to transform all troponin cDNAs in this project. About 1 µl of the desired expression construct DNA was transformed into 10-20 µl of competent cells in sterile eppendorf tube, cells were then gently mixed by flicking the tube gently few times, the tube then incubated on ice for 30 minutes. The

cells were heat shocked at 42 °C for 1 minute without shaking in a water bath. The tube was placed back in ice immediately for 2 minutes. 200-400 µl of autoclaved LB media were used to dilute the transformed cells, diluted cells then were incubated at 37 °C with shaking at 220 rpm for 60-90 minutes. 100 µl of cell culture were spread on LB agar plate with appropriate antibiotic and incubated at 37 °C overnight. The rest of cell culture was spun down at 13,000 rpm for 10-15 seconds at room temperature. Supernatant discarded and the pellet re-suspended in fresh 100 µl of autoclaved LB media. The resuspended culture was then spread on another LB agar plate and incubated at 37 °C overnight.

2.1.4 Glycerol Stocks

A single colony was picked up from a transformation plate and placed into 5 ml of autoclaved LB broth containing the appropriate antibiotics. The cells were incubated to grow at 37 °C for 5-6 hours at 200 rpm. The grown culture was diluted in autoclaved glycerol (75% culture + 25% glycerol). The stocks were transferred into 1 ml aliquots and stored at -80 °C.

2.1.5 Reconstitution of troponin complexes

Since all troponin subunits (TnI, TnC, and TnT) were expressed in E.coli and the contaminant proteins were the same, we decided to shorten the troponin reconstitution method by reconstituting the complex before a single purification. Recombinant human cardiac troponin was reconstituted by mixing 2:1.5:1 volume ratio of recombinant troponins T, I, and C culture pellets that were broken using French press after they were dissolved in lysis buffer (25 mM Tris-HCl, pH 7.5, 1 mM EDTA, 20% sucrose, 200 mM NaCl, 6 M urea, 0.1% Triton X 100). After 4 hours dialysis

against the following reconstitution buffers contained different KCl and urea concentrations (10 mM Imidazole, pH 7, 1 mM DTT, 0.01% Sodium azide, 100 μ M CaCl₂) at 4 °C, the concentrations of urea and KCl were decreased using a stepwise dialysis protocol (2 M Urea, 1 M KCl for the first buffer, 0.75 M KCl for the second buffer, and 0.5 M KCl for the last one). Aggregated protein was removed by centrifugation using 14,000 rpm for 10 minutes at 4 °C. The reconstituted troponin were further purified and concentrated using ammonium sulphate (0-30% and 30-50%), the 50% pellet was resuspended in the minimum volume of gel filtration column buffer (10 mM Imidazole, pH 7, 1 mM DTT, 0.01% Sodium azide, 100 μ M CaCl₂, and 0.2 M KCl) and dialyzed against the same buffer overnight. Gel filtration column (Sephacryl S-200 or S-300) was used for further purification and to show that this reconstitution method using either wild type or TnI mutants resulted in a single species (the 1:1:1 complex), and this was confirmed by SDS-PAGE. All the previous protocols (Szczesna et al., 2000; Burton et al., 2002) were based on purifying each of troponin subunits TnT, TnI, and TnC separately before the reconstitution. These protocols take at least three weeks to get the final troponin complex in a modest yield (Szczesna et al., 2000; Burton et al., 2002).

2.1.6 IAANScys35ser-cTnC and IAANScys84ser-cTnC preparation and purification-

Recombinant human cTnC (C35S and C84S) mutants in PLEICS-05 vector were over expressed in Escherichia coli strain BL21 (DE3) plys. cTnC cell pellets were broken using French press after they were resuspended in lysis buffer (25 mM Tris-HCl, pH 7.5, 1 mM EDTA, 20% sucrose, 200 mM NaCl, 6 M urea, 0.1% TritonX100). Cell lysis supernatant was diluted with equal volume of dialysis buffer (50 mM Tris-HCl, pH 7.5,

1 mM EDTA, 1 mM β -mercaptoethanol, and 6 M urea) and dialysed against same buffer overnight. The TnC crude was spun down at 10,000 rpm for 10 minutes at 4 °C, and then it was loaded onto a Q-sepharose column that had been equilibrated by the dialysis buffer. TnC was eluted by using 0-2M NaCl linear gradient. Fractions of 10 ml have been collected and monitored at 280 nm. The peak fractions were run on a 15% SDS gel to check for purity, figure 2.2.

A 5-fold molar excess of IAANS was added to cTnC (C35S or C84S) at 2 mg/ml (in 6 M urea, 150 mM KCl, 50 mM Tris HCl (pH 7.5), and 0.2 mM DTT) and incubated in the dark for 5 hours at room temperature. The labelling reaction was stopped by adding 10 mM L-cystine, the mixture was spun down and the supernatant was dialysed extensively to remove the free label. The amount of label incorporated was determined by the absorbance at 325 nm using a molar extinction coefficient of 24900 M⁻¹ adjusting for the absorbance of unlabelled cTnC (Robinson et al., 2007). Labelled cTnC was dialysed against first reconstitution buffer to start the reconstitution process as mentioned in the previous section.

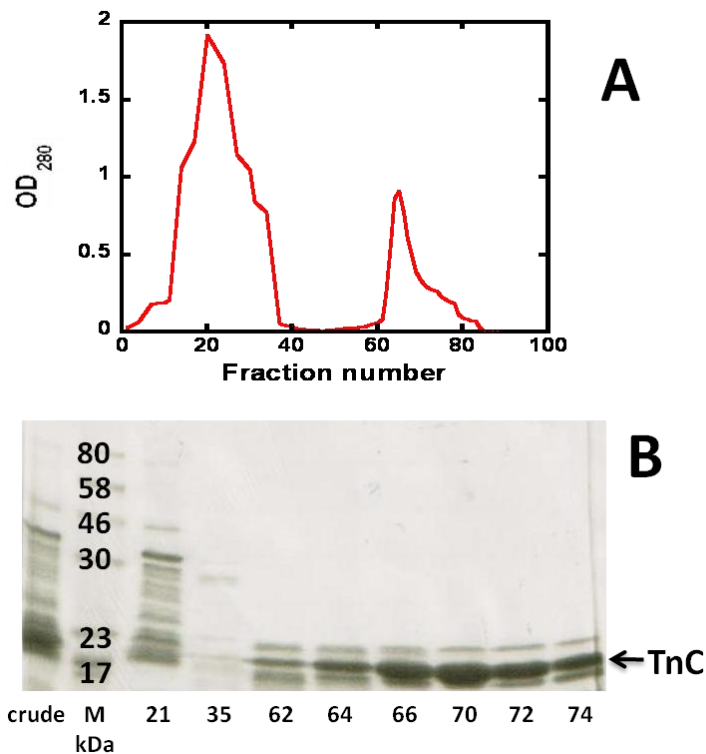


Figure 2.2 The purification of cTnC^{C84S} by using Q-sepharose column. A is a trace from the chart recorder of the absorbance at 280 nm. B is the SDS-PAGE analysis of the fractions by using 15% gel. Numbers along the bottom correspond to the fraction numbers that related to A.

2.2 Fluorescent phosphate binding protein (MDCC-PBP) preparation and purification -

Bacterial phosphate binding protein (PBP) containing the mutation (Ala-197-Cys) was isolated as described before (Brune et al., 1994). The PBP was expressed in *Escherichia coli* strain under the control of rhamnose promoter (Haldimann et al., 1998). A starter culture has been started by adding one vial of PBP glycerol stock culture into 10 ml of LB broth media and 10 µl of tetracycline stock (0.5 g tetracycline in 40 ml of 40% ethanol) in a 50 ml sterile eppendorf. The starter culture was rapidly shaken at 200 rpm for 6-10 hours at 37 °C. The entire content of the eppendorf was transferred into

500 ml flask contained 90 ml of LB media and 90 μ l tetracycline stock. The culture was grown for 16 hours at 37 °C by shaking at 220 rpm. 10 ml of this culture and 0.6 ml of tetracycline stock were diluted into 500 ml of the minimal media (100 mM HEPES, 20 mM KCl, 15 mM (NH₄)₂SO₄, 1 mM MgCl₂, 10 μ M FeSO₄, 1 μ g/ml thiamine, 0.25% glycerol, and 2 mM KH₂PO₄). The minimal culture was incubated at 37 °C by shaking at 200 rpm. The OD at 600 nm for the culture was followed. When the OD at 600 nm reached 0.1, 5 ml of 200 mM rhamnose was added. The culture was then incubated at the same conditions for 16 hours. The culture was spun down at 4,000 rpm for 20 minutes at room temperature. The pellets were resuspended by using 650 ml of (10 mM Tris-HCl, and 30 mM NaCl). Resuspended cells were spun down at 4,000 rpm for 20 minutes at room temperature. The pellets were resuspended again in 350 ml of the same buffer and then spun down at 5,000 rpm for 20 minutes at room temperature. The pellets were resuspended in 100 ml of 33 mM Tris-HCl, and then it was rapidly stirred at room temperature. A 100 ml of (40% (w/v) sucrose, 33 mM Tris-HCl, and 0.1 mM EDTA) was added to the resuspended pellets and then left to be stirred for another 10 minutes. The cells were spun down at 10,000 rpm for 20 minutes at 4 °C, and then the pellets were rapidly resuspended in 200 ml of 0.5 mM ice cold MgCl₂. The cells were stirred for 15 minutes at 4 °C, and then spun down at 10,000 rpm for 20 minutes at 4 °C. The supernatant that contained the PBP was dialysed against 10 mM Tris-HCl overnight. The dialysed supernatant was filtered through glass wool and loaded on Q-sepharose column which had been equilibrated against 10 mM Tris-HCl buffer. After loading, the column was washed by 1.5 volumes of equilibration buffer. 0-200 mM NaCl linear gradient (in Tris-HCl buffer) was applied to elute the pure PBP.

The PBP was the major protein present and was pure and confirmed by SDS-PAGE. The pure PBP was pooled, shell frozen, and lyophilised to dryness overnight.

Fluorescent phosphate binding protein (MDCC-PBP) was prepared as described (Brune et al., 1994). 80 mg of Lyophilised PBP prepared from E.coli was rehydrated in 18 ml of 20 mM Tris-HCl (pH 8.1) and dialysed overnight against 2 L of the same buffer. After dialysis, the PBP was removed from dialysis and the concentration was determined. The concentration was maintained at about 3.7 mg/ml based on MWt of 35 kDa for PBP. The PBP solution was warmed up to room temperature before adding 0.2 ml of 20 mM MEG stock and 40 μ l PNPase at 0.1 U/ μ l stock. The solution left at room temperature for 10 minutes. 0.12 ml of 25 mM MDCC dissolved in DMF was added to adjust the PBP solution to 150 mM MDCC. The solution was covered in foil and tightly sealed in Nesco film before using rotator to mix it for 30 minutes at room temperature. To remove the free label, the labelled -PBP was loaded onto Bio-Gel p4 column which had been equilibrated by using 20 mM Tris-HCl buffer. The column was washed by 1.5 volumes of 20 mM Tris-HCl, and 3mls of fraction were collected. OD at 280 nm and 430 nm were read for protein and label respectively. Also the labelling ratio was calculated. The lower the ratio is the better the labelling. 15% SDS gel was run and fraction contained MDCC-PBP were pooled and the concentration was determined by using extinction coefficient of $1.78 \text{ mg}^{-1}\text{ml}^{-1}$. The MDCC-PBP pooled was loaded onto Q-sepharose column which had been equilibrated in 10 mM Tris-HCl. The protein was eluted with a 400 ml gradient from 0-50 mM NaCl in 10 mM Tris buffer (pH 8). 4 ml fractions were collected after running a 15% SDS gel, figure 2.3. The pooled fractions were shell frozen and lyophilised to dryness. The PBP powder was

then rehydrated with 5 ml of 5 mM MOPS (pH 7) and dialysed overnight in the same buffer.

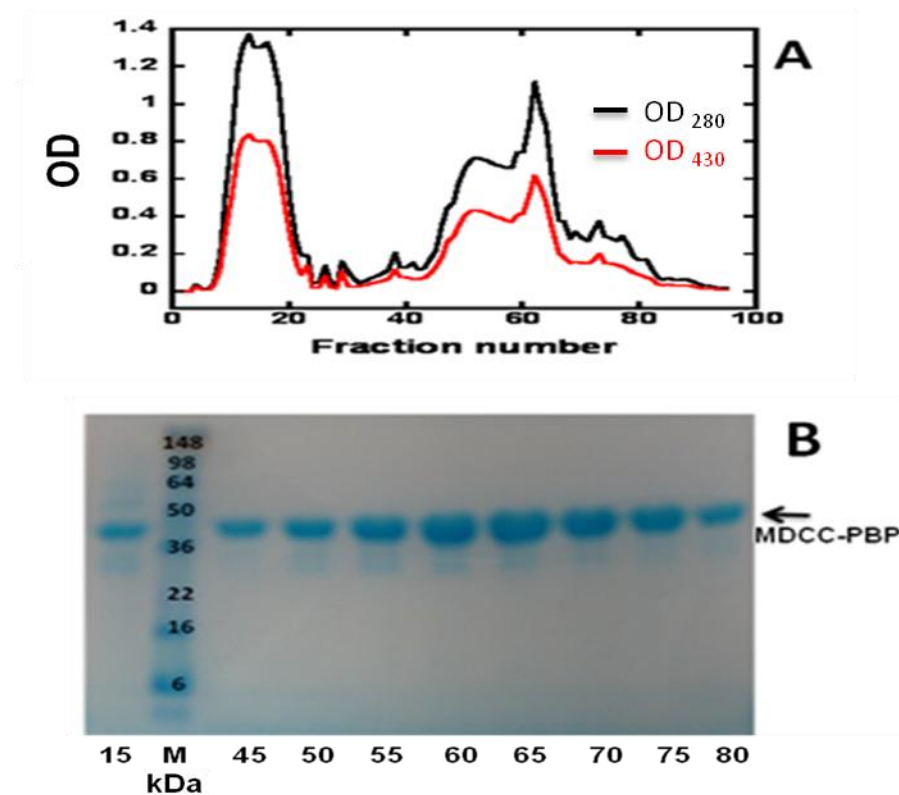


Figure 2.3 The purification of MDCC-PBP by using Q-sepharose column. A is a trace from the chart recorder of the absorbance at 280 and 430 nm. B is the SDS-PAGE analysis of the fractions by using 15% gel. Numbers along the bottom correspond to the fraction numbers that related to A.

2.3 Protein purification from tissues

Cardiac muscle contractile proteins: actin, tropomyosin, troponin, myosin, and myosin subfragment-1 (S1) were purified from sheep heart muscle. Skeletal muscle contractile proteins: actin, troponin, tropomyosin, myosin, and myosin subfragment-1 (S1) were purified from rabbit skeletal muscle.

2.3.1 Cardiac muscle proteins purification

2.3.1.1 Cardiac myosin preparation

Cardiac muscle myosin was prepared by using the method of Margossian and Lowey (Margossian and Lowey 1982). Sheep heart left ventricle muscles were dissected, cut, and placed at 4 °C. The connective tissues and fat were removed, and then the muscle was minced and weighed. Double volume of Guba-Straub buffer (0.3 M KCl, 1 mM EDTA, 0.1 M K₂HPO₄, and 0.05 M KH₂PO₄) was added to the minced muscle and stirred at 4 °C for about 30 minutes. The mixture was centrifuged at 5,000 rpm, using SLC 6000 rotor for 20 minutes. The pellets were kept for the preparation of actin acetone powder and the supernatant was used for the myosin preparation. The supernatant was filtered through a glass wool and about 14 volumes of cold water were added. Water was slowly added with continuous stirring to precipitate the myosin. The mixture left in the cold room without disturbance for about 4-6 hours to settle and myosin to sediment. The top transparent layers were sucked away and the remaining solution was spun down at 5,000 rpm, using SLC 6000 rotor for about 10 minutes. The pellets that contained the myosin were weighed and dissolved in 0.25 volume of (3 M KCl, 30 mM imidazole, pH 7.0) and left overnight to completely dissolve. To precipitate the actomyosin, an equal volume of cold water was slowly added with stirring, then it was spun down at 5,000 rpm, using SLC 6000 rotor for about 10 minutes (The size of the pellet should be small, if not an extra cycle of precipitation was needed). Eight volumes of cold water were added to the supernatant to precipitate the myosin. The myosin was collected by centrifugation at 5,000 rpm, using SLC 6000 rotor for about 10 minutes. The pellet was weighed and dissolved in 1.5 volumes of 3 M KCl, 2.5 mM DTT, 30 mM imidazole, pH 7.0. The myosin solution left at 4 °C overnight to

completely dissolve. Myosin concentration was determined by Lowry method and the myosin was diluted in an equal volume of glycerol. The myosin stock was stored at -20 °C.

2.3.1.2 Cardiac myosin subfragment-1 (S1) preparation

The Weeds and Taylor method (Weeds and Taylor 1975) was used to purify myosin subfragment-1 from myosin. Myosin stock in glycerol was diluted in 20 volumes of cold water. The diluted myosin was manually stirred till the solution became cloudy. Myosin was pelleted by centrifugation at 13,000 rpm, using SLA 1500 rotor for 10 minutes, and the pellets were dissolved in 0.6 M NaCl at about 10 mg/ml myosin concentration. The dissolved myosin was dialysed versus 120 mM NaCl, 20 mM NaH₂PO₄, and 1 mM EDTA, pH 7.0 overnight. Next day the myosin was digested at 25 °C by incubating the myosin solution in 0.05 mg/ml chymotrypsin for 10 minutes. The digestion reaction was stopped by adding of 0.1 mM PMSF (PMSF stock was in ethanol so it was diluted in 2 ml of water) and cocktail protease inhibitor tablets (1 tablet for 50 ml myosin solution). The digested myosin was dialysed versus 5 mM MOPS pH 7.0, 5 mM MgCl₂, 1 mM DTT, and 0.1 mM PMSF. The light meromyosin was precipitated by centrifugation at 20,000 rpm, using SS34 rotor for 20 minutes. The supernatant (contained the S1) was filtered then loaded onto ion-exchange column (Q-Sepharose column) which had been equilibrated with dialysis buffer (5 mM MOPS pH 7.0, 5 mM MgCl₂, 1 mM DTT, and 0.1 mM PMSF). After loading the column with S1, the column was washed with the same buffer, and the S1 was eluted by using 0.5 L gradient of 0-250 mM NaCl. 10 ml fractions were collected and monitored at OD at 280 nm. The S1 purity was checked by 15% SDS-PAGE, figure 2.4. The pure S1 fractions were pooled

and brought to 65% ammonium sulphate. The ammonium sulphate was added slowly over 30 minutes with continuous stirring at 4 °C. The S1 solution was spun down at 13,000 rpm, using SLA 1500 rotor for 10 minutes. The pellets were dissolved in ATPase high salt buffer (140 mM KCl, 10 mM MOPS pH 7.2, 3.5 mM MgCl₂, 1 mM DTT, and 1 mM NaN₃) and S1 was dialysed against same buffer overnight. The S1 concentration was determined by using extinction coefficient A_{1%} of 6.4 at OD 280 nm. The S1 was instantly frozen by using liquid nitrogen and then stored at -80 °C.

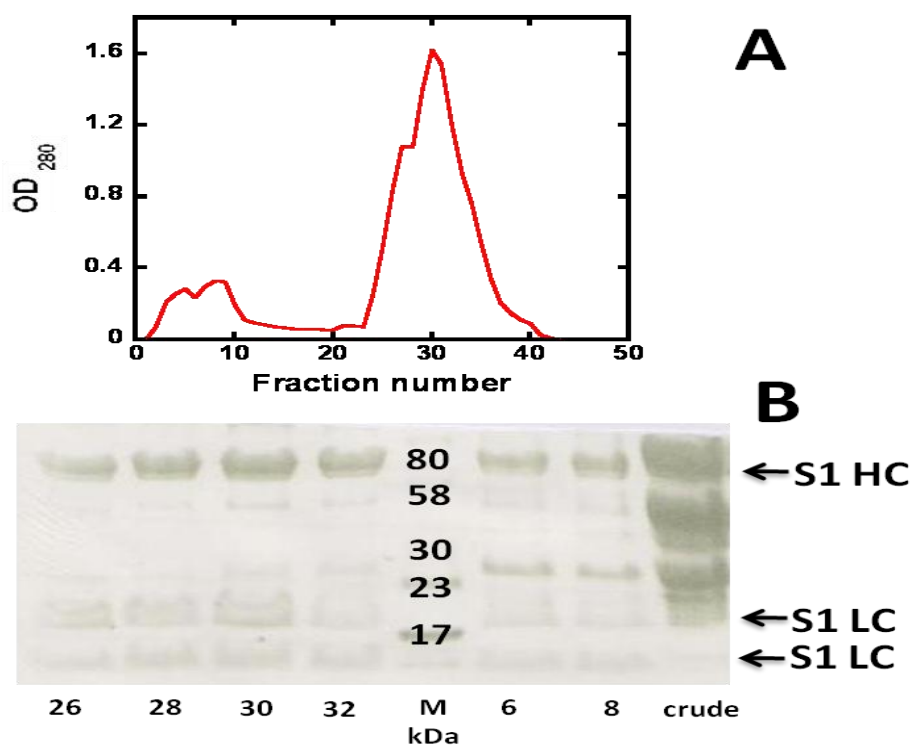


Figure 2.4 The purification of cardiac myosin subfragment-1(S1) by using Q-sepharose column. A is a trace from the chart recorder of the absorbance at 280 nm. B is the SDS-PAGE analysis of the fractions by using 15% gel. Numbers along the bottom correspond to the fraction numbers that related to A.

2.3.2 Sheep cardiac muscle acetone powder preparation

Cardiac muscle acetone powder was prepared by using the first pellet (2.3.1.1 Cardiac myosin preparation) (Pardee and Spudich 1982). The pellet was washed by different buffers. Every wash the pellet was stirred, filtered through a fine nylon mesh, and finally squeezed as dry as possible. A number of wash procedures was followed: two times in ten volumes of cold water at 4 °C, one time in four volumes of 0.4% NaHCO₃ at 4 °C, and finally four times with four volumes of cold acetone. The acetone powder was dried overnight at room temperature in the fume hood. Next day the powder was weighed and stored at -20 °C.

2.3.2.1 Preparation of cardiac F-actin

The method of Spudich and Watt (Spudich and Watt 1971) was used to prepare the cardiac F-actin from sheep heart acetone powder. 2.5 g of acetone powder was stirred for 20 minutes in 50 ml of G-actin buffer (2 mM Tris-HCl pH 8.0, 0.2 mM ATP, 0.1 mM CaCl₂, 0.5 mM DTT, and 1 mM NaN₃), then it was spun down at 18,000 rpm, using SS34 rotor for 20 minutes. The supernatant was filtered through glass wool and the pellets were re-extracted by another 50 ml G-actin buffer. G-actin (that was in the pooled supernatants) was polymerised by using 0.1 volume of 10 x KME buffer (100 mM Tris-HCl pH 8.0, 500 mM KCl, 25 mM MgCl₂, 10 mM EGTA, and 10 mM NaN₃). After adding the KME it was incubated in water bath at 30 °C for 1 hour. The F-actin solution was brought to 0.8 M KCl and kept manually stirred for about 45 minutes. The F-actin was spun down at 42,000 rpm, using T-1250 rotor for 2 hours. The F-actin pellets were washed and soaked in G-buffer. The pellets were dissolved and brought to 5-5.5 mg/ml then dialysed against G-buffer for 48 hours. The G-actin spun down at 42,000

rpm, using T-1250 rotor for 2 hours. The supernatants was filtered through glass wool and loaded on gel filtration column (Sepharyl S200 or S300) that had been equilibrated by G-buffer. Fractions of 4 ml were collected and monitored at 290 nm. The purity of G-actin was checked by 15% SDS gel, figure 2.5. Fractions of pure G-actin were pooled, polymerised by using 0.1 volume of 10×KME, and incubated at 30 °C for 45 minutes. The F-actin was spun down at 42,000 rpm, using T-1250 rotor for 2 hours. The cardiac F-actin pellets were soaked and resuspended in ATPase buffer. The concentration of F-actin was determined and it was stored at 4 °C.

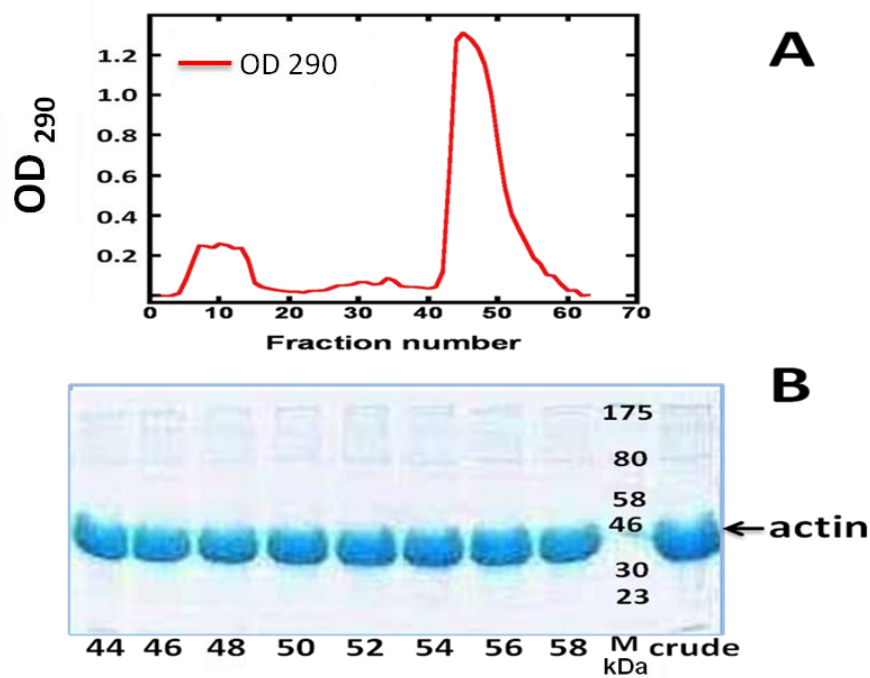


Figure 2.5 The purification of actin by using gel filtration column. A is a trace from the chart recorder of the absorbance at 290 nm. B is the SDS-PAGE analysis of the fractions by using 15% gel. Numbers along the bottom correspond to the fraction numbers that related to A.

2.3.2.2 Preparation of *N*-(1-pyrenyl)-iodoacetamide-labelled cardiac F-actin

N-(1-pyrenyl)-iodoacetamide-labelled cardiac F-actin was prepared according to the method of Kouyama and Mihashi (Kouyama and Mihashi 1981). Cys-374 was labelled with *N*-(1-pyrenyl)iodoacetamide (PIA). We followed the same method as previously mentioned in section 2.3.2.1 to purify the F-actin, but the pellets were soaked and resuspended in labelling buffer (25 mM Tris-HCl pH 7.5, 100 mM KCl, 2 mM MgCl₂, 3 mM NaN₃, and 0.3 mM ATP) and dialysed at 1 mg/ml against same labelling buffer overnight. 7 moles of *N*-(1-pyrenyl)iodoacetamide were added per 1 mol of F-actin. The mixture was slowly mixed in dark at room temperature for 3 hours. The mixture was spun down at 10,000 rpm, using SS34 rotor for 10 minutes. The supernatant was spun down at 42,000 rpm, using T-1250 rotor for two hours. The pellets were soaked, resuspended in G-buffer (at 5-5.5 mg/ml) and dialysed against G-buffer for 48 hours. The *N*-(1-pyrenyl)iodoacetamide G-actin was spun down at 42,000 rpm, using T-1250 rotor for two hours and the supernatant was filtered and loaded onto gel filtration column (Sepharyl S200 or S300) that had been equilibrated with G-buffer. Fractions of 4 ml were collected and monitored at 290 nm. The purity of *N*-(1-pyrenyl)iodoacetamide G-actin was checked by 15% SDS gel. The pure fractions were pooled, polymerised by 0.1 volume of 10xKME buffer, and incubated at 30 °C for 45 minutes. The PIA F-actin was spun down at 42,000 rpm, using T-1250 rotor for two hours. The pellets soaked and resuspended in ATPase buffer. The degree of pyrene labelling was determined by comparing the actin concentration at 290 ((A₂₉₀ - (A₃₄₄*0.127))* 38.5 μM/OD with the concentration of pyrene label at 344 (A₃₄₄*45.5

$\mu\text{M}/\text{OD}$). The labelling ratio was between 85-95%. The N-(1-pyrenyl)iodoacetamide-labelled cardiac F-actin was stored at 4 °C.

2.3.2.3 Cardiac Troponin Preparation

Troponin complex was extracted from sheep heart acetone powder according to the method of Potter (Potter 1982). 30 g of sheep heart acetone powder was extracted in 20 volumes of extraction buffer (1 M KCl, 20 mM TES pH 7 and 15 mM β -mercaptoethanol) by continuous stirring overnight at 4 °C. The suspension was centrifuged at 14,000 rpm for 20 minutes at 4 °C using a SLA 3000 rotor. The pellet was discarded and the supernatant was adjusted to pH 8.0 with 1 M potassium hydroxide. 30% ammonium sulphate saturation (167 g/L) was added slowly over 1 hour at 4 °C with a continuous gentle stirring. During addition of ammonium sulphate, the pH was maintained between 7 and 8. The new solution was spun down at 12,000 rpm for 20 minutes at 4 °C using a SLA 1500 rotor. The pellet was discarded and the 30% supernatant was then brought to 42.5% ammonium sulphate saturation (73 g/L added) that was gently added over 1 hour to precipitate the troponin complex. Centrifugation was carried out at 12,000 rpm for 20 minutes at 4 °C using a SLA 1500 rotor. The 42.5% supernatant was kept for tropomyosin preparation and the pellet was dissolved in ATPase buffer (10 mM MOPS pH 7, 50 mM KCl, 3.5 mM MgCl_2 , 1 mM DTT, and 1 mM NaN_3) and left to dialyse extensively against two litres of the same ATPase buffer overnight. The troponin complex was spun down at 10,000 rpm for 10 minutes at 4 °C, and then it was loaded onto a DEAE column which had been equilibrated with the same dialysis buffer. The column was washed and the troponin was eluted by applying a linear gradient of 50-600 mM KCl. 6 ml fractions were

collected and monitored at 280 nm. 15 % SDS gel was run to check the purity. The fractions with pure cardiac Tn were pooled, concentrated and stored at -80 °C.

2.3.2.4 Purification of cardiac tropomyosin

The 42.5% supernatant (2.3.2.3 Cardiac Troponin Preparation) brought up to 65% saturated ammonium sulphate to precipitate the tropomyosin. Ammonium sulphate was added slowly over 1 hour at 4 °C with a continuous gentle stirring. The new solution was spun down to pellet the tropomyosin at 12,000 rpm for 20 minutes at 4 °C. The 65% pellet which contained the tropomyosin was dissolved in dialysis buffer (10 mM MOPS pH 7.2, 50 mM KCl, 3.5 mM MgCl₂, 1 mM DTT, and 1 mM NaN₃) and dialysed against the same buffer overnight. The tropomyosin crude was spun down at 18,000 rpm for 10 minutes at 4 °C, and then it was loaded onto a DEAE column which had been equilibrated with the same dialysis buffer. The column was washed and the tropomyosin was eluted by applying a linear gradient of 50-500 mM KCl. 5 ml fractions were collected and monitored at 280 nm. The purity of tropomyosin was checked by running 15% SDS gel, figure 2.6. The pure tropomyosin fractions were pooled and concentrated by using 65% ammonium sulphate that was added slowly over 1 hour at 4 °C with gentle stirring. The 65% pellet was dissolved in minimum volume of high salt ATPase buffer and dialysed against same buffer overnight. The pure concentrated tropomyosin was spun down at 10,000 rpm for 10 minutes at 4 °C. The tropomyosin concentration was checked and the protein was stored at -80 °C.

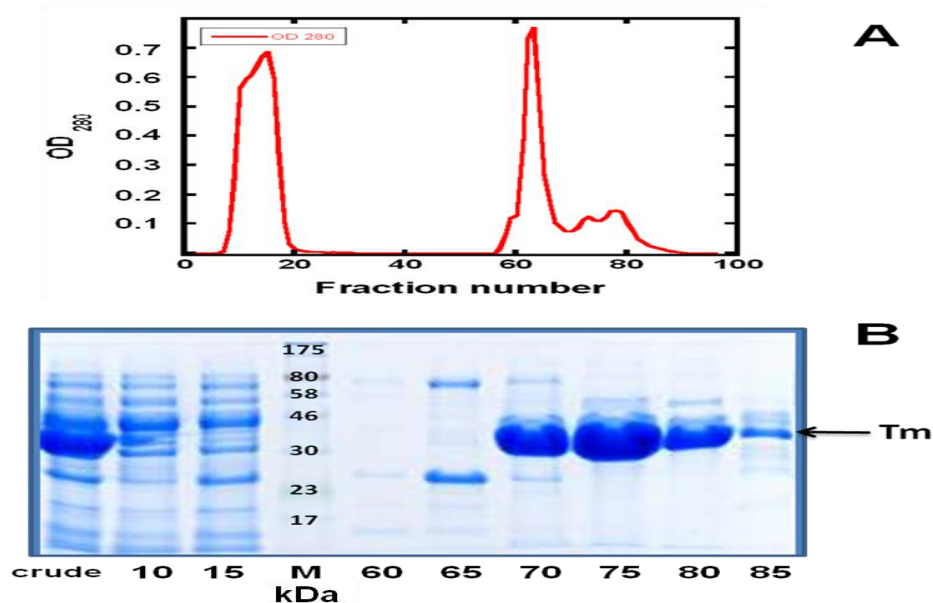


Figure 2.6 The purification of cardiac tropomyosin by using DEAE column. A is a trace from the chart recorder of the absorbance at 280 nm. B is the SDS-PAGE analysis of the fractions by using 15% gel. Numbers along the bottom correspond to the fraction numbers that related to A.

2.3.2.5 Preparation of N-(1-pyrenyl)iodoacetamide -labelled tropomyosin

Cardiac tropomyosin was labelled with N-(1-pyrenyl)iodoacetamide (PIA) according to the method of Lehrer and Morris (Lehrer and Morris 1982). Native cardiac tropomyosin was reduced with DTT (100 mM) at 40 °C for twenty minutes. To denature the tropomyosin, the reduced tropomyosin at 3 mg/ml was dialysed against 5 M GuHCl, 30 mM MES pH 7.5, 0.6 mM DTT overnight. Next day the tropomyosin was labelled with six fold molar excess of PIA for 2-3 hours at room temperature. The labelling reaction was stopped by adding 20 mM DTT. To remove the un-dissolved PIA, the labelled tropomyosin was spun down at 13,000 rpm in a bench centrifuge for 5 minutes at room temperature. The PIA-tropomyosin was renatured by dialysing against renaturing buffer (1 M NaCl, 5 mM MOPS pH 7.5, 1 mM EDTA).

2.4 Skeletal muscle proteins purification

We used the same protocols (section 2.3) to prepare the skeletal myosin, skeletal myosin subfragment-1 (S1), skeletal actin, skeletal troponin, and skeletal tropomyosin using rabbit skeletal muscles (back and legs)(euthanized white New Zealand rabbits (7-8 kg), University of Leicester).

2.5 General Methods

2.5.1 Determination of Protein Concentration

Protein concentrations were spectrophotometrically measured by using a Varian Cary 50 spectrophotometer. Samples were scanned from 250 nm to 350 nm. Absorption $A_{1\%}$ extinction coefficients were used for each protein (Table 2.1).

Table 2.1 Extinction coefficients

protein	$A_{1\%}$ Extinction coefficient at 280 nm
actin	11.5
tropomyosin	3.3
Skeletal troponin	13.0
Cardiac troponin	12.0
myosin	5.4
Skeletal Myosin subgragment-1	7.9
cardiac Myosin subgragment-1	6.4
Phosphate binding protein	17.8

Lowry method was used to determine the concentration of labelled proteins (Lowry et al., 1951). 1-100 µl samples of labelled protein were transferred into different tubes and made up to 0.5 ml by adding 1 M NaOH. A 5 ml of solution A (1 ml 0.5% CuSO₄ + 1 ml K⁺Na⁺tartrate + 48 ml 2% Na₂CO₃) was added to each tube and the solution mixed and incubated for 10 minutes at room temperature. A 0.5 ml of solution B (Folin and Cioculteau's phenol reagent in water, 1:1 (v / v)) was added into each tube and the solution was mixed and then left for 30 minutes at room temperature. The concentration of protein was determined by measurement of the absorbance at 700 nm using a spectrophotometer, and interpolating this value using a calibration chart determined by assay of total nitrogen content of actin and myosin. The protein concentration was the average of at least three samples.

2.5.2 Polyacrylamide Gel Electrophoresis

Electrophoresis comprising a 15% separating gel with a 4% stacking gel was used to resolve Proteins. The proteins samples were diluted with an equal volume of 2xSDS sample buffer (20 mM Tris-HCl pH 8, 5% SDS, 10% mercaptoethanol, 20% ethanol, and 0.02% bromophenol blue) then boiled for 3-5 minutes prior loading. The gels were run using the Biorad minigel system at 40-50 mA and 200 V until the dye front reached the end of the gel. The gels were removed, washed immediately in deionised water before immersing in Coomassie blue staining solution (0.5% PAGE blue 83 in 50% methanol, and 10% acetic acid) for 30 minutes. The gel was then destained in several changes of Coomassie destaining solution (40% methanol, and 10% acetic acid) until the background was clear.

2.5.3 Agarose Gel Electrophoresis

60 ml of 1xTAE buffer (40 mM Tris-base pH 8, 0.35 mM EDTA, and 1.14 ml glacial acetic acid) was used to dissolve 0.6 g of agarose completely by using the microwave. The solution temperature brought down to about 50 °C, and then ethidium bromide solution (final concentration of 0.5 µg/ml) was added. The gel was poured into a casting tray with a well comb and left to set at room temperature. The set gel is placed in the electrophoretic chamber and covered with 1xTAE buffer. DNA samples were diluted in DNA loading buffer and electrophoretically resolved, by comparison with a DNA size standard (1 kb plus ladder, Invitrogen). The gel was run at 100 mA and the DNA visualised under UV light.

2.5.4 Co-sedimentation Assay

The co-sedimentation assay was performed by gentle mixing of 7 µM actin with 2 µM tropomyosin and incubated for at least 20 minutes at 4 °C. 2 µM of various troponin complexes were then added, mixed, and incubated with the actin.tropomyosin complex mixture. The total volume of the samples was brought up to 1 ml by using ATPase buffer. The samples were then incubated for about 10 minutes at room temperature before spinning down at 85,000 rpm for 30 minutes at 4 °C by using a Beckman TLA110 rotor. Equivalent samples of the pellets and supernatants were then analysed on a 15% SDS-PAGE gel which was stained in Coomassie blue staining solution and then destained.

2.6 Determination of Actomyosin Mg²⁺ ATPase Activity

Mixtures of actin, tropomyosin and troponin were incubated in a final volume of 95 µl of ATPase buffer. Assay blanks contained S1 only. The ATPase reaction was started by adding of 5 µl of 100 mM MgATP at timed intervals and the mixtures were incubated for 5 minutes at 37 °C. The assay was stopped by addition of 0.5 ml of 10% Trichloroacetic acid to give a final volume of 600 µl. Precipitated protein was sedimented by centrifuging at 13,000 rpm for 5 minutes. 500 µl of the supernatant was taken and placed in a test tube. Free inorganic phosphate (Pi) was determined by using the method of Taussky and Schorr (Taussky and Schorr 1953). 1 ml of 1% ammonium molybdate in 0.5 M H₂SO₄ was added into each tube and vortexed, then 0.5 ml of freshly prepared 10 g FeSO₄ dissolved in 25 ml 0.5 M H₂SO₄ was added and vortexed. The solution left for 5 minutes for the blue colour to develop. Standards containing 0, 65 and 130 nmoles of inorganic phosphate were processed in the same way.

The concentration of inorganic phosphate was determined by measurement of absorbance at 700 nm using spectrophotometer. Standard buffer contained zero nmoles of inorganic phosphate was used as a blank buffer. The OD at 700 nm was read for all samples and standard buffers. The equation below was used to work out the optical density per nmole of Pi.

$$\text{Average OD per nmoles of Pi} = \frac{[(\text{OD}_{700} \text{ for } 100\mu\text{l of Pi}/65\text{nmoles of Pi}) + (\text{OD}_{700} \text{ for } 200\mu\text{l of Pi}/130\text{nmoles of Pi})]}{2}$$

For every ATPase reaction, a control with S1 in the absence of actin was carried out. The OD measured for S1 only and its contribution to the total Pi release was

subtracted from the acto-S1 OD. This difference divided by the average OD per nmole of Pi determines the amount of Pi produced from the acto-S1 ATPase. Since the OD measured was for a 0.5 ml reaction as opposed to the actual total quenching volume of 0.6 ml, 6/5 volume correction had to be made. To work out the rate at which ATP hydrolyse, the amount of Pi nmoles produced was divided by the total reaction time in seconds. The ATPase rate (equation below) was expressed as nmoles of Pi per second.

$$\text{ATPase rate} = (\text{nmoles of Pi produced}) / ((6/5) \times \text{reaction time})$$

2.7 Circular Dichroism

A Jasco –J715 spectropolarimeter using a cell path length of 0.1 cm was used to do the CD measurements at 4 °C and 25 °C in a 10 mM sodium phosphate, pH 7.0 and 0.3 M NaF solution. The spectra recorded ranged between 190-250 nm in the far UV region with a bandwidth of 1nm at a speed of 50 nm per min at a resolution of 1 nm. 10 scans were averaged, baseline corrected and no numerical smoothing was applied. Troponin wild type and troponin I mutants concentrations used were 5 µM.

Thermal stability measurements forward and reverse were made by following the molar ellipticity of troponin complex at 222 nm as a function of temperature in buffer containing 0.3 M NaF, 10 mM sodium phosphate, pH 7.0. Data were obtained at 1.0 °C intervals from 15 to 85 °C using a protein concentration of 5 µM.

2.8 Isothermal titration calorimetry (ITC) experiment

Isothermal titration microcalorimetry (ITC) was performed at 25 °C on a VP-ITC instrument (Microcal LLC, Northampton, MA, USA). Proteins were dialyzed extensively against ATPase buffer (140 mM KCl, 10 mM Mops pH 7.2, 3.5 mM MgCl₂, 0.1 mM DTT, 1 mM NaN₃, and 50 µM CaCl₂). Protein samples were clarified by centrifugation at

13,000 rpm for 10 min at 4 °C using bench centrifuge prior to protein concentration determination. The sample cell was filled with 1.4 ml of pre-incubated actin.tropomyosin mixture solution (7 μ M and 1.2 μ M respectively) and titrated with 300 μ l of 70 μ M wild type or TnI mutations incorporated into troponin complexes. For the first 13 injections, the injection size was 7 μ l, with duration of 14 sec, at 240 sec intervals with a stirring at 300 rpm. For the last 15 injections, the injection size was 14 μ l, with duration of 28 sec, at 240 sec intervals with a stirring at 300 rpm. Control titration of buffer with actin.Tm indicated that heats of dilution were small and constant. Origin ITC data analysis software (Microcal Inc.) was used to analyze all binding isotherms.

2.9 Enzyme Kinetics

2.9.1 Transient State Kinetic Measurements

The Hi-tech Scientific SF61 stopped flow apparatus equipped with a 100 watt Xe/Hg lamp was used for all transient kinetic measurements. KinetAsyst software package was used for the interpretation and analysis of the kinetic data. Both single and double mixing modes were used in this project. The manual set up was used to select the desired excitation wavelength and to maximise the signal. To maximise the signal; the Live Display was used by adjusting the photomultiplier voltage. Once the excitation wavelength is set up and the signal optimised, Acquire Control Panel was used to adjust the run time and the channel.

2.9.1.1 Myosin subfragment-1 (S1) Binding to PIA-actin thin filament – switch between blocked and closed states

Relatively large excess of PIA-labelled actin was rapidly mixed with a small amount of S1 (1/10th), and the kinetics of binding of S1 to PIA-actin.Tm.Tn (7:1:1) in the presence and absence of Ca^{2+} (Head et al., 1995) was followed. The pyrene iodoacetamide fluorescence (labelled actin) was excited at 364 nm and emission of fluorescence was monitored through a 400 nm cut-off filter (GG400 filter). The measurements were carried out in ATPase buffer (10 mM Mops, pH 7.2, 140 mM KCl, 4 mM MgCl_2 , 1 mM DTT, 1 mM NaN_3) at 25 °C. 6 to 8 transients were collected and averaged. The average data was then fitted to one exponential equation by a non linear least square curve fit using the Fit control Panel of the Fit Asystant. The exponential change in fluorescence was observed and used to determine the value of the equilibrium constant between blocked and closed states:

$$k_{\text{obs}} (+ \text{ or } - \text{Ca}^{2+}) / k_{\text{obs}} (\text{actin alone}) = K_B / (1+K_B)$$

Where k_{obs} is the observed rate constant (in the presence or absence of calcium, or for actin alone), and K_B is the equilibrium constant between blocked and closed states.

2.9.1.2 ATP Induced S1 dissociation from Actin Thin Filament – Switch between open to closed state

The excimer fluorescence of PIA-tropomyosin (Tm^*) was used to monitor the kinetics of the ON/OFF state change of actin. Tm^* .Tn filaments (Lehrer and Geeves 1998). The pyrene iodoacetamide fluorescence (labelled cTm) was excited at 364 nm and emission of excimer fluorescence was monitored through a 455 nm cut-off filter. Light scattering was observed at 90° to the incident beam using a UG filter (light over 400

nm was cut off). The measurements were carried out in ATPase buffer (10 mM Mops, pH 7.2, 140 mM KCl, 5 mM MgCl₂, 1 mM DTT, 1 mM NaN₃) at 20 °C. 6 to 10 transients were collected and averaged. The average data was then fitted to one exponential equation by a non linear least square curve fit using the Fit control Panel of the Fit Asystant. The transient was normalized and a number of simulation curves for different n values are presented. A good estimate of the value of n can be obtained by super-imposing computer generated curves at the various different values of n on the experimental curve and using the equation:

$$f_{on} = 1 - (1 - \exp(-k_{LS} * t))^n$$

where f_{on} is the fraction of the cooperative unit in the on-state, k_{LS} is the observed rate constant of S1 binding (light scattering), t is the time, and n is the size of cooperative unit.

2.9.1.3 Phosphate release experiment

Pi release was measured using the same stopped-flow in the double-mixing configuration. MDCC-PBP the phosphate sensor (Brune et al., 1994) was used to measure the transient of Pi release. MDCC fluorescence changes were measured using $\lambda_{ex}=435$ nm and a 455 nm cut-off filter for emission. 7-methyl guanosine (0.1 mM) and purine nucleoside phosphorylase (0.01 unit/ml) were used to remove the phosphate contamination. 5 mM Mops and 3 mM MgCl₂ buffer, pH 7 at 25 °C was used to carry out the measurements. All solutions of S1, ATP, and thin filaments have contained MDCC-PBP (10 μ M) to eliminate the contribution of residual phosphate to the signal. 5

to 7 transients were averaged for analysis. The data were fitted to two exponential by using the software provided by Hi-Tech.

2.9.1.4 Calcium Dissociation Kinetics Measurements

Quin-2 was used to measure the Ca^{2+} dissociation kinetics. The excitation wavelength was 334 nm and the emission was measured with a GG455 cut-off filter. In these measurements, the Ca^{2+} dissociation was monitored by the increase of Quin-2 fluorescence. The measurements were carried out in ATPase buffer (140 mM KCl, 4 mM MgCl_2 , 50 mM MOPS pH 7.2). In this experiment, one syringe contained Actin.Tm.Tn.S1 in the ratio of 7:1.3:1.3:2.7 μM in same ATPase buffer contained 50 μM CaCl_2 . The other syringe contained 150 μM Quin-2. The traces obtained were an average of 5-7 shots and the resulting tracing was fitted to a sum of exponentials by a non-linear least-squares method.

For measurements of IAANS fluorescence, the excitation monochromator was 334 nm and the emission was measured with a GG455 cut-off filter. In this experiment, one syringe contained Actin.Tm.Tn^{IAANS}.S1 in the ratio of 7:1.3:1.3:2.7 μM in ATPase buffer (140 mM KCl, 4 mM MgCl_2 , 50 mM MOPS pH 7.2) contained 50 μM CaCl_2 . The other syringe contained the same solution without the proteins and added 1 mM EGTA. The traces obtained were an average of 7-10 shots and the resulting tracing was fitted to a sum of exponentials by a non-linear least-squares method.

2.10 Steady State Kinetic Measurements

2.10.1 Calcium Binding Measurements

cTnC was labelled with IAANS at Cys35 and Cys84 and reconstituted with TnT and TnI as described in (section 2.1.6). Troponin complexes were dialyzed extensively against experiment buffer (50 mM MOPS pH 7.2, 140 mM KCl, 4 mM MgCl₂ and 1 mM EGTA). Two methods were used to obtain reconstituted thin filament: 1) mixed 21 μM actin, 3 μM Tm and 3 μM IAANS-labelled troponin or 2) 21 μM actin mixed in with excess Tm·Tn was cosedimented and resuspended in experiment buffer. The free Ca²⁺ concentration was calculated using Maxchelator programme WINMAXC version 2.0. The titrations were carried out by the addition of a concentrated stock solution of 20 mM Ca²⁺ into a 2 ml volume cuvette (table 2.2) which is constantly stirred by a magnetic stirrer. The change in fluorescence was monitored with the final ΔF values adjusted for the difference in assay mix volume following each incremental addition. The adjusted and normalised ΔF_i was plotted as a function of Ca²⁺ concentration and the following equation was used to analyse the titration curve (Kobayashi and Solaro 2006):

$$\Delta F_i = \sum \Delta F_{\max} X \left(\frac{X_i^{n_H}}{K^{n_H}} \right) / 1 + \left(\frac{X_i^{n_H}}{K^{n_H}} \right)$$

where ΔF_i is the total fluorescence signal change after *i*th addition of stock of Ca²⁺ solution, X_i is the free Ca²⁺ concentration after *i*th addition and n_H and K are the Hill coefficient and association constant for a Ca²⁺ binding site respectively. ΔF_{max} is the maximum fluorescence change.

Table 2.2 Ca²⁺ - EGTA buffer for calcium titration experiment (2.10.1)

[Ca] mM	[Ca] Free	pCa	Volume of 20mM CaCl₂ (μl)	Volume of 20mM CaCl₂ Added (μl)	Volume correction
0.05	4.82E-09M	8.32	2.5	2.50	2002.5
0.10	9.89E-09M	8.00	5.00	2.50	2005
0.20	2.09E-08M	7.68	10.0	5.00	2010
0.30	3.32E-08M	7.48	15.0	5.00	2015
0.40	4.71E-08M	7.33	20.0	5.00	2020
0.50	6.28E-08M	7.20	25.0	5.00	2025
0.60	8.08E-08M	7.09	30.0	5.00	2030
0.70	1.01E-07M	7.00	35.0	5.00	2035
0.80	1.26E-07M	6.90	40.0	5.00	2040
0.90	1.55E-07M	6.81	45.0	5.00	2045
1.00	1.89E-07M	6.72	50.0	5.00	2050
1.10	2.31E-07M	6.64	55.0	5.00	2055
1.20	2.86E-07M	6.54	60.0	5.00	2060
1.30	3.54E-07M	6.45	65.0	5.00	2065
1.40	4.45E-07M	6.35	70.0	5.00	2070
1.50	5.72E-07M	6.24	75.0	5.00	2075
1.60	7.63E-07M	6.12	80.0	5.00	2080
1.70	1.07E-06M	5.97	85.0	5.00	2085
1.80	1.71E-06M	5.77	90.0	5.00	2090
1.90	3.52E-06M	5.45	95.0	5.00	2095
1.95	1.20E-05M	4.92	97.5	2.50	2097.5
2.00	1.99E-05M	4.70	100	2.50	2100
2.05	5.75E-05M	4.24	102.5	2.50	2102.5
2.10	1.04E-04M	3.98	105	2.50	2105

CHAPTER 3

**Structural and functional characterization
of cardiomyopathy associated troponin I
mutants**

3.1 Introduction

Troponin I is a basic protein that complexes with the acidic TnC and TnT to form the troponin complex. Mutations in the cardiac TnI gene occur in 5% of families with genetic cardiomyopathies and 29 HCM and 1 DCM mutations have been described. Clinical manifestations of cardiac TnI mutations are diverse ranging from asymptomatic with high life expectancy to severe heart failure and sudden cardiac death (Gomes and Potter 2004).

In order to investigate the functional implications of TnI mutations, the expression of sufficient amount of TnI mutants and reconstitution with TnC and TnT into a functional troponin complex is necessary. The methodologies we used in our biochemical investigations, in particular isothermal calorimetry and transient kinetics rely on the use of substantial amount of proteins. In this project we established a shortened method that allowed successful purification and reconstitution of the seven TnI mutations.

The current chapter aims to evaluate the functional and structural effects of the TnI mutations causing HCM and DCM. We analysed the effect of TnI mutations on the structure of the whole troponin complex using circular dichroism. In order to assess the effect of TnI mutations on the binding of the troponin complex to the actin-tropomyosin complex, we performed isothermal calorimetry experiments and co-sedimentation assays. Finally we examined the effect of TnI mutations on the ability of Tn complex to activate and inhibit the actomyosin ATPase activity in the presence or absence of Ca^{2+} respectively and on the Ca^{2+} sensitivity of the actomyosin ATPase. Overall, we have generated seven troponin I HCM and DCM mutants; that were

expressed, purified, and reconstituted with troponin T and troponin C. The reconstituted troponin complexes were obtained reasonably pure and in large quantities sufficient for kinetics investigation. We found that TnI mutations did not compromise the formation of a soluble trimeric Tn-ITC complex or its overall folding. Remarkably actin binding in the presence of Ca^{2+} was strengthened for all mutants. In the absence of Ca^{2+} , inhibition of the actomyosin ATPase was drastically reduced by the R145G mutation but not by any other mutations. In the presence of Ca^{2+} , activation was reduced by two mutations, R145G and A2V. The actomyosin ATPase Ca^{2+} sensitivity was enhanced for three mutations: R145G, A157V and K206Q.

3.2 Results

3.2.1 Cloning and Expression of TnI Mutations

Single amino acid substitutions were generated by PCR based site directed mutagenesis using the overlap extension method (Higuchi et al., 1988). Figure 3.1 shows the PCR products run on an agarose gel. All lanes show a band at the predicted size of 500 bp. All TnI generated constructs were verified by sequencing.

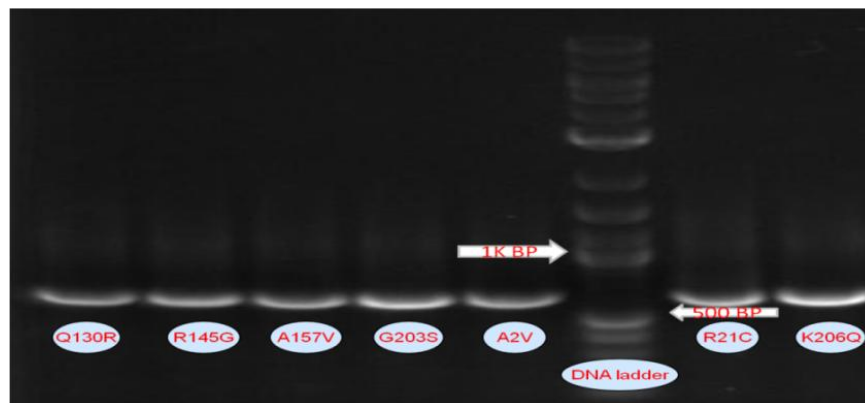


Figure 3.1 Agarose gel of the PCR products of HCTnI mutants obtained by the overlap extension method. Each lane represented the PCR product of one human construct as labelled. The DNA ladder lane represents a marker of molecular weight (carried out by Dr. Xiaowen Yang at the University of Leicester).

Following sequence analysis of the mutant constructs, expression trials of the seven constructs were performed. We monitored the protein expression levels for wild type and TnI mutants at 25 °C and 37 °C using either 0.2 mM or 0.4 mM IPTG for induction of expression. Cell lysates were analysed by SDS-gels and we monitored the time dependent increase in intensity of the troponin I band (24 kDa molecular weight). Figure 3.2.A shows TnI expression levels at 25 °C using the two IPTG concentrations. Lanes 1 and 5 show cell lysates before induction. In these lanes a number of faint bands corresponding to bacterial proteins are identifiable. Lanes 2-4 and 6-8 are cell

lysates taken every two hours and overnight after IPTG addition. A very faint band corresponding to the molecular weight of TnI (24 kDa) is observed 2 hours after induction of protein expression and gradually increases with time. Figure 3.2.B shows trial expression at 37 °C. Both 0.2 mM and 0.4 mM IPTG concentrations (lanes 10-12 and 14-16 respectively) gave much higher level of expression of TnI than at 25 °C. We concluded that the optimal conditions that give the highest level of expression of TnI constructs were: 0.4 mM IPTG at 37 °C for 5-6 hours after induction.

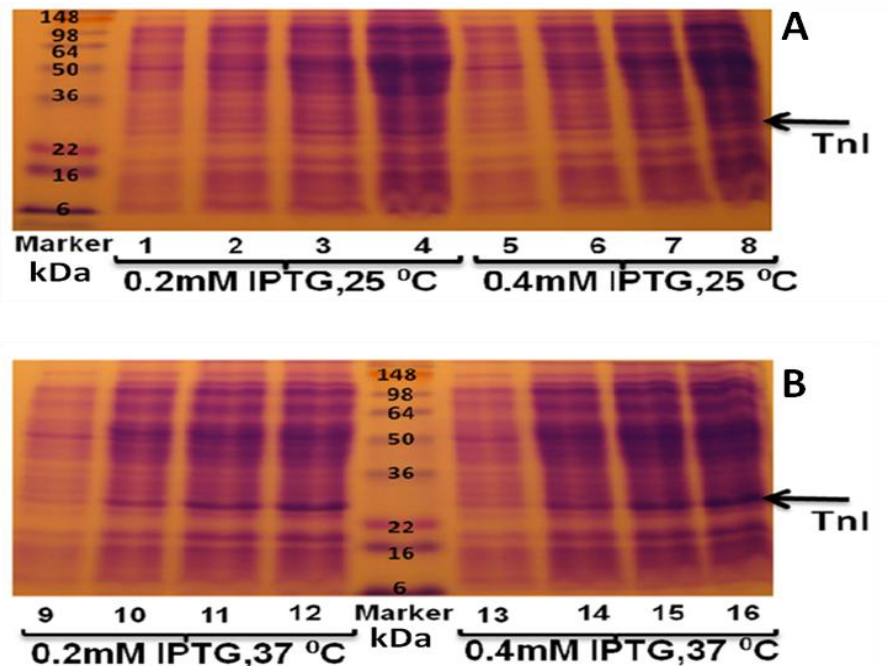


Figure 3.2 15% SDS-Polyacrylamide gel electrophoresis. Human cardiac TnI expression. A) lanes 1-4 show the expression by using 0.2 mM IPTG at 25 °C for 0, 2, 4 hours and overnight after induction, lanes 5-8 show the expression by using 0.4 mM IPTG at 25 °C for 0, 2, 4 hours and overnight after induction. B) lanes 9-12 show the expression by using 0.2 mM IPTG at 37 °C for 0, 2, 4, and 6 hours after induction, lanes 13-16 show the expression by using 0.4 mM IPTG at 37 °C for 0, 2, 4, and 6 hours after induction.

3.2.2 Reconstitution of Troponin Complex

All previous protocols (Szczesna et al., 2000; Burton et al., 2002) were based on purifying each of troponin subunits TnT, TnI, and TnC separately before the reconstitution. These protocols take longer time to obtain the final troponin complex and produce lower yield. Since all troponin subunits (TnI, TnC, and TnT) were expressed in E.coli and the contaminant proteins were the same, the troponin reconstitution method was shortened by reconstituting the expressed proteins using the cell lysates directly before purification using ammonium sulphate fractionation and gel filtration chromatography. Figure 3.3.A shows the elution profile of the gel filtration column. Figure 3.3.B shows gel electrophoresis of cell lysates obtained from the expression of cTnT (lane 1), cTnI (lane 2) and cTnC (lane 3). Protein bands corresponding to TnT, TnI and TnC are visible as indicated by the arrows. In addition a number of other proteins bands can be seen. They represent various bacterial proteins. Bacteria do not express troponin and consequently there is no endogenous troponin. The unpurified reconstituted troponin solution was brought to 30% ammonium sulphate concentration and the precipitated protein pelleted and analysed by gel electrophoresis (lane 4). Striated muscle troponin precipitates at around 42% ammonium sulphate concentration and therefore is not present in this pellet as indicated by the absence of major protein bands at the predicted level of the three troponin subunits. This lane does however show a number of bacterial proteins and so this step allowed a slight increase in the purity of the protein complex. In contrast increasing the ammonium concentration to 50% led to the precipitation of the troponin complex (crude). However, this fraction contained additional impurities as seen by the various bands on the gel. In addition, another potential source of

contamination is the possibility of forming dimeric complexes of troponin (for example TnI-C or TnI-T) or tetrameric complexes as has been reported for troponin T (Lounes et al. 2008) which can have different biochemical properties than the physiological trimeric complex. Gel electrophoresis under denaturing conditions cannot distinguish between these various troponin species. We used size exclusion chromatography to assess the stoichiometry of the troponin subunits and purify the troponin complex further. Figure 3.3.C, lanes 29-35 show the protein content of fractions 29-35 obtained from a gel filtration column (Sephacryl S-200 or S-300). Fractions 29-35 show a protein pattern containing mainly the troponin subunits TnT, TnI and TnC. Fractions 38 and 41 show a protein band of a molecular weight around 58 kDa. The troponin complex is therefore eluted after a protein of molecular mass 80 kDa and before a protein of 58 kDa molecular mass (lane 38-41). The only combination of troponin subunits that give this range of molecular weight is the trimeric TnT-I-C complex with a 1:1:1 stoichiometry (native molecular weight on size exclusion chromatography: 79 kDa). In addition the fractions showed that the troponin complex is largely pure (minor contamination even if the amount of troponin loaded on the gel is large). Our new protocol allows the reconstitution of the troponin complex within 5-6 days with a yield of 10-15 mg from each expression and purification (4 L of TnT, 3 L of TnI, and 2 L of TnC cell culture).

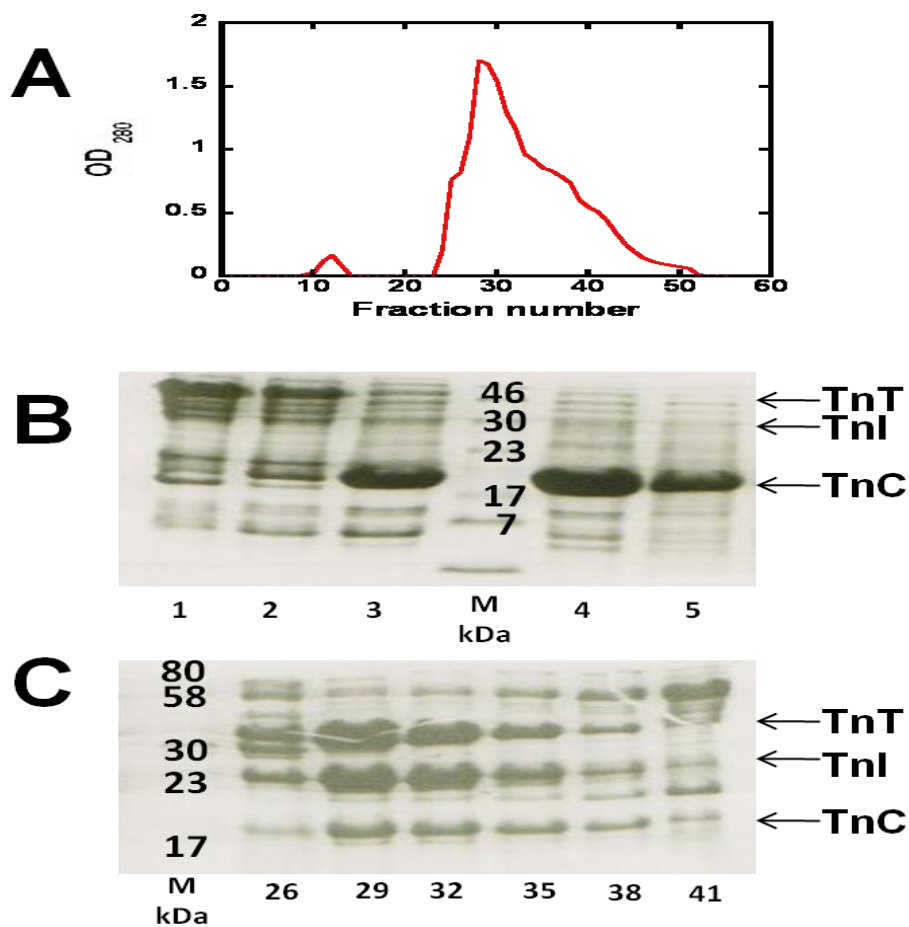


Figure 3.3 The reconstitution and purification of troponin complex using gel filtration chromatography. A is a trace from the chart recorder of the absorbance at 280 nm. B is the SDS-PAGE analysis of the reconstitution process using a 15% polyacrylamide gel. lane 1-3 are cell lysate obtained after expression of TnT, TnI and TnC respectively, lane 4 and 5 are the 30% and 50% ammonium sulphate pellet and supernatant respectively. C is the SDS-PAGE analysis of the gel filtration column fractions. Numbers along the bottom indicate fraction numbers.

3.2.3 Circular Dichroism of TnI Mutations

Circular dichroism (CD) is an excellent method for rapidly evaluating the secondary structure of proteins. Circular dichroism is based on the unequal absorption of left-handed and right-handed circularly polarized light by proteins (Greenfield 2006). The shape of the spectra of a protein is dependent on its α -helical, β -sheet and random

coil content. Hence, CD spectra can be used to estimate the secondary structure of unknown proteins and monitor the effect of mutations on protein structure.

We used CD to evaluate the effect of TnI mutations on the secondary structure of the troponin complex. We have not tried to deconvolute the proportion of the various secondary structure components since this requires a high level of protein purity and an accurate determination of protein concentration (Miles and Wallace, 2006). Our purified proteins showed minor protein contaminants (Figure 3.3.C). However a comparative study of the CD spectra between the various TnI mutants is still valuable to uncover any mutation induced large change in the troponin structure. All TnI mutants reconstituted into troponin complexes showed α -helical ($\Theta=222$) and beta-sheet ($\Theta=208$) contents (Figures 3.4). R145G and A2V TnI mutations showed no effect on the CD spectra of the troponin complexes, suggesting that these mutations had no impact on the secondary structure of troponin. TnI R21C, Q130R, G203S and K206Q give the same shape of the CD spectra but a slight decrease in the amplitude of the signal. The absence of major change indicates that overall these mutations did not affect substantially the secondary structure of troponin.

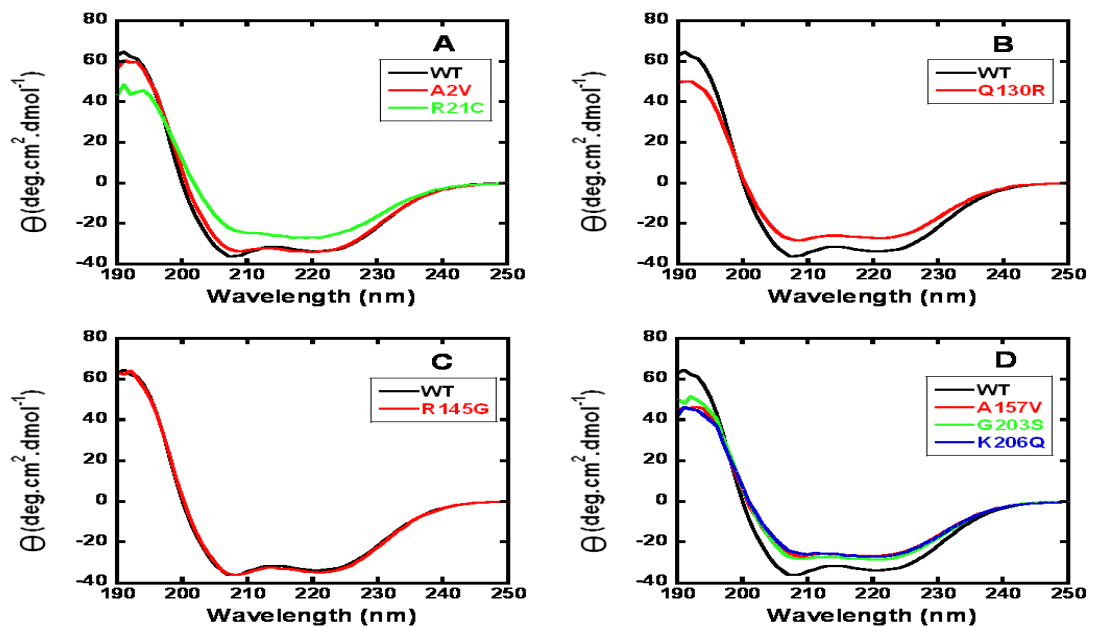


Figure 3.4 Circular Dichroism spectra of TnI WT and HCM and DCM mutants reconstituted in troponin complexes. CD spectra of the troponin complexes using the different TnI mutants (Panel A, A2V and R21C; Panel B, Q130R; Panel C, R145G and Panel D A157V, G203S and K206K) were measured in the presence of 10 mM NaH₂PO₄, pH 7.0 and 0.3 M NaF. All samples were used at a concentration of 2.5 μM. Each data point is an average of two experiments at 10 °C and each curve consisted of an average of 10 scans.

Circular dichroism can also be used to evaluate the thermal stability of a protein and how is it affected by temperature. Figure 3.5 shows the change in ellipticity at 222 nm with increasing temperature from 15 °C to 85 °C. The curves obtained for the different TnI mutants are indistinguishable. Therefore the thermal stability of the troponin complexes reconstituted is not affected by any of the TnI mutations.

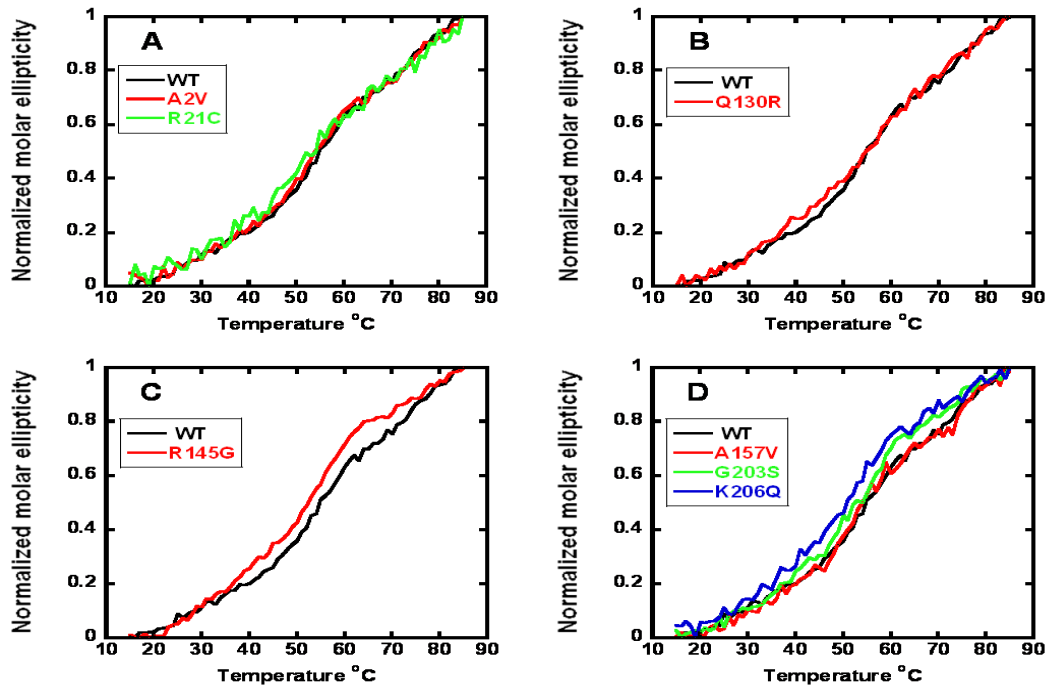


Figure 3.5 Thermal denaturation of TnI WT and HCM and DCM mutants reconstituted in troponin complexes. Thermal denaturation spectra of (A) N-terminal TnC binding region (B) TnT binding region (C) Inhibitory region (D) C-terminal TnC binding region HCM and DCM mutations. All samples were in 10 mM NaH_2PO_4 , pH 7.0 and 0.3 M NaF. It was monitored at 222 nm between 15-85 °C at a rate of 1° C/min.

3.2.4 Effect of TnI HCM and DCM mutations on the ability of the troponin complex to regulates the actomyosin ATPase in a Ca^{2+} dependent manner.

Having established that the mutants did not overly affect the structure of the troponin complex reconstituted with TnI mutants, we aimed to characterise the effect of TnI mutations on its biochemical properties by steady state methods. Troponin I main biochemical property is to regulate the actomyosin ATPase. We used three experimental strategies to investigate the effect of TnI mutations on the actomyosin ATPase:

1- Effect of increasing concentrations of troponin on the actomyosin ATPase. This experimental design allows the determination of the effect of mutation on the maximal inhibition (in the absence of Ca^{2+}) and maximal activation (in the presence of Ca^{2+}) of the actomyosin ATPase by the troponin complex.

2- Effect of increasing concentrations of myosin head. This type of actomyosin ATPases give sigmoidal curves which depend on the cooperativity within the thin filament and the transition between the inhibited and activated states.

3- Finally we determined the Ca^{2+} sensitivity of the actomyosin ATPase by varying the concentration of Ca^{2+} . The results of this experiment depend on the Ca^{2+} affinity of troponin, the cooperativity of thin filament and the transition between the inhibited and activated states of thin filaments.

3.2.4.a. Effect of increasing troponin concentration on maximal inhibition and activation of the actomyosin ATPase:

Actin-Tm-activated myosin subfragment-1 ATPase rates were measured using 1-12 μM rabbit skeletal S1, 5-7 μM cardiac actin, and 2 μM cardiac Tm in ATPase low salt buffer contained 5mM ATP at 37 °C in the presence of 0-2 μM troponin complex. The actomyosin ATPase activity in the absence of Tn, is used as the reference level for both activation and inhibition and is set at 100%.

Figure 3.6 shows the ability of wild type and TnI mutants to activate and inhibit the actin-Tm-activated myosin ATPase activity in reconstituted thin filament systems. In the absence of Ca^{2+} , the wild type troponin and 6 mutants A2V, R21C, Q130R, A157V, G203S and K206Q gave comparable maximal inhibition of the actomyosin ATPase

(between 75 and 92% inhibition). In contrast, the mutation in the inhibitory region of troponin I, R145G, dramatically reduced the ability of the troponin complex to inhibit the actomyosin ATPase in the absence of Ca^{2+} .

In the presence of Ca^{2+} , wild type troponin potentiated the actin-tropomyosin activated myosin subfragment-1 ATPase activity by about 291 ± 7.76 %. TnI mutations A2V and R145G reduced the activation of the reconstituted thin filament to 180 ± 8.14 % and 156 ± 8.31 % respectively (Figure 3.6, panels A and C). In contrast mutation A157V increased the maximal activation to 330 ± 7.78 % (Figure 3.6., panel D). TnI mutations R21C, Q130R, G203S and K206Q did not change the level of maximal activation of the actomyosin ATPase by the troponin complex (Figure 3.6. panels A, B and D).

Figure 3.7 and table 3.1 shows the maximal activation and inhibition obtained by TnI wild type and HCM and DCM mutants.

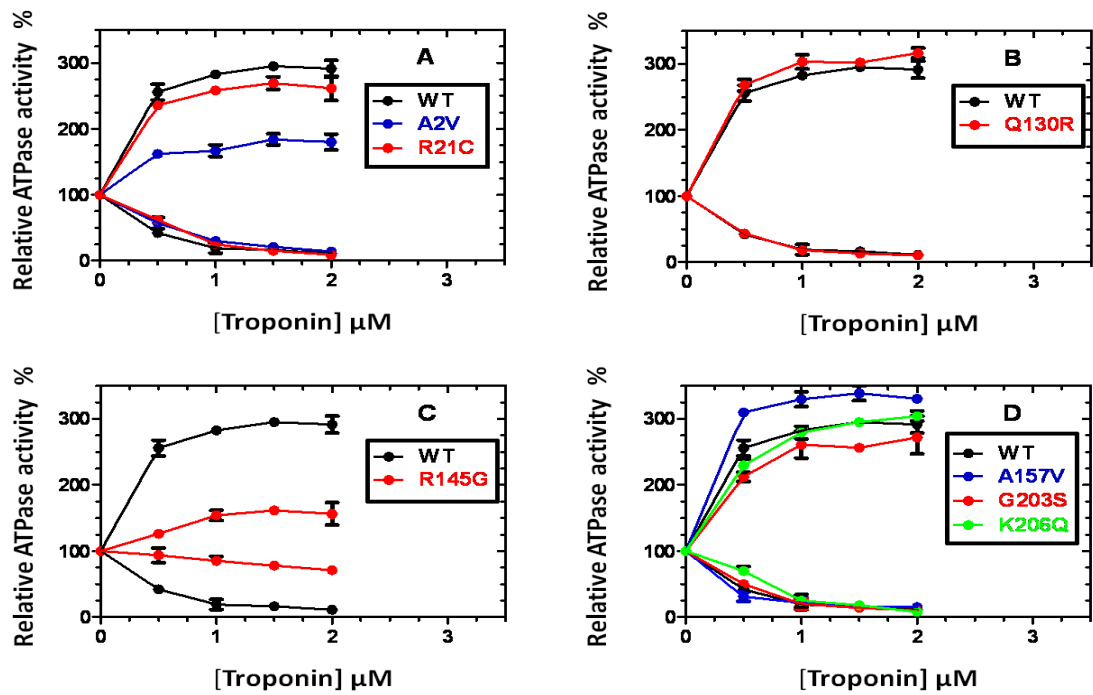


Figure 3.6 Effect of increasing TnI mutants concentration on Actin-Tm activated Myosin-S1 ATPase in the presence and absence of calcium. Actin-Tm-activated myosin subfragment-1 ATPase assays were carried out in the presence of 0-2 μM troponin. The assay consisted of 7 μM cardiac actin, 2 μM cardiac Tm, and 1 μM skeletal S1 (low S1 concentration) in the presence of either 0.2 mM CaCl₂ or 1 mM EGTA at 37 °C in low salt ATPase buffer (10 mM KCl, 10 mM MOPS pH 7.2, 3.5 mM MgCl₂, 1 mM DTT, and 1 mM NaN₃). 3-5 experiments were performed and are expressed as an average.

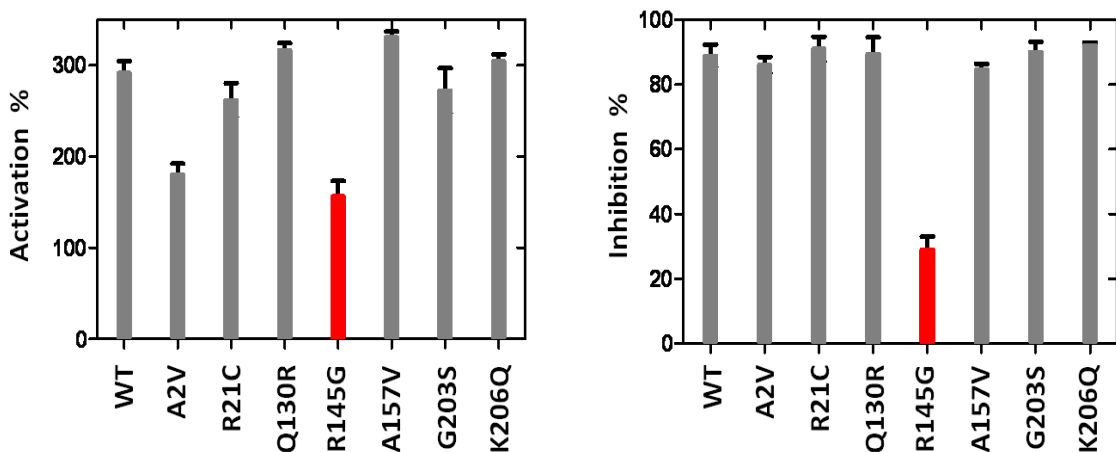


Figure 3.7 Bar chart of the maximal activation or inhibition obtained with each mutation. The last data point from figure 3.6 data shown is used to calculate the percentage of ATPase activation or inhibition using the actin-Tm (no Tn) as a reference point.

Table 3.1 The maximal activation and inhibition obtained by wild type and TnI mutants (Data are shown as mean \pm S.E).

TnI	Maximal activation %	Maximal inhibition %
WT	291 \pm 7.76	89 \pm 4.16
A2V	180 \pm 8.14	86 \pm 4.34
R21C	260 \pm 9.61	91 \pm 5.21
Q130R	310 \pm 7.49	90 \pm 2.81
R145G	156 \pm 8.31	29 \pm 2.78
A157V	330 \pm 7.78	84 \pm 5.18
G203S	265 \pm 14.8	90 \pm 4.22
K206Q	295 \pm 7.08	92 \pm 5.32

3.2.4.b Effect of TnI mutations on the cooperative activation of actin-Tm-Tn-myosin ATPase by myosin heads.

Figure 3.8 shows the dependence of the thin filament activation of myosin ATPase on the concentration of S1. The ATPase obtained with S1 myosin head alone (Orange triangles) or in the presence of actin (green diamonds) is linearly dependent on S1 concentration. For regulated cardiac thin filament (actin.Tm.Tn), the ATPase dependence on S1 concentration is sigmoidal in both presence and absence of Ca²⁺ as previously reported for skeletal muscle thin filaments (Lehrer and Morris 1982).

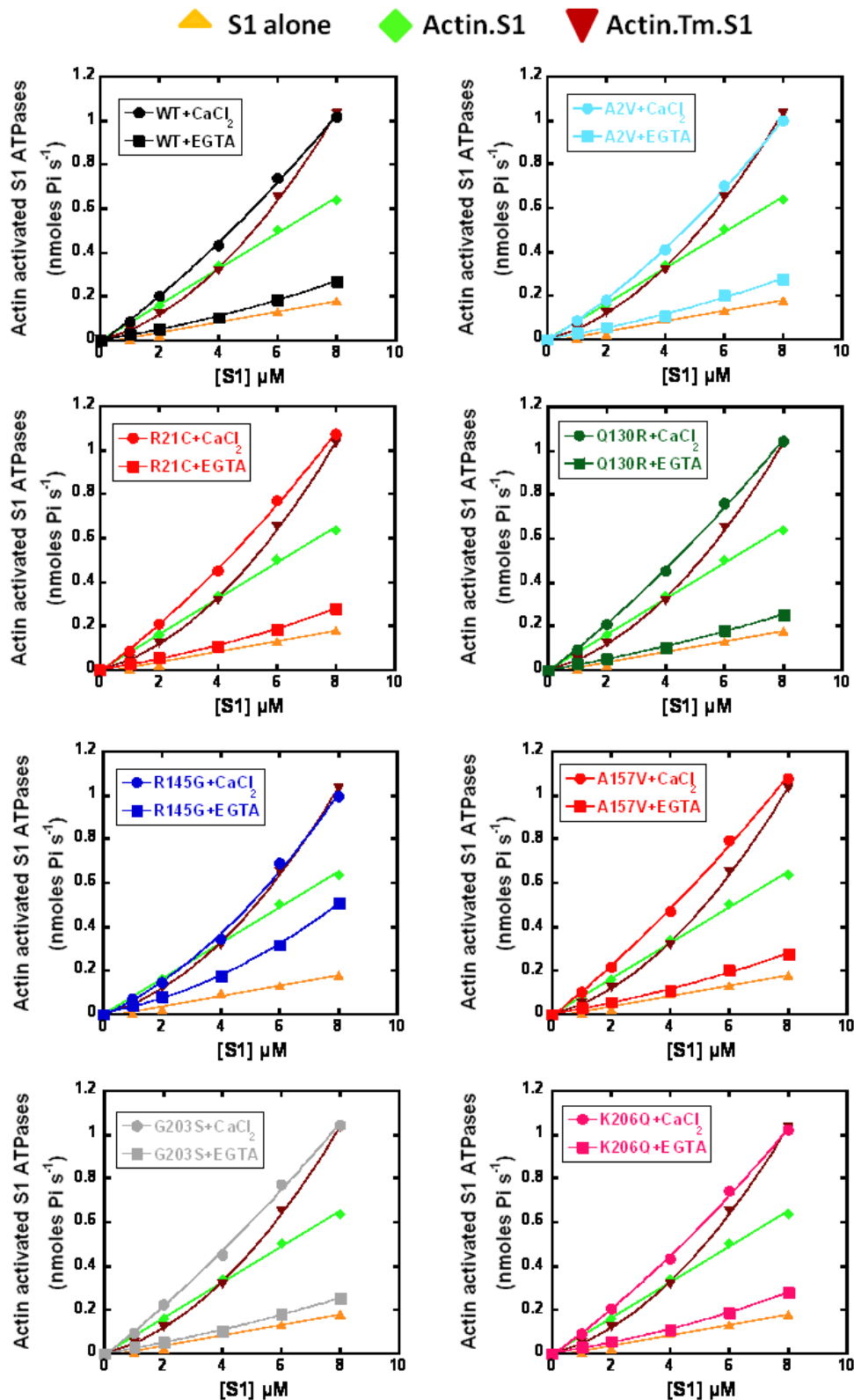


Figure 3.8 Effect of TnI mutations on the S1 dependence of the actomyosin ATPase. Thin filament activation of S1 ATPase at increasing concentration of S1 in the presence and absence of calcium. Activity was measured in the presence of 5 μM cardiac actin, 2 μM cardiac Tm, 2 μM Tn, and 1-8 μM skeletal S1 at 37 $^{\circ}\text{C}$ in ATPase low salt buffer (10 mM KCl, 10 mM MOPS pH 7.2, 3.5 mM MgCl_2 , 1 mM DTT, and 1 mM NaN_3).

In the presence of Ca^{2+} the curves are well above the curves obtained in the absence of Ca^{2+} due to the activatory role of Ca^{2+} . All mutants except R145G displayed similar behaviour to the wild type. TnIR145G, however, showed less activation in the presence of Ca^{2+} (curve shifted to the right) and less inhibition in the absence of Ca^{2+} (curve shifted to the left). These results are in agreement with the data obtained in the previous section.

3.2.4.c Effect of TnI mutations on the Ca^{2+} sensitivity of the actin-Tm-Tn activation of S1 myosin head ATPase.

In this chapter we determined the effect of HCM and DCM mutations on the Ca^{2+} concentration dependence of the actomyosin ATPase. Figure 3.9 shows the relative normalized ATPase activity curves (pCa-ATPase curve) comparing thin filaments containing TnI wild type and mutants. The data were fitted to the Hill equation:

$[100 / (1 + 10^{(n_H * (pCa - pCa_{50}))})]$ and the pCa_{50} and n_H were determined.

The Ca^{2+} dependence of thin filament activation of the myosin ATPase using wild type TnI gave a pCa_{50} value of 5.86 and a Hill coefficient n_H value of 1.33. A n_H higher than 1 is indicative of cooperativity in the system.

Mutations A2V, R21C, Q130R and G203S showed no change in the pCa_{50} values (less than 0.1 pCa units). In contrast mutations R145G, A157V and K206Q increased the pCa_{50} of the ATPase dependence on Ca^{2+} (by 0.6 pCa unit).

Hill coefficient values were unchanged for TnI mutants A157V (1.32), G203S (1.39) and K206Q (1.27), increased for R21C (1.62) and Q130R (1.47) and decreased for A2V (1.15) and R145G (1.15), table 3.2.

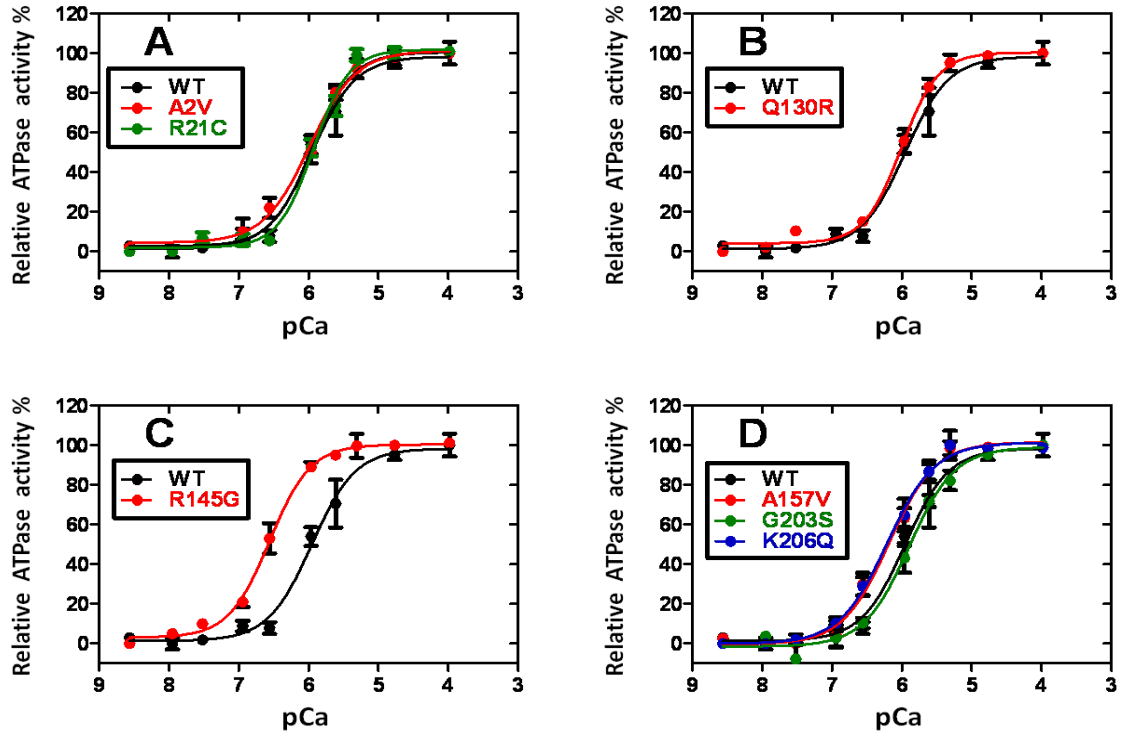


Figure 3.9 Effect of TnI mutations on Ca²⁺ dependent Actin.Tm activated S1 ATPase activity. The experiments were performed using 7 μ M actin, 2 μ M Tm, 2 μ M Tn and 1 μ M S1 and 5 mM ATP in 50 mM MOPS, 10 mM KCl, 3.5 mM MgCl₂, and 1 mM EGTA pH 7.0, 37 $^{\circ}$ C. Increasing concentrations of Ca²⁺ were added to achieve the desired pCa. The basal ATPase activity at pCa 8.5 was considered 0% and the maximal ATPase activity at pCa 4 to be 100%. The rate of S1 alone was subtracted.

Table 3.2 The effect of cTnI mutations on the Ca²⁺ binding dependent actin-activated acto-S1 ATPase activity (Data are shown as mean ± S.E).

TnI	pCa₅₀	Hill Coefficient
WT	5.96 ± 0.06	1.33 ± 0.26
A2V	6.03 ± 0.05	1.15 ± 0.19
R21C	5.94 ± 0.03	1.62 ± 0.22
Q130R	6.04 ± 0.03	1.47 ± 0.19
R145G	6.51 ± 0.04	1.15 ± 0.18
A157V	6.18 ± 0.05	1.32 ± 0.16
G203S	5.88 ± 0.05	1.39 ± 0.19
K206Q	6.20 ± 0.05	1.27 ± 0.16

3.2.5 Binding of troponin complexes containing WT and TnI mutants into actin.Tm thin filament.

In this section we examined the effects of TnI mutants on the ability of troponin complex to interact with actin.Tm thin filament using two different methods: co-sedimentation and isothermal calorimetry.

3.2.5.1 Co-sedimentation of TnI WT and mutants with thin filament

The thin filament proteins were premixed at a ratio of 7:2:2 Actin:Tm:Tn and spun down as detailed in section 2.5.4. Pellets and supernatants were analysed using 15% SDS-gels. SDS-PAGE analysis of WT and TnI mutant thin filaments showed no apparent

changes in the ability of the troponin complexes to bind to actin-Tm thin filaments. No changes were seen in the protein content in the pellet (P) and supernatant (S) between troponin complexes containing TnI WT and mutants, figure 3.10. Since we used two folds saturated concentrations of both troponin and tropomyosin, the same protein quantity of troponin complexes and Tm were found in both pellets and supernatants

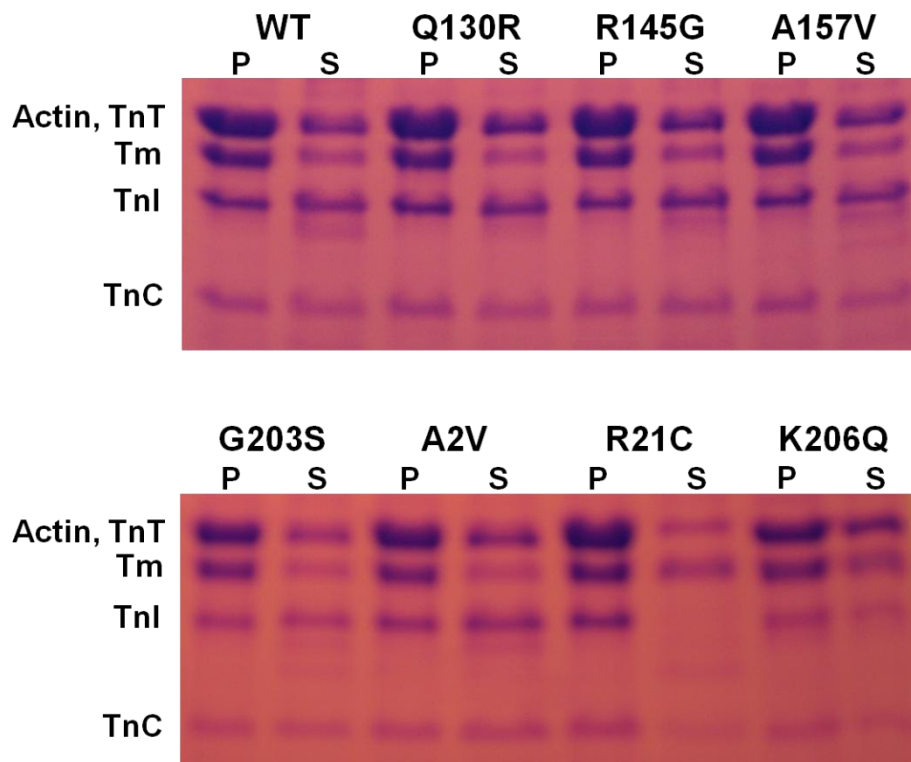


Figure 3.10 15% SDS-PAGE for of WT and TnI mutations cosedimented to Actin-Tm. From left to right pellets (P) and supernatants (S) are shown: wild type, Q130R, R145G, A157V, G203S, A2V, R21C and K206Q. Thin filaments were reconstituted by incubating 7 μ M actin, 2 μ M Tm, and 2 μ M Tn in 10 mM MOPS, 140 mM KCl, 4 mM MgCl₂, 0.1 mM CaCl₂ and 1 mM DTT (pH 7.2) for 30 min and then spun down for 30 minutes at 85,000 rpm at 4 °C.

3.2.5.2 Binding of troponin complexes to actin-Tm thin filaments by using ITC assay

The results of a typical ITC experiments are illustrated in figures 3.11-3.14. Traces of calorimetric titrations of troponin complexes with actin-Tm thin filaments showed negative peaks, the interactions are exothermic. Each deflection represents the heat released by troponin complex binding to thin filament with each injection. The binding isotherms derived from these data are plotted. These graphs show the integrated heats for each troponin complex injection versus the molar ratio of troponin complex to actin.

The stoichiometry (n), association constants (K_a), and enthalpy of binding (ΔH) were obtained directly. Entropy ($T\Delta S$) and change in Gibbs free energy (ΔG) were calculated by using the following equation.

$$\Delta G = -RT \ln K_d = \Delta H - T\Delta S$$

Wild type troponin complex binding to thin filament showed a dissociation constant K_d of 1.1 μM and a stoichiometry of 0.16. TnI mutants reconstituted into troponin complexes showed stronger ability to bind to actin-Tm thin filaments (lower dissociation constants), in addition they all showed stoichiometry values of 0.14-0.17 close to the wild type value (table 3.3) and agreeing well with the physiological ratio of one troponin per seven actin monomers.

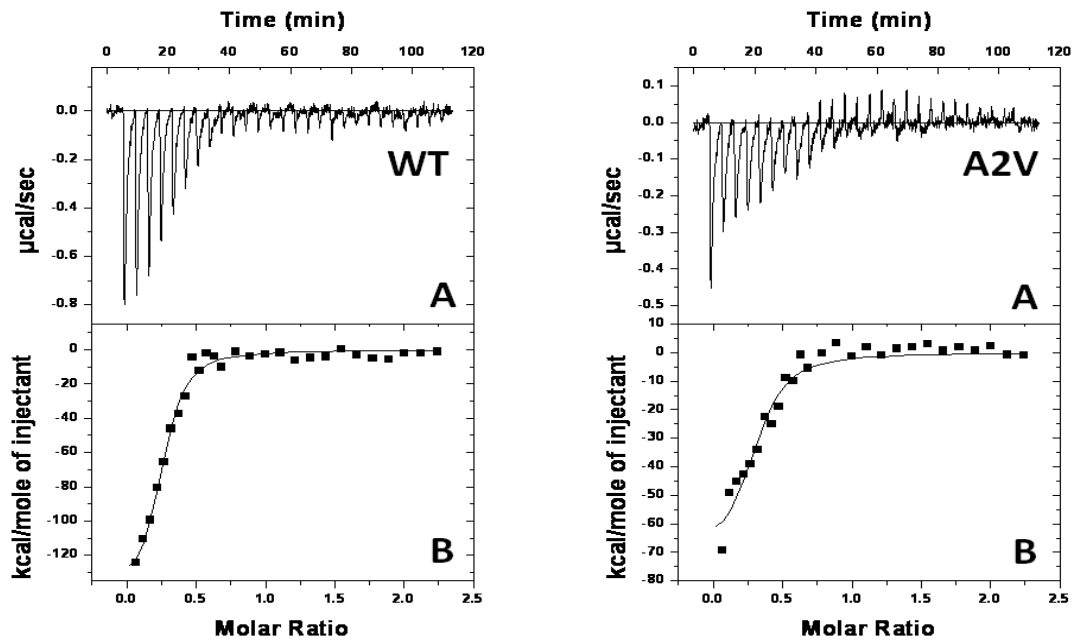


Figure 3.11 Microcalorimetric titration of actin.tropomyosin with troponin complexes (wild type and A2V) in the presence of $50 \mu\text{M CaCl}_2$. (A) The traces of titration obtained by 27 injections of $70 \mu\text{M}$ troponin complex into $7 \mu\text{M}:1.2 \mu\text{M}$ actin:tropomyosin at 25°C , 140 mM KCl , $10 \text{ mM Mops pH } 7.2$, 3.5 mM MgCl_2 , 1 mM NaN_3 , 0.1 mM DTT , and $50 \mu\text{M CaCl}_2$. (B) Integrated heats for each injection versus the molar ratio of troponin complex to actin.tropomyosin. The solid lines indicate the curve fit of the data.

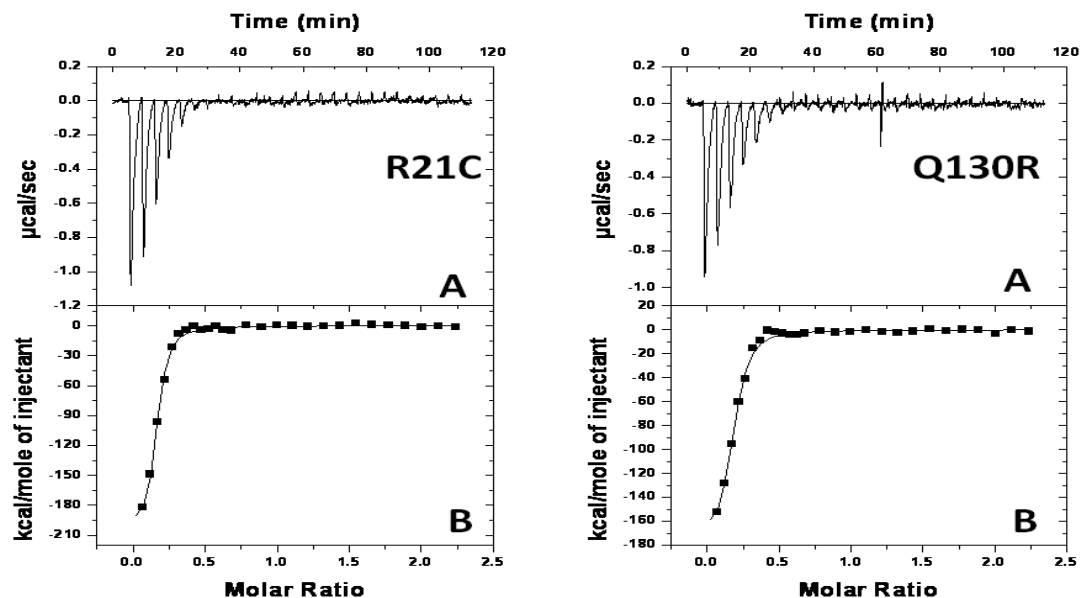


Figure 3.12 Microcalorimetric titration of actin.tropomyosin with troponin complexes (R21C and Q130R) in the presence of $50 \mu\text{M CaCl}_2$. (A) The traces of titration obtained by 27 injections of $70 \mu\text{M}$ troponin complex into $7 \mu\text{M}:1.2 \mu\text{M}$ actin:tropomyosin at 25°C , 140 mM KCl , $10 \text{ mM Mops pH } 7.2$, 3.5 mM MgCl_2 , 1 mM NaN_3 , 0.1 mM DTT , and $50 \mu\text{M CaCl}_2$. (B) Integrated heats for each injection versus the molar ratio of troponin complex to actin.tropomyosin. The solid lines indicate the curve fit of the data.

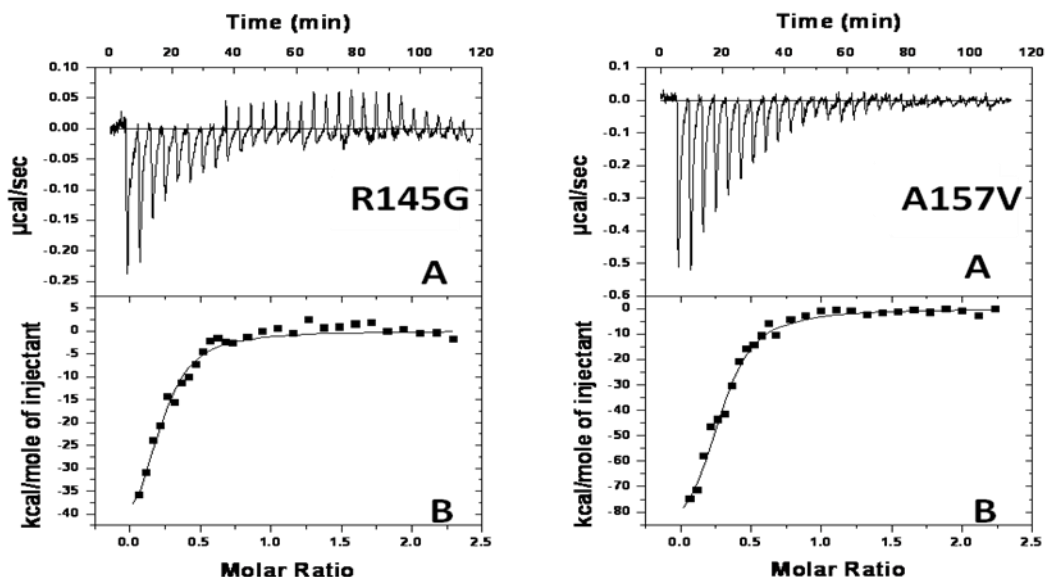


Figure 3.13 Microcalorimetric titration of actin.tropomyosin with troponin complexes (R145G and A157V) in the presence of 50 μM CaCl_2 . (A) The traces of titration obtained by 27 injections of 70 μM troponin complex into 7 μM :1.2 μM actin:tropomyosin at 25 $^\circ\text{C}$, 140 mM KCl, 10 mM Mops pH 7.2, 3.5 mM MgCl_2 , 1 mM NaN_3 , 0.1 mM DTT, and 50 μM CaCl_2 . (B) Integrated heats for each injection versus the molar ratio of troponin complex to actin.tropomyosin. The solid lines indicate the curve fit of the data.

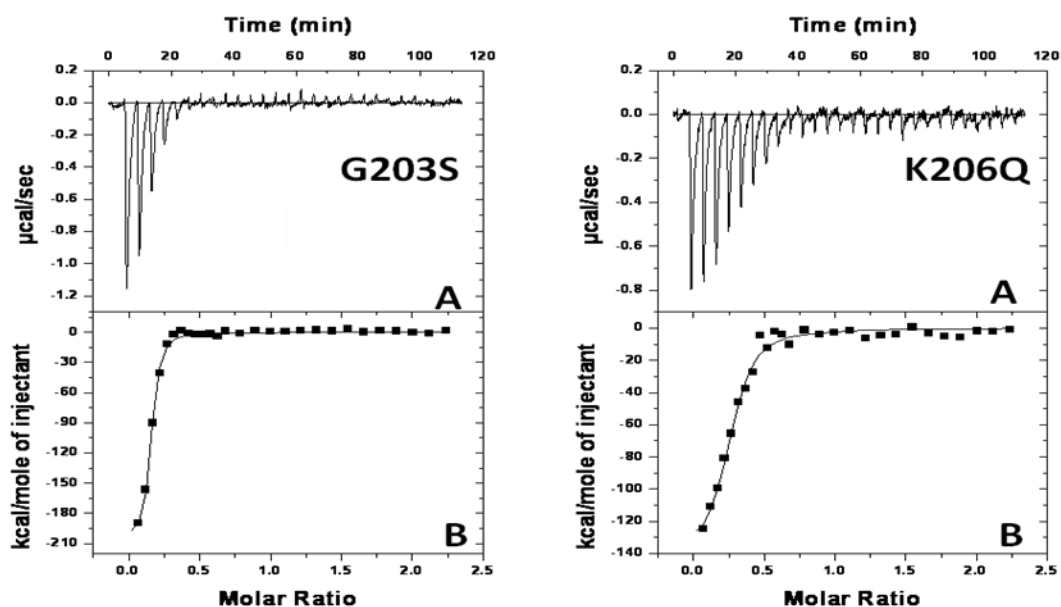


Figure 3.14 Microcalorimetric titration of actin.tropomyosin with troponin complexes (G203S and K206Q) in the presence of 50 μM CaCl_2 . (A) The traces of titration obtained by 27 injections of 70 μM troponin complex into 7 μM :1.2 μM actin:tropomyosin at 25 $^\circ\text{C}$, 140 mM KCl, 10 mM Mops pH 7.2, 3.5 mM MgCl_2 , 1 mM NaN_3 , 0.1 mM DTT, and 50 μM CaCl_2 . (B) Integrated heats for each injection versus the molar ratio of troponin complex to actin.tropomyosin. The solid lines indicate the curve fit of the data.

Table 3.3 Binding parameters for complexation between troponin complexes and actin.Tm thin filaments

Troponin complex	K_d (μM)	Stoichiometry (n)	ΔH (kJmol⁻¹)	ΔG (kJmol⁻¹)	TΔS (kJmol⁻¹)
Wild type	1.10	0.16	-122	-34.4	-87.6
A2V	0.47	0.15	-71	-24.4	-46.6
R21C	0.68	0.15	-207	-33.0	-174
Q130R	0.52	0.17	-175	-32.0	-143
R145G	0.92	0.17	-43	-34.0	-9.00
A157V	0.47	0.15	-98	-31.4	-66.6
G203S	0.75	0.14	-192	-33.0	-159
K206Q	0.61	0.16	-142	-35.0	-107

3.3 Discussion

Here, we describe the mutagenesis of TnI, protein expression and purification, and the initial steps in biochemical characterisation. Since transient kinetic rely on the use of a large amount of protein and since studying an integrated system such as thin filaments required the preparation of 14 proteins (myosin head, actin, tropomyosin, troponin T, troponin C, troponin I wild type and 7 mutants and phosphate binding protein), a large effort was dedicated to set up expression, purification and reconstitution methods for the troponin that yielded sufficient amount of proteins, in a reasonably pure form and in a relatively short time frame. To this end, we cloned the troponin cDNA into the pLEICS-05 vector (a vector designed for high yield protein expression). We have also established the optimum conditions for expression (0.4 mM IPTG for induction, 5-6 hours incubation at 37 °C after induction). We have also developed a shortened procedure for the reconstitution and purification of a soluble trimeric complex. Overall these efforts allowed us to obtain troponin complexes reconstituted with TnI mutants at a yield of 10-15 mg sufficient for structural, biochemical and biophysical characterisation.

3.3.1 TnI HCM and DCM mutations have no deleterious effect on the structure of troponin.

Having established that all TnI mutants were able to combine with the two other troponin subunits in a trimeric complex, we aimed to determine the effect of these mutations on the secondary structure of the troponin complex using circular dichroism. We found that R145G and A2V TnI mutations showed no effect on the CD spectra of the troponin complexes, suggesting that these mutations had no impact on

the secondary structure of troponin. The result on R145G is in agreement with a previous study (Lang et al., 2002). TnI R21C, Q130R, G203S and K206Q give the same shape of the CD spectra but a slight decrease in the amplitude of the signal. The small reduction in the CD signal could be due to small difference in protein concentrations. Alternatively a small decrease in the α -helical content is possible. Deng et al reported a slight decrease in helicity for G203S and K206Q (Deng et al., 2003).

The absence of major change indicates that overall, these mutations did not affect substantially the secondary structure of troponin.

3.3.2. Effect of TnI mutations on the steady state actomyosin ATPase.

We have investigated the effect of the TnI mutants A2V, R21C, Q130R, R145G, A157V, G203S, and K206Q on the ability of Ca^{2+} and troponin to regulate the actin-Tm- myosin subfragment-1 ATPase activity using three different experimental designs: by increasing concentrations of troponin, increasing concentration of S1 and increasing concentration of Ca^{2+} . We investigated the effect of mutations on maximal inhibition, maximal activation (in the presence of Ca^{2+}) of the actomyosin ATPase, on the cooperativity of the thin filament inhibition and activation, on the transition between the inhibited and activated states and on the Ca^{2+} sensitivity.

We found that DCM mutation A2V decrease maximal activation and the Hill coefficient. TnI mutation R21C and Q130R had no effect on any ATPase parameters except a slight increase in the Hill coefficient of Ca^{2+} dependent activation of actin-Tm-myosin head ATPase. This is in agreement with a previous study that showed that R21C mutation did not affect the ATPase activity (Gomes et al., 2005).

The most remarkable effect was obtained with mutation R145G. This mutation led to a substantial decrease in the ability of the troponin to inhibit actomyosin ATPase in the absence of Ca^{2+} in agreement with previous studies (Elliot et al., 2000; Lang et al., 2002). This is not surprising since this mutation occurs in the inhibitory region at a conserved position. Even more surprising was the observed decrease in the ability of troponin to activate the actomyosin ATPase in the presence of Ca^{2+} . This suggests that amino acids in the so called inhibitory regions are not only important for the inhibited state of thin filament but also for the activated state.

Mutation in the switch region A157V increased maximal activation and the pCa_{50} . Finally mutation in the C-terminal region did not affect the activation or inhibition of the actomyosin ATPase. Mutation K206Q affected Ca^{2+} sensitivity and increased pCa_{50} .

3.3.3. TnI mutations enhanced troponin binding affinity for actin-tropomyosin.

We performed two types of actin binding experiments: co-sedimentation and isothermal calorimetry. Co-sedimentation experiments showed no difference in the actin binding ability of troponin complexes reconstituted with TnI mutations. However this method is only qualitative and is not sensitive enough to detect small affinity changes. We have used the isothermal calorimetry to quantitatively analyse troponin binding to actin-Tm. This method directly measures the binding constant K_a and the stoichiometry. The ITC data uncovered a remarkable effect. All TnI mutants showed higher ability than the wild type to bind to the actin-tropomyosin filament in the presence of Ca^{2+} . This is the first time this effect has been reported. This is remarkable and may be significant in relation to the biochemical basis of HCM and DCM since in

normal heart, Ca^{2+} decrease of the affinity of troponin for actin-tropomyosin is important for thin filament activation. Therefore mutations in TnI may uncouple Ca^{2+} binding from the weakening of the troponin affinity to actin-tropomyosin. It was not possible to measure the affinity of the troponin for actin-tropomyosin in the absence of Ca^{2+} (no heat change in this experiment) probably because of the larger affinity of troponin for actin-tropomyosin in the absence of Ca^{2+} . We are the first to report the effect of these mutants by using the ITC technique.

CHAPTER 4

Effects of cTnI mutations on the affinity and kinetics of Ca^{2+} binding to and release from troponin.

4.1 Introduction

Ca^{2+} plays a fundamental role in the regulation of cardiac muscle contraction (Ebashi and Endo 1968). Ca^{2+} binding to TnC represent the first step in the activation of myofilament. Ca^{2+} binds the high affinity sites III and IV in the C-terminus of TnC with a high affinity (K_d nearly 10^{-8} M). The binding to the regulatory site II in cardiac TnC is weaker (K_d nearly 10^{-5} - 10^{-6} M) (Kobayashi and Solaro 2006). The affinity of site II to Ca^{2+} is affected by incorporation in thin filament (Davis and Tikunova 2008). In addition, myosin head binding to regulated actin enhances calcium affinity (Bremel and Weber 1972). Thin filament affinity for Ca^{2+} is an important determinant of thin filament Ca^{2+} -sensitivity. Alterations in calcium sensitivity in functional studies such as ATPase, in vitro motility assays, and force measurements has been widely reported (our data from chapter 3, Kobayashi and Solaro 2006; Robinson et al., 2007). We hypothesized that changes in Ca^{2+} affinity of the regulatory site of TnC may contribute to the observed changes in myofilament Ca^{2+} sensitivity observed with various TnI mutations (Gordon et al., 2000). Another important parameter describing the interaction of troponin with Ca^{2+} is the Ca^{2+} dissociation rate constant. This rate has been suggested to play an important role in cardiac muscle relaxation (Davis and Tikunova 2008).

Cardiac TnC contains two cysteine residues; Cys-35 which is located in the first calcium binding site and Cys-84 that is located at the C-terminal end of helix D where the TnI-TnC interaction occurs. They can be used to attach fluorophore labels to monitor Ca^{2+} interaction with troponin C. To avoid the pitfalls of labelling the two cysteines and having signals emanating from the two labels, in our lab we generated two

monocysteine mutants of cTnC (cTnC^{C35S} and cTnC^{C84S}) by substitution of either of the two cysteines into a serine. We have used IAANS fluorescence (at both Cys 35 and Cys 84) to measure the Ca²⁺ affinity and Ca²⁺ dissociation kinetics from Ca²⁺ specific site of TnC within troponin complex, reconstituted thin filament, and thin filament in the presence of myosin heads (Dong et al., 1997). Quin-2 is a Ca²⁺ chelator and a fluorophore. This fluorophore was also used to measure the Ca²⁺ dissociation kinetics (Rosenfeld and Taylor 1985).

4.2 Results

4.2.1 Effect of TnI mutation on calcium binding properties

4.2.1.1 Fluorescence Properties of IAANS-Cys 35/84 Labelled TnC

TnC was expressed in E.coli and purified as described in chapter 2. The cysteine at residue 84 was mutated to serine and then the cysteine at position 35 was labelled with IAANS (TnC^{IAANSC35}) to measure the calcium binding at the regulatory site II of cTnC in whole Tn complex. Alternatively cysteine at residue 35 was mutated to serine and then cysteine at position 84 was modified with IAANS (TnC^{IAANSC84}) to measure the calcium binding at the regulatory site II of TnC in thin filament and calcium binding at the regulatory site II of TnC in thin filament in the presence of myosin heads. The proteins were dialysed against a buffer that contained 4 mM Mg²⁺ to saturate the high calcium affinity sites (III and IV) with Mg²⁺.

To measure the calcium binding for TnC in the troponin complex, we have used TnC labelled with IAANS at C35. For TnC^{IAANSC35} alone, the fluorescence emission spectrum was relatively insensitive to Ca²⁺ (Fig. 4.1.A, blue curves). Reconstitution with TnI and TnT to form the Tn complex led to a decrease in the fluorescence emission at 450 nm to about 50% of that in the absence of bound Ca²⁺ (Fig. 4.1.A, green curves). The small difference in fluorescence for TnC^{IAANSC35} reconstituted fully with the thin filament proteins (red curves) made it unsuitable since the signal from free Tn will contribute substantially to the signal obtained with thin filaments. For that we have used TnC^{IAANSC35} to measure the calcium binding for troponin complex.

TnC^{IAANSC84} gave a bigger difference upon Ca²⁺ binding to reconstituted thin filament (red curves) than for the troponin complex (green curves), figure 4.1.B. Hence TnC^{IAANSC84} is suitable to determine Ca²⁺ binding affinity of the thin filament and thin

filament in the presence of myosin head (no interference from any free troponin as this gives only a small signal).

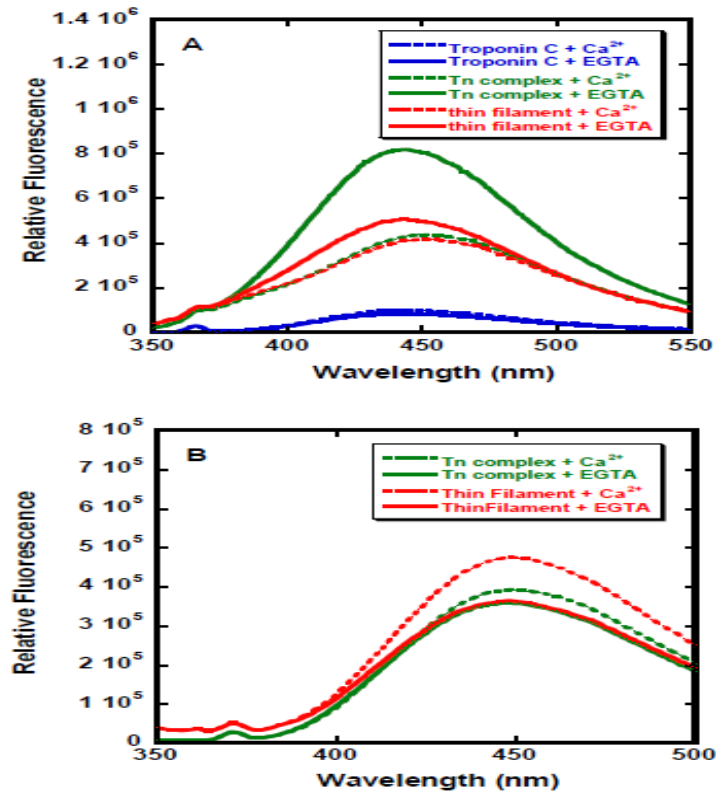


Figure 4.1 Emission spectra of (A) IAANS attached to Cys-35 of cTnC^{C84S} and (B) Cys-84 of cTnC^{C35S} in various regulatory complexes. The TnC subunit (blue), troponin complex (green) and the reconstituted thin filament (red). IAANS was excited at 329 nm. Conditions were 50 mM MOPS pH 7.0, 140 mM KCl, 4 mM MgCl₂, and either 2 mM EGTA (solid lines) or 0.1 mM CaCl₂ (dashed lines) at 25 °C.(adapted from Zimna Wazeer, PhD thesis, University of Leicester)

4.2.1.2 Effect of TnI Mutations on Ca²⁺ affinity of the Tn Complex

We aimed to investigate the effect of TnI mutations on the calcium binding to TnC reconstituted in the troponin complex. Here we used the TnC^{IAANSC35}. Structural sites III and IV were saturated and blocked by 4 mM Mg²⁺. Upon calcium binding to the single regulatory site II, the fluorescence intensity was decreased. Figure 4.2 shows the

fluorescence change given by Ca^{2+} binding to the cTn complex with TnI mutations (given by IAANS-Cys35-TnC). We noted that most mutations affected the start point and end point of the fluorescence despite the fact that we used the same concentration of TnC (and therefore fluorophore concentrations and labelling ratio were the same). Figure 4.3 shows a plot of normalised fluorescence versus pCa. The data were fitted to the Hill equation.

$$\left(\frac{1}{1 + 10^{(n_H \cdot (pCa - pCa_{50}))}} \right) \quad \dots \quad \text{Hill equation (4.1)}$$

The pCa_{50} , K_d , and n_H were determined, table 4.1.

WT Troponin bound Ca^{2+} with a $K_d = 2.13 \times 10^{-7}$ M (pCa_{50} 6.67) which is in agreement with previously determined values (Kobayashi and Solaro 2006; Pinto et al., 2009).

TnI mutations A2V, Q130R, R145G, G203S, and K206Q did not change the pCa_{50} values of fluorescence changes in comparison to the wild type (Figure 4.3). TnIR145G reconstituted in troponin complex showed a Ca^{2+} dissociation constant of ($K_d = 2.09 \times 10^{-7}$ M) which is in agreement with previously determined value ($K_d = 2.24 \times 10^{-7}$ M) (Kobayashi and Solaro 2006). In contrast, TnIR21C gave lower pCa_{50} . Therefore TnI R21C mutation slightly reduced the troponin complex affinity for Ca^{2+} ($K_d = 3.46 \times 10^{-7}$ M) while TnIA157V mutation increased troponin affinity for Ca^{2+} ($K_d = 1.38 \times 10^{-7}$ M).

Since cardiac TnC has only one Ca^{2+} specific site (site II), we expected Ca^{2+} binding to the isolated Tn complex to be non cooperative. Indeed, for all troponin complexes, the Hill coefficient n_H was around 1.0 which indicates the absence of cooperativity in Ca^{2+} binding to cTn as previously reported (Kobayashi and Solaro 2006).

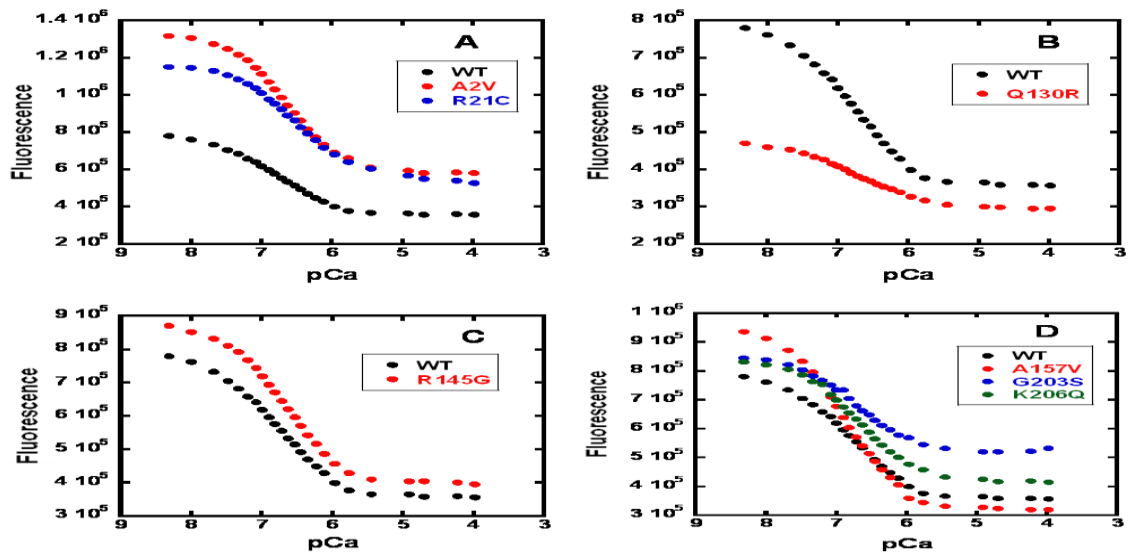


Figure 4.2 Ca^{2+} binding to the cTn complex with TnI mutations given by IAANS-Cys35-TnC. Fluorescence emission intensity change was plotted against free Ca^{2+} concentration. (A) N-terminal TnC binding region (B) TnT binding region (C) Inhibitory region (D) C-terminal TnC binding region HCM and DCM mutations reconstituted in troponin complexes.

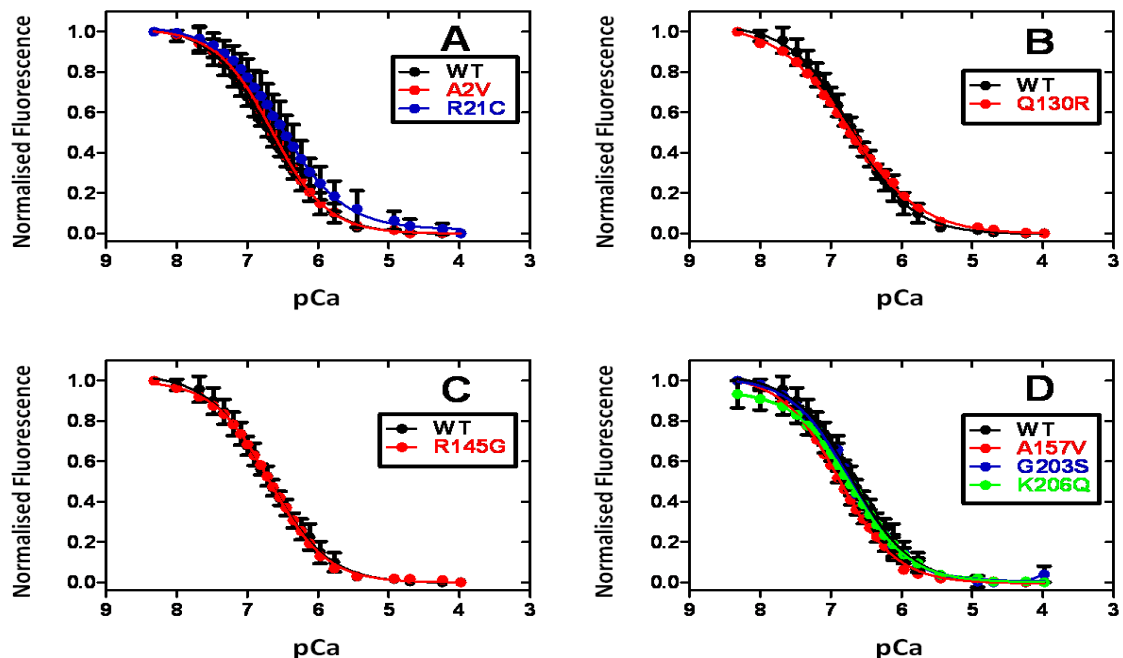


Figure 4.3 Representative data for the Ca^{2+} binding to the cTn complex with TnI mutations given by IAANS-Cys35-TnC. Relative fluorescence emission intensity change was plotted against free Ca^{2+} concentration. (A) N-terminal TnC binding region (B) TnT binding region (C) Inhibitory region (D) C-terminal TnC binding region HCM and DCM mutations reconstituted in troponin complexes. The data obtained are from at least three experiments and the curves are fit to equation (4.1).

Table 4.1 Summary of the effect of TnI mutations on the calcium binding properties of Tn complex by using TnC^{IAANSC35}

Troponin I	pCa₅₀	Hill coefficient (n_H)	K_d (M)
Wild Type	6.67 ± 0.04	1.08 ± 0.03	2.13 ± 0.02 x 10⁻⁷
A2V	6.63 ± 0.004	1.14 ± 0.004	2.34 ± 0.003 x 10⁻⁷
R21C	6.46 ± 0.07	1.00 ± 0.06	3.46 ± 0.07 x 10⁻⁷
Q130R	6.70 ± 0.01	1.00 ± 0.01	1.99 ± 0.02 x 10⁻⁷
R145G	6.68 ± 0.01	1.09 ± 0.008	2.09 ± 0.03 x 10⁻⁷
A157V	6.87 ± 0.02	1.11 ± 0.01	1.38 ± 0.02 x 10⁻⁷
G203S	6.71 ± 0.03	1.09 ± 0.02	1.95 ± 0.02 x 10⁻⁷
K206Q	6.75 ± 0.03	0.97 ± 0.03	1.78 ± 0.03 x 10⁻⁷

(Data are shown as mean ± S.E)

4.2.1.3 Effect of TnI mutations on the Ca²⁺ affinity of Thin Filaments

In this experiment, we have used the TnC^{IAANSC84} to measure the Ca²⁺ binding to reconstituted thin filament. Since the Ca²⁺ dependent IAANS-C35 fluorescence change of free troponin is bigger than the change in thin filament reconstituted with Tn complex (section 4.2.1.2), it is not accurate to measure the Ca²⁺ binding to reconstituted thin filament using TnC^{IAANSC35} because of the potential contribution of fluorescence change from free troponin complex.

The fluorescence intensity of TnC^{IAANS84} was increased upon calcium binding. The IAANSC84 probe gave very little change upon Ca²⁺ binding to free troponin and a bigger change upon Ca²⁺ binding to troponin reconstituted in thin filaments, so any excess amount of free Tn complex would not affect the fluorescence measurements (Kobayashi and Solaro 2006). Figure 4.4 shows the fluorescence change given by Ca²⁺ binding to thin filament reconstituted with TnI mutations (given by IAANS-Cys84-TnC). Figure 4.5 shows a plot of normalised fluorescence versus pCa. The data were fitted to the Hill equation (equation 1), table 4.2. For the wild type troponin reconstituted in thin filament, we found that the pCa₅₀ was 6.29 ($K_d = 5.12 \times 10^{-7}$ M). Hence Ca²⁺ binding to thin filament is 2 fold weaker than Tn complex in agreement with previous report (Rosenfeld and Taylor 1986). The Hill coefficient increased to a value of 2.25 which suggests that calcium binding to cardiac thin filament is cooperative.

All TnI mutation showed tighter calcium affinity for thin filament compared to the wild type. However the increase in the affinity for Ca²⁺ is rather small (less than 2 fold). The data obtained with R145G ($K_d = 3.24 \times 10^{-7}$ M) are in close agreement with previous reports (Kobayashi and Solaro 2006).

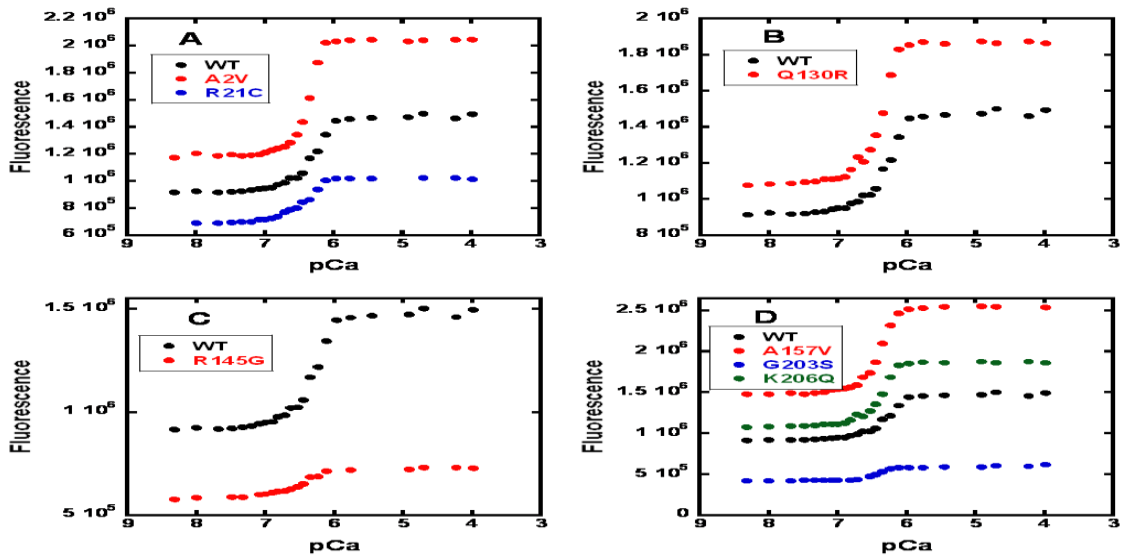


Figure 4.4 Ca^{2+} binding to the thin filament reconstituted with TnI mutations given by IAANS-Cys84-TnC. Fluorescence emission intensity change was plotted against free Ca^{2+} concentration. (A) N-terminal TnC binding region (B) TnT binding region (C) Inhibitory region (D) C-terminal TnC binding region HCM and DCM mutations reconstituted in thin filaments.

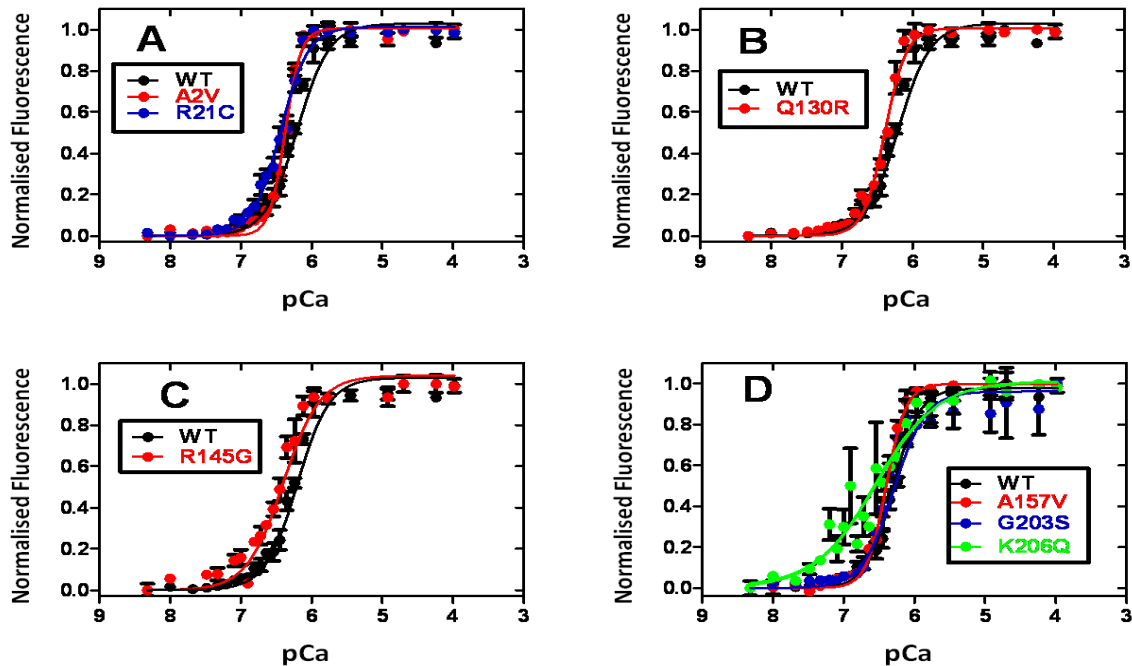


Figure 4.5. Representative data for the Ca^{2+} binding to the thin filament reconstituted with TnI mutations given by IAANS-Cys84-TnC. Relative fluorescence emission intensity change was plotted against free Ca^{2+} concentration. (A) N-terminal TnC binding region (B) TnT binding region (C) Inhibitory region (D) C-terminal TnC binding region HCM and DCM mutations reconstituted in thin filaments. The data obtained are from at least three experiments and the curves are fit to equation (4.1).

Table 4.2 Summary of the effect of TnI mutations on the calcium binding properties of regulated thin filament by using TnC^{IAANSC84}

Troponin I	pCa₅₀	Hill coefficient (n_H)	K_d (M)
Wild Type	6.29 ± 0.01	2.25 ± 0.28	5.12 ± 0.02 x10⁻⁷
A2V	6.37 ± 0.03	3.93 ± 0.50	4.26 ± 0.03 x10⁻⁷
R21C	6.44 ± 0.03	2.25 ± 0.27	3.63 ± 0.03 x10⁻⁷
Q130R	6.39 ± 0.01	2.90 ± 0.37	4.07 ± 0.02 x10⁻⁷
R145G	6.49 ± 0.03	1.66 ± 0.22	3.24 ± 0.04 x10⁻⁷
A157V	6.40 ± 0.02	3.11 ± 0.42	3.98 ± 0.02 x10⁻⁷
G203S	6.37 ± 0.03	2.12 ± 0.56	4.26 ± 0.03 x10⁻⁷
K206Q	6.56 ± 0.07	1.02 ± 0.54	2.75 ± 0.04 x10⁻⁷

(Data are shown as mean ± S.E)

4.2.1.4 Effect of TnI mutations on the Ca²⁺ affinity of Thin Filaments in the presence of rigor myosin heads

It has been shown that when myosin heads bind to regulated actin as a rigor complex in the absence of MgATP, the thin filament exhibits an increased affinity for Ca²⁺ (Bremel and Weber 1972). In this experiment, we have used the TnC^{IAANSC84} to measure the Ca²⁺ binding to reconstituted thin filament in the presence of rigor myosin heads for the same reasons cited in the previous section (namely bigger signal and absence of potential contribution from free Tn), figure 4.1. Figure 4.6 shows the fluorescence change given by Ca²⁺ binding to the thin filament in the presence of myosin heads (given by IAANS-Cys84-TnC).

Figure 4.7 shows a plot of normalised fluorescence versus pCa. The data were fitted to the Hill equation (equation 1), Table 4.3. For the wild type troponin reconstituted in thin filament and in the presence of myosin heads, the pCa₅₀ was 6.78 ($K_d = 1.66 \times 10^{-7}$ M). In the presence of myosin heads, the Ca²⁺ affinity increased to the same level of Tn complex. The Hill coefficient reduced to a value close to 1 and that suggests that calcium binding to thin filament in the presence of myosin heads is not cooperative (table 4.3).

All TnI mutations showed the same trend as the wild type, in the presence of myosin heads, the affinity of thin filament for Ca²⁺ was increased. In addition there was little effect of TnI mutations on the affinity of Ca²⁺ to thin filaments in the presence of rigor.

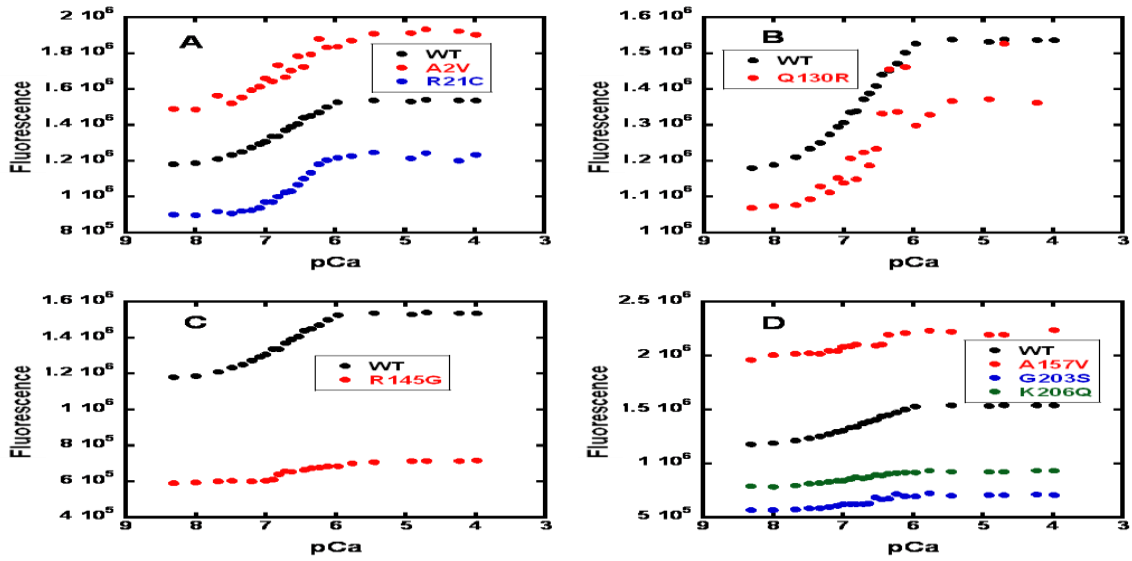


Figure 4.6 Ca^{2+} binding to the thin filament reconstituted with TnI mutations in the presence of myosin heads given by IAANS-Cys84-TnC. Fluorescence emission intensity change was plotted against free Ca^{2+} concentration. (A) N-terminal TnC binding region (B) TnT binding region (C) Inhibitory region (D) C-terminal TnC binding region HCM and DCM mutations reconstituted in thin filaments in the presence of myosin heads.

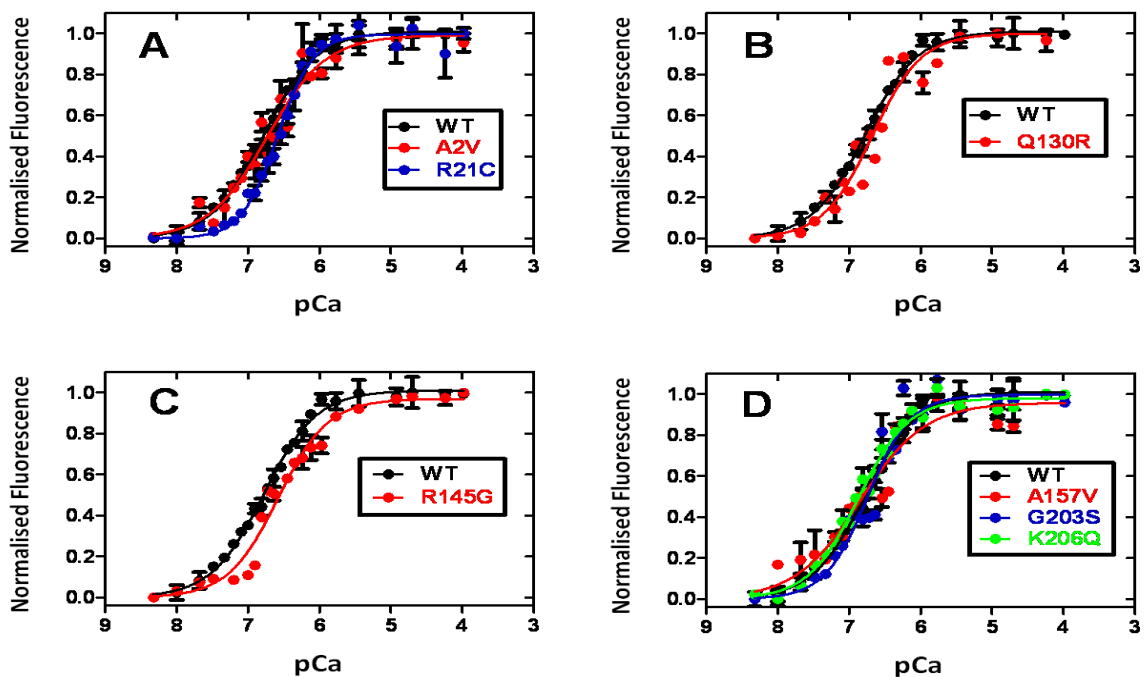


Figure 4.7 Representative data for the Ca^{2+} binding to the thin filament reconstituted with TnI mutations in the presence of myosin heads given by IAANS-Cys84-TnC. Relative fluorescence emission intensity change was plotted against free Ca^{2+} concentration. (A) N-terminal TnC binding region (B) TnT binding region (C) Inhibitory region (D) C-terminal TnC binding region HCM and DCM mutations reconstituted in thin filaments in the presence of myosin heads. The data obtained are from at least three experiments and the curves are fit to equation (4.1).

Table 4.3 Summary of the effect of TnI mutations on the calcium binding properties of regulated thin filament in the presence of myosin heads by using TnC^{IAANSC84}

Troponin I	pCa₅₀	Hill coefficient (n_H)	K_d (M)
Wild Type	6.78 ± 0.02	1.19 ± 0.02	1.66 ± 0.03 x10⁻⁷
A2V	6.72 ± 0.04	1.04 ± 0.04	1.90 ± 0.04 x10⁻⁷
R21C	6.58 ± 0.02	1.72 ± 0.02	2.63 ± 0.03 x10⁻⁷
Q130R	6.74 ± 0.04	2.01 ± 0.03	1.82 ± 0.05 x10⁻⁷
R145G	6.55 ± 0.03	1.16 ± 0.02	2.82 ± 0.04 x10⁻⁷
A157V	6.80 ± 0.06	0.89 ± 0.05	1.58 ± 0.07 x10⁻⁷
G203S	6.74 ± 0.03	1.43 ± 0.03	1.82 ± 0.04 x10⁻⁷
K206Q	6.85 ± 0.02	1.20 ± 0.02	1.41 ± 0.03 x10⁻⁷

(Data are shown as mean ± S.E)

4.2.2 Effect of TnI mutations on the kinetics of Ca²⁺ dissociation

4.2.2.1 Ca²⁺ Dissociation kinetics of cTnI mutations using TnC^{IAANSC35}

Ca²⁺ dissociation from thin filament is critical for thin filament switching to the inhibited states (Closed and Blocked) and consequently for Cardiac muscle relaxation. The Ca²⁺ dissociation rate from TnC reconstituted with thin filament in the presence of rigor of myosin heads is thought to play an important role in cardiac muscle relaxation

In this section, we investigated the effect of TnI mutations on the kinetics of Ca²⁺ dissociation from TnC reconstituted within a Tn complex, the thin filament, and the thin filament in the presence of rigor myosin heads. Here, we have used the same TnC^{IAANSC35} to monitor Ca²⁺ dissociation from the Tn complex as has been done in equilibrium binding. Figures 4.8, 4.10, and 4.12 show the stopped-flow kinetic transients of TnC^{IAANSC35} fluorescence change upon Ca²⁺ dissociation from troponin complex, thin filaments, and thin filaments in the presence of rigor myosin heads respectively. The observed rate constant of Ca²⁺ dissociation was obtained after chasing bound Ca²⁺ by an excess of EGTA (the Ca²⁺ chelator). Ca²⁺ dissociation from TnC^{IAANSC35} resulted in fluorescence increase and the rate constant of this fluorescence increase reflected the observed rate constant of Ca²⁺ dissociation.

Figures 4.9, 4.11, and 4.13 show the normalised transients of TnC^{IAANSC35} reconstituted in troponin complex, thin filament, and thin filament in the presence of rigor myosin heads respectively.

The average data was fitted to one exponential equation by a non linear least square curve fit using the Fit control Panel of the Fit Asystant. In figure 4.9, the wild type

troponin complex reconstituted with TnC^{IAANSC35} showed similar rate of calcium dissociation constant as previously reported (Davis et al., 2007). The observed rate constant of Ca²⁺ dissociation from the regulatory domain of WT is 10.8 s⁻¹, table 4.4. All TnI mutation showed the same rate constant of dissociation except the A157 HCM mutation. TnIA157V (4.9.D) showed almost three fold decrease of Ca²⁺ dissociation rate constant (4.1 s⁻¹) compared to the wild type.

As previously reported (Kobayashi and Solaro 2006; Davis et al., 2007), thin filament desensitized and reduced the affinity of the regulatory N-terminal domain of TnC to Ca²⁺. For the TnC^{IAANSC35} reconstituted with thin filament, all TnI mutations and wild type showed about two fold increase of Ca²⁺ dissociation rate. The observed rate constant of Ca²⁺ dissociation of wild type reconstituted with thin filament was 18.4 s⁻¹, two fold higher than for the Tn complex alone (10.8 s⁻¹), (figure 4.11 and table 4.4). TnIA157V showed an increase in Ca²⁺ dissociation rate constant (7.0 s⁻¹) compared to the Tn complex (4.1 s⁻¹), but was still lower than for the wild type Tn reconstituted thin filaments (figure 4.11.D and table 4.4).

The observed rate constant of calcium dissociation from thin filament in the presence of rigor myosin heads was decreased to nearly the same value as for the troponin complex (11 s⁻¹)(figure 4.13 and table 4.4). Again TnI mutations A2V, R21C, Q130R, R145G, G203S, and K206Q did not affect the observed rate constant of Ca²⁺ dissociation from rigor bound thin filaments. TnIA157V showed a lower observed rate constant of Ca²⁺ dissociation (4 s⁻¹) compared to the wild type.

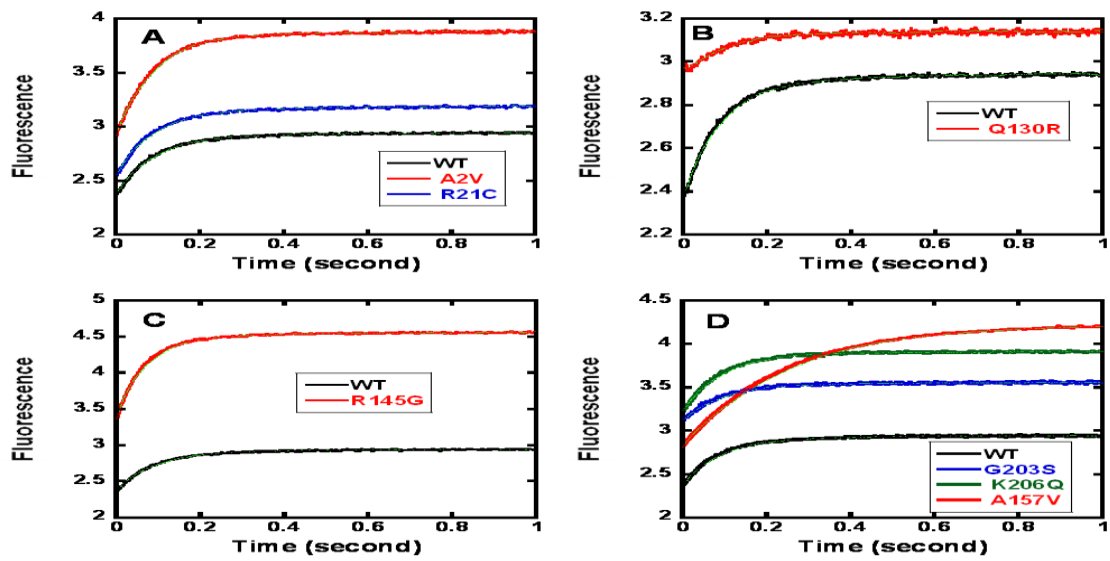


Figure 4.8 Ca^{2+} dissociation fluorescence given by $\text{TnC}^{\text{IAANSC35}}$ reconstituted in Tn complex. (A) N-terminal TnC binding region (B) TnT binding region (C) Inhibitory region (D) C-terminal TnC binding region HCM and DCM mutations. Stopped flow kinetic traces obtained from mixing $4.8 \mu\text{M}$ Tn complexes with an equal volume of the same experiment buffer containing an excess of the Ca^{2+} chelator EGTA (1 mM) at 15°C . Final conditions: 50 mM MOPS pH 7.2, 140 mM KCl, 4 mM MgCl_2 , and $100 \mu\text{M}$ CaCl_2 .

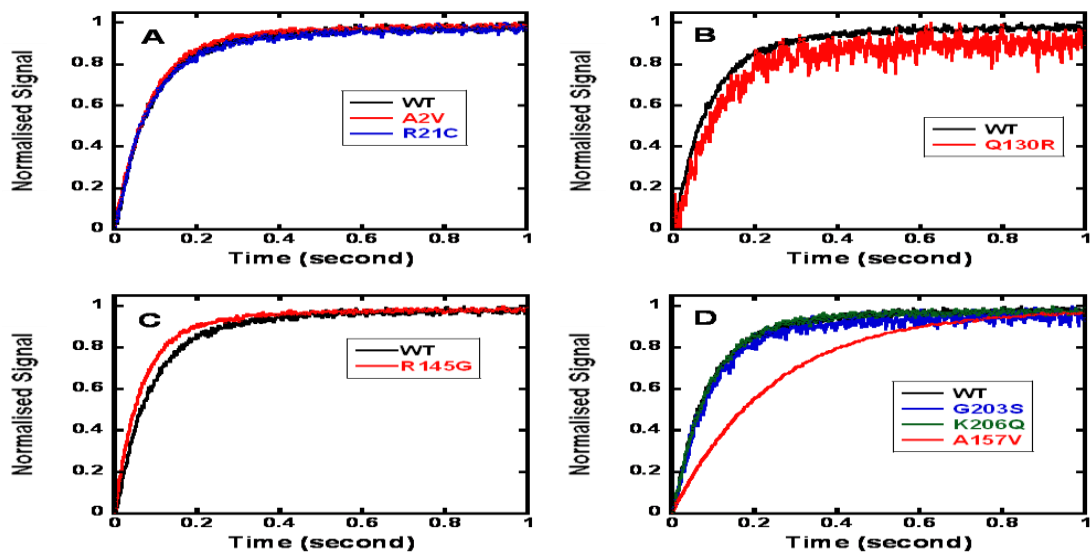


Figure 4.9 Ca^{2+} dissociation normalised fluorescence given by $\text{TnC}^{\text{IAANSC35}}$ reconstituted in Tn complex. (A) N-terminal TnC binding region (B) TnT binding region (C) Inhibitory region (D) C-terminal TnC binding region HCM and DCM mutations. Stopped flow kinetic normalised traces obtained from mixing $4.8 \mu\text{M}$ Tn complexes with an equal volume of the same experiment buffer containing an excess of the Ca^{2+} chelator EGTA (1 mM) at 15°C .

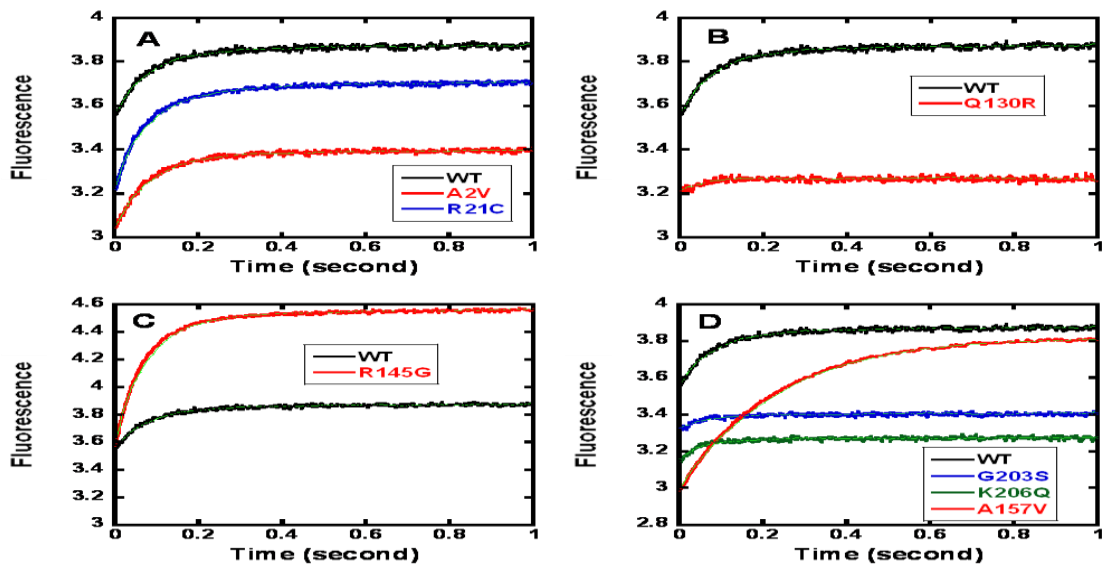


Figure 4.10 Ca^{2+} dissociation fluorescence given by $\text{TnC}^{\text{IAANSC35}}$ reconstituted in thin filament. (A) N-terminal TnC binding region (B) TnT binding region (C) Inhibitory region (D) C-terminal TnC binding region HCM and DCM mutations. Stopped flow kinetic traces obtained from mixing $4.8 \mu\text{M}$ Tn complexes reconstituted in thin filament ($28 \mu\text{M}$ c-Actin and $5.6 \mu\text{M}$ c-Tm) with an equal volume of the same experiment buffer containing an excess of the Ca^{2+} chelator EGTA (1 mM) at $15 \text{ }^\circ\text{C}$. Final conditions: 50 mM MOPS pH 7.2, 140 mM KCl, 4 mM MgCl_2 , and $100 \mu\text{M}$ CaCl_2 .

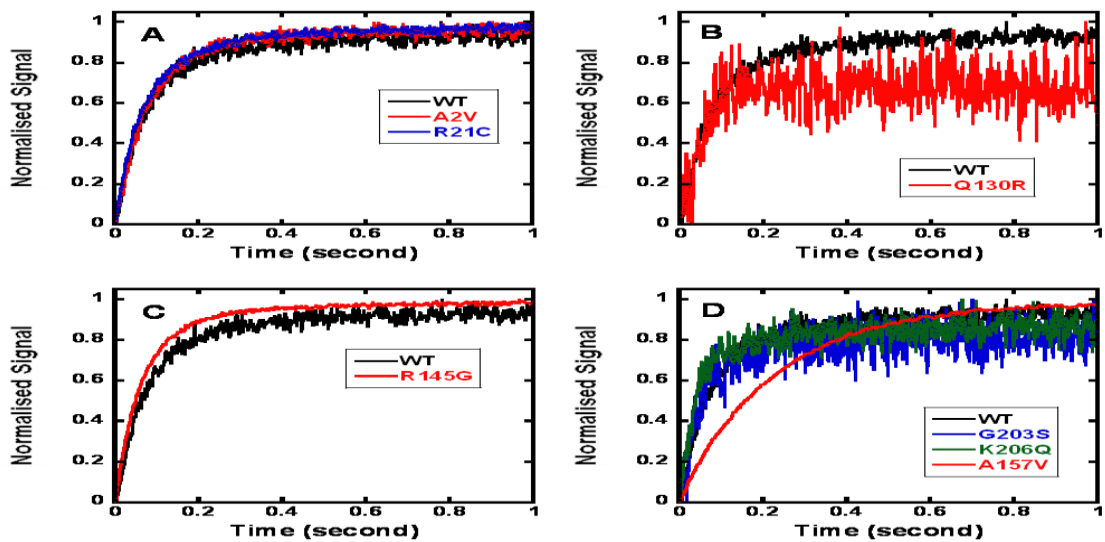


Figure 4.11 Ca^{2+} dissociation normalised fluorescence given by $\text{TnC}^{\text{IAANSC35}}$ reconstituted in thin filament. (A) N-terminal TnC binding region (B) TnT binding region (C) Inhibitory region (D) C-terminal TnC binding region HCM and DCM mutations. Stopped flow kinetic normalised traces obtained from mixing $4.8 \mu\text{M}$ Tn complexes reconstituted in thin filament ($28 \mu\text{M}$ c-Actin and $5.6 \mu\text{M}$ c-Tm) with an equal volume of the same experiment buffer containing an excess of the Ca^{2+} chelator EGTA (1 mM) at $15 \text{ }^\circ\text{C}$.

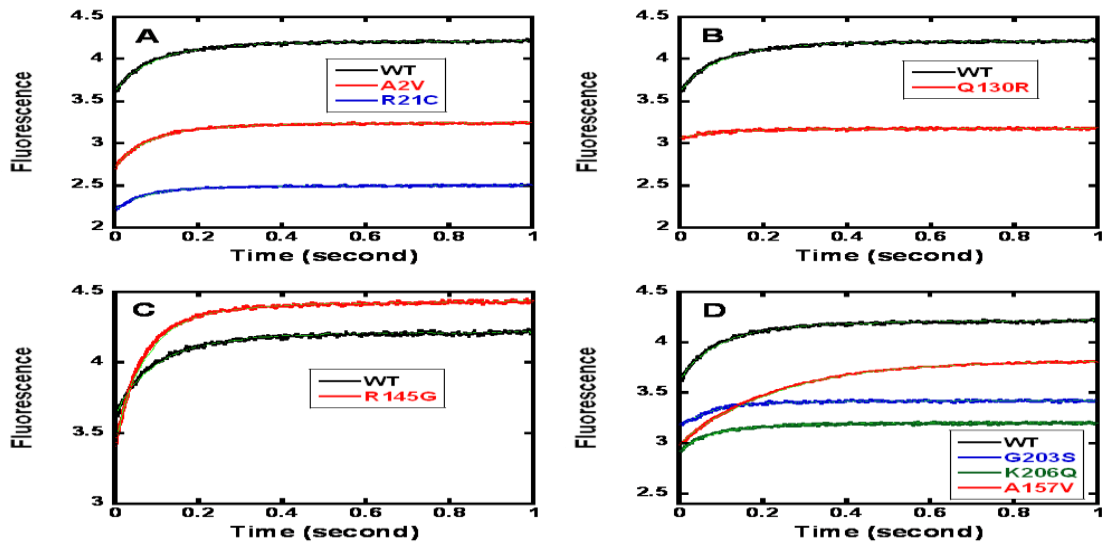


Figure 4.12 Ca^{2+} dissociation fluorescence given by $\text{TnC}^{\text{IAANSC35}}$ reconstituted in thin filament + rigor myosin heads. (A) N-terminal TnC binding region (B) TnT binding region (C) Inhibitory region (D) C-terminal TnC binding region HCM and DCM mutations. Stopped flow kinetic traces obtained from mixing $4.8 \mu\text{M}$ Tn complexes reconstituted in thin filament + rigor myosin heads ($28 \mu\text{M}$ c-Actin, $5.6 \mu\text{M}$ c-Tm, and $7 \mu\text{M}$ sk-S1) with an equal volume of the same experiment buffer containing an excess of the Ca^{2+} chelator EGTA (1 mM) at 15°C . Final conditions: 50 mM MOPS pH 7.2, 140 mM KCl, 4 mM MgCl_2 , and $100 \mu\text{M}$ CaCl_2 .

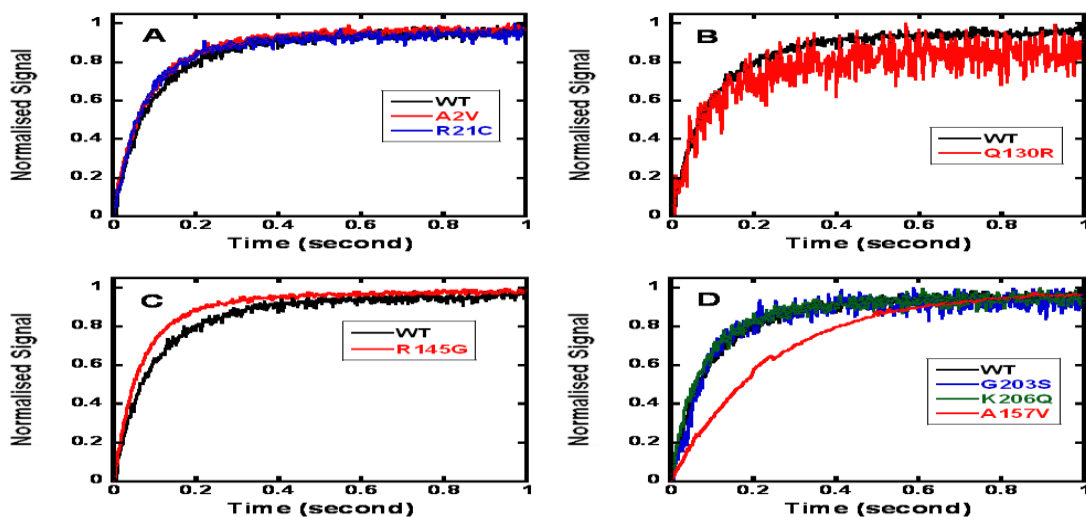


Figure 4.13 Ca^{2+} dissociation normalised fluorescence given by $\text{TnC}^{\text{IAANSC35}}$ reconstituted in thin filament + rigor myosin heads. (A) N-terminal TnC binding region (B) TnT binding region (C) Inhibitory region (D) C-terminal TnC binding region HCM and DCM mutations. Stopped flow kinetic normalised traces obtained from mixing $4.8 \mu\text{M}$ Tn complexes reconstituted in thin filament + rigor myosin heads ($28 \mu\text{M}$ c-Actin, $5.6 \mu\text{M}$ c-Tm, and $7 \mu\text{M}$ sk-S1) with an equal volume of the same experiment buffer containing an excess of the Ca^{2+} chelator EGTA (1 mM) at 15°C .

Table 4.4 Summary of the effect of cTnI mutations on the Ca²⁺ dissociation rate constant obtained by using TnC^{IAANSC35} probe.

Troponin I	Troponin complex Rate (s⁻¹)	Thin filament Rate (s⁻¹)	Thin filament + S1 Rate (s⁻¹)
Wild Type	10.8 ± 2.5	18.4 ± 3.2	11.0 ± 2.9
A2V	11.2 ± 3.1	19.4 ± 2.7	10.3 ± 3.5
R21C	10.7 ± 2.7	20.5 ± 3.4	11.7 ± 1.8
Q130R	9.60 ± 3.3	16.6 ± 4.1	9.90 ± 2.2
R145G	13.9 ± 3.3	19.0 ± 3.7	13.2 ± 2.8
A157V	4.10 ± 0.9	7.00 ± 1.5	4.00 ± 1.3
G203S	10.7 ± 2.7	16.8 ± 2.9	12.0 ± 3.0
K206Q	11.1 ± 2.9	23.0 ± 3.6	11.2 ± 2.7

(Data are shown as mean ± S.E)

4.2.2.2 Ca²⁺ Dissociation kinetics of cTnI mutations using TnC^{IAANSC84}

We used TnC^{IAANSC84} to measure the Ca²⁺ dissociation constant for Tn complex, thin filament, and thin filament in the presence of rigor myosin heads. Figures 4.14, 4.16 and 4.18 show the transients of TnC^{IAANSC84} fluorescence change upon Ca²⁺ dissociation for TnI mutations reconstituted in troponin complex, thin filament, and thin filament in the presence of rigor myosin heads respectively. Figure 4.15 shows the Ca²⁺ dependent decrease in IAANS-Cys84 fluorescence in the Tn complex for wild type and TnI HCM and DCM mutations. The average data was fitted to two exponential equations by a non linear least square curve fit using the Fit control Panel of the Fit Assistant. For WT Tn complex, an observed rate constant of 42 s⁻¹ was obtained which is in a strong agreement with the value previously reported using TnC^{IAANST53C} (41.9 s⁻¹) (Davis et al., 2007). Although the signal of TnC^{IAANSC84} reconstituted in Tn complex is small, the experimental design is different from equilibrium binding experiments. In the later experiments, the total amplitude should be sufficiently large to divide it over a number of incremental points. In the kinetic approach the total amplitude is used every point and the measured parameter (observed rate constant) is not dependent on the amplitude. All TnI mutation showed similar rate constants as the wild type except the DCM mutation A2V (35 s⁻¹) and the HCM mutation A157V (30 s⁻¹). With the exception of TnIA157V, all TnI mutants reconstituted with the thin filament showed no difference in the rate of Ca²⁺ dissociation compared to the wild type (89 s⁻¹), figure 4.17 and table 4.5. This value is also close to the value that has been obtained by using TnC^{IAANST53C} (Davis et al., 2007). TnIA157V reconstituted in thin filament showed slower Ca²⁺ dissociation rate (74 s⁻¹) than the wild type (89 s⁻¹). Rigor myosin binding wild type and all TnI mutants reconstituted in thin filament showed decrease Ca²⁺ dissociation

rate constants (rate for wild type is 38 s^{-1}). TnIA2V DCM mutant and TnIA157V HCM mutant showed lower observed rate constant of Ca^{2+} dissociation in comparison to the wild type (31 s^{-1} and 24 s^{-1} respectively)(figure 4.19 and table 4.5).

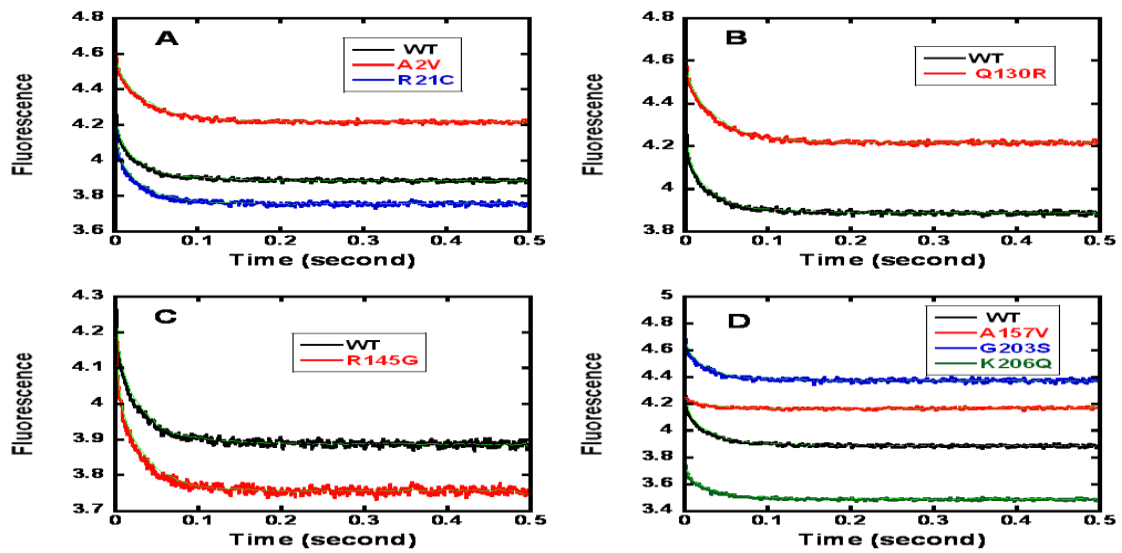


Figure 4.14 Ca^{2+} dissociation fluorescence given by $\text{TnC}^{\text{IAANSC84}}$ reconstituted in Tn complex. (A) N-terminal TnC binding region (B) TnT binding region (C) Inhibitory region (D) C-terminal TnC binding region HCM and DCM mutations. Stopped flow kinetic traces obtained from mixing $4.8 \mu\text{M}$ Tn complexes with an equal volume of the same experiment buffer containing an excess of the Ca^{2+} chelator EGTA (1 mM) at 15°C . Final conditions: 50 mM MOPS pH 7.2, 140 mM KCl, 4 mM MgCl_2 , and $100 \mu\text{M}$ CaCl_2 .

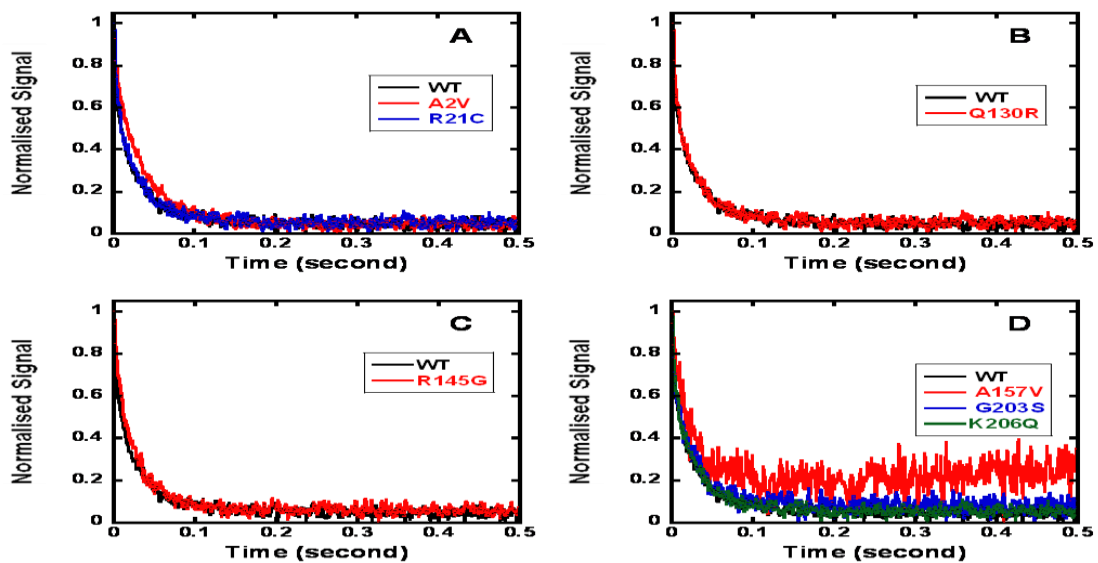


Figure 4.15 Ca^{2+} dissociation normalised fluorescence given by $\text{TnC}^{\text{IAANSC84}}$ reconstituted in Tn complex. (A) N-terminal TnC binding region (B) TnT binding region (C) Inhibitory region (D) C-terminal TnC binding region HCM and DCM mutations. Stopped flow kinetic normalised traces obtained from mixing $4.8 \mu\text{M}$ Tn complexes with an equal volume of the same experiment buffer containing an excess of the Ca^{2+} chelator EGTA (1 mM) at 15°C .

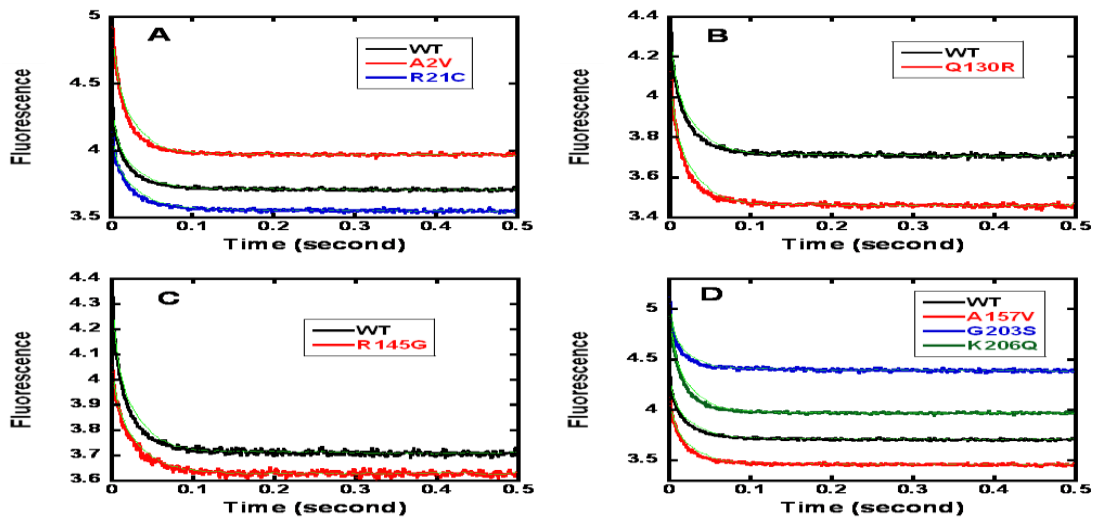


Figure 4.16 Ca^{2+} dissociation fluorescence given by $\text{TnC}^{\text{IAANSC84}}$ reconstituted in thin filament. (A) N-terminal TnC binding region (B) TnT binding region (C) Inhibitory region (D) C-terminal TnC binding region HCM and DCM mutations. Stopped flow kinetic traces obtained from mixing $4.8 \mu\text{M}$ Tn complexes reconstituted in thin filament ($28 \mu\text{M}$ c-Actin and $5.6 \mu\text{M}$ c-Tm) with an equal volume of the same experiment buffer containing an excess of the Ca^{2+} chelator EGTA (1 mM) at $15 \text{ }^\circ\text{C}$. Final conditions: 50 mM MOPS pH 7.2, 140 mM KCl, 4 mM MgCl_2 , and $100 \mu\text{M}$ CaCl_2 .

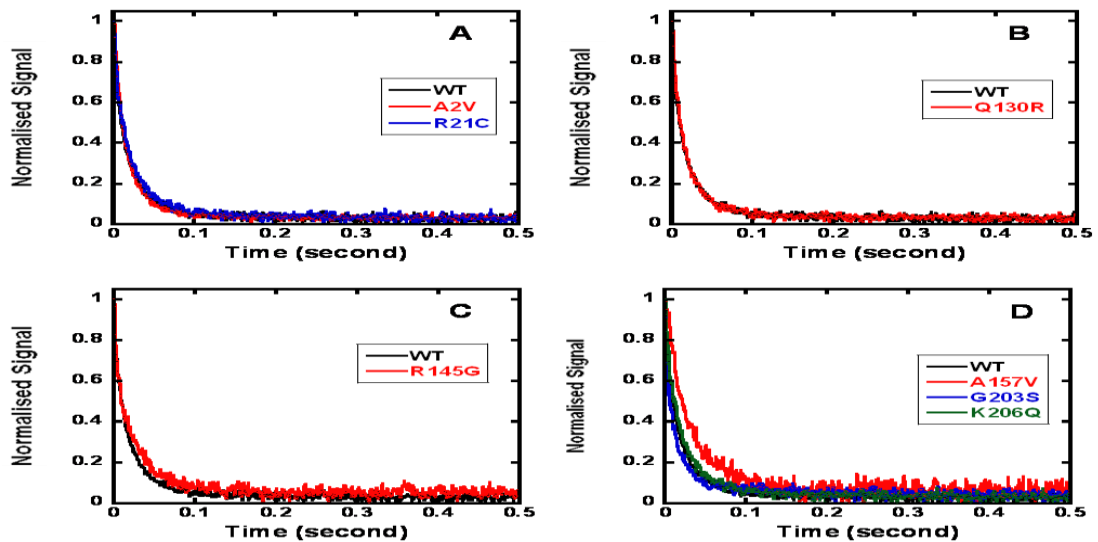


Figure 4.17 Ca^{2+} dissociation normalised fluorescence given by $\text{TnC}^{\text{IAANSC84}}$ reconstituted in thin filament. (A) N-terminal TnC binding region (B) TnT binding region (C) Inhibitory region (D) C-terminal TnC binding region HCM and DCM mutations. Stopped flow kinetic normalised traces obtained from mixing $4.8 \mu\text{M}$ Tn complexes reconstituted in thin filament ($28 \mu\text{M}$ c-Actin and $5.6 \mu\text{M}$ c-Tm) with an equal volume of the same experiment buffer containing an excess of the Ca^{2+} chelator EGTA (1 mM) at $15 \text{ }^\circ\text{C}$.

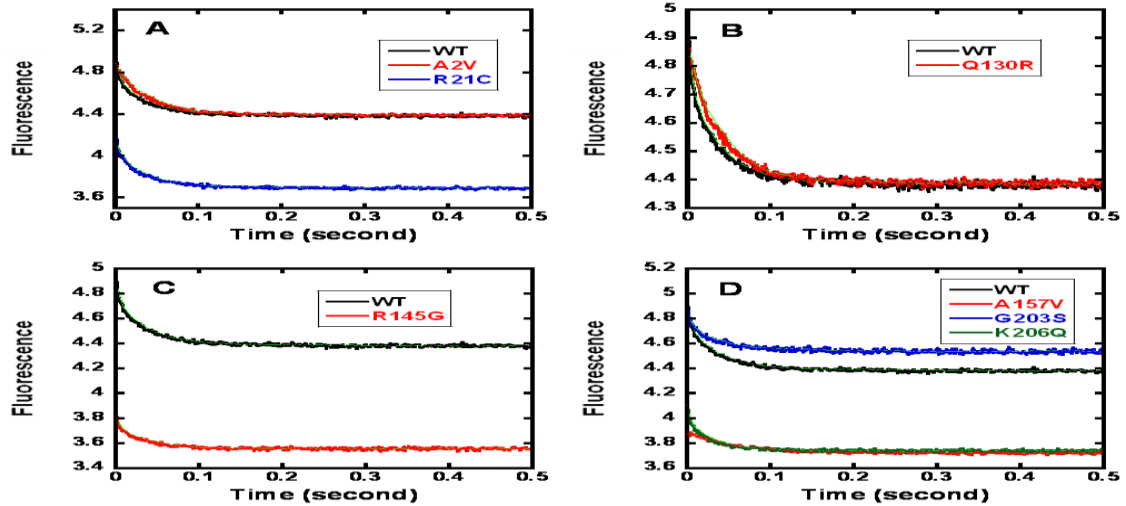


Figure 4.18 Ca^{2+} dissociation fluorescence given by $\text{TnC}^{\text{IAANSC84}}$ reconstituted in thin filament + rigor myosin heads. (A) N-terminal TnC binding region (B) TnT binding region (C) Inhibitory region (D) C-terminal TnC binding region HCM and DCM mutations. Stopped flow kinetic traces obtained from mixing $4.8 \mu\text{M}$ Tn complexes reconstituted in thin filament + rigor myosin heads ($28 \mu\text{M}$ c-Actin, $5.6 \mu\text{M}$ c-Tm, and $7 \mu\text{M}$ sk-S1) with an equal volume of the same experiment buffer containing an excess of the Ca^{2+} chelator EGTA (1 mM) at 15°C . Final conditions: 50 mM MOPS pH 7.2, 140 mM KCl, 4 mM MgCl_2 , and $100 \mu\text{M}$ CaCl_2 .

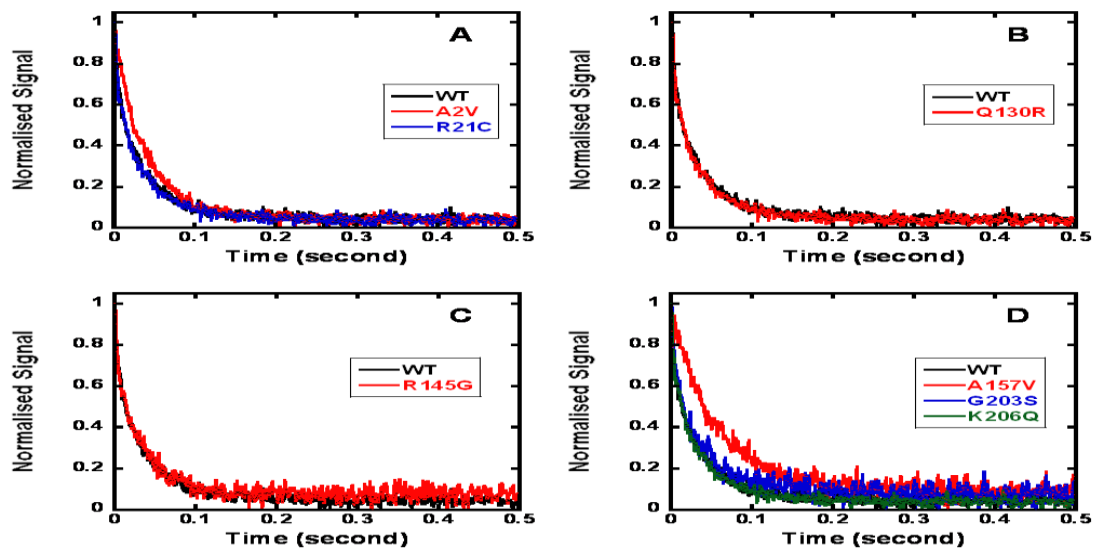


Figure 4.19 Ca^{2+} dissociation normalised fluorescence given by $\text{TnC}^{\text{IAANSC84}}$ reconstituted in thin filament + rigor myosin heads. (A) N-terminal TnC binding region (B) TnT binding region (C) Inhibitory region (D) C-terminal TnC binding region HCM and DCM mutations. Stopped flow kinetic normalised traces obtained from mixing $4.8 \mu\text{M}$ Tn complexes reconstituted in thin filament + rigor myosin heads ($28 \mu\text{M}$ c-Actin, $5.6 \mu\text{M}$ c-Tm, and $7 \mu\text{M}$ sk-S1) with an equal volume of the same experiment buffer containing an excess of the Ca^{2+} chelator EGTA (1 mM) at 15°C .

Table 4.5 Summary of the effect of cTnI mutations on the Ca²⁺ dissociation rate constant obtained by using TnC^{IAANSC84} probe.

Troponin I	Troponin complex	Rate (s⁻¹)	Thin filament	Rate (s⁻¹)	Thin filament + S1	Rate (s⁻¹)
Wild Type	42 ± 5.7		89 ± 5.1		38 ± 2.7	
A2V	35 ± 4.9		91 ± 3.2		31 ± 3.3	
R21C	43 ± 5.7		86 ± 3.2		39 ± 1.7	
Q130R	40 ± 4.1		93 ± 4.6		37 ± 2.2	
R145G	44 ± 3.9		88 ± 2.8		37 ± 3.6	
A157V	30 ± 2.1		74 ± 1.9		24 ± 2.3	
G203S	43 ± 3.3		95 ± 5.4		37 ± 3.8	
K206Q	42 ± 4.5		92 ± 2.6		38 ± 2.7	

(Data are shown as mean ± S.E)

4.2.2.3 Ca²⁺ dissociation kinetics of cTnI mutations using Quin-2

Ca²⁺ dissociation from troponin complex, thin filament, and thin filament + rigor myosin heads was also measured using the fluorophores and Ca²⁺ chelator Quin-2 (Tsien 1983). Native troponin complexes or troponin complexes reconstituted with thin filament in the presence and absence of rigor myosin heads were mixed with a large excess of Quin-2. The results were very close to the measurements using IAANS-Cys 84.

Figures 4.20, 4.22, and 4.24 show the stopped-flow kinetic transients of calcium dissociation from troponin complex, thin filament, and thin filament in the presence of rigor myosin heads respectively by using Quin-2.

The normalised fluorescent signal for Ca²⁺ dissociation from wild type troponin complex at 15 °C is shown in figure 4.21. The fitting gave two observed rate constants of fast phase at 49 s⁻¹ and slow phase at 6 s⁻¹ which is in agreement with previously determined values (Gomes et al., 2004; Davis et al., 2007). It has been shown before that the fast step measures the calcium dissociation from the regulatory site (Rosenfeld and Taylor 1985; Martin et al., 1992).

No significant differences were seen for all mutations studied here except for TnIA157V. This mutation showed lower calcium dissociation rate compared to WT in all three systems, troponin, thin filaments and rigor bound thin filaments (figure 4.21, 4.23, and 4.25 and table 4.6).

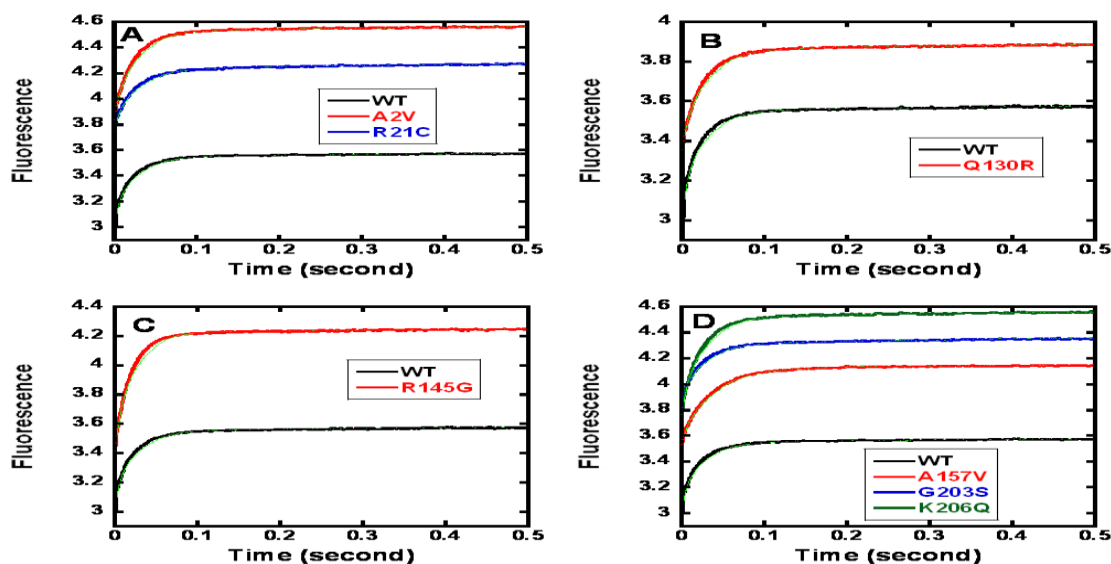


Figure 4.20 Ca^{2+} dissociation fluorescence given by Quin-2 of reconstituted Tn complex. (A) N-terminal TnC binding region (B) TnT binding region (C) Inhibitory region (D) C-terminal TnC binding region HCM and DCM mutations. Stopped flow kinetic traces obtained from mixing 16 μM Tn complexes with an equal volume of the same experiment buffer containing an excess of Quin-2 (150 μM) at 15 $^{\circ}\text{C}$. Final conditions: 50 mM MOPS pH 7.2, 140 mM KCl, 4 mM MgCl_2 , and 30 μM CaCl_2 .

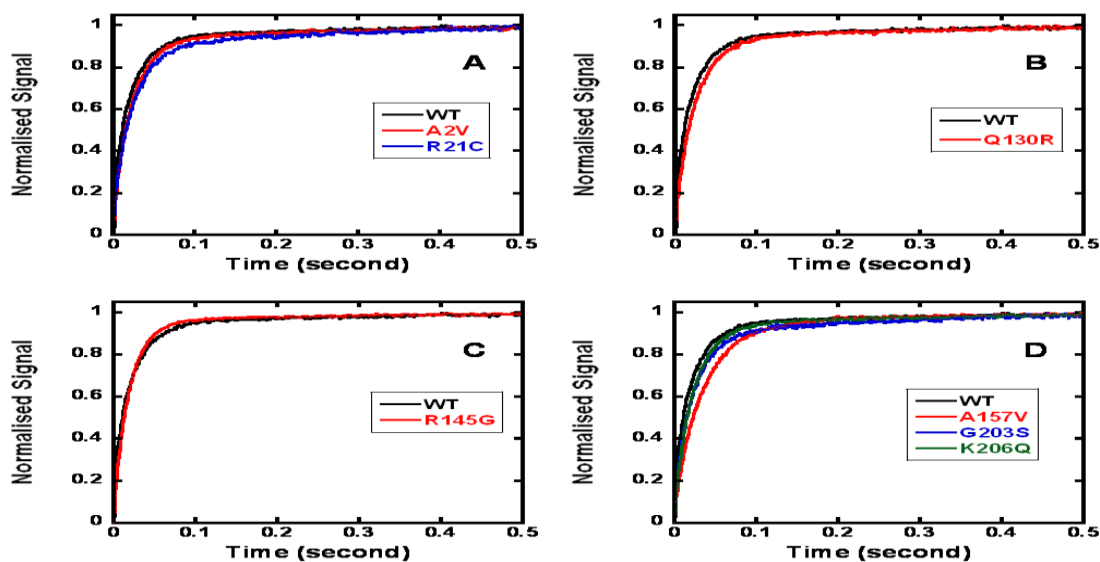


Figure 4.21 Ca^{2+} dissociation normalised fluorescence given by Quin-2 of reconstituted Tn complex. (A) N-terminal TnC binding region (B) TnT binding region (C) Inhibitory region (D) C-terminal TnC binding region HCM and DCM mutations. Stopped flow kinetic normalised traces obtained from mixing 16 μM Tn complexes with an equal volume of the same experiment buffer containing an excess of Quin-2 (150 μM) at 15 $^{\circ}\text{C}$.

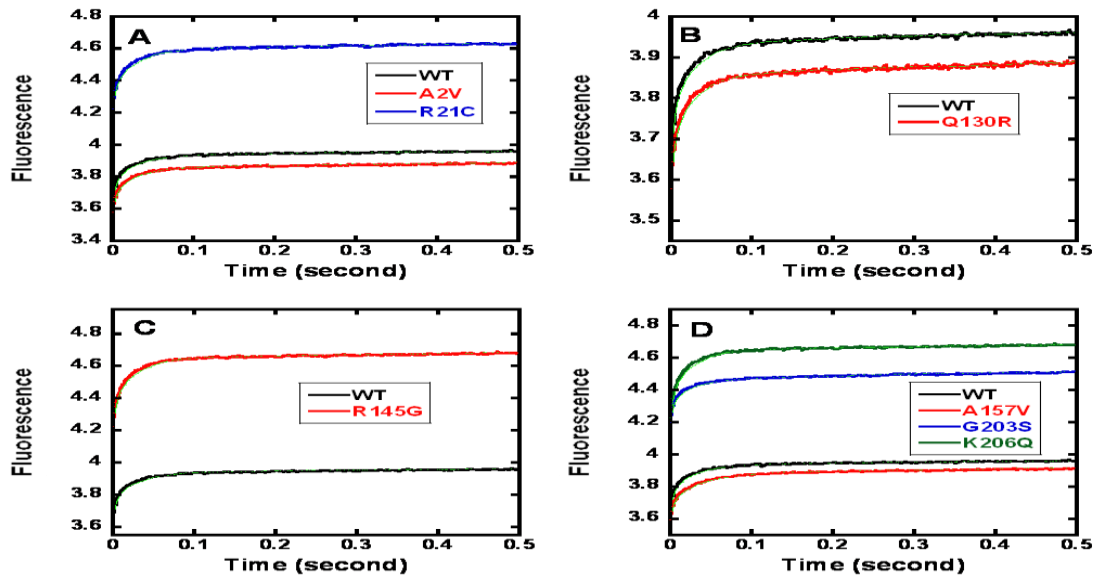


Figure 4.22 Ca^{2+} dissociation fluorescence given by Quin-2 of thin filament. (A) N-terminal TnC binding region (B) TnT binding region (C) Inhibitory region (D) C-terminal TnC binding region HCM and DCM mutations. Stopped flow kinetic traces obtained from mixing $8 \mu\text{M}$ Tn complexes reconstituted in thin filament ($48 \mu\text{M}$ c-Actin and $9.6 \mu\text{M}$ c-Tm) with an equal volume of the same experiment buffer containing an excess of Quin-2 ($150 \mu\text{M}$) at 15°C . Final conditions: 50 mM MOPS pH 7.2, 140 mM KCl, 4 mM MgCl_2 , and $30 \mu\text{M}$ CaCl_2 .

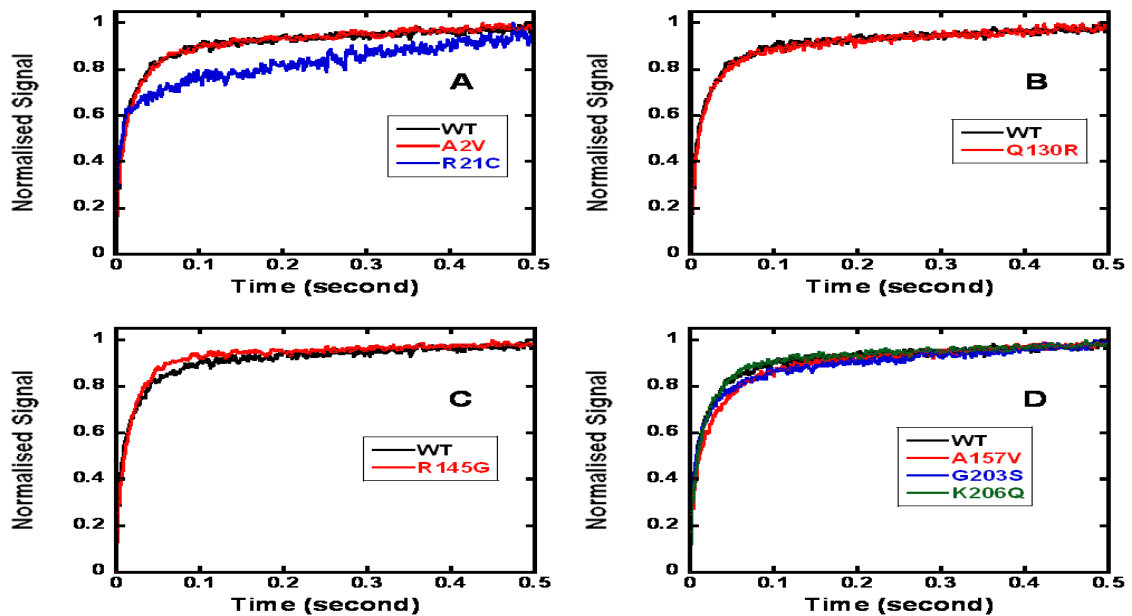


Figure 4.23 Ca^{2+} dissociation normalised fluorescence given by Quin-2 of thin filament. (A) N-terminal TnC binding region (B) TnT binding region (C) Inhibitory region (D) C-terminal TnC binding region HCM and DCM mutations. Stopped flow kinetic normalised traces obtained from mixing $8 \mu\text{M}$ Tn complexes reconstituted in thin filament ($48 \mu\text{M}$ c-Actin and $9.6 \mu\text{M}$ c-Tm) with an equal volume of the same experiment buffer containing an excess of Quin-2 ($150 \mu\text{M}$) at 15°C .

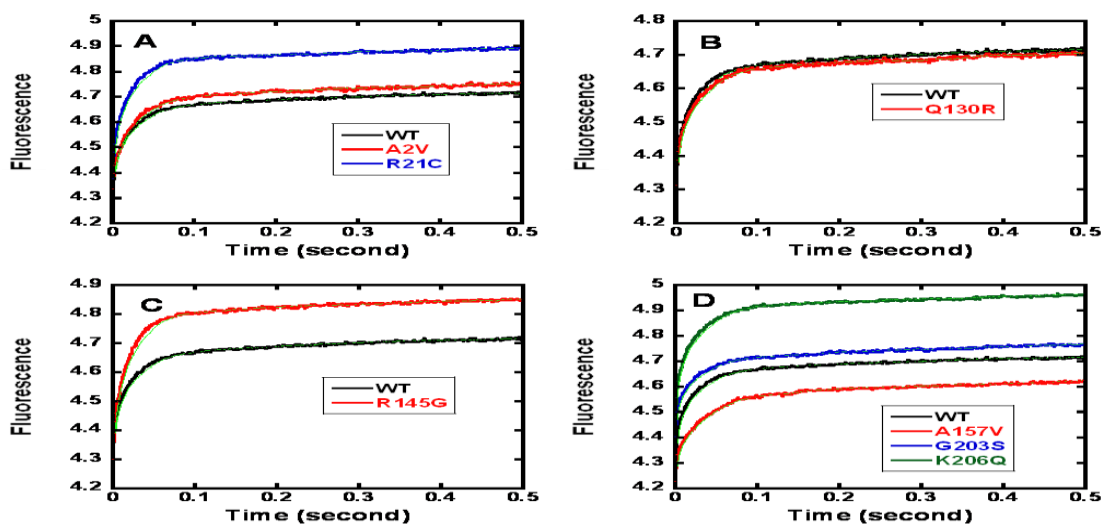


Figure 4.24 Ca^{2+} dissociation fluorescence given by Quin-2 of thin filament + rigor myosin heads. (A) N-terminal TnC binding region (B) TnT binding region (C) Inhibitory region (D) C-terminal TnC binding region HCM and DCM mutations. Stopped flow kinetic traces obtained from mixing $8 \mu\text{M}$ Tn complexes reconstituted in thin filament + rigor myosin heads ($48 \mu\text{M}$ c-Actin, $9.6 \mu\text{M}$ c-Tm, and $12 \mu\text{M}$ sk-S1) with an equal volume of the same experiment buffer containing an excess of Quin-2 ($150 \mu\text{M}$) at 15°C . Final conditions: 50 mM MOPS pH 7.2, 140 mM KCl, 4 mM MgCl_2 , and $30 \mu\text{M}$ CaCl_2 .

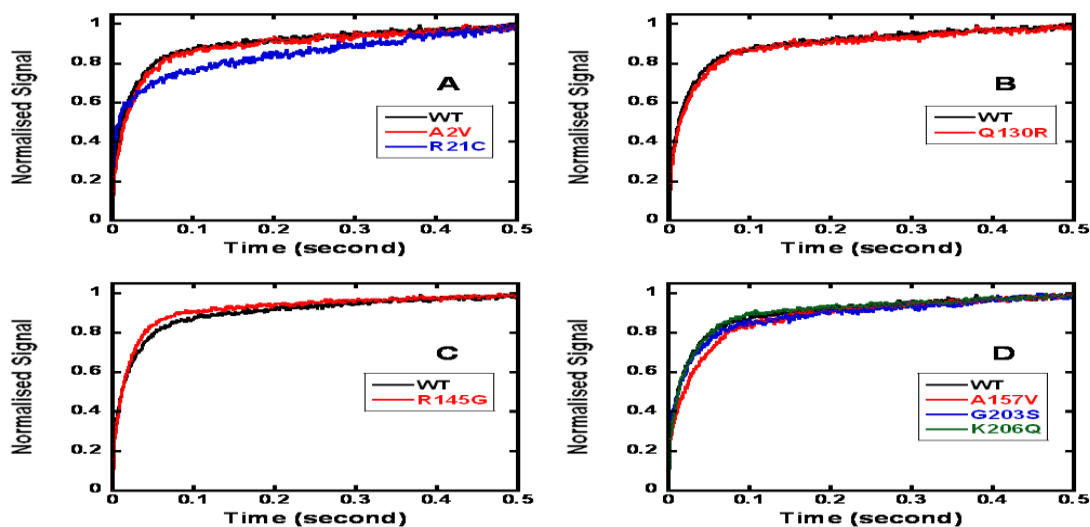


Figure 4.25 Ca^{2+} dissociation normalised fluorescence given by Quin-2 of thin filament + rigor myosin heads. (A) N-terminal TnC binding region (B) TnT binding region (C) Inhibitory region (D) C-terminal TnC binding region HCM and DCM mutations. Stopped flow kinetic normalised traces obtained from mixing $8 \mu\text{M}$ Tn complexes reconstituted in thin filament + rigor myosin heads ($48 \mu\text{M}$ c-Actin, $9.6 \mu\text{M}$ c-Tm, and $12 \mu\text{M}$ sk-S1) with an equal volume of the same experiment buffer containing an excess of Quin-2 ($150 \mu\text{M}$) at 15°C .

Table 4.6 Summary of the effect of cTnI mutations on the Ca²⁺ dissociation rate constant obtained by using Quin-2.

Troponin I	Troponin complex	Rate (s⁻¹)	Thin filament	Rate (s⁻¹)	Thin filament + S1	Rate (s⁻¹)
	Fast	Slow	Fast	Slow	Fast	Slow
Wild Type	49 ± 4.3	6 ± 1.1	92 ± 6.7	8 ± 0.8	44 ± 5.2	6 ± 1.0
A2V	44 ± 3.8	5 ± 0.9	94 ± 5.8	7 ± 0.9	42 ± 3.9	4 ± 0.8
R21C	42 ± 3.2	4 ± 0.8	93 ± 4.9	9 ± 1.2	48 ± 4.5	7 ± 1.1
Q130R	42 ± 4.7	5 ± 1.0	96 ± 5.9	9 ± 1.0	40 ± 3.3	5 ± 0.9
R145G	51 ± 5.6	6 ± 0.7	95 ± 7.7	7 ± 0.6	50 ± 4.6	5 ± 0.8
A157V	31 ± 2.6	2 ± 0.3	74 ± 4.8	6 ± 0.8	29 ± 1.9	3 ± 0.4
G203S	43 ± 3.6	5 ± 0.9	94 ± 6.9	8 ± 0.9	41 ± 4.1	6 ± 0.8
K206Q	43 ± 4.4	4 ± 1.2	90 ± 8.1	6 ± 1.0	43 ± 2.7	5 ± 1.1

(Data are shown as mean ± S.E)

4.3 Discussion

Ca^{2+} plays a major role in myofilaments activation and inhibition. Ca^{2+} levels in the cytoplasm of cardiomyocytes are therefore tightly controlled by various Ca^{2+} channels and Ca^{2+} binding proteins that act as buffers. The high concentrations of troponin C in cardiomyocytes make this protein play a major role in intracellular Ca^{2+} buffering in these cells. In addition the dissociation of Ca^{2+} from troponin is a prerequisite for cardiac relaxation. Therefore, the affinity of troponin for Ca^{2+} and Ca^{2+} dissociation rate constants are important parameters in cardiomyocytes biochemistry. In this chapter, we used the $\text{TnC}^{\text{IAANSC35}}$ and $\text{TnC}^{\text{IAANSC84}}$ to study the effect of TnI mutations on these parameters. We measured the Ca^{2+} affinity for the Tn complex, thin filament, and thin filament + rigor myosin heads since previous studies have shown that these different protein complexes affect the mentioned parameters differently. The same two labels have been used also in addition to the fluorophore Quin-2 to investigate the Ca^{2+} dissociation constant of Tn complex, thin filament, and thin filament + rigor myosin heads.

In the WT Troponin complex, $\text{TnC}^{\text{IAANSC35}}$ bound Ca^{2+} with a $K_d = 2.13 \times 10^{-7}$ M (pCa_{50} 6.67) which is in agreement with previously determined values (Kobayashi and Solaro 2006; Pinto et al., 2009). R145G reconstituted in troponin complex showed a dissociation constant value of ($K_d = 2.09 \times 10^{-7}$ M) which is in agreement with previous report (Kobayashi and Solaro 2006). TnI R21C gave lower pCa_{50} ($K_d = 3.46 \times 10^{-7}$ M), we concluded that troponin complex reconstituted with this mutation would bind calcium slightly weaker compared to the wild type. In contrast TnI A157V mutation

reconstituted with troponin complex bind calcium stronger than the wild type ($K_d = 1.38 \times 10^{-7}$ M).

The fluorescence intensity of TnC^{IAANSC84} gave a small fluorescence change for troponin complex but a bigger fluorescence change for thin filament upon calcium binding. This makes this probe suitable for monitoring thin filaments affinity for Ca^{2+} . For the wild type thin filament, we found that the pCa_{50} was 6.29 ($K_d = 5.12 \times 10^{-7}$ M), suggesting a weaker affinity than Tn complex. The Hill coefficient increased to a value of 2.25 and this suggests that calcium binding to thin filament is cooperative.

All TnI mutation showed higher calcium affinity for thin filament compared to the wild type. R145G showed higher affinity to thin filament ($K_d = 3.24 \times 10^{-7}$ M) as previously reported (Kobayashi and Solaro 2006).

It has been shown that when myosin heads bind to regulated actin as a rigor complex in the absence of MgATP, the thin filament exhibits an increased affinity for Ca^{2+} (Bremel and Weber 1972). For the wild type troponin reconstituted in thin filament and in the presence of myosin heads, the pCa_{50} was 6.78 ($K_d = 1.66 \times 10^{-7}$ M). We found that the addition of myosin heads has increased the affinity for calcium but that the mutants showed little difference than the wild type.

We also investigated the effect of TnI mutations on the kinetics of Ca^{2+} dissociation from TnC reconstituted within Tn complex, thin filament, and thin filament in the presence of rigor myosin heads using IAANSC35, IAANSC84 and Quin-2.

TnC^{IAANSC35} showed a similar rate of calcium dissociation (10.8 s^{-1}). These findings are in agreement with the value obtained using IAANS attached to Cys53 on TnC (Davis et al., 2007). TnC^{IAANSC84} and Quin-2 gave a faster rate (around 45 s^{-1}). Using the three

different probes, all TnI mutations showed the same rate constant of dissociation except the A157 HCM mutation which showed two-three fold decrease of Ca^{2+} dissociation rate constant compared to the wild type. The decrease in calcium dissociation rate constant of A157V corresponds to the increased affinity observed for the Tn complex contained this mutation ($K_d = 1.38 \times 10^{-7}$ M). The difference in the observed rate constant between $\text{TnC}^{\text{IAANSC35}}$, $\text{TnC}^{\text{IAANSC84}}$ and Quin-2 suggest that the fluorescence of $\text{TnC}^{\text{IAANSC35}}$ report a different event or step in the Ca^{2+} dissociation pathway than $\text{TnC}^{\text{IAANSC84}}$ and Quin-2 while the last are likely monitoring the same step.

Thin filament desensitizes and reduces the affinity of the regulatory N-terminal domain of TnC to Ca^{2+} . For the $\text{TnC}^{\text{IAANSC35}}$ reconstituted with thin filament, all TnI mutations and wild type showed about an increase of Ca^{2+} dissociation rate constant using all three probes. Again TnIA157V showed decreased Ca^{2+} dissociation rate constant.

Addition of S1 has been shown to reverse thin filament induced desensitisation (Fitzsimons et al., 1998; Fitzsimons et al., 2001). Again, all TnI mutations except A157V, displayed the same observed rate constant of Ca^{2+} dissociation from thin filaments saturated with S1. TnIA157V showed lower observed rate constant of Ca^{2+} dissociation. The presence of this mutation may therefore decrease the rate of cardiac muscle relaxation.

CHAPTER 5

**Effect of cTnI mutations on thin filaments
dynamics.**

5.1 Introduction

Biochemical investigations of HCM and DCM mutations in troponin I, have focused on steady state parameters mainly maximal activation and inhibition of actomyosin ATPase (or force or in vitro filament sliding velocity), pCa_{50} and Hill coefficient of Ca^{2+} sensitivity. However these parameters are composite parameters and depend on many elements. For instance the Hill coefficient, while a measure of thin filament cooperativity, depend on cooperativity of Ca^{2+} binding, cooperativity of transitions between the various thin filament states and cooperativity in S1 binding. The pCa_{50} depend on Ca^{2+} affinity, on Tn conformational change and on the equilibrium constants between inhibited and activated states. Maximal activation and inhibition are dependent on the level of thin filament activation (dependent on Ca^{2+} affinity, thin filament cooperativity and equilibrium constants) and cross bridge kinetics. The complexity of these parameters hampered the formulation of a molecular mechanism linking the effect of mutations to the onset and progression of the disease.

The Ca^{2+} dependent regulatory switch of cardiac muscle is a formidable example of cooperative allosteric systems. Lehrer and Geeves reviewed the evidence supporting that the muscle thin filaments act as a cooperative-allosteric system switching between three states and described the different role of the various components of this system (Lehrer and Geeves 1998). Thin filament dynamics has been intensively studied using various biochemical and biophysical methods (Ishii and Lehrer 1990; Fraser and Marston 1995; Craig and Lehman, 2001; Maytum et al., 2003). This led to the development of a number of techniques to study thin filament dynamics.

Thin filaments can switch between different states of different biochemical activities (allostery) in a cooperative manner. Cooperativity is a consequence of the Tm molecule interacting with seven actin subunits and wrapping the entire actin filament because adjacent Tm molecules communicate via end-to-end interactions (Lehrer 1994). It has been shown that the size of cooperative unit can be defined as the average number of actin subunits trapped in the open state by binding of one or more myosin heads (Lehrer et al., 1997). Structural and biochemical studies have shown that the thin filament can exist in three distinct states, figure 1.20 (McKillop and Geeves 1993). The transitions between these states are characterised by the equilibrium constants K_B and K_T . K_B is defined by the proportion of thin filament in the closed state over the proportion of thin filament in the blocked state. K_T is defined by the proportion of thin filament in the open state to the proportion of thin filament in the closed state.

In this chapter, we have studied the effect of TnI mutations associated with HCM and DCM on the thin filament dynamics including n , K_B , and K_T parameters and some of these mutations have substantially affected the values of these parameters.

5.2 Results

5.2.1 Effect of TnI mutations on K_B

Relaxation of the heart is triggered by the removal of Ca^{2+} from the myoplasm. The decrease of intracellular Ca^{2+} concentration leads to the dissociation of Ca^{2+} from TnC and the switch of the thin filament to a state unable to activate the myosin head ATPase. This state is named a blocked state. We measured K_B by comparing the kinetics of S1 binding to thin filaments at low and high Ca^{2+} . S1 is rapidly mixed with 10 fold excess of actin and the binding process is monitored by the quenching of the fluorescence using pyrenes-iodoacetamide-labelled actin at Cys-374 of actin (Head et al., 1995). The transient decrease in the fluorescence signal is fit well by a single exponential.

As shown in figure 5.1, the observed rate constant obtained for actin alone and actin.Tm.Tn in the presence of calcium were similar, this suggests that the actin.Tm.Tn+ Ca^{2+} is fully in the ON state (Head et al., 1995). Thin filament reconstituted with wild type troponin in the absence of calcium gave much lower observed rate constants of S1 binding to actin. The observed rate constants are linearly dependent on the actin concentration. K_B is calculated from the ratio of the slopes of the lines obtained in the absence and presence of Ca^{2+} . A K_B value of 0.52 is obtained for the wild type troponin. Our results were similar to those previously published for wild type Tn (Maytum et al., 1999; Maytum et al., 2003).

To investigate the effect of TnI mutations on the equilibrium constant K_B , the kinetics of S1 binding to thin filaments was followed for each mutation. The k_{obs} obtained in both the presence and absence of calcium as well as actin alone are linearly

dependent upon actin concentration over the range 1-6 μM for all mutants. In figures 5.2- 5.5, k_{obs} is plotted versus increasing thin filament concentration. Apart of R145G, all Tnl mutations behaved similarly to the wild type and they gave K_{B} values in the range of 0.42-0.70, table 5.1. Mutation R145G gave a drastic change in the S1 binding to thin filaments. In the absence of EGTA, the observed rate constant of S1 binding are much different from the data obtained with Wild type in the absence of Ca^{2+} and much closer to the values obtained in the presence of Ca^{2+} for wild type or R145G. This suggests that thin filaments reconstituted with this Tnl mutant do not occupy the blocked state in the absence of Ca^{2+} . The K_{B} value calculated for thin filaments reconstituted with R145G in the absence of Ca^{2+} is 4.6.

Table 5.1 summarizes the effect of cTnl mutations on the thin filament switching parameter K_{B} , while figure 5.6 illustrates the blocked state population in the absence of calcium.

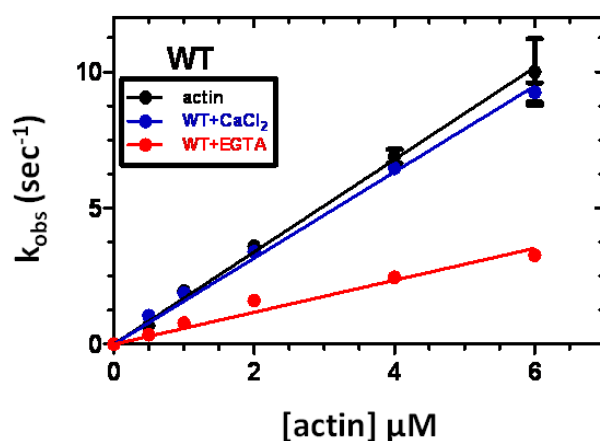


Figure 5.1 Binding of S1 to PIA-actin and to actin.Tm.Tn WT in the presence and absence of calcium. The observed rate of S1 binding as a function of PIA-labelled actin concentration in the presence and absence of calcium. Conditions: 140 mM KCl, 10 mM Mops pH 7.2, 4 mM MgCl₂, 1 mM DTT, 0.2 mM CaCl₂ or 1 mM EGTA, at 25 °C. The graph has slopes of $1.59 \pm 0.03 \times 10^6 \text{ M}^{-1} \cdot \text{s}^{-1}$ (+Ca²⁺) and $0.58 \pm 0.02 \times 10^6 \text{ M}^{-1} \cdot \text{s}^{-1}$ (-Ca²⁺)

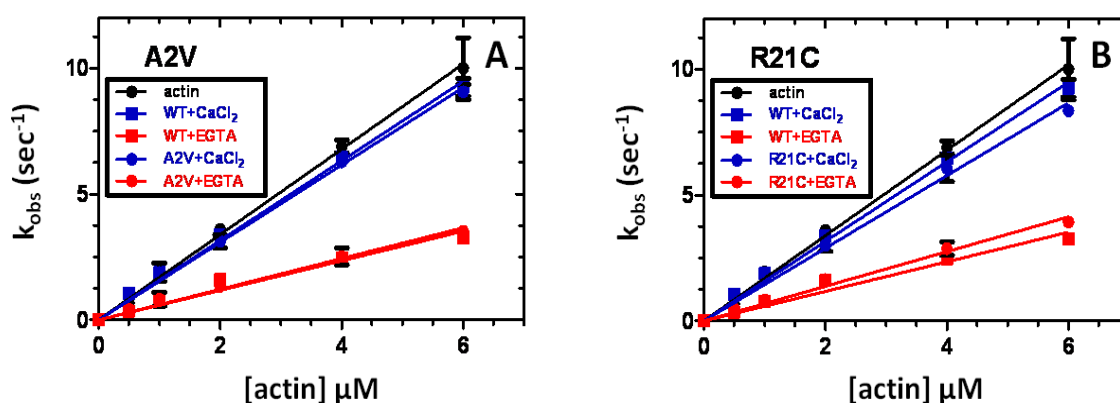


Figure 5.2 Binding of S1 to PIA-actin in the presence and absence of calcium for TnI mutations in the N-terminal TnC binding region. The observed rate of S1 binding as a function of PIA-labelled actin concentration in the presence and absence of calcium. Conditions: 140 mM KCl, 10 mM Mops pH 7.2, 4 mM MgCl₂, 1 mM DTT, 0.2 mM CaCl₂ or 1 mM EGTA, at 25 °C. The graphs have slopes of (A) $1.58 \pm 0.03 \times 10^6 \text{ M}^{-1} \cdot \text{s}^{-1}$ (+Ca²⁺) and $0.59 \pm 0.03 \times 10^6 \text{ M}^{-1} \cdot \text{s}^{-1}$ (-Ca²⁺) and (B) $1.54 \pm 0.04 \times 10^6 \text{ M}^{-1} \cdot \text{s}^{-1}$ (+Ca²⁺) and $0.61 \pm 0.02 \times 10^6 \text{ M}^{-1} \cdot \text{s}^{-1}$ (-Ca²⁺).

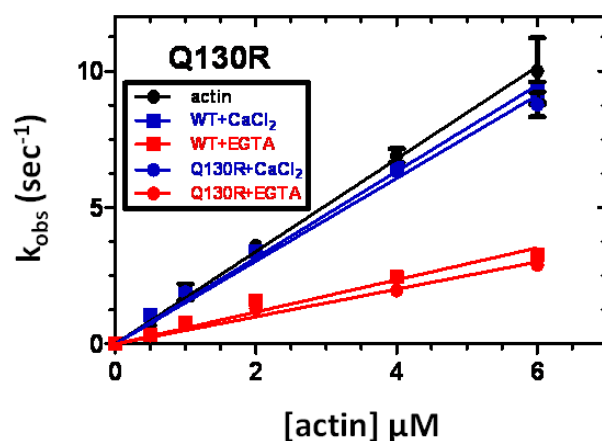


Figure 5.3 Binding of S1 to PIA-actin in the presence and absence of calcium for TnI mutation in TnT binding region. The observed rate of S1 binding as a function of PIA-labelled actin concentration in the presence and absence of calcium. Conditions: 140 mM KCl, 10 mM Mops pH 7.2, 4 mM MgCl₂, 1 mM DTT, 0.2 mM CaCl₂ or 1 mM EGTA, at 25 °C. The graphs has slopes of $1.52 \pm 0.04 \times 10^6 \text{ M}^{-1} \cdot \text{s}^{-1}$ (+Ca²⁺) and $0.50 \pm 0.02 \times 10^6 \text{ M}^{-1} \cdot \text{s}^{-1}$ (-Ca²⁺).

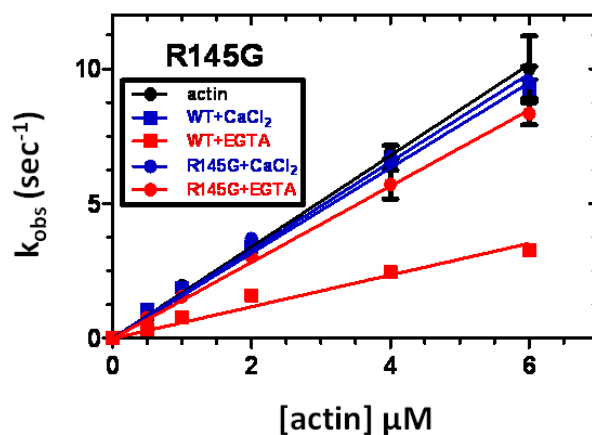


Figure 5.4 Binding of S1 to PIA-actin in the presence and absence of calcium for TnI mutations in inhibitory region. The observed rate of S1 binding as a function of PIA-labelled actin concentration in the presence and absence of calcium. Conditions: 140 mM KCl, 10 mM Mops pH 7.2, 4 mM MgCl₂, 1 mM DTT, 0.2 mM CaCl₂ or 1 mM EGTA, at 25 °C. The graphs have slopes of $1.63 \pm 0.04 \times 10^6 \text{ M}^{-1} \cdot \text{s}^{-1}$ (+Ca²⁺) and $1.41 \pm 0.03 \times 10^6 \text{ M}^{-1} \cdot \text{s}^{-1}$ (-Ca²⁺).

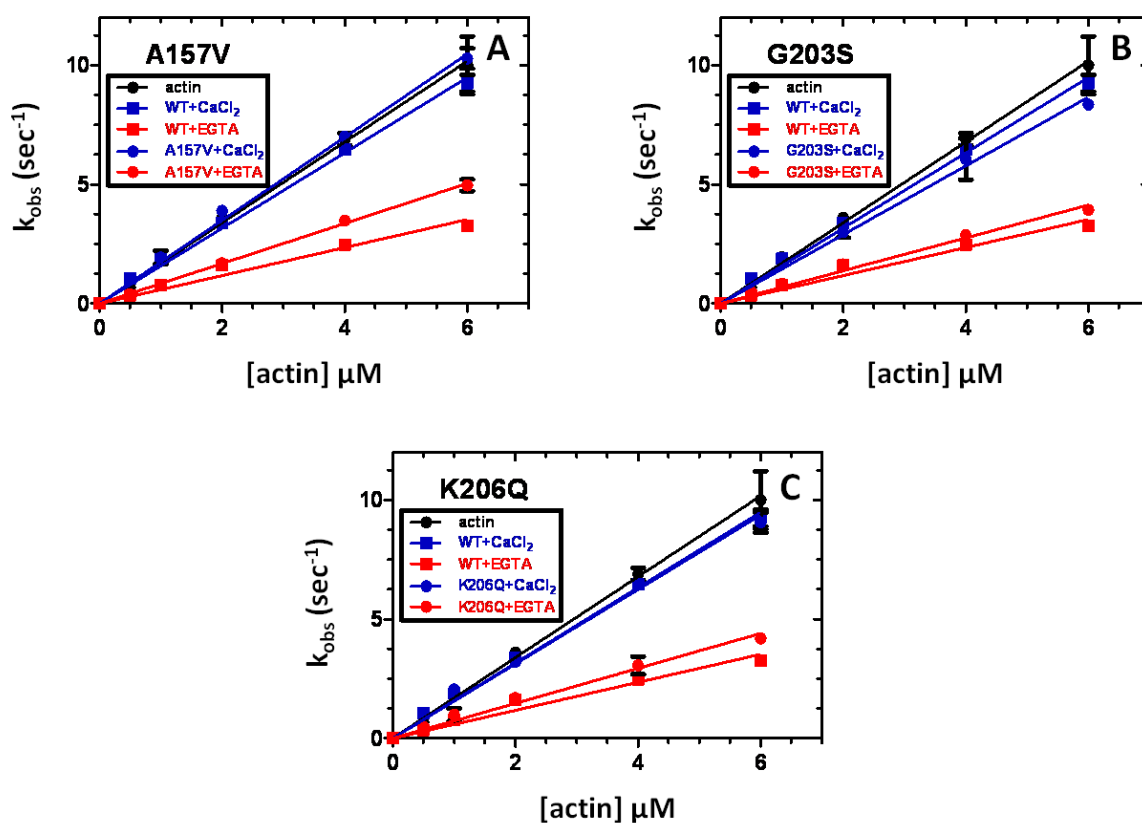


Figure 5.5 Binding of S1 to PIA-actin in the presence and absence of calcium for TnI mutations in C-terminal TnC binding region. The observed rate of S1 binding as a function of PIA-labelled actin concentration in the presence and absence of calcium. Conditions: 140 mM KCl, 10 mM Mops pH 7.2, 4 mM MgCl₂, 1 mM DTT, 0.2 mM CaCl₂ or 1 mM EGTA, at 25 °C. The graphs have slopes of (A) $1.72 \pm 0.03 \times 10^6 \text{ M}^{-1} \cdot \text{s}^{-1}$ (+Ca²⁺) and $0.84 \pm 0.02 \times 10^6 \text{ M}^{-1} \cdot \text{s}^{-1}$ (-Ca²⁺) (B) $1.44 \pm 0.05 \times 10^6 \text{ M}^{-1} \cdot \text{s}^{-1}$ (+Ca²⁺) and $0.69 \pm 0.02 \times 10^6 \text{ M}^{-1} \cdot \text{s}^{-1}$ (-Ca²⁺) and (C) $1.56 \pm 0.03 \times 10^6 \text{ M}^{-1} \cdot \text{s}^{-1}$ (+Ca²⁺) and $0.73 \pm 0.03 \times 10^6 \text{ M}^{-1} \cdot \text{s}^{-1}$ (-Ca²⁺)

Table 5.1 The effect of cTnI mutations on the thin filament switching parameter K_B (slope for actin alone = $1.72 \pm 0.05 \times 10^6 \text{ M}^{-1} \cdot \text{s}^{-1}$)

Troponin	K_B	Number of experiments
WT + CaCl ₂	>5	4
WT + EGTA	0.52 ± 0.10	4
A2V+ CaCl ₂	>5	4
A2V+ EGTA	0.57 ± 0.12	4
R21C+ CaCl ₂	>5	3
R21C+ EGTA	0.55 ± 0.07	3
Q130R+ CaCl ₂	>5	3
Q130R+ EGTA	0.42 ± 0.09	3
R145G+ CaCl ₂	>5	5
R145G+ EGTA	4.6 ± 0.23	5
A157V+ CaCl ₂	>5	3
A157V+ EGTA	0.70 ± 0.13	3
G203S+ CaCl ₂	>5	3
G203S+ EGTA	0.67 ± 0.09	3
K206Q+ CaCl ₂	>5	3
K206Q+ EGTA	0.63 ± 0.11	3

(Data are shown as mean \pm S.E)

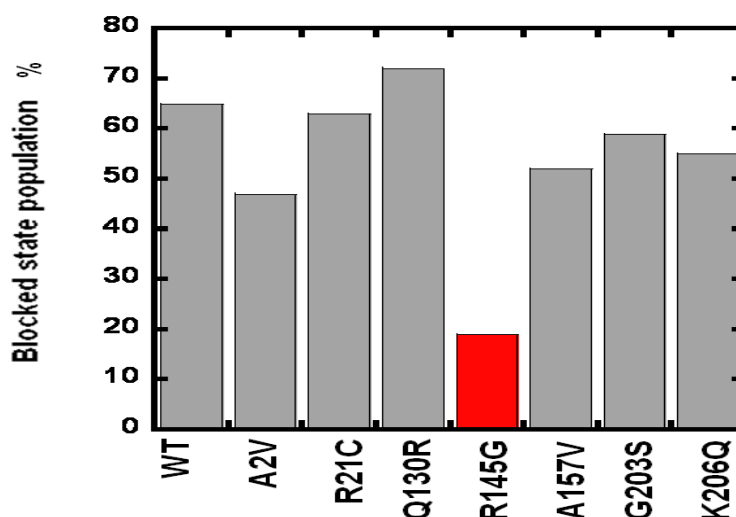


Figure 5.6 The blocked state population in the absence of calcium for TnI WT and HCM and DCM mutations

5.2.1.1 Calcium dependence of K_B

It has been shown before that k_{obs} for S1 binding to thin filament is calcium dependent (Head et al., 1995). In this study we determined the effect of HCM and DCM TnI mutations on the Ca^{2+} concentration dependence of K_B . Figure 5.7 shows a plot of k_{obs} of S1 binding versus increasing thin filament concentration at different Ca^{2+} concentrations. Each line is used to calculate K_B at that Ca^{2+} concentration. Figure 5.8 shows a plot of K_B 's versus pCa and they are typical cooperative binding curves. The data were fitted to the Hill equation and the pCa_{50} and n_H were determined (table 5.2). The wild type showed a $pCa_{50} = 5.64$ and a Hill coefficient of 1.3, which is in agreement with previous published work (Reiffert et al., 1996). All TnI mutations showed increased calcium sensitivity of K_B compared to the wild type (increased pCa_{50}). R145G showed higher K_B (decreased population of thin filaments in the blocked states) at all low Ca^{2+} concentration. None of the other mutants showed any effect at low Ca^{2+} . At high Ca^{2+} concentration, however all mutants showed a decreased value of K_B (from 4 to 2.5).

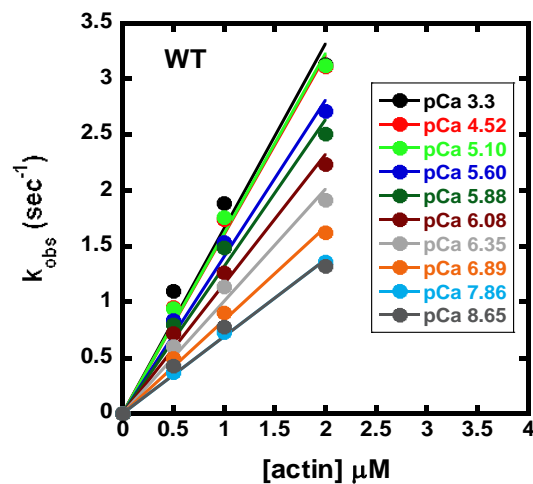


Figure 5.7 Binding of S1 to PIA-actin.Tm.Tn WT. The observed rate of S1 binding as a function of PIA-labelled actin concentration at different pCa. Conditions: 50 mM Mops pH 7.0, 140 mM KCl, 4 mM $MgCl_2$, and 2 mM EGTA, at 25 °C

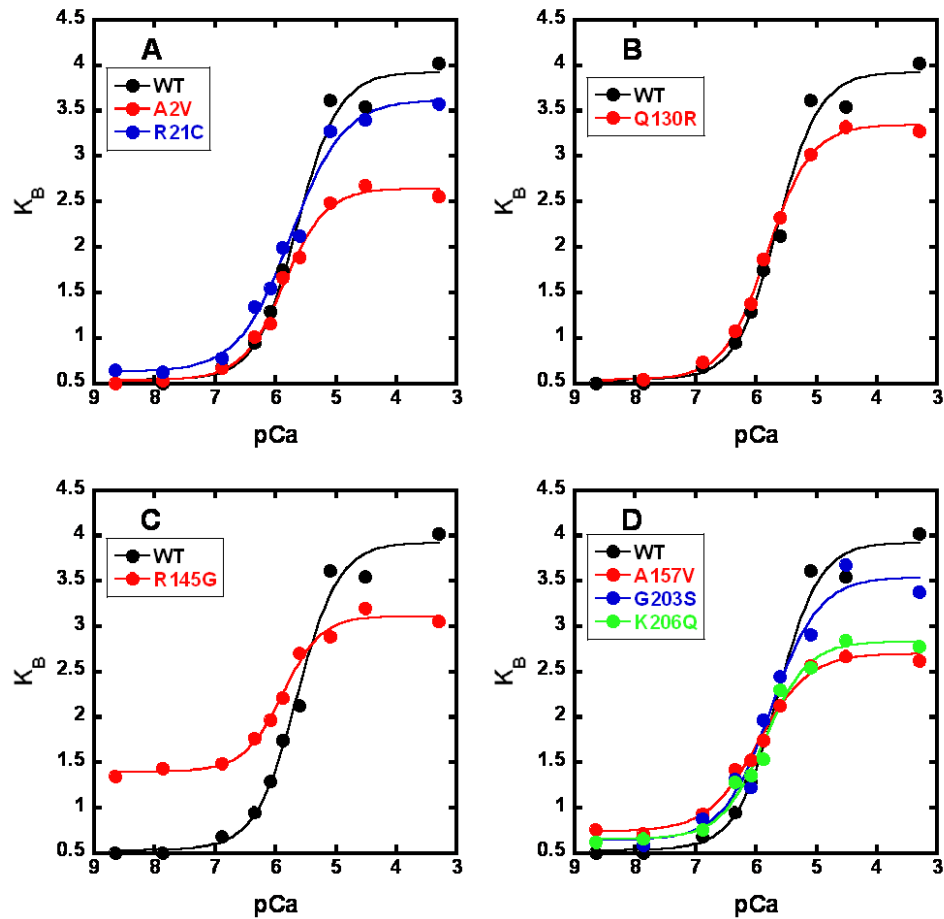


Figure 5.8 The equilibrium constant K_B as a function of pCa. (A) N-terminal TnC binding region (B) TnT binding region (C) Inhibitory region (D) C-terminal TnC binding region HCM and DCM mutations reconstituted in thin filament. The experiments were performed in 50 mM Mops pH 7.0, 140 mM KCl, 4 mM $MgCl_2$, and 2 mM EGTA, at 25 °C.

Table 5.2 Calcium dependence of K_B

Troponin	pCa_{50}	Hill Coefficient
WT	5.64	1.30
A2V	5.86	1.30
R21C	5.74	1.10
Q130R	5.81	1.20
R145G	5.88	1.40
A157V	5.96	1.10
G203S	5.75	1.20
K206Q	5.86	1.20

5.2.1.2 Electron microscopy and helical reconstruction of thin filaments containing TnIR145G.

Previous studies using electron microscopy and helical reconstruction have showed that the three thin filament biochemical states correspond to three thin filaments structural states in which the position of tropomyosin is different. Since we have shown in the previous section using S1 binding experiments, that R145G substantially decreased the population in the blocked state, we aimed to assess the effect of this mutation on the position of tropomyosin on the surface of the actin filament. This work was undertaken by Dr Jung (Korea Basic Science Institute, South Korea). Figure 5.9 shows the 3-dimensional reconstructions of tropomyosin on actin reconstituted with troponin complexes (wild type and TnI R145G mutant) in the presence and absence of calcium. Panels B and C show an actin filament decorated with tropomyosin and troponin in the absence of Ca^{2+} . The arrow indicates the position of tropomyosin on the outer domain of actin. Addition of Ca^{2+} led to a movement of tropomyosin towards the centre of the actin filament. In the absence of Ca^{2+} , thin filament reconstituted with TnIR145G shows tropomyosin located not in the outer part of the actin (as for the wild type) but rather towards the centre of the actin (like wild type thin filaments in the presence of Ca^{2+}). These data confirm that in the absence of Ca^{2+} thin filaments reconstituted with R145G occupy the closed state, not the blocked state unlike the wild type troponin. This is in agreement with our biochemical measurements (in the absence of calcium, K_B for TnIR145G =4.6). In the presence of Ca^{2+} the position of tropomyosin does not look different in comparison to the absence of Ca^{2+} .

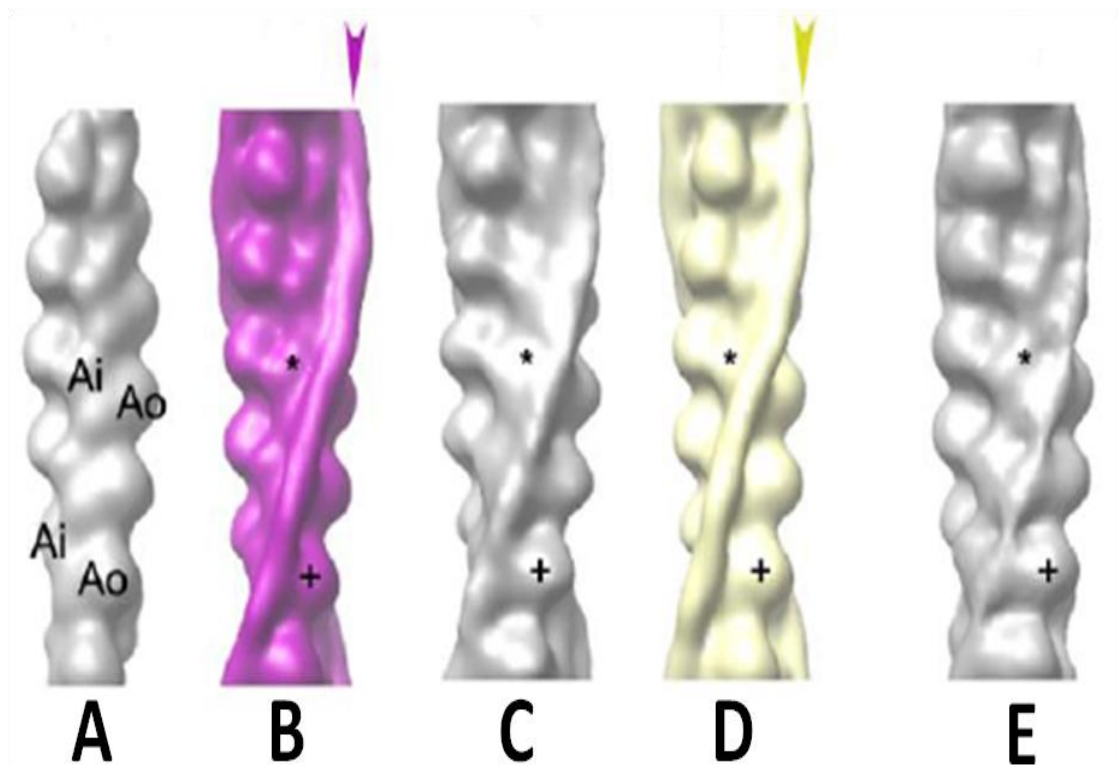


Figure 5.9 Surface views of actin and thin filament reconstructions showing the position of tropomyosin. A represents actin alone, B and D represent thin filament reconstituted with WT Tn in the absence and presence of calcium respectively, C and E represent thin filament reconstituted with R145G Tn in the absence and presence of calcium respectively (Collaboration with Dr Jung, South Korea).

5.2.2 Effect of Tnl mutations on K_T

Phosphate release is an important step in the actomyosin cross-bridge cycle. This step seems to be the rate limiting step and the step associated with force generation in the cross-bridge cycle. In addition this step is affected by regulatory proteins in smooth and skeletal muscle (Alahyan et al., 2008; Heeley et al, 2002). According to the three state model activation of phosphate release require the thin filament to switch to the open state. Hence following the kinetics of phosphate release allows the determination of both K_B and K_T . We used the fluorescent phosphate binding protein in a double-mixing stopped flow experiments to monitor the kinetics of phosphate release and to calculate K_T . The rate of phosphate release was measured in single turnover double mixing stopped-flow experiments directly using the fluorescence of MDCC-PBP (Heeley et al., 2002; Alahyan et al., 2006; Houmeida et al., 2010). The fluorescence emission of MDCC-PBP increases 8-fold upon saturation by Pi.

8 μ M of skeletal S1 and 10 μ M of ATP were combined in the first mix and allowed to incubate for 2 seconds for ATP to be bound and hydrolyzed by S1. In the second mix the S1-nucleotide complex was combined with thin filaments in the presence and absence of calcium and in the presence of rigor myosin head and calcium. The rate of phosphate release from the thin filament.S1 complex was measured from the fluorescence enhancement because of the rapid binding of phosphate to MDCC-PBP, figure 5.10. In this experiment it is necessary to use high actin concentration and low salt to obtain a measurable amount of S1.ADP.Pi bound to actin thin filament (because actin-S1.ADP.Pi complex is a weak binding complex and the interaction is further decreased by ionic strength).

The transient of phosphate release was best fit with a double exponential. The fast component correspond to the observed rate constant of phosphate dissociation from S1.ADP.Pi bound to thin filament while the slower component correspond to ATP hydrolysis by S1 bound to thin filaments (Heeley et al., 2002). The observed rate constant of phosphate release is dependent on thin filament concentration. The data are best fit by the following equation describing a rectangular hyperbola (Alahyan et al., 2006):

$$k_{obs} = k_{obs\ max}(\text{rigor} + \text{CaCl}_2) * [\text{actin}] / ((1 + (1/K_B) + (1/K_T)) * K_d + (1 + (1/K_B) + (1/K_T)) * [\text{actin}])$$

Where $k_{obs\ max}$ is the rate constant of phosphate release for thin filament + rigor myosin heads in the presence of Ca^{2+} .

Using the experimentally determined K_B values in the presence of calcium (from section 5.2.1); we calculated the values of K_T . Table 5.3 summarize the values of K_T that have been obtained by this experiment. By floating both K_B and K_T and using the same fit equation, we have obtained values of K_B comparable to the values from section 5.2.1.

Figures 5.11-5.14 illustrate the effect of Troponin I mutation on the phosphate release from thin filament.myosinS1-ADP-Pi in the absence of calcium, in the presence of calcium alone and with both calcium and rigor myosin head.

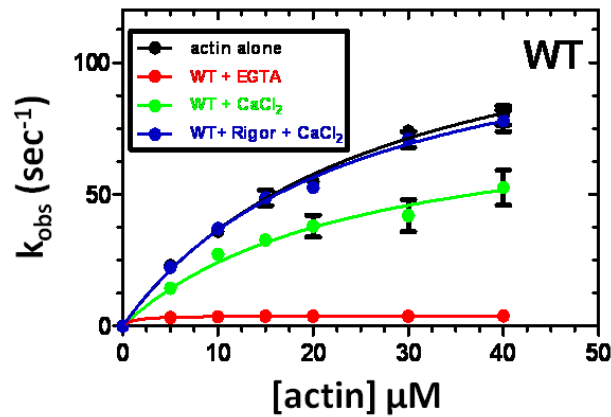


Figure 5.10 Dependence of the rates of phosphate release from acto(TmTn)myosinS1-ADP-Pi on thin filament concentration and calcium and rigor S1 bound to the thin filament. Double mixing stopped-flow experiment were performed by mixing 8 μM sk S1 with 10 μM ATP, incubated for 2 sec and then mixed with variant thin filament concentration in the presence of calcium, calcium and rigor and in the absence of calcium. The dependence of k_{obs} of thin filament concentration was fit to the equation

$k_{\text{obs}} = k_{\text{obs}} \max(\text{rigor} + \text{CaCl}_2) * [\text{actin}] / ((1 + (1/K_B) + (1/K_T)) * K_d + (1 + (1/K_B) + (1/K_T)) * [\text{actin}])$.
 Conditions: 5 mM Mops pH 7, 3 mM MgCl_2 , 6 μM MDCC-PBP, 0.1 mM 7-methyl guanosine, 0.01 unit/ml purine nucleoside phosphorylase, at 25 $^\circ\text{C}$.

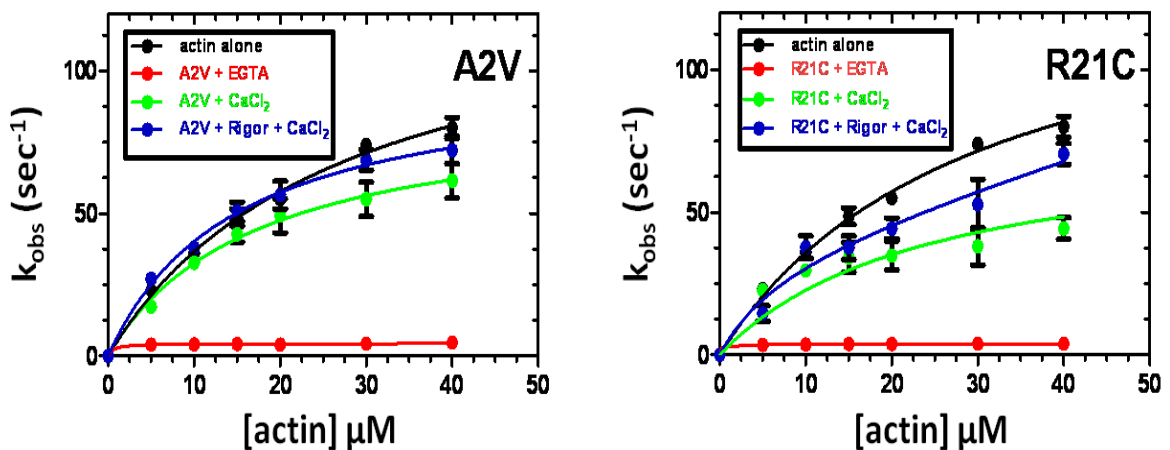


Figure 5.11 Dependence of the rates of phosphate release from acto(TmTn)myosinS1-ADP-Pi on thin filament concentration and calcium and rigor S1 bound to the thin filament. Troponin I mutations in the N-terminal TnC binding region. Double mixing stopped-flow experiment were performed by mixing 8 μM sk S1 with 10 μM ATP, incubated for 2 sec and then mixed with variant thin filament concentration in the presence of calcium, calcium and rigor and in the absence of calcium. The dependence of k_{obs} of thin filament concentration was fit to the equation $k_{\text{obs}} = k_{\text{obs}} \max(\text{rigor} + \text{CaCl}_2) * [\text{actin}] / ((1 + (1/K_B) + (1/K_T)) * K_d + (1 + (1/K_B) + (1/K_T)) * [\text{actin}])$.
 Conditions: 5 mM Mops pH 7, 3 mM MgCl_2 , 6 μM MDCC-PBP, 0.1 mM 7-methyl guanosine, 0.01 unit/ml purine nucleoside phosphorylase, at 25 $^\circ\text{C}$.

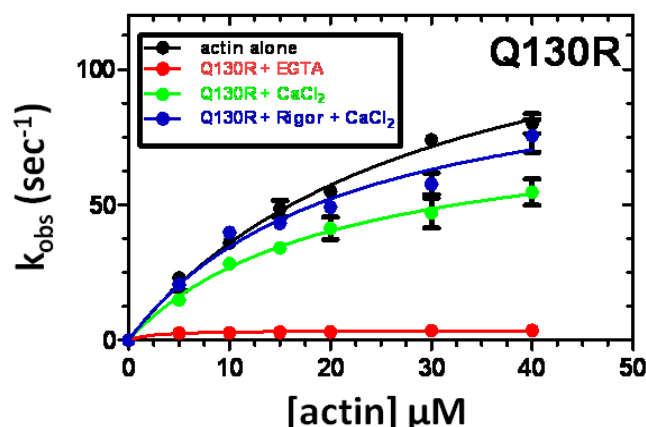


Figure 5.12 Dependence of the rates of phosphate release from acto(TmTn)myosinS1-ADP-Pi on thin filament concentration and calcium and rigor S1 bound to the thin filament. Troponin I mutations in the TnT binding region. Double mixing stopped-flow experiment were performed by mixing 8 μM sk S1 with 10 μM ATP, incubated for 2 sec and then mixed with variant thin filament concentration in the presence of calcium, calcium and rigor and in the absence of calcium. The dependence of k_{obs} of thin filament concentration was fit to the equation $k_{obs} = k_{obs}max(rigor+CaCl_2)*[actin] / ((1+(1/K_B)+(1/K_T))*K_d + (1+(1/K_B)+(1/K_T))*[actin])$. Conditions: 5 mM Mops pH 7, 3 mM MgCl₂, 6 μM MDCC-PBP, 0.1 mM 7-methyl guanosine, 0.01 unit/ml purine nucleoside phosphorylase, at 25 °C.

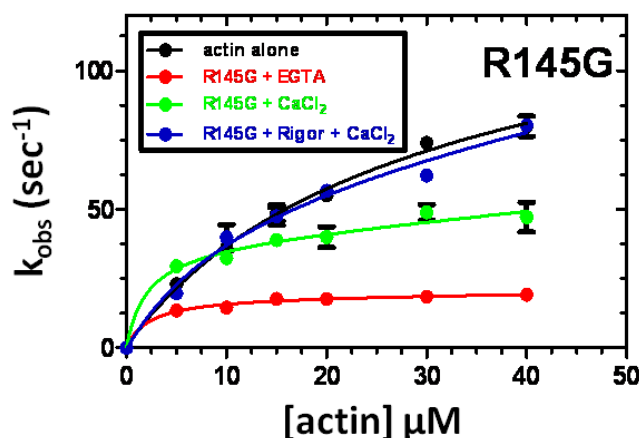


Figure 5.13 Dependence of the rates of phosphate release from acto(TmTn)myosinS1-ADP-Pi on thin filament concentration and calcium and rigor S1 bound to the thin filament. Troponin I mutations in the inhibitory region. Double mixing stopped-flow experiment were performed by mixing 8 μM sk S1 with 10 μM ATP, incubated for 2 sec and then mixed with variant thin filament concentration in the presence of calcium, calcium and rigor and in the absence of calcium. The dependence of k_{obs} of thin filament concentration was fit to the equation $k_{obs} = k_{obs}max(rigor+CaCl_2)*[actin] / ((1+(1/K_B)+(1/K_T))*K_d + (1+(1/K_B)+(1/K_T))*[actin])$. Conditions: 5 mM Mops pH 7, 3 mM MgCl₂, 6 μM MDCC-PBP, 0.1 mM 7-methyl guanosine, 0.01 unit/ml purine nucleoside phosphorylase, at 25 °C.

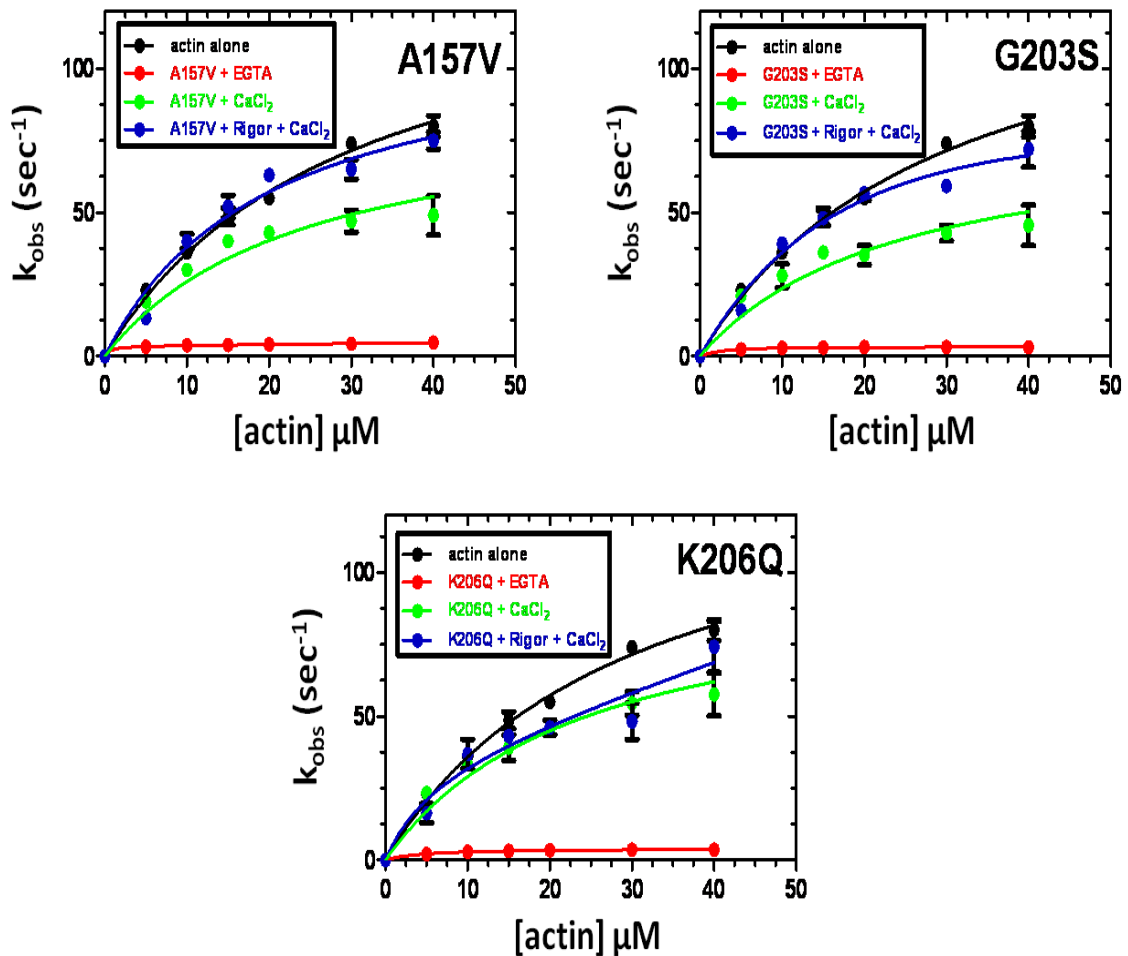


Figure 5.14 Dependence of the rates of phosphate release from acto(TmTn)myosinS1-ADP-Pi on thin filament concentration and calcium and rigor S1 bound to the thin filament. Troponin I mutations in the C-terminal TnC binding region. Double mixing stopped-flow experiment were performed by mixing 8 μM sk S1 with 10 μM ATP, incubated for 2 sec and then mixed with variant thin filament concentration in the presence of calcium, calcium and rigor and in the absence of calcium. The dependence of k_{obs} of thin filament concentration was fit to the equation $k_{obs} = k_{obs} \max(\text{rigor} + \text{CaCl}_2) * [\text{actin}] / ((1 + (1/K_B) + (1/K_T)) * K_d + (1 + (1/K_B) + (1/K_T)) * [\text{actin}])$. Conditions: 5 mM Mops pH 7, 3 mM MgCl₂, 6 μM MDCC-PBP, 0.1 mM 7-methyl guanosine, 0.01 unit/ml purine nucleoside phosphorylase, at 25 °C.

The presence of rigor and calcium was needed to fully activate the thin filament for the wild type troponin. The rate of phosphate release for all mutants and wild type was very close to the rate of phosphate release from actin alone (Heeley et al., 2002).

In figure 5.13, Troponin I R145G displayed less inhibition of the rate of phosphate release in the absence of calcium. This result support a reduction in the population of the blocked state occupied by thin filaments reconstituted with this mutant (section 5.2.1), figures 5.4 and 5.6. Thin filaments reconstituted with TnI R145G also displayed less activation of the rate of phosphate release.

Table 5.3 The effect of cTnI mutations on the equilibrium constant K_T

Troponin	K_T	K_B	K_d μM	$k_{\text{obs max}}$ (s^{-1})	No. of experiments
WT	24 ± 3	>5	20 ± 0.9	75 ± 11	4
A2V	15 ± 1	>5	17 ± 1.1	89 ± 9	3
R21C	27 ± 9	>5	13 ± 0.6	59 ± 7	4
Q130R	21 ± 6	>5	20 ± 0.7	81 ± 12	4
R145G	22 ± 5	>5	3 ± 0.4	43 ± 6	3
A157V	20 ± 6	>5	10 ± 0.3	63 ± 7	3
G203S	18 ± 5	>5	11 ± 0.9	55 ± 8	3
K206Q	30 ± 8	>5	13 ± 1.1	75 ± 9	3

(Data are shown as mean \pm S.E)

5.2.3 Effect of TnI mutations on the size of cooperative unit

The cooperative unit is the number of actin monomers switched simultaneously between the ON and OFF states by the binding of an allosteric inhibitor (such as troponin in the absence of Ca^{2+}) or activator (such as S1 myosin head). We used a method developed by Geeves and Lehrer for the study of skeletal muscle Tm to measure the size of the cooperative unit (Geeves and Lehrer 1994). The method is based on monitoring simultaneously the ON-OFF transition and myosin association/dissociation to thin filaments. It has been shown that pyrene-labelled tropomyosin dimers exhibit excimer fluorescence which decreases when the thin filament switches from the ON state to the OFF state. Myosin binding to actin is monitored by light scattering.

We used freshly purified sheep cardiac tropomyosin to investigate the effect of TnI mutations on the size of cooperative unit. Since Cardiac Tm consists of α -molecules and each α -molecule contains a single cysteine at residue 190, the degree of labelling is typically close to two pyrenes per molecule of Tm and this gives the maximum signal of excimer fluorescence.

The emission spectrum of PIA-labelled Tm (cys-190) is composed of monomer peaks at about 385 nm and 410 nm, and an excimer peak centred at 480 nm. By adding actin, the monomer fluorescence was unchanged while the excimer fluorescence was slightly decreased. Upon addition of S1 the excimer fluorescence level was substantially increased. The effect of S1 was reversed by adding Mg^{2+} -ATP (Figure 5.15). The change in the level of the excimer fluorescence in the presence of troponin was relatively

small (Figure 5.16) but it was good enough to monitor the transition to the ON state in the presence of troponin.

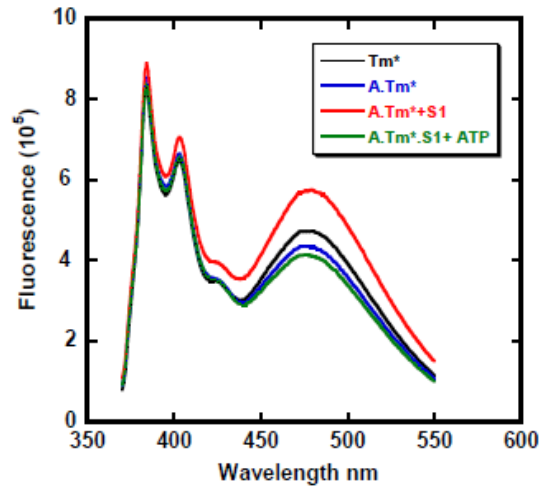


Figure 5.15 Fluorescence emission spectra of PIA-labelled Tm (Tm*). Experiment conditions: 6 μM actin, 1 μM Tm*, 3 μM S1, 1 mM Mg^{2+} -ATP in 10 mM Mops pH 7.2, 140 mM KCl, 4 mM MgCl_2 , and 1 mM DTT, at 25 °C (Adapted from Zimna Wazeer, PhD thesis, University of Leicester).

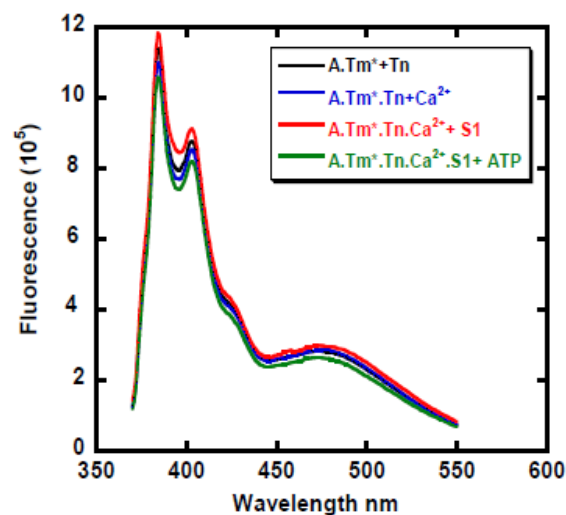


Figure 5.16 Fluorescence emission spectra of PIA-labelled Tm (Tm*) in the presence of troponin complex. Experiment Conditions: 6 μM actin, 1 μM Tm*, 1 μM Tn, 3 μM S1, 1 mM Mg^{2+} -ATP and 0.2 mM CaCl_2 in 10 mM Mops pH 7.2, 140 mM KCl, 4 mM MgCl_2 , and 1 mM DTT, at 25 °C (Adapted from Zimna Wazeer, PhD thesis, University of Leicester).

We used a kinetic method to measure the size of cooperative unit based on ATP induced S1 dissociation and subsequent switch of the thin filament from the ON to the OFF states (Geeves and Lehrer 1994). The experiment has been performed by mixing actin.Tm*.S1 with 56 μ M ATP. ATP binding to S1 lead to its dissociation from thin filament monitored by a decrease in light scattering signal (figure 5.17.A) while the fluorescence (FI) signal remained constant (delayed) until the amount of S1 bound to the thin filament is not sufficient to keep it in the ON state and the filament is switched to the OFF state. The delay or lag duration depends upon the size of n.

The size of the cooperative unit n is determined by generating a number of curves with different values of n (blue, green and cyan curves in figures 5.17-5.21) from the equation $f_{on} = 1-(1-\exp(-k_{LSt}))^n$ and comparing the experimental curve (red curve in figures 5.17-5.21) to these simulated curves.

As shown in figure 5.17, in the presence of troponin, the change in the excimer fluorescence was much smaller than for Actin.Tm* alone. We averaged a large number of transients (10-15 transients) to reduce the noise and to obtain a measureable fluorescence signal change when troponin was incorporated into thin filament. In addition, in order to remove any excess amount of Tm* molecules that would contribute to the fluorescence background, we cosedimented actin.Tm*.Tn.S1 at 6:1:1:6 ratio and the pellets were re-suspended in experimental buffer. Figure 5.17 illustrates the comparison of the difference in amplitude of the fluorescence between actin.Tm* and actin.Tm*.Tn thin filaments. Thin filament reconstituted with wild type troponin in the presence of calcium gave a size of cooperative unit in the range of 14-21 which is similar to previous findings (Maytum et al., 1999; Maytum et al., 2003).

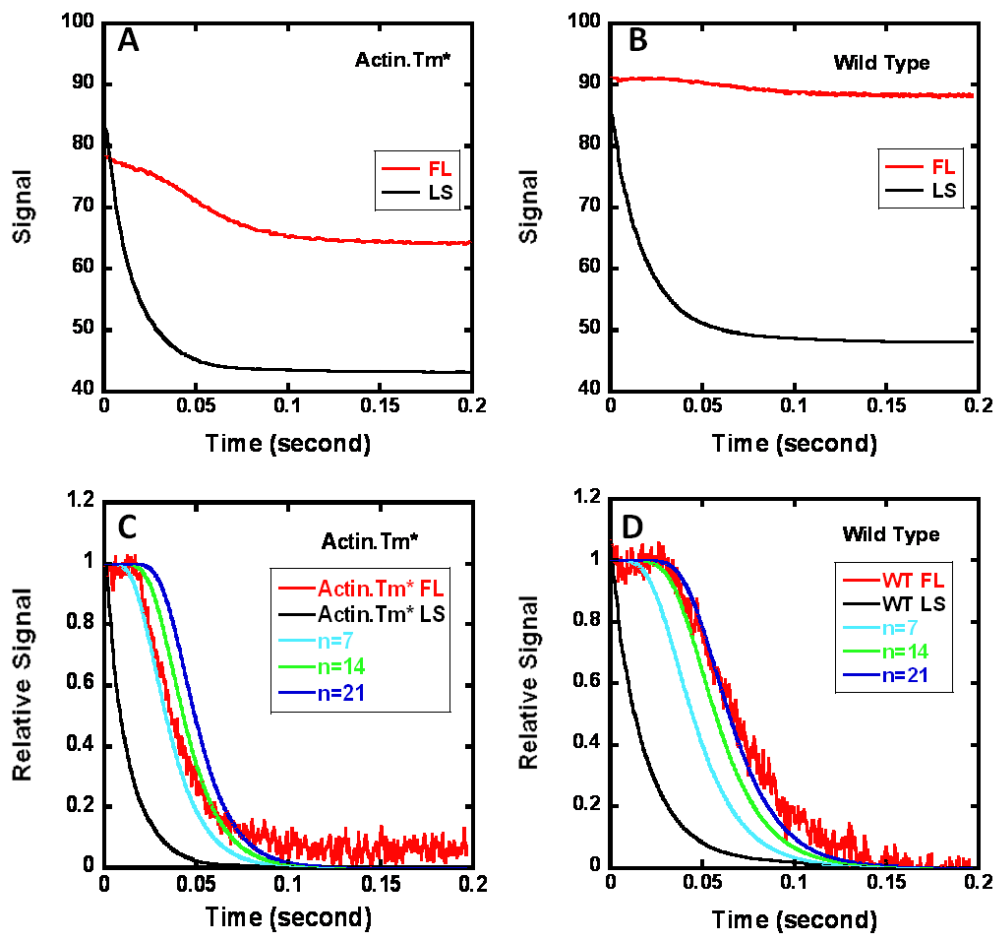


Figure 5.17 Kinetics of ATP induced dissociation of S1 from Actin.Tm* and Actin.Tm*.Tn thin filament (wild type). A and B are time courses of fluorescence and light scattering for actin.Tm* and actin.Tm*.Tn wild type. The signals are an average of 10-15 transients. C and D are normalised time courses of light scattering (black lines) and fluorescence (red lines) signals when 56 μ M ATP was mixed with 6 μ M S1, 6 μ M actin, 1 μ M Tm* and 1 μ M Tn. The other coloured lines are the computer generated simulation curves. The experiments were performed in 140 mM KCl, 20 mM Mops pH 7.2, 4 mM MgCl₂, 0.2 mM CaCl₂, and 1 mM DTT, at 25 °C.

Thin filaments reconstituted with TnI A2V (figure 5.18), TnI R21C (figure 5.18), Q130R (figure 5.19), A157V (figure 5.21), G203S (figure 5.21) and K206Q (figure 5.21) gave n values in the range 14-21 similar to the wild type cardiac troponin I. Surprisingly the excimer fluorescence curve obtained in the presence of troponin I R145G (figure 5.20) showed no lag unlike all other mutants and the troponin wild type. Since the excimer fluorescence reports the transition from the open to the closed state and that the size

of the lag is proportional to the size of the cooperative unit, two possible explanations can be put forward to explain the absence of a lag in this experiment. Firstly, that the filament lost all cooperativity ($n=1$ means no lag). This explanation is however excluded because of the values of the Hill coefficient obtained in the Ca^{2+} sensitivity of ATPase reported in section 3.2.4.c ($n>1$ and comparable to the wild type value). An alternative interpretation is the absence or a substantial decrease of the population of the filaments in the open state. In other words, the closed state is stabilized by this TnI mutation. This explanation is supported by the ATPase experiments (chapter three) and Phosphate release experiments (previous section) which indicate that thin filaments reconstituted with this mutant may not be switched fully to the open state by S1 binding (Lower activation of ATPase activity and of Pi release in contrast to the Wild type and other mutants). However because of the absence of a lag, it is not possible to determine the size of the cooperative unit for this mutant.

All experiments were carried out a minimum of 3 times using different preparations of proteins. We used different protein batches of cardiac actin, PIA-labelled Tm* prepared from freshly purified sheep heart muscles, skeletal S1, and troponin complexes.

Table 5.4 summarises the results from these experiments. The values obtained for n remained consistent between experiments using different protein batches and ATP concentrations.

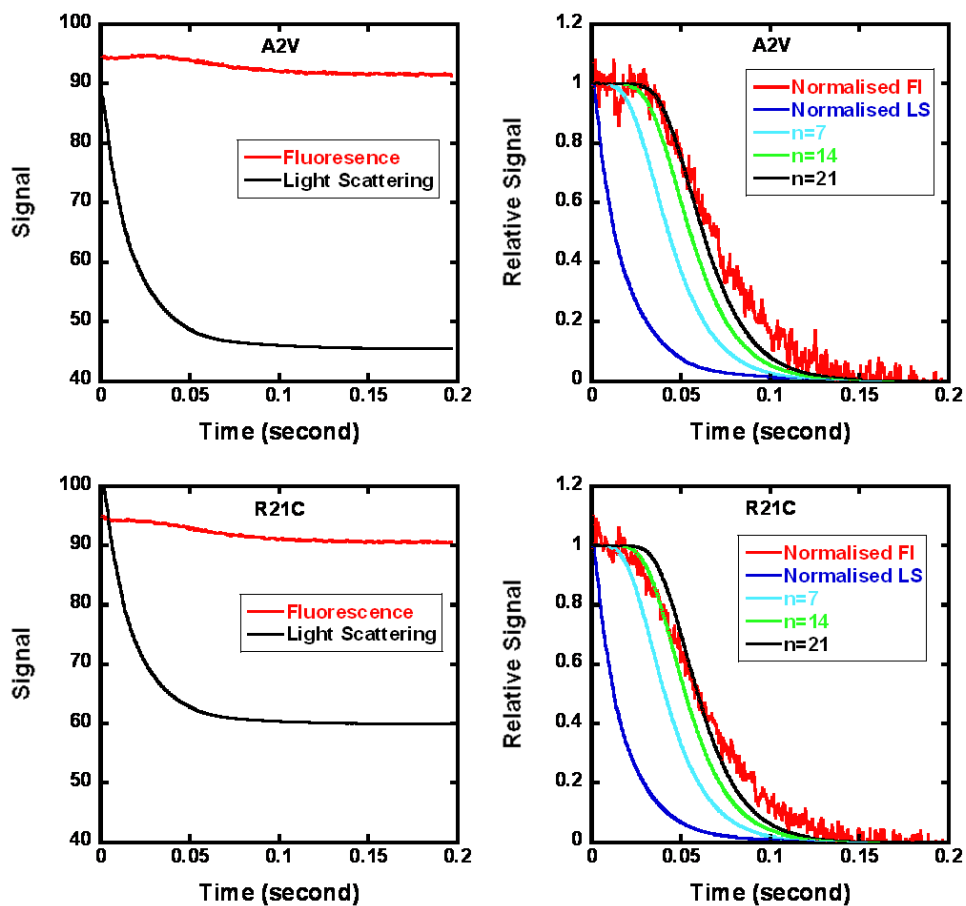


Figure 5.18 Kinetics of ATP induced dissociation of S1 from TnI mutations in the N-terminal TnC binding region. Left panels are time courses of fluorescence and light scattering, the signals are an average of 10-15 transients. Right panels are normalised time courses of light scattering (blue line) and fluorescence (red line) signals for A2V and R21C TnI mutation respectively when 56 μM ATP was mixed with 6 μM S1, 6 μM actin, 1 μM Tm* and 1 μM Tn. The other coloured lines are the computer generated simulation curves. The experiments were performed in 140 mM KCl, 20 mM Mops pH 7.2, 4 mM MgCl_2 , 0.2 mM CaCl_2 , and 1 mM DTT, at 25 $^\circ\text{C}$.

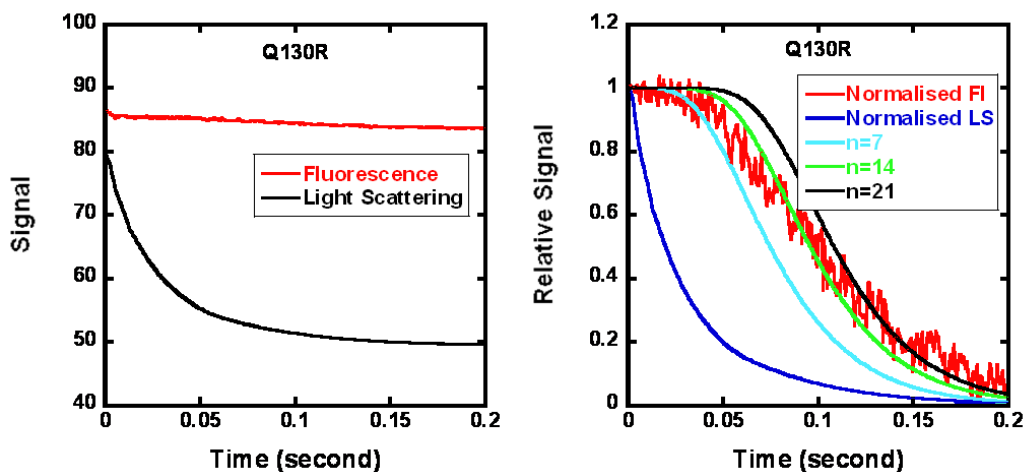


Figure 5.19 Kinetics of ATP induced dissociation of S1 from TnI mutation in TnT binding region. Left panel is time course of fluorescence and light scattering; the signals are an average of 10-15 transients. Right panel is normalised time course of light scattering (blue line) and fluorescence (red line) signals for Q130R TnI mutation when 56 μM ATP was mixed with 6 μM S1, 6 μM actin, 1 μM Tm* and 1 μM Tn. The other coloured lines are the computer generated simulation curves. The experiments were performed in 140 mM KCl, 20 mM Mops pH 7.2, 4 mM MgCl₂, 0.2 mM CaCl₂, and 1 mM DTT, at 25 °C.

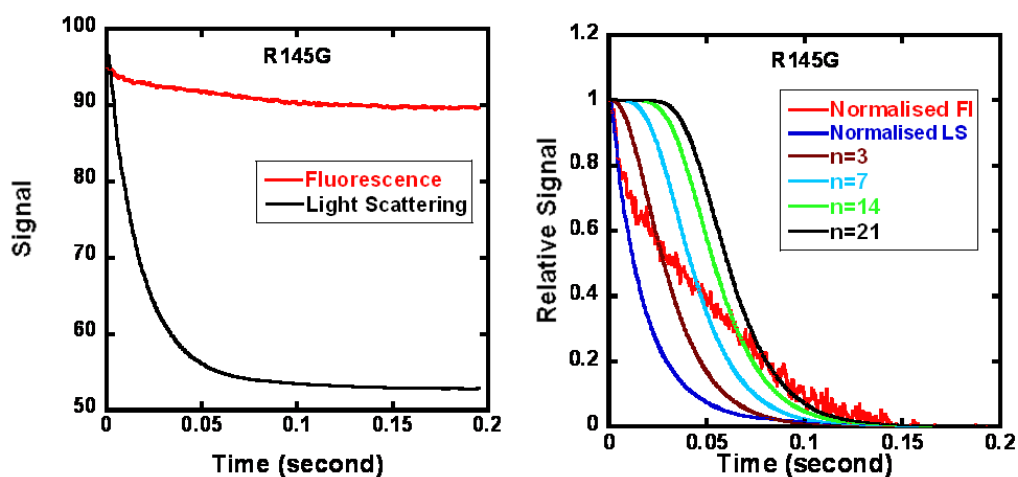


Figure 5.20 Kinetics of ATP induced dissociation of S1 from TnI mutation in inhibitory region. Left panel is time course of fluorescence and light scattering; the signals are an average of 10-15 transients. Right panel is normalised time course of light scattering (blue line) and fluorescence (red line) signals for R145G TnI mutation when 56 μM ATP was mixed with 6 μM S1, 6 μM actin, 1 μM Tm* and 1 μM Tn. The other coloured lines are the computer generated simulation curves. The experiments were performed in 140 mM KCl, 20 mM Mops pH 7.2, 4 mM MgCl₂, 0.2 mM CaCl₂, and 1 mM DTT, at 25 °C.

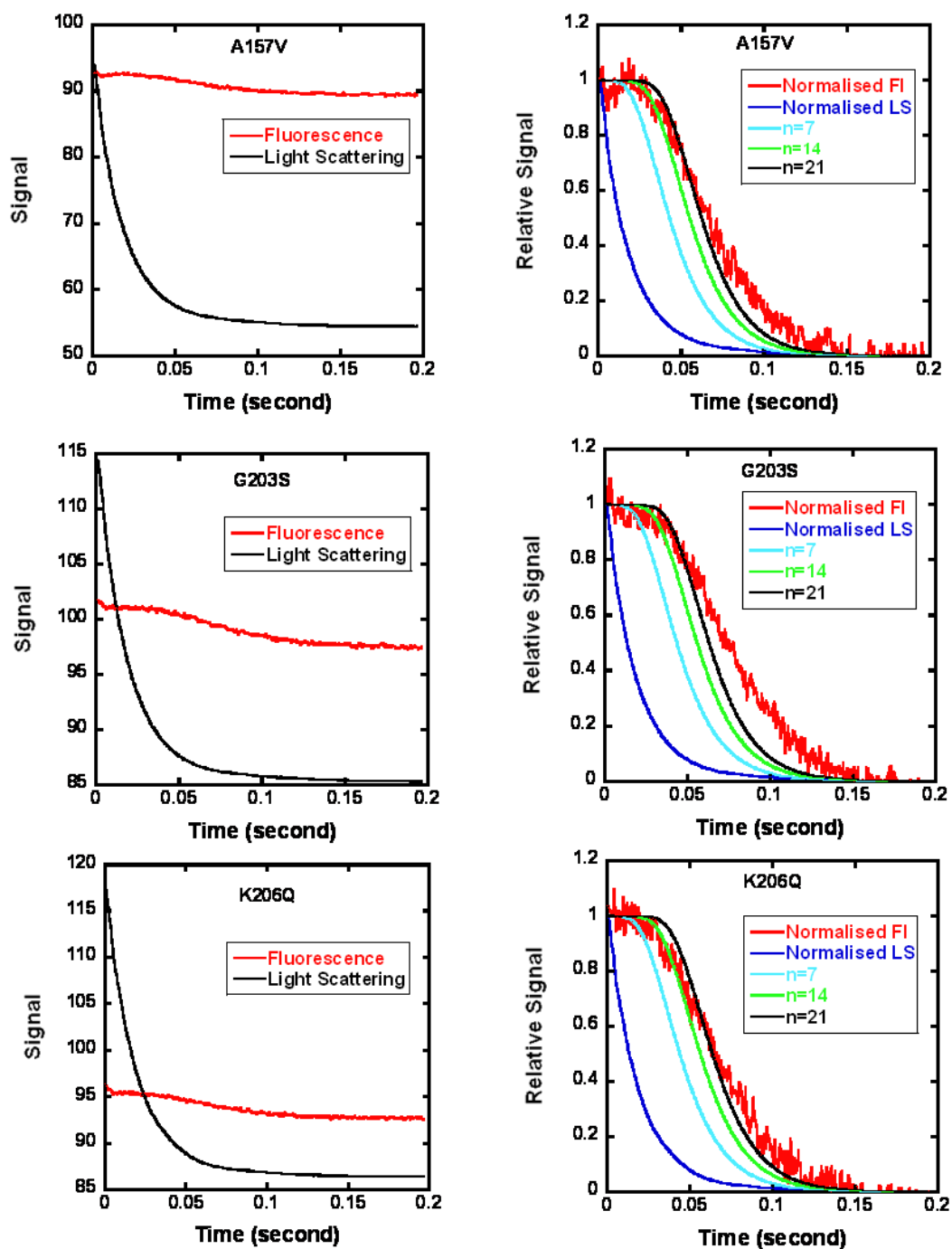


Figure 5.21 Kinetics of ATP induced dissociation of S1 from TnI mutations in the C-terminal TnC binding region. Left panels are time courses of fluorescence and light scattering, the signals are an average of 10-15 transients. Right panels are normalised time courses of light scattering (blue line) and fluorescence (red line) signals for A157V G203S and K206Q TnI mutation respectively when 56 μM ATP was mixed with 6 μM S1, 6 μM actin, 1 μM Tm* and 1 μM Tn. The other coloured lines are the computer generated simulation curves. The experiments were performed in 140 mM KCl, 20 mM Mops pH 7.2, 4 mM MgCl_2 , 0.2 mM CaCl_2 , and 1 mM DTT, at 25 $^\circ\text{C}$.

Table 5.4 Summary of the effect of Tnl mutations on the size of cooperative unit n

Tnl	Size of cooperative unit (n)	Observed rate constant of switch (ON-OFF transition) sec⁻¹	Number of experiments
WT	14-21	28 ± 4.2	4
A2V	14-21	29 ± 3.9	3
R21C	14	28 ± 1.8	3
Q130R	14	36 ± 3.2	3
R145G	Not possible	22 ± 2.5	4
A157V	14-21	28 ± 2.8	3
G203S	14-21	25 ± 2.6	3
K206Q	14	28 ± 3.3	3

(Data are shown as mean ± S.E)

5.3 Discussion

Regulation of cardiac muscle contraction depends on a set of allosteric and cooperative transitions in thin filaments. Cardiac thin filaments can exist in a blocked, closed or open state. Complete relaxation at low Ca^{2+} requires the thin filament to be switched to the blocked state, while contraction requires thin filaments to be in the open state. TnI and TnC act as allosteric effectors that bias the equilibrium towards one state depending on the Ca^{2+} concentration. The cooperative nature of thin filaments allow for a more efficient switching between these states. In muscle thin filaments cooperativity is primarily due to tropomyosin, and is affected by the TnT subunit of troponin that interacts with Tm in the head to tail overlap regions. Hence both the equilibria (K_B and K_T) between these states and the cooperativity (defined by the size of the cooperative unit n) are important determinant of cardiac muscle contraction and relaxation. In this chapter we examined the effect of the DCM and HCM TnI mutants A2V, R21C, Q130R, R145G, A157V, G203S, and K206Q on the three parameters; size of cooperative unit, equilibrium constant between blocked and closed states, and equilibrium constant between closed and open states; that characterise thin filaments dynamics.

a) Effect of TnI mutations on thin filament cooperativity.

The PIA-labelled Tm excimer fluorescence was used to measure the size of cooperative unit. Before assessing the effect of TnI mutations on the size of the cooperative unit, it is important to examine the limitations of the method used. Although the use of a probe attached to tropomyosin is less prone to ambiguities in the interpretation unlike probes attached to actin or troponin, this method has two limitations: 1) first the

amplitude of the signal obtained in the presence of troponin is small and the noise to signal ratio is big. 2) As can be seen from the simulations in figures 5.17 to 5.21, the method is only accurate for n values between 1 and 10. For n values higher than 10, the differences between the curves are small and therefore not accurate. We found that all TnI mutations did not affect the size of the cooperative unit and gave values of n comparable to the wild type (values in the range 14-21). This is not surprising since only the TnT subunit influences Tm-Tm communication along the thin filament via its interaction at the Tm-Tm overlap region (Schaertl et al., 1995) and TnI does not interact with tropomyosin. These results suggest that TnI mutations are unlikely to affect the propagation of the Ca^{2+} binding or dissociation along the actin filament.

b) Effect of TnI mutation on the transition between the blocked and closed states:

Structural and biochemical studies have shown that the thin filament can exist in three distinct states, figure 1.21 (McKillop and Geeves 1993). The blocked state has been only shown to be occupied in the absence of calcium when the troponin I is tightly bound to the thin filament. The proportion of thin filament in the blocked state is an important determinant of cardiac muscle relaxation. In the blocked state (In the absence of calcium) the troponin-tropomyosin complex is located in the outer domain of actin totally covering the S1 binding sites.

The large fluorescence change of PIA-labelled actin upon S1 myosin heads binding makes the monitoring of the transition between blocked and closed states possible (Head et al., 1995; Alahyan et al., 2006). To monitor K_B , we followed the kinetics of the binding of S1 in the presence and absence of calcium to an excess of actin. The difference in the gradient obtained in the absence of Ca^{2+} to the gradient obtained for

actin alone allow the determination of K_B . Thin filaments reconstituted with TnIR145G gave a higher value of K_B at low Ca^{2+} suggesting that it is not fully switched off in the absence of calcium (low blocked state population). Electron microscopy and helical reconstruction showed that tropomyosin is not positioned on the outer domain in the absence of Ca^{2+} as it normally does with wild type troponin. This suggests that cardiac muscle expressing this TnI mutant will not relax fully. The other mutants did not show major differences compared to the wild type. All TnI mutations showed increase calcium sensitivity of K_B compared to the wild type.

c) Effect of TnI mutations on the transition between the closed and open states.

Contraction of the heart muscle requires the switch to the open state that allows myosin head binding and force generation. Force generation is associated with phosphate release. We have used measurement of phosphate release to monitor the transition between the closed and open state. The rate of phosphate release from the thinfilament.S1.ADP.Pi complex was measured from the fluorescence enhancement of a fluorescently labelled phosphate binding protein (MDCC-PBP). In the absence of Ca^{2+} , Troponin I R145G displayed less inhibition of the rate of phosphate release. This result supports a reduction in the population of the blocked state occupied by thin filaments reconstituted with this mutant. TnIR145G also decreased the activation of phosphate release in the presence of Ca^{2+} . This suggests that this mutation inhibit the transition from the closed to the open state. The absence of a lag in the excimer fluorescence change upon switching from the open to the closed state suggests that this mutation stabilises the closed state. All other mutants did not affect this transition.

CHAPTER 6

**A comparative study of skeletal muscle
and cardiac muscle thin filaments
activation of the actomyosin ATPase.**

6.1 Introduction

Although skeletal muscle and cardiac muscle share a number of similarities, there are considerable differences between these two types of muscle. For example, in cardiac muscle, the in vivo tuning of contraction varies from beat to beat depending on sympathetic tone and circulatory load. While in skeletal muscle the contraction is modulated by the delivery of Ca^{2+} to the myoplasm during excitation-contraction coupling (Moss and Fitzsimons 2010). At the level of contractile proteins, cardiac and skeletal muscles have different isoforms of actin, myosin, troponin and tropomyosin. cTm is composed of $\alpha\alpha$ -homodimers while skeletal muscle contains mainly $\alpha\beta$ -heterodimers. cTnI contains an extra 32-amino acid as N-terminal extension that contains two phosphorylation sites, ser23 and 24. In addition the cTnC contains only a single calcium binding site in the N terminal of TnC, whereas in the N terminal of skeletal TnC, there are two Ca^{2+} binding sites (Zhang et al., 1995; Perry 1998). Also, unlike skeletal troponin C, cardiac troponin C undergoes only a partial opening upon Ca^{2+} binding to the N terminal region and further opening is achieved after TnI binding to TnC (Li et al., 1999). The whole N terminal of skTnC found to be tilted substantially with respect to the C terminal, IT arm, and thin filament during activation, but this motion does not occur in the cardiac muscle (Sun et al., 2009).

Furthermore, in skeletal muscle Ca^{2+} alone is insufficient to fully activate thin filaments and the binding of myosin heads to actin is necessary for myofilament full activation. In skeletal muscle a cooperative allosteric three state model has been suggested to account for both Ca^{2+} and myosin heads activation of actin filaments. Previous assumptions by a number of authors (including our lab) extrapolated the nature of skeletal muscle thin filament transitions and their effectors to cardiac muscle thin

filaments (Fitzsimons et al., 2001 a and b; Mirza et al., 2007). They suggested that cardiac thin filaments also exist in three states with similar properties to those in skeletal muscle and that Ca^{2+} also controls the blocked to closed transition while myosin heads controls the closed to open state. However, a couple of papers published during the course of this thesis (Sun et al., 2009; Houmeida et al., 2010) challenged this assumption and argued that the physiological regulation of cardiac contractility by Ca^{2+} is rather an intrinsic property of thin filaments with no contribution from myosin cross bridges.

Finally the step in the cardiac actomyosin ATPase pathway regulated by Ca^{2+} is thought to be phosphate release but without direct experimental evidence.

In the present studies, we used rapid reaction kinetics to uncover the step in the actomyosin ATP hydrolysis pathway regulated by Ca^{2+} . We also aimed to compare the mechanism of cardiac thin filament activation by Ca^{2+} with that of skeletal muscle thin filaments. Our results suggest that phosphate release is the step regulated by Ca^{2+} during cardiac thin filament activation of myosin ATPase. Our finding also shows that unlike skeletal muscle, in cardiac muscle Ca^{2+} alone is sufficient to maximally activate thin filaments.

6.2 Results

6.2.1 The dual effect of the regulatory proteins on the acto-S1.

Figure 6.1 shows the ATPase dependence on the concentration of S1 in the presence of a combination of the thin filament proteins (fully cardiac actin-tropomyosin-troponin-S1 and fully skeletal actin-tropomyosin-troponin-S1 systems).

For the skeletal system, at low S1 concentration the ATPase of regulated skeletal thin filament (actin.Tm.Tn) is inhibited compared to pure actin in the presence and absence of Ca^{2+} , but the inhibition is greater when Ca^{2+} is absent which is in agreement with previous published work (Lehrer and Morris 1982). When the S1 concentration is increased, the ATPase increases sigmoidally for both presence and absence of Ca^{2+} .

In contrast, for the cardiac system at low S1 concentration the ATPase of regulated cardiac thin filament (actin.Tm.Tn) is activated compared to pure actin in the presence of Ca^{2+} , and it is inhibited in the absence of Ca^{2+} . Similar to the skeletal system, when the S1 concentration is increased, the ATPase for cardiac system increases sigmoidally for both presence and absence of Ca^{2+} ; in the presence of Ca^{2+} the increase is greater.

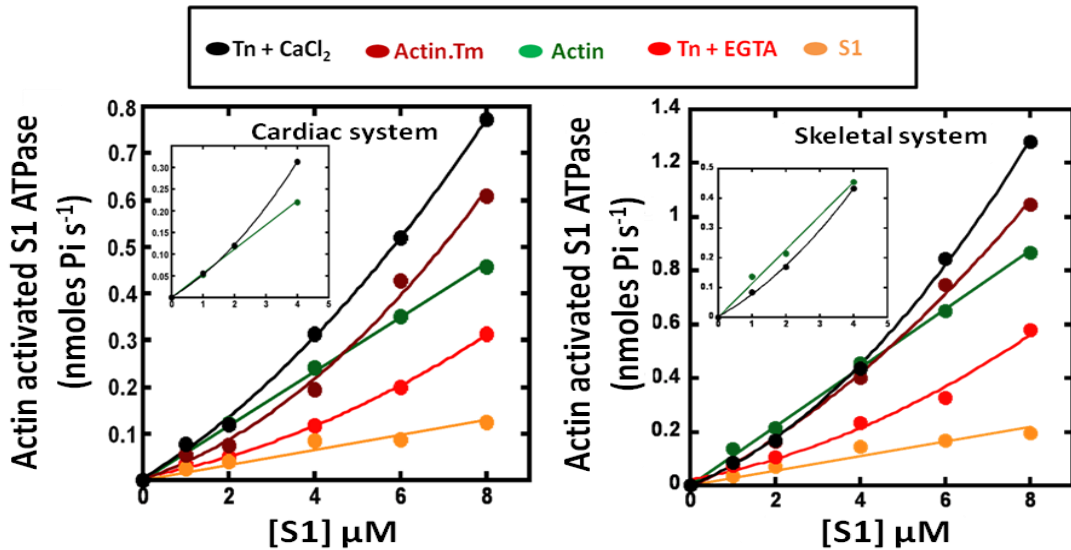


Figure 6.1 The dual effect of the regulatory proteins on the acto-S1. Activation and Inhibition of acto-S1 ATPase for cardiac and skeletal systems at increasing concentration of S1 in the presence and absence of calcium. Activity was measured in the presence of 12 μM actin, 2 μM tropomyosin, 2 μM troponin, and 1-8 μM S1 at 37 $^{\circ}\text{C}$ in ATPase low salt ATPase buffer.

6.2.2 Kinetics of phosphate release

The rate of phosphate release was measured in single turnover double mixing stopped-flow experiments directly using the fluorescence of MDCC-PBP (Heeley et al., 2002; Alahyan et al., 2006). We optimized conditions for the stopped flow experiments. Figure 6.2 shows the dependence of the rates of phosphate release from acto(TmTn)myosinS1-ADP-Pi on thin filament concentration at two different ATP concentration. 8 μM of S1 and either 10 μM or 20 μM of ATP were combined in the first mix and allowed to incubate for 2 seconds so that S1 can bind and hydrolyse ATP. In the second mix the S1-nucleotide complex was combined with thin filaments in the presence and absence of calcium and in the presence of rigor myosin head and calcium. Figure 6.3 (A and B) shows the transients of fluorescence increase upon phosphate release while figure 6.3 (C and D) shows the actin dependence of the

observed rate constants of phosphate release. In the cardiac system the observed rate constant of phosphate release was slower (around 1.5 s^{-1}) compared to the skeletal system (70 s^{-1}). In the presence of rigor myosin head and at low and high calcium, the fluorescence changes were biphasic for skeletal muscle system and single exponential for the cardiac system. The k_{obs} dependence on thin filament concentration was fit by a hyperbola. The values of the maximum observed rate constant and the apparent dissociation constant (K_d) are summarized in table 6.1. For the cardiac system, calcium alone and calcium + rigor gave observed rate constant of Pi release comparable to actin alone (Figure 6.3.C), while in the skeletal system calcium + rigor gave higher values than calcium alone (Figure 6.3.D). We repeated the experiment for Ca^{2+} saturated cardiac thin filaments with $20 \text{ }\mu\text{M}$ ATP to assess if the ATP concentration was not enough to saturate S1, which could lead to the presence of rigor. We found that the two ATP concentrations gave similar level of activation of phosphate release, figure 6.2. In the absence of Ca^{2+} , both systems has substantially reduced observed rate constant of phosphate release (values around the steady state values obtained from ATPase experiments).

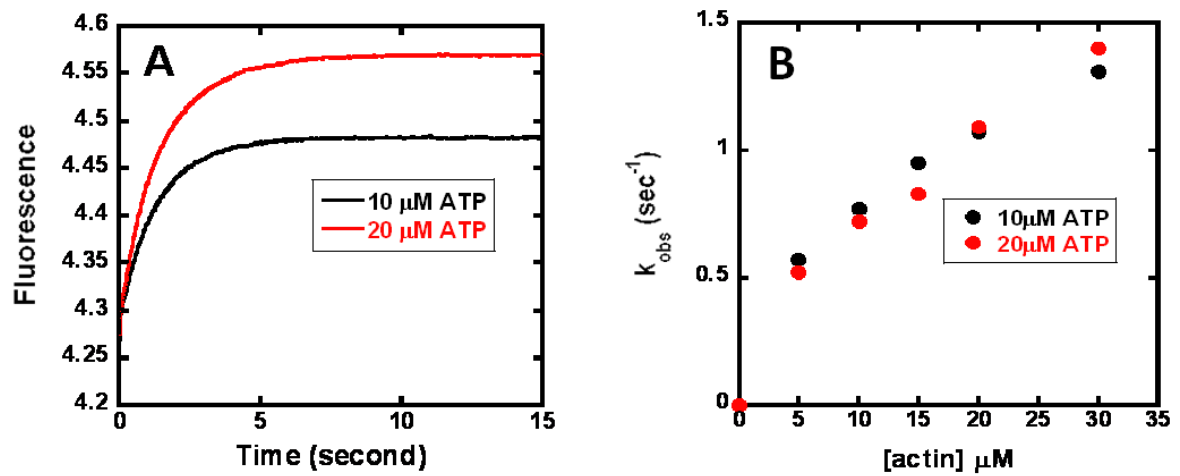


Figure 6.2 The effect of ATP concentration on the rates of phosphate release from acto(TmTn)myosinS1-ADP-Pi in the presence of calcium. A is a stopped flow kinetic traces for cardiac system at 10 and 20 μM ATP. Double mixing stopped-flow experiments were performed by mixing 8 μM S1 with 10 and 20 μM ATP and incubated for 2 sec and then mixed with 20 μM (actin subunit concentration) thin filaments in the presence of calcium. B the dependence of k_{obs} on thin filament concentration for cardiac system. Double mixing stopped-flow experiments were performed by mixing 8 μM S1 with both 10 and 20 μM ATP and incubated for 2 sec and then mixed with thin filaments in the presence of calcium. Conditions: 5 mM MOPS pH 7, 3 mM MgCl_2 , 6 μM MDCC-PBP, 0.1 mM 7-methyl guanosine, 0.01 unit/ml purine nucleoside phosphorylase, at 25 $^\circ\text{C}$.

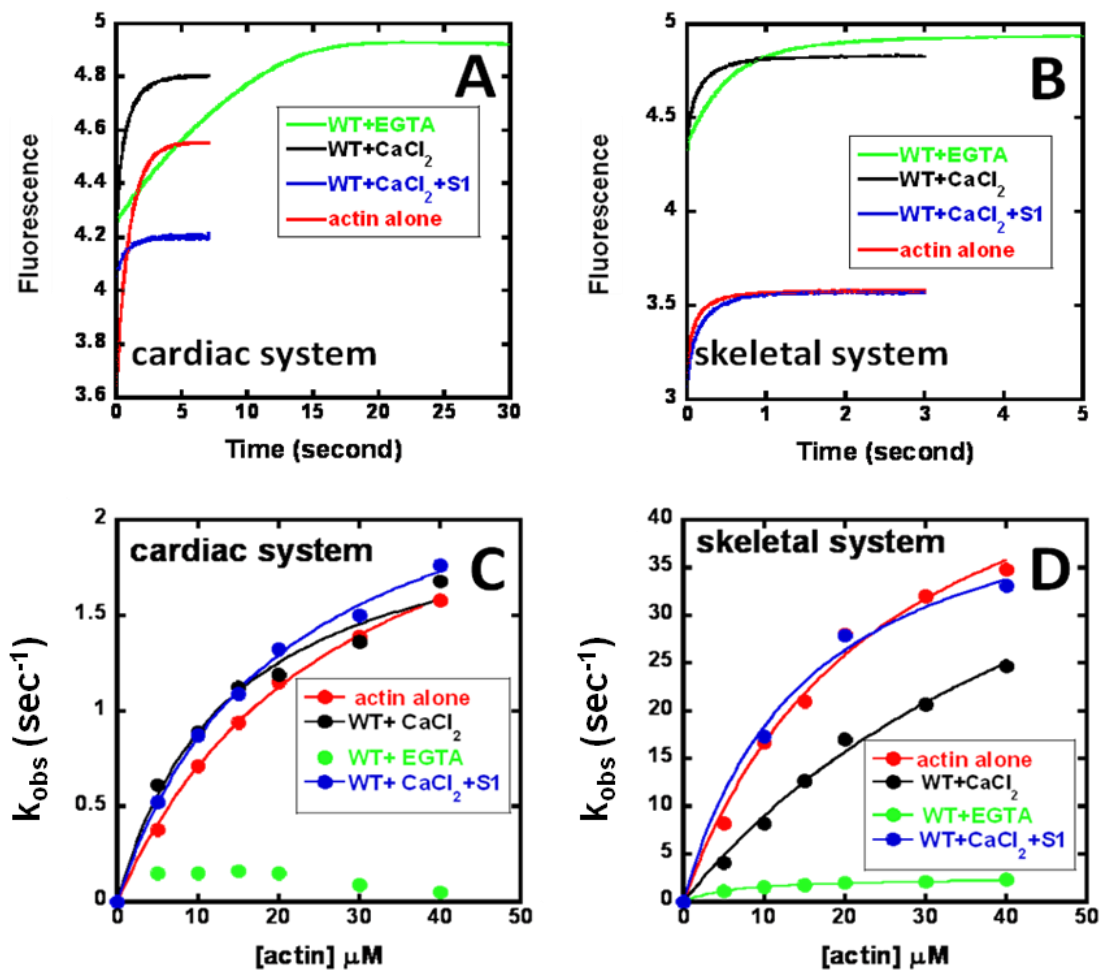


Figure 6.3 Dependence of the rates of phosphate release from acto(TmTn)myosinS1-ADP-Pi on thin filament concentration and calcium and rigor S1 bound to the thin filament. A and B are Stopped flow kinetic traces for cardiac and skeletal systems. Double mixing stopped-flow experiments were performed by mixing 8 μM S1 with 10 μM ATP and incubated for 2 sec and then mixed with 30 μM (actin subunit concentration) thin filaments in the presence of calcium, calcium and rigor and in the absence of calcium for both skeletal and cardiac systems. C and D are the dependence of k_{obs} on thin filament concentration for cardiac and skeletal systems. The dependences were fitted to hyperbolas. Conditions: 5 mM Mops pH 7, 3 mM MgCl₂, 6 μM MDCC-PBP, 0.1 mM 7-methyl guanosine, 0.01 unit/ml purine nucleoside phosphorylase, at 25 °C.

Table 6.1 Maximum rate constant of phosphate release, and dissociation constant for cardiac and skeletal system

	K_d (μM)	Maximum rate constant of phosphate release (s^{-1})
Cardiac system		
Actin alone	28	2.7
Thin filament + Ca^{2+}	14	2.1
Thin filament + EGTA	-	-
Thin filament + Ca^{2+} + Rigor	21	2.6
Skeletal system		
Actin alone	58	61
Thin filament + Ca^{2+}	16	47
Thin filament + EGTA	6.7	2.6
Thin filament + Ca^{2+} + Rigor	25	58

6.2.3 The equilibrium constant between blocked and closed states

K_B was measured by comparing the kinetics of S1 binding to thin filaments at low and high calcium. A 10 fold excess of actin was rapidly mixed with S1 and the binding event was monitored by the quenching of the fluorescence using PIA-label actin at Cys-374. Figure 6.4 (A and B) show the change in fluorescence that were observed by mixing 0.4 μ M S1 with 4 μ M PIA-actin/0.8 μ M Tm.Tn in the stopped flow apparatus in the presence and absence of calcium. Figure 6.4 (C and D) shows the actin dependence of the rate of S1 binding to actin. For both skeletal and cardiac systems, the observed rate constant of S1 binding to actin alone, and to actin.Tm.Tn in the presence of calcium were similar within experimental errors. This suggests that the actin.Tm.Tn+Ca²⁺ is mostly in the open state for both systems as it would be expected for actin alone (Head et al., 1995). The ratio of the values of k_{obs} in the absence of calcium to the value of k_{obs} for actin alone (or presence of calcium) gave a K_B value of 0.40 for skeletal system but a higher value of 0.74 for the cardiac system. Our results were similar to those published previously for both cardiac and skeletal systems (Maytum et al., 1999; Maytum et al., 2003).

Figure 6.5 shows a plot of K_B 's versus pCa for both systems; they are typical cooperative binding curves. The data were fitted to the Hill equation and the pCa₅₀ and n_H were determined. Both systems showed pCa₅₀= 5.88, and a Hill coefficient of 1.9 and 1.5 for skeletal and cardiac system respectively. However an important difference is in the minimum values (Obtained in the absence of Ca²⁺) and in the maximum values (obtained in the presence of Ca²⁺). Both of them are much higher for cardiac thin filaments.

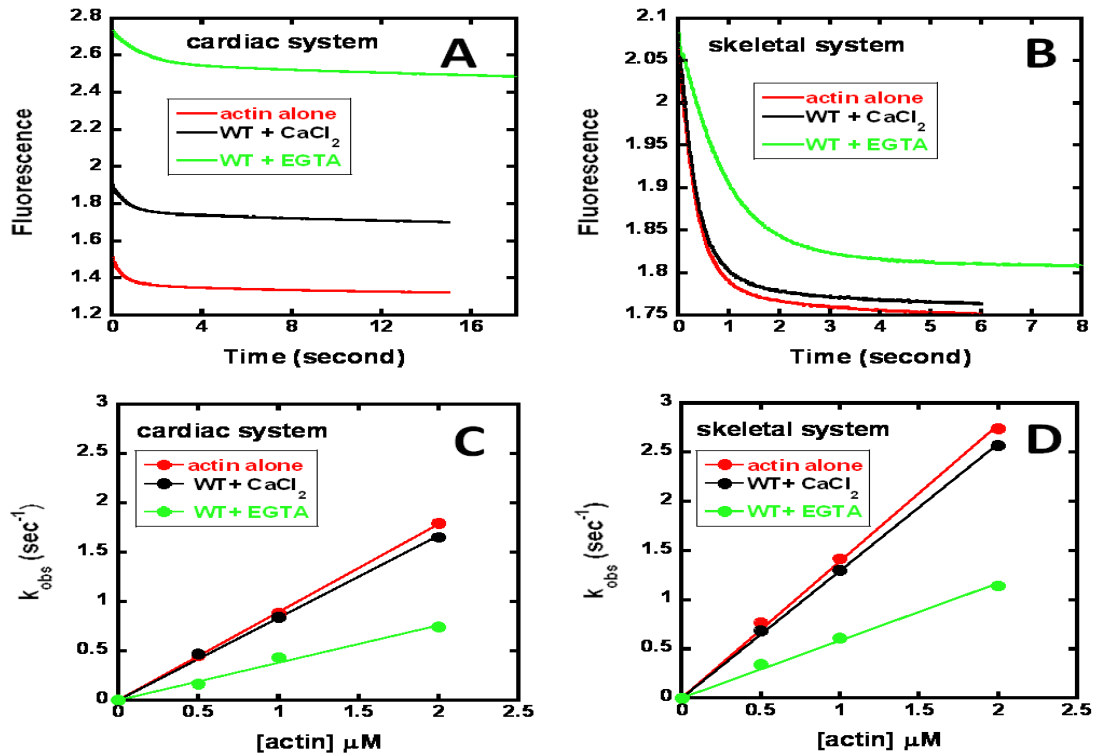


Figure 6.4 Binding of S1 to PIA-actin and to actin.Tm.Tn in the presence and absence of calcium for both cardiac and skeletal systems. A and B are the fluorescence transients (for cardiac and skeletal systems) that were observed by mixing 0.4 μM S1 with 4 μM PIA-actin/0.8 μM Tm.Tn in the stopped flow apparatus in the presence and absence of calcium. C and D are the observed rate of S1 binding as a function of PIA-labelled actin concentration in the presence and absence of calcium. Conditions: 140 mM KCl, 10 mM Mops pH 7.2, 4 mM MgCl₂, 1 mM DTT, 0.2 mM CaCl₂ or 1 mM EGTA, at 25 °C.

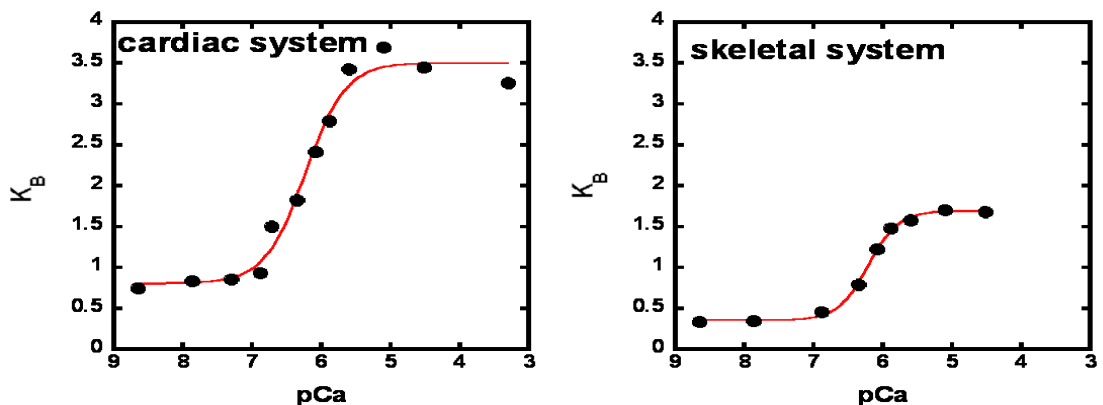


Figure 6.5 The equilibrium constant K_B as a function of pCa for cardiac and skeletal systems. The experiments were performed in 50 mM Mops pH 7.0, 140 mM KCl, 4 mM MgCl₂, and 2 mM EGTA, at 25 °C.

6.2.4 The size of cooperative unit

As mentioned in the introduction, cardiac and skeletal muscle tropomyosin isoforms are different. Skeletal muscle tropomyosin is made of $\alpha\beta$ -heterodimers while cardiac tropomyosin is made of $\alpha\alpha$ -homodimers. Many functional studies have pointed to differences between α and β isoforms of tropomyosin. Since one of the important functions of tropomyosin is to introduce long range cooperativity to the thin filaments, we aimed to investigate the cooperativity of these two isoforms. We used the method described in chapter 5 to determine the size of the cooperative unit n for both skeletal muscle and cardiac muscle thin filaments.

Figure 6.6 shows the normalised transients obtained for both sheep cardiac tropomyosin (cardiac system) and skeletal muscle tropomyosin (skeletal system). Both experimental curves describing the fluorescence change for cardiac and skeletal muscle labelled tropomyosin are positioned between the simulated curves using $n=14$ and $n=21$. Therefore, the apparent size of cooperative unit (n) is similar between both cardiac and skeletal systems (actin.Tm.Tn thin filament) in the presence of Ca^{2+} (around 14-21).

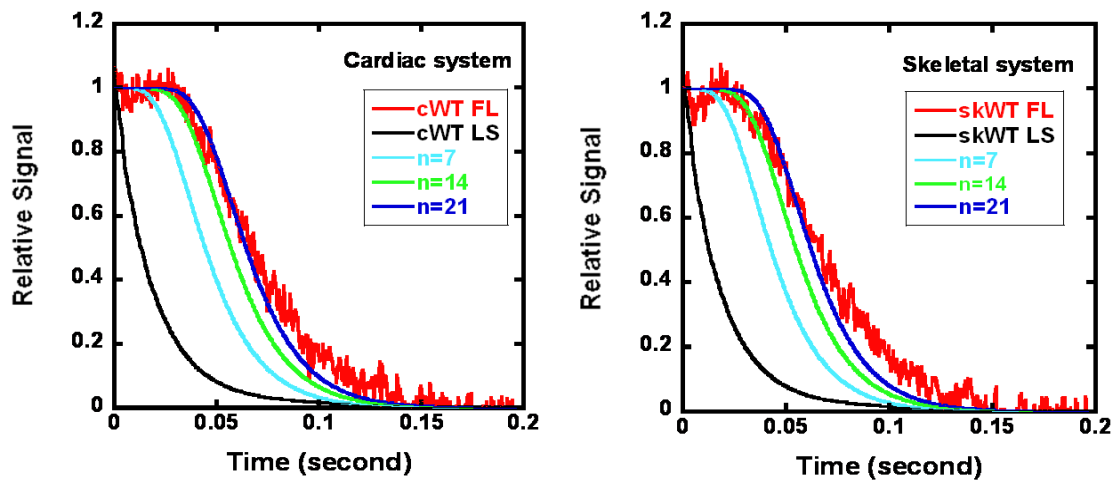


Figure 6.6 Kinetics of ATP induced dissociation of S1 from Actin.Tm*.Tn thin filament (cardiac and skeletal systems). Normalised time courses of light scattering (black lines) and fluorescence (red lines) signals when 56 μM ATP was mixed with 6 μM S1, 6 μM actin, 1 μM Tm* and 1 μM Tn. The other coloured lines are the computer generated simulation curves. The experiments were performed in 140 mM KCl, 20 mM Mops pH 7.2, 4 mM MgCl_2 , 0.2 mM CaCl_2 , and 1 mM DTT, at 25 $^\circ\text{C}$.

6.3 Discussion

In this chapter we compared skeletal and cardiac muscle thin filaments and their activation by Ca^{2+} and myosin. We assessed the impact of these isoform differences on the occupancy of blocked state, the transition to the open state, the size of the cooperative unit n and the activation of phosphate release.

We have used recombinant human cardiac troponin, sheep heart cardiac actin, tropomyosin and myosin heads. Skeletal muscle thin filaments were reconstituted from rabbit skeletal muscle actin, tropomyosin, troponin and the myosin heads.

The main findings from these investigations are:

1) Cardiac thin filaments have a lower population of the blocked state in the absence of Ca^{2+} than skeletal muscle. This has been suggested previously on the basis of activation of resting force by low level of NEM S1 (Moss et al., 2004). In a previous work, they showed that in the absence of calcium, the cardiac system showed a 2-3 fold reduction in the rate constant of S1 binding to actin, while the skeletal system showed a 3-4 fold reduction, as a result the cardiac system is less off than skeletal system in the absence of calcium (Maytum et al., 2003). The high proportion of cardiac thin filaments not in the blocked state could lead to a higher level of diastolic wall stress due to small variation in Ca^{2+} intracellular concentration. This effect may be exacerbated in mutations that increase cardiac thin filaments sensitivity.

2) In the presence of troponin and Ca^{2+} the size of the cooperative unit is similar. This is rather surprising since the main protein determinant of the size of the cooperative unit is tropomyosin and the isoform content of cardiac tropomyosin ($\alpha\alpha$ -homodimers) and skeletal muscle tropomyosin ($\alpha\beta$ -heterodimers) is different. However, the method

used is not sensitive enough to detect differences above an n value of 14 and so small differences may have not been detected in our experiment. Geeves and co-workers found that the cardiac TnT has the same effect as the skeletal TnT in increasing the size of cooperative unit (Maytum et al., 2003).

3) At high Ca^{2+} , skeletal muscle thin filaments still contain a significant proportion in the blocked state (about 40%) while cardiac muscle thin filaments contain less than 20%. Maytum et al. reported that in the absence of calcium, the cardiac system shows a higher occupancy of closed and open states compared to the skeletal system (Maytum et al., 2003).

4) The rate of phosphate release is the rate limiting step for cardiac thin filament activation of cardiac myosin ATPase (White et al., 1997; Houmeida et al., 2010).

5) The rate of phosphate release is the step regulated by Ca^{2+} . This is similar to the regulation of phosphate release reported in skeletal muscle (Heeley et al., 2002) and smooth muscle (Alahyan et al., 2006).

6) Ca^{2+} is sufficient to fully activate the rate of phosphate release from cardiac thin filaments-cardiac S1.ADP.Pi, while in skeletal muscle thin filaments, Ca^{2+} alone is not sufficient but rather full activation needs both Ca^{2+} and S1 activation.

Our data are in agreement with the recent report that myosin binding does not contribute significantly to cardiac thin filament activation under physiological conditions, the mechanism of cooperativity in cardiac system should be intrinsic to the thin filaments (Sun et al., 2009).

CHAPTER 7

General Discussion

7.1 Introduction

Genetic hypertrophic and dilated cardiomyopathies are characterized by a conspicuous change in contractile dysfunction and in the heart morphology. The genetics of these cardiomyopathies have been established and many mutations in the contractile proteins including the troponin complex have been found. A major effort has been made to unravel how mutations in these proteins can alter their function and lead to pathological states. The main aim of this thesis is to understand, at the molecular level, how mutations in TnI that cause cardiomyopathies alter the regulation of the cardiac contractile cycle.

There are 29 mutations in human cardiac TnI that were associated with HCM and one mutation associated with DCM. Many mutations in the TnI gene are severe and patients carrying these TnI mutations are at risk of heart failure and sudden death.

Biochemical investigations have focused on steady state parameters mainly maximal activation and inhibition of actomyosin ATPase (or force or in vitro filament sliding velocity), pCa_{50} and Hill coefficient of Ca^{2+} sensitivity. However these parameters are composite parameters and depend on many elements. For instance the Hill coefficient, while a measure of thin filament cooperativity, depends on cooperativity of Ca^{2+} binding, cooperativity of transitions between the various thin filament states and cooperativity in S1 binding. The pCa_{50} depends on Ca^{2+} affinity, on Tn conformational change and on the equilibrium constants between inhibited and activated states. Maximal activation and inhibition are dependent on the level of thin filament activation (itself dependent on Ca^{2+} affinity, thin filament cooperativity and equilibrium constants) and cross bridge kinetics. The complexity of these parameters

hampered the formulation of a molecular mechanism linking the effect of mutations to the onset and progression of the disease.

In this thesis we aimed to approach the investigation of TnI linked mutations using a different strategy. We investigated the effect of TnI on single parameters using a combination of steady state and transient kinetics methods. Although transient kinetics is more complex and demanding, but it is a good method for unravelling the molecular mechanism of proteins action. The main findings are outlined in the following section.

7.2 Main Findings in the Thesis

We have chosen six HCM mutations and the only DCM mutation (A2V). These mutations were classified into four groups based on their positions within TnI functional regions. Two mutations are located in the N-terminal part of cTnI (unique to the cardiac isoform), A2V and R21C. One mutation is located in the TnT binding site, Q130R. One mutation is present in the inhibitory region. Finally three mutations are localised in the C-terminus of TnI, A157V, G203S and K206Q, figure 7.1 and figure 7.2. Overall analysis of these mutations showed that some biochemical parameters were affected similarly between all the mutations while other parameters were affected differently between these mutations.

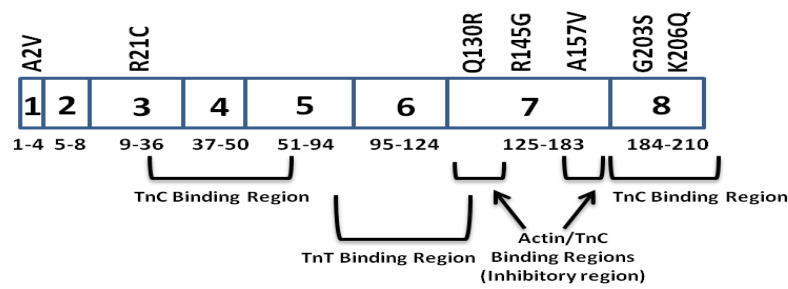


Figure 7.1 Exon organisation and TnI HCM localisation in human cardiac troponin I. (adapted from Gomes and Potter 2004).

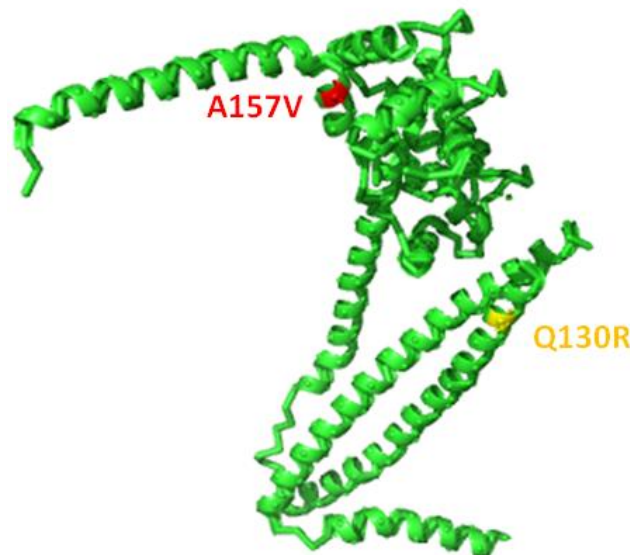


Figure 7.2 Locations of TnIQ130R and TnIA157V in troponin structure.

7.2.1 Common effects between the TnI mutations:

Circular dichroism measurement at room temperature or at various temperatures demonstrated that none of the TnI mutations affected the secondary structure or the thermal stability of the Tn complex. This is in agreement with previous studies (Lang et al., 2002; Deng et al., 2003). In addition, other studies in our lab on TnT have shown that even for deletions mutations that affected the structure of isolated TnT,

reconstitution with other Tn subunits stabilised the TnT structure and abolished this effect (Zimna Wazeer, PhD thesis, University of Leicester).

Our measurements of the size of the cooperative unit n , showed that no TnI mutation, affected this parameter ($n = 14-21$ for wild type troponin and mutants). This is also expected since thin filament cooperativity is a property of tropomyosin.

More importantly, it is well established that Ca^{2+} and actin binding weakens their mutual binding to troponin. Our measurements indicate that all TnI mutations increased the affinity of the troponin complex for actin in the presence of Ca^{2+} . This may be an important finding since, in the absence of mutations, Ca^{2+} binding to TnC weakens the interaction of the troponin complex with thin filaments and this facilitates thin filament activation. TnI mutations seem to interfere with this property. We also found that all mutations increase the Ca^{2+} affinity of thin filament. Therefore, the two effects suggest that TnI mutations may lead to uncoupling of Ca^{2+} binding and actin binding.

Finally, while most mutants did not affect K_B (at low Ca^{2+}) in the same way, all increased the Ca^{2+} sensitivity of this parameter (increased pCa_{50} of K_B).

7.2.2 Functional consequences of TnI mutations

Functional consequences associated with TnI mutations in the N-terminal TnC binding region (A2V and R21C)

TnI mutants A2V incorporated into troponin complexes reduced the activation of the reconstituted thin filament to 180 ± 8.14 , while the TnIR21C showed 260 ± 9.61 % activation. In the absence of Ca^{2+} , both TnIA2V and TnIR21C showed same inhibition

level as the wild type (86 ± 5.21 % and 91 ± 4.34 % inhibitions respectively). Consistent with our findings, in a previous study, they showed that the TnIR21C mutant did not affect the ATPase activity (Gomes et al., 2005).

The R21C mutant displayed less activation of the rate of phosphate release; in this case it is the contraction of the heart muscle which will be affected not the extent of cardiac relaxation.

Functional consequences associated TnI mutations in the TnT binding region (Q130R)

The TnIQ130R mutant reconstituted into troponin complex showed 310 ± 7.49 % activation of ATPase in the presence of Ca^{2+} , higher than the actin-Tm-activated myosin subfragment-1 ATPase activity for the wild type, in the absence of calcium it showed same level of inhibition same as the wild type (90 ± 2.81). This mutant displayed no effect on the rate of phosphate release. This mutant showed an increase in the calcium affinity for the troponin complex and thin filament, and it showed a decrease in calcium affinity for the thin filament in the presence of myosin head rigor.

Functional consequences associated TnI mutations in the C-terminal TnC binding region (G203S, and K206Q)

For the C-terminal TnC binding region HCM mutants, the TnIK206Q showed no difference in the activation (295 ± 7.08) and inhibition (92 ± 5.32) of actin-Tm-activated myosin subfragment-1 ATPase compared to the wild type, while the TnI HCM mutant G203S showed lower activation level (265 ± 14.8 %) and same inhibition level as the wild type (90 ± 4.22 % inhibition).

G203S displayed less activation of the rate of phosphate release. In this case it is the contraction of the heart muscle which will be affected not the extent of cardiac relaxation. K206Q showed no differences in the rate of phosphate release.

7.2.3 Mutations specific effects:

Among the mutations we studied, 5 mutations (A2V, R21C, Q130R, G203S and K206Q) showed no additional effect to the common effect reported above. None of these mutations affected the other biochemical parameters investigated (n , K_B , K_T , Ca^{2+} Off rate), table 7.1.

In contrast, two mutations R145G and A157V showed compromised cardiac relaxation.

7.2.3.1 TnI R145G

Cardiac troponin I is the inhibitory subunit of the troponin complex, and its interaction with cardiac troponin C plays a crucial role in transmitting the signal of Ca^{2+} to the other myofilament proteins in heart muscle contraction. The inhibitory region of cTnI is a twenty amino acid motif encompassing residues 128-147. The inhibitory region binds to either cTnC or actin-tropomyosin, depending on the intracellular concentration of Ca^{2+} . The inhibitory region of cTnI during diastole binds strongly to actin-tropomyosin, and that inhibits the actin-myosin interaction and consequently cardiac interaction. The inhibition is released when cTnI binding shifts from actin to cTnC, due to Ca^{2+} binding to the Ca^{2+} binding site within the N-domain of cTnC (Lindhout et al., 2002). The movement of the inhibitory region of cTnI from actin-tropomyosin to cTnC constitutes the key switch between muscle relaxation and contraction (Lindhout et al., 2002).

Half of the residues of the inhibitory region are thought to be essential for inhibitory activity; therefore the interaction of a small region of TnI with actin is the minimum requirement to prevent actin activation of myosin ATPase (Patchell et al., 2002).

Multiple mutations in cTnI have been associated with heart diseases. A specific missense mutation within the inhibitory region -R145G- has been associated with familial hypertrophic cardiomyopathy (Kimura et al., 1997). TnIR145G mutation is located in the critical inhibitory region (residues 128-147). The HCTnIR145G mutation occurs at a highly conserved position and causes a change from a basic arginine residue to a non polar glycine residue at the 145 position.

The effect of TnIR145G on the steady state ATPase activity was significantly different from the wild type as has been previously reported by other groups (Elliot et al., 2000; Lang et al., 2002). In the absence of Ca^{2+} this mutant reconstituted into troponin complex showed a reduced inhibition, while in the presence of Ca^{2+} , TnIR145G showed less activation (156%).

This reduced inhibition can be explained if the TnIR145G mutation only moderately holds Tm in the closed state, and as a result it could partially blocks the binding of strong myosin heads to the actin thin filament; therefore at low Ca^{2+} concentration, the ATPase activity remains high. This can support the notion that the interaction between actin-Tm and cTnIR145G is disrupted by the missense mutation in cTnI.

There is a potential that the TnIR145G mutation can lead to a structural perturbation in the cTnI subunit and as a result in the entire troponin complex. To determine whether this mutation causes a change in the secondary structure of TnI, CD spectroscopy was carried out on wild type cTnI and the TnIR145G mutant. The TnI mutant (R145G) showed no difference in the secondary structure when it is compared

to the wild type cTnI, our finding is consistent with previous findings (Lang et al., 2002). R145G mutation had a dramatic increase of the equilibrium constant between blocked and closed states (K_B) in the absence of Ca^{2+} , table 7.1. This effect was also observed using 3-dimensional reconstructions of tropomyosin on actin reconstituted with TnI R145G. This effect explains the observed decreased inhibitory activity of TnIR145G. It has been suggested that TnI may pin the troponin-tropomyosin complex in the blocked state (Lang et al., 2002; Kobayashi et al., 2004). The abolition of K_B by R145G suggests that TnIR145 may be the amino acid (or one of the few amino acids) involved in pinning the troponin-tropomyosin complex in the blocked state.

In their study, Lindhout and his colleagues suggested that the removal of the positive charge on the arginine side chains by mutation to glycine results in the loss of the hydrophobic methylene side-chain carbon group, this replacement might affect the side-chain packing required for proper complex formation. It is possible that the loss of this critical salt-bridge is sufficient to change the important electrostatic balance in this region of cTnI, and this in turn negatively alter the interaction of TnI with actin in the absence of Ca^{2+} (Lindhout et al., 2005).

Burton et al. found that the TnIR145G mutation would lead to a complete loss of relaxation when it was studied in an invitro motility assay, the TnIR145G mutation is a lethal mutation and patients with TnIR145G mutation most likely express the mutated protein at low levels (Burton et al., 2002).

It has been suggested that TnIR145 is essential for the appropriate interaction of TnI with TnC in calcium bound state. The human cardiac TnIR145G mutation can disturb the interactions between TnI-TnC and TnI-actin, in that way affecting cross bridge turnover kinetics (Kruger et al., 2005).

7.2.3.2 TnI A157V

Cardiac muscle activation is triggered by Ca^{2+} binding to the single regulatory site of cardiac troponin C, this binding leads to structural changes between cTnC and the two key regions of cardiac troponin I: the inhibitory region (residues 128–147) and the switch region (residues 150–159). When Ca^{2+} binds to cTnC during systole, the switch region of cTnI pulls the inhibitory region away from its binding site on actin, leading to tropomyosin movement and myosin binding sites exposure on actin, allowing the actin–myosin interaction (Takeda et al., 2003; Dong et al., 2003; Oleszczuk et al., 2010).

A particular missense mutation within the switch region –A157V- has been associated with familial hypertrophic cardiomyopathy (Richard et al., 2003).

TnIA157V was the only mutation to show decreased calcium dissociation rate compared to wild type in all three systems (troponin complex, thin filament, and thin filament + myosin heads), table 7.1. This mutation showed slower calcium dissociation kinetics in IAANSC35, IAANSC84 and Quin-2 experiments, and we suggest that this could compromise the kinetics of relaxation. A slower relaxation may affect cardiac relaxation in a more dramatic way under conditions of strenuous exercise since the cardiac cycle is shortened and relaxation is much faster.

Table 7.1 Summary of general findings in this thesis

TnI	Structural changes		Thermal stability		ATPase activity				K _B			K _T		Ca ²⁺ affinity			Rate of Ca ²⁺ dissociation using IAANSC35			Rate of Ca ²⁺ dissociation using IAANSC84			Rate of Ca ²⁺ dissociation using Quin-2				
	Structural changes	Thermal stability	Affinity for Thin filament	activation	inhibition	pCa ₅₀ Sensitivity	n _H	Absence of Ca ²⁺	pCa ₅₀ Sensitivity	n _H	Size of coop	Unit (n)	Tn complex using IAANSC35	Thin filament using IAANSC84	Thin filament + S1 using IAANSC 84	Tn complex	Thin filament	Thin filament+S1	Tn complex	Thin filament	Thin filament+S1	Tn complex	Thin filament	Thin filament+S1	Tn complex	Thin filament	Thin filament+S1
A2V	↔	↔	↑	↓	↓	↔	↓	↔	↑	↔	↔	↓	↑	↓	↔	↔	↔	↓	↔	↓	↔	↔	↔	↔	↔	↔	↔
R21C	↔	↔	↑	↓	↔	↔	↑	↔	↑	↔	↔	↓	↑	↓	↔	↔	↔	↔	↔	↔	↔	↔	↔	↔	↔	↔	↔
Q130R	↔	↔	↑	↑	↔	↔	↑	↔	↑	↔	↔	↑	↑	↓	↔	↔	↔	↔	↔	↔	↔	↔	↔	↔	↔	↔	↔
R145G	↔	↔	↑	↓	↓	↑	↓	↑	↑	↔	↔	↔	↑	↑	↓	↔	↔	↔	↔	↔	↔	↔	↔	↔	↔	↔	↔
A157V	↔	↔	↑	↑	↔	↔	↔	↔	↑	↔	↔	↔	↑	↑	↑	↓	↓	↓	↓	↓	↓	↓	↓	↓	↓	↓	↓
G203S	↔	↔	↑	↓	↔	↔	↔	↔	↑	↔	↔	↑	↑	↓	↔	↔	↔	↔	↔	↔	↔	↔	↔	↔	↔	↔	↔
K206Q	↔	↔	↑	↔	↔	↑	↔	↔	↑	↔	↔	↑	↑	↑	↔	↔	↔	↔	↔	↔	↔	↔	↔	↔	↔	↔	↔

7.2.4 Comparison of Cardiac and skeletal muscle thin filament activation:

Cardiac and skeletal muscles share a number of similarities; however there are considerable differences between these two types of muscle. In skeletal muscle, the contraction is modulated by Ca^{2+} delivery to the myoplasm during excitation-contraction coupling, while the contraction of heart muscle is activated on a beat to beat basis by a transient increase in intracellular free Ca^{2+} ion concentration (Moss and Fitzsimons 2010).

Cardiac and skeletal muscles have different isoforms of actin, myosin, troponin and tropomyosin. Cardiac and skeletal actins are almost identical to each other (Collins and Elzinga 1975). cTm is composed of $\alpha\alpha$ -homodimers, while skeletal muscle contains mainly $\alpha\beta$ -heterodimers. Fast skeletal and cardiac myosins have drastically different kinetic mechanisms; the former have faster ADP dissociation rates from actomyosin (Siemankowski et al., 1985). In the N terminal of skeletal TnC, there are two Ca^{2+} binding sites, while in cTnC there is only one calcium binding site in the N terminal regulatory lobe of TnC (Zhang et al., 1995; Perry 1998). Unlike skeletal troponin C, cardiac troponin C undergoes only a partial opening upon Ca^{2+} binding to the N terminal region and further opening is achieved after TnI binding to TnC (Li et al., 1999). The whole N terminal of skeletal TnC found to be tilted substantially with respect to the C terminal, IT arm, and thin filament during activation, but this motion does not happen in the cardiac muscle (Sun et al., 2009). cTnI contains an extra 32-amino acid as N-terminal extension that contains two phosphorylation sites, ser23 and 24.

In the present study, we compared cardiac and skeletal muscle thin filaments and their activation by myosin and Ca^{2+} . We assessed the impact of these isoform differences on

the occupancy of blocked state, the size of the cooperative unit n , the transition to the open state, and the activation of phosphate release.

We have used recombinant human cardiac troponin, sheep heart cardiac actin, tropomyosin and myosin heads. Skeletal muscle thin filaments were reconstituted from rabbit skeletal muscle actin, tropomyosin, troponin and the myosin heads.

Here, we used rapid reaction kinetics to uncover the step in the actomyosin ATP hydrolysis pathway regulated by Ca^{2+} . We also aimed to compare the mechanism of cardiac thin filament activation by Ca^{2+} with that of skeletal muscle thin filaments.

It has been found previously that the cardiac thin filaments have lower population of the blocked state in the absence of Ca^{2+} compared to the skeletal thin filaments (Moss et al., 2004). Maytum et al. showed that in the absence of calcium, the skeletal system showed a 3-4 fold reduction in the rate constant of S1 binding to actin, while the cardiac system showed a 2-3 fold reduction, as a result the cardiac system is less off than skeletal system in the absence of calcium (Maytum et al., 2003).

Consistent with previous findings (Maytum et al., 2003), we found that in the presence of troponin and Ca^{2+} the size of the cooperative unit is similar for both skeletal and cardiac systems. However, the method used is not sensitive enough to detect differences above an n value of 14 and so small differences may have not been detected in our experiment (Maytum et al., 2003).

At high Ca^{2+} , cardiac muscle thin filaments contains lower proportion in the blocked state (about 20%) compared to the skeletal muscle thin filaments (contains about 40%)(Maytum et al., 2003).

Previous published work found that the rate of phosphate release is the rate limiting step for skeletal thin filament activation of myosin ATPase (White et al., 1997;

Houmeida et al., 2010). The rate of phosphate release is also the step regulated by Ca^{2+} in skeletal muscle.

In skeletal muscle, a cooperative allosteric three state model has been suggested to account for both Ca^{2+} and myosin heads activation of actin filaments. It has been suggested that cardiac thin filaments also exist in three states with similar properties to those in skeletal muscle, and that Ca^{2+} also controls the blocked to closed transition, while myosin heads controls the closed to open state (Fitzsimons et al., 2001 a and b; Mirza et al., 2007). Recently, two groups argued that the physiological regulation of cardiac contractility by Ca^{2+} is an intrinsic property of thin filaments with no contribution from myosin cross bridges (Sun et al., 2009; Houmeida et al., 2010).

In summary, we have found that calcium alone is sufficient to fully activate the cardiac thin filament, while skeletal muscle thin filaments complete activation required both Ca^{2+} and myosin heads. This is a fundamental difference between skeletal muscle and cardiac muscle activation and relaxation. This could have important clinical consequences since many drugs used for cardiac diseases therapy affect the Ca^{2+} level in the heart. Our findings are also important for the studies of disease associated mutations in Tn and Tm.

7.3 Mechanism of pathogenesis

Since the discovery of the linkage of genetic hypertrophic and dilated cardiomyopathies to mutations in contractile proteins, a major effort is aimed at uncovering the molecular defects that could represent the initial insult on the cardiac function. However relating structural and biochemical changes inflicted by mutations to the actual consequences at the level of the heart is a challenging task. This is

because the sarcomere (which is the muscle contractile unit) is an integrated cooperative system and therefore perturbation of any part of this functional unit is likely to affect the properties of the whole system. Nevertheless making predictions on the basis of these biochemical studies is a useful starting point for understanding the disease process.

All studied mutations showed two important features: an increase in Ca^{2+} affinity and an uncoupling of actin binding from Ca^{2+} binding. Since troponin C plays an important role in buffering Ca^{2+} in the myoplasm of cardiomyocyte, it has been suggested that a change in Ca^{2+} affinity may affect intracellular Ca^{2+} homeostasis (Bers et al 2008). Indeed a transgenic animal expressing TnIG203S has been shown to have altered Ca^{2+} cycling (Tsoutsman et al 2006). Ca^{2+} has many more roles in cardiomyocyte than just regulation of cardiac muscle contraction. It is involved in apoptosis and growth programs.

One mutation studied (R145G) decreased the population of the blocked state at low Ca^{2+} . We therefore suggest that this mutation may compromise cardiac relaxation in the low Ca^{2+} resting state (Diastole). Indeed Kruger et al. have shown that R145G mutation slowed the kinetics of force relaxation in mechanical experiments (Kruger et al., 2005).

In contrast the A157V mutation decrease the Ca^{2+} dissociation rate constant, and we suggest that this could also compromise the kinetics of relaxation. Although a slightly slower kinetics of relaxation may not alter cardiac function under normal physiological conditions (since the diastole is relatively long: 0.7 sec), a slower relaxation may affect cardiac relaxation in a more dramatic way under conditions of strenuous exercise.

During exercises the relaxation process needs to be fast to accommodate the increased heart rate, so lowering the rate of relaxation could compromise the functioning of the heart under these conditions.

We have not identified any specific effect due to mutation R21C. However the side chain of this Arginine is supposed to interact with the phosphate group attached to serine 23 of TnI upon its phosphorylation by PKA. Phosphorylation of TnI is the major effect of β -adrenergic stimulation (Metzger and Westfall 2004). We have not studied the effect of phosphorylation and we suggest that this mutation may affect phosphorylation mediated effects.

Finally it has been shown that the heart muscle can tolerate mild ischemic conditions and that this effect is cTnI mediated through the bisphosphorylation at Ser-23 and Ser-24, which results in more weakening of the interaction between the cardiac N terminal extension of TnI and the regulatory lobe of TnC and that lead to muscle relaxation (Solaro et al., 2008; Dorn and force 2005). Mutation in cTnI may hamper this natural mechanism of cardiac protection from mild ischemic conditions.

7.4 Limitations of study:

In this section we wish to discuss the potential limitations of our studies. Three main points need to be raised in relation to our findings and their relevance to the mechanism of pathogenesis:

- 1) The source of the proteins studied, in particular the isoform and the species from which it is derived. We have shown in chapter 6 that cardiac myosin heads affect thin filaments differently from skeletal muscle myosin heads. These differences could

explain the differences in the data obtained for the same mutation between different laboratories.

2) The dosage effect. HCM and DCM diseases are autosomal dominant diseases and therefore only one copy of the genes (of the 2 copies of each gene that humans have) is defective (Bonne et al., 1998; Vikstrom and Leinwand 1996). The expression of the mutant protein has been shown to range from as little as 5% and no more than 50%.

3) All our studies are done under unloaded conditions. In vivo, thin filaments act under load and there is evidence that the load may affect certain steps in thin filament activation and in cross-bridge kinetics. At the level of the myofilaments, the increase in the length of the sarcomere within the physiological range is associated with the increase in the Ca^{2+} sensitivity of force, at each submaximal $[\text{Ca}^{2+}]$, force would increase steeply as length is increased (Moss et al., 2004).

7.5 Conclusion:

In this thesis we have studied in depth the effect of mutations in cardiac TnI on thin filament Ca^{2+} mediated regulation. We uncovered molecular defects that are in agreement with the known role of these regions. In particular the effect of mutations R145G and A157V on the switch to the blocked state and on the Ca^{2+} dissociation rate constant respectively. We have found for the first time an uncoupling between Ca^{2+} binding and actin binding of cTnI by all TnI mutations studied. It will be interesting (but possibly challenging) to model these changes and predict their effect on cardiac function under basal activity and under conditions of increased stress such as exercise or mild ischemia.

APPENDICES

Appendix A

Buffers

Guba-Straub buffer

(0.3 M KCl, 1 mM EDTA, 0.1 M K_2HPO_4 , and 0.05 M KH_2PO_4)

ATPase high salt buffer (AHSB)

(140 mM KCl, 10 mM MOPS pH 7.2, 3.5 mM $MgCl_2$, 1 mM DTT, and 1 mM NaN_3)

ATPase medium salt buffer (AMSB)

(50 mM KCl, 10 mM MOPS pH 7.2, 3.5 mM $MgCl_2$, 1 mM DTT, and 1 mM NaN_3)

ATPase low salt buffer (ALSB)

(10 mM KCl, 10 mM MOPS pH 7.2, 3.5 mM $MgCl_2$, 1 mM DTT, and 1 mM NaN_3)

G-actin buffer

(2 mM Tris-HCl pH 8.0, 0.2 mM ATP, 0.1 mM $CaCl_2$, 0.5 mM DTT, and 1 mM NaN_3)

KME buffer

(100 mM Tris-HCl pH 8.0, 500 mM KCl, 25 mM $MgCl_2$, 10 mM EGTA, and 10 mM NaN_3)

Lysis buffer

(25 mM Tris-HCl, pH 7.5, 1 mM EDTA, 20% sucrose, 200 mM NaCl, 6 M urea, 0.1% TritonX100)

Appendix B

Ca²⁺-EGTA buffers

Ca²⁺ - EGTA buffer for K_B experiment

Total [Ca ²⁺] mM	Free [Ca ²⁺] M	pCa
0.01	2.23 * 10 ⁻⁹	8.65
0.03	6.76 * 10 ⁻⁹	8.17
0.06	1.37 * 10 ⁻⁸	7.86
0.10	2.34 * 10 ⁻⁸	7.63
0.20	4.93 * 10 ⁻⁸	7.30
0.30	7.84 * 10 ⁻⁸	7.10
0.45	1.29 * 10 ⁻⁷	6.89
0.60	1.90 * 10 ⁻⁷	6.72
0.80	2.96 * 10 ⁻⁷	6.53
1.00	4.45 * 10 ⁻⁷	6.35
1.30	8.28 * 10 ⁻⁷	6.08
1.50	1.33 * 10 ⁻⁶	5.88
1.70	2.51 * 10 ⁻⁶	5.60
1.90	7.89 * 10 ⁻⁶	5.10
2.00	3.01 * 10 ⁻⁵	4.52
2.50	5.02 * 10 ⁻⁴	3.30

Ca²⁺ - EGTA buffer for ATPase experiment

Total [Ca²⁺] mM	Free [Ca²⁺] M	pCa
0.01	2.73 * 10⁻⁹	8.56
0.04	1.12 * 10⁻⁸	7.95
0.10	3.00 * 10⁻⁸	7.52
0.30	1.16 * 10⁻⁷	6.94
0.50	2.73 * 10⁻⁷	6.56
0.80	1.09 * 10⁻⁶	5.96
0.90	2.44 * 10⁻⁶	5.61
0.95	4.81 * 10⁻⁶	5.31
1.00	1.67 * 10⁻⁵	4.77
1.10	1.03 * 10⁻⁴	3.98

Ca²⁺ - EGTA buffer for K_T experiment

Total [Ca²⁺] mM	Free [Ca²⁺] M	pCa	Total 25 mM CaCl₂ (μl) added for 1 ml
0.05	2.91 * 10⁻⁸	7.53	2.0
0.07	4.27 * 10⁻⁸	7.37	2.8
0.10	6.55 * 10⁻⁸	7.18	4.0
0.15	1.12 * 10⁻⁷	6.95	6.0
0.17	1.35 * 10⁻⁷	6.87	6.8
0.20	1.75 * 10⁻⁷	6.75	8.0
0.25	2.62 * 10⁻⁷	6.58	10
0.30	3.94 * 10⁻⁷	6.40	12
0.35	6.12 * 10⁻⁷	6.21	14
0.40	1.04 * 10⁻⁶	5.98	16
0.45	2.27 * 10⁻⁶	5.64	18
0.50	1.14 * 10⁻⁵	4.94	20
0.60	1.01 * 10⁻⁴	3.99	24

REFERENCES

Alahyan, M., Webb, M. R., Marston, S. B., and El-Mezgueldi, M. (2006) The mechanism of smooth muscle caldesmon-tropomyosin inhibition of the elementary steps of the actomyosin ATPase, *J Biol Chem* 281, 19433-19448.

Al-Hillawi, E., Minchin, S. D., and Trayer, I. P. (1994) Overexpression of human cardiac troponin-I and troponin-C in *Escherichia coli* and their purification and characterisation. Two point mutations allow high-level expression of troponin-I, *Eur J Biochem* 225, 1195-1201.

Arad, M., Seidman, J. G., and Seidman, C. E. (2002) Phenotypic diversity in hypertrophic cardiomyopathy, *Hum Mol Genet* 11, 2499-2506.

Ashrafian, H., and Watkins, H. (2007) Reviews of translational medicine and genomics in cardiovascular disease: new disease taxonomy and therapeutic implications cardiomyopathies: therapeutics based on molecular phenotype, *J Am Coll Cardiol* 49, 1251-1264.

Barry, W. H., and Bridge, J. H. (1993) Intracellular calcium homeostasis in cardiac myocytes, *Circulation* 87, 1806-1815.

Barta, J., Toth, A., Jaquet, K., Redlich, A., Edes, I., and Papp, Z. (2003) Calpain-1-dependent degradation of troponin I mutants found in familial hypertrophic cardiomyopathy, *Mol Cell Biochem* 251, 83-88.

Bers, D. M. (2008) Calcium cycling and signaling in cardiac myocytes, *Annu Rev Physiol* 70, 23-49.

Bonne, G., Carrier, L., Bercovici, J., Cruaud, C., Richard, P., Hainque, B., Gautel, M., Labeit, S., James, M., Beckmann, J., Weissenbach, J., Vosberg, H. P., Fiszman, M., Komajda, M., and Schwartz, K. (1995) Cardiac myosin binding protein-C gene splice acceptor site mutation is associated with familial hypertrophic cardiomyopathy, *Nat Genet* 11, 438-440.

Bonne, G., Carrier, L., Richard, P., Hainque, B., and Schwartz, K. (1998) Familial hypertrophic cardiomyopathy: from mutations to functional defects, *Circ Res* 83, 580-593.

Bonnemann, C. G., and Laing, N. G. (2004) Myopathies resulting from mutations in sarcomeric proteins, *Curr Opin Neurol* 17, 529-537.

Bremel, R. D., and Weber, A. (1972) Cooperation within actin filament in vertebrate skeletal muscle, *Nat New Biol* 238, 97-101.

Brito, D., and Madeira, H. (2005) Malignant mutations in hypertrophic cardiomyopathy: fact or fancy?, *Rev Port Cardiol* 24, 1137-1146.

Brown, J. H., Kim, K.H., Jun, G., Greenfield, N. J., Dominguez, R., Volkmann, N., Hitchcock- DeGregori, S. E. & Cohen, C. (2001) *Proc. Natl. Acad. Sci. USA* **98**, 8496–8501.

Brown, J. H., Zhou, Z., Reshetnikova, L., Robinson, H., Yammani, R. D., Tobacman, L. S., and Cohen, C. (2005) Structure of the mid-region of tropomyosin: bending and binding sites for actin, *Proc Natl Acad Sci U S A* 102, 18878-18883.

Brune, M., Hunter, J. L., Corrie, J. E., and Webb, M. R. (1994) Direct, real-time measurement of rapid inorganic phosphate release using a novel fluorescent probe and its application to actomyosin subfragment 1 ATPase, *Biochemistry* 33, 8262-8271.

Burton, D., Abdulrazzak, H., Knott, A., Elliott, K., Redwood, C., Watkins, H., Marston, S., and Ashley, C. (2002) Two mutations in troponin I that cause hypertrophic cardiomyopathy have contrasting effects on cardiac muscle contractility, *Biochem J* 362, 443-451.

Chalovich, J. M., and Eisenberg, E. (1982) Inhibition of actomyosin ATPase activity by troponin-tropomyosin without blocking the binding of myosin to actin, *J Biol Chem* 257, 2432-2437.

Chang, A. N., and Potter, J. D. (2005) Sarcomeric protein mutations in dilated cardiomyopathy, *Heart Fail Rev* 10, 225-235.

Chen, R., Tsuji, T., Ichida, F., Bowles, K. R., Yu, X., Watanabe, S., Hirono, K., Tsubata, S., Hamamichi, Y., Ohta, J., Imai, Y., Bowles, N. E., Miyawaki, T., and Towbin, J. A. (2002) Mutation analysis of the G4.5 gene in patients with isolated left ventricular noncompaction, *Mol Genet Metab* 77, 319-325.

Cheng, T. O. (2005) Frequency of cardiac troponin I mutations in families with hypertrophic cardiomyopathy in China, *J Am Coll Cardiol* 46, 180-181; author reply 181.

Collins, J. H., and Elzinga, M. (1975) The primary structure of actin from rabbit skeletal muscle. Completion and analysis of the amino acid sequence, *J Biol Chem.* 250, 5915–5920.

Craig, R., and Lehman, W. (2001) Crossbridge and tropomyosin positions observed in native, interacting thick and thin filaments, *J Mol Biol* 311, 1027-1036.

Criddle, A. H., Geeves, M. A., and Jeffries, T. (1985) The use of actin labelled with N-(1-pyrenyl)iodoacetamide to study the interaction of actin with myosin subfragments and troponin/tropomyosin, *Biochem J* 232, 343-349.

Crilley, J. G., Boehm, E. A., Blair, E., Rajagopalan, B., Blamire, A. M., Styles, P., McKenna, W. J., Ostman-Smith, I., Clarke, K., and Watkins, H. (2003) Hypertrophic cardiomyopathy due to sarcomeric gene mutations is characterized by impaired energy metabolism irrespective of the degree of hypertrophy, *J Am Coll Cardiol* 41, 1776-1782.

Dalloz, F., Osinska, H., and Robbins, J. (2001) Manipulating the contractile apparatus: genetically defined animal models of cardiovascular disease, *J Mol Cell Cardiol* 33, 9-25.

Davis, J. P., Norman, C., Kobayashi, T., Solaro, R. J., Swartz, D. R., and Tikunova, S. B. (2007) Effects of thin and thick filament proteins on calcium binding and exchange with cardiac troponin C, *Biophys J* 92, 3195-3206.

Davis, J. P., and Tikunova, S. B. (2008) Ca²⁺ exchange with troponin C and cardiac muscle dynamics, *Cardiovasc Res* 77, 619-626.

Deng, Y., Schmidtman, A., Kruse, S., Filatov, V., Heilmeyer, L. M., Jr., Jaquet, K., and Thieleczek, R. (2003) Phosphorylation of human cardiac troponin I G203S and K206Q linked to familial hypertrophic cardiomyopathy affects actomyosin interaction in different ways, *J Mol Cell Cardiol* 35, 1365-1374.

Deng, Y., Schmidtman, A., Redlich, A., Westerdorf, B., Jaquet, K., and Thieleczek, R. (2001) Effects of phosphorylation and mutation R145G on human cardiac troponin I function, *Biochemistry* 40, 14593-14602.

Dong, W., Rosenfeld, S. S., Wang, C. K., Gordon, A. M., and Cheung, H. C. (1996) Kinetic studies of calcium binding to the regulatory site of troponin C from cardiac muscle, *J Biol Chem* 271, 688-694.

Dong, W. J., Robinson, J. M., Stagg, S., Xing, J., and Cheung, H. C. (2003) Ca²⁺-induced conformational transition in the inhibitory and regulatory regions of cardiac troponin I, *J Biol Chem* 278, 8686-8692.

Dong, W. J., Wang, C. K., Gordon, A. M., and Cheung, H. C. (1997) Disparate fluorescence properties of 2-[4'-(iodoacetamido)anilino]-naphthalene-6-sulfonic acid attached to Cys-84 and Cys-35 of troponin C in cardiac muscle troponin, *Biophys J* 72, 850-857.

Dong, W. J., Xing, J., Robinson, J. M., and Cheung, H. C. (2001) Ca²⁺ induces an extended conformation of the inhibitory region of troponin I in cardiac muscle troponin, *J Mol Biol* 314, 51-61.

Doolan, A., Tebo, M., Ingles, J., Nguyen, L., Tsoutsman, T., Lam, L., Chiu, C., Chung, J., Weintraub, R. G., and Semsarian, C. (2005) Cardiac troponin I mutations in Australian families with hypertrophic cardiomyopathy: clinical, genetic and functional consequences, *J Mol Cell Cardiol* 38, 387-393.

Dorn, G. W., 2nd, and Force, T. (2005) Protein kinase cascades in the regulation of cardiac hypertrophy, *J Clin Invest* 115, 527-537.

Dorn, G. W., 2nd, Robbins, J., and Sugden, P. H. (2003) Phenotyping hypertrophy: eschew obfuscation, *Circ Res* 92, 1171-1175.

Ebashi, S. (1963) Third Component Participating in the Superprecipitation of 'Natural Actomyosin', *Nature* 200, 1010.

Ebashi, S., and Endo, M. (1968) Calcium ion and muscle contraction, *Prog Biophys Mol Biol* 18, 123-183.

Elliott, K., Watkins, H., and Redwood, C. S. (2000) Altered regulatory properties of human cardiac troponin I mutants that cause hypertrophic cardiomyopathy, *J Biol Chem* 275, 22069-22074.

Farah, C. S., and Reinach, F. C. (1995) The troponin complex and regulation of muscle contraction, *FASEB J* 9, 755-767.

Fitzsimons, D. P., Patel, J. R., Campbell, K. S., and Moss, R. L. (2001) (a) Cooperative mechanisms in the activation dependence of the rate of force development in rabbit skinned skeletal muscle fibers, *J Gen Physiol* 117, 133-148.

Fitzsimons, D. P., Patel, J. R., and Moss, R. L. (1998) Role of myosin heavy chain composition in kinetics of force development and relaxation in rat myocardium, *J Physiol* 513 (Pt 1), 171-183.

Fitzsimons, D. P., Patel, J. R., and Moss, R. L. (2001) (b) Cross-bridge interaction kinetics in rat myocardium are accelerated by strong binding of myosin to the thin filament, *J Physiol* 530, 263-272.

Flicker, P. F., Phillips, G. N., Jr., and Cohen, C. (1982) Troponin and its interactions with tropomyosin. An electron microscope study, *J Mol Biol* 162, 495-501.

Franz, W. M., Muller, M., Muller, O. J., Herrmann, R., Rothmann, T., Cremer, M., Cohn, R. D., Voit, T., and Katus, H. A. (2000) Association of nonsense mutation of dystrophin gene with disruption of sarcoglycan complex in X-linked dilated cardiomyopathy, *Lancet* 355, 1781-1785.

Franz, W. M., Muller, O. J., and Katus, H. A. (2001) Cardiomyopathies: from genetics to the prospect of treatment, *Lancet* 358, 1627-1637.

Fraser, I. D., and Marston, S. B. (1995) In vitro motility analysis of actin-tropomyosin regulation by troponin and calcium. The thin filament is switched as a single cooperative unit, *J Biol Chem* 270, 7836-7841.

Fu, J. D., and Yang, H. T. (2006) Developmental regulation of intracellular calcium homeostasis in early cardiac myocytes, *Sheng Li Xue Bao* 58, 95-103.

Fujii, T., Iwane, A. H., Yanagida, T., and Namba, K. Direct visualization of secondary structures of F-actin by electron cryomicroscopy, *Nature* 467, 724-728.

Geeves, M. A., and Holmes, K. C. (1999) Structural mechanism of muscle contraction, *Annu Rev Biochem* 68, 687-728.

Geeves, M. A., and Lehrer, S. S. (1994) Dynamics of the muscle thin filament regulatory switch: the size of the cooperative unit, *Biophys J* 67, 273-282.

Geisterfer-Lowrance, A. A., Kass, S., Tanigawa, G., Vosberg, H. P., McKenna, W., Seidman, C. E., and Seidman, J. G. (1990) A molecular basis for familial hypertrophic cardiomyopathy: a beta cardiac myosin heavy chain gene missense mutation, *Cell* 62, 999-1006.

Gergely, J. (1998) Molecular switches in troponin, *Adv Exp Med Biol* 453, 169-176.

Gerull, B., Gramlich, M., Atherton, J., McNabb, M., Trombitas, K., Sasse-Klaassen, S., Seidman, J. G., Seidman, C., Granzier, H., Labeit, S., Frenneaux, M., and Thierfelder, L.

(2002) Mutations of TTN, encoding the giant muscle filament titin, cause familial dilated cardiomyopathy, *Nat Genet* 30, 201-204.

Gimona, M. (2008) Dimerization of tropomyosins, *Adv Exp Med Biol* 644, 73-84.

Gomes, A. V., Harada, K., and Potter, J. D. (2005) A mutation in the N-terminus of troponin I that is associated with hypertrophic cardiomyopathy affects the Ca²⁺-sensitivity, phosphorylation kinetics and proteolytic susceptibility of troponin, *J Mol Cell Cardiol* 39, 754-765.

Gomes, A. V., and Potter, J. D. (2004) Molecular and cellular aspects of troponin cardiomyopathies, *Ann N Y Acad Sci* 1015, 214-224.

Gomes, A. V., and Potter, J. D. (2004) Cellular and molecular aspects of familial hypertrophic cardiomyopathy caused by mutations in the cardiac troponin I gene, *Mol Cell Biochem* 263, 99-114.

Gomes, A. V., Potter, J. D., and Szczesna-Cordary, D. (2002) The role of troponins in muscle contraction, *IUBMB Life* 54, 323-333.

Gomes, A. V., Venkatraman, G., Davis, J. P., Tikunova, S. B., Engel, P., Solaro, R. J., and Potter, J. D. (2004) Cardiac troponin T isoforms affect the Ca²⁺ sensitivity of force development in the presence of slow skeletal troponin I: insights into the role of troponin T isoforms in the fetal heart, *J Biol Chem* 279, 49579-49587.

Gordon, A. M., Homsher, E., and Regnier, M. (2000) Regulation of contraction in striated muscle, *Physiol Rev* 80, 853-924.

Greaser, M. L., and Gergely, J. (1971) Reconstitution of troponin activity from three protein components, *J Biol Chem* 246, 4226-4233.

Greenfield, N. J. (2006) Using circular dichroism spectra to estimate protein secondary structure, *Nat Protoc* 1, 2876-2890.

Gregorio, C. C., and Antin, P. B. (2000) To the heart of myofibril assembly, *Trends Cell Biol* 10, 355-362.

Haldimann, A., Daniels, L. L., and Wanner, B. L. (1998) Use of new methods for construction of tightly regulated arabinose and rhamnose promoter fusions in studies of the *Escherichia coli* phosphate regulon, *J Bacteriol* 180, 1277-1286.

- Harada, K., and Morimoto, S. (2004) Inherited cardiomyopathies as a troponin disease, *Jpn J Physiol* 54, 307-318.
- Hartshorne, D. J., and Mueller, H. (1968) Fractionation of troponin into two distinct proteins, *Biochem Biophys Res Commun* 31, 647-653.
- Hasenfuss, G., Mulieri, L. A., Leavitt, B. J., Allen, P. D., Haeberle, J. R., and Alpert, N. R. (1992) Alteration of contractile function and excitation-contraction coupling in dilated cardiomyopathy, *Circ Res* 70, 1225-1232.
- Head, J. G., Ritchie, M. D., and Geeves, M. A. (1995) Characterization of the equilibrium between blocked and closed states of muscle thin filaments, *Eur J Biochem* 227, 694-699.
- Heeley, D. H., Belknap, B., and White, H. D. (2002) Mechanism of regulation of phosphate dissociation from actomyosin-ADP-Pi by thin filament proteins, *Proc Natl Acad Sci U S A* 99, 16731-16736.
- Hernandez, G., Blumenthal, D. K., Kennedy, M. A., Unkefer, C. J., and Trewhella, J. (1999) Troponin I inhibitory peptide (96-115) has an extended conformation when bound to skeletal muscle troponin C, *Biochemistry* 38, 6911-6917.
- Hernandez, O. M., Housmans, P. R., and Potter, J. D. (2001) Invited Review: pathophysiology of cardiac muscle contraction and relaxation as a result of alterations in thin filament regulation, *J Appl Physiol* 90, 1125-1136.
- Herskowitz, I. (1987) Functional inactivation of genes by dominant negative mutations, *Nature* 329, 219-222.
- Hill, T. L., Eisenberg, E., and Greene, L. (1980) Theoretical model for the cooperative equilibrium binding of myosin subfragment 1 to the actin-troponin-tropomyosin complex, *Proc Natl Acad Sci U S A* 77, 3186-3190.
- Hitchcock-DeGregori, S. E. (2008) Tropomyosin: function follows structure, *Adv Exp Med Biol* 644, 60-72.
- Ho, C. Y., Lever, H. M., DeSanctis, R., Farver, C. F., Seidman, J. G., and Seidman, C. E. (2000) Homozygous mutation in cardiac troponin T: implications for hypertrophic cardiomyopathy, *Circulation* 102, 1950-1955.

Holmes, K. C., Popp, D., Gebhard, W., and Kabsch, W. (1990) Atomic model of the actin filament, *Nature* 347, 44-49.

Houdusse, A., Love, M., Dominguez, R., Grabarek, Z., and Cohen, C. (1997) Structures of four Ca²⁺-bound troponin C at 2.0 Å resolution: further insights into the Ca²⁺-switch in the calmodulin superfamily, *Structure* 5, 1695-1711.

Houmeida, A., Heeley, D. H., Belknap, B., and White, H. D. Mechanism of regulation of native cardiac muscle thin filaments by rigor cardiac myosin-S1 and calcium, *J Biol Chem* 285, 32760-32769.

Howard, J. (1997) Molecular motors: structural adaptations to cellular functions, *Nature* 389, 561-567.

Hunkeler, N. M., Kullman, J., and Murphy, A. M. (1991) Troponin I isoform expression in human heart, *Circ Res* 69, 1409-1414.

Ichida, F., Tsubata, S., Bowles, K. R., Haneda, N., Uese, K., Miyawaki, T., Dreyer, W. J., Messina, J., Li, H., Bowles, N. E., and Towbin, J. A. (2001) Novel gene mutations in patients with left ventricular noncompaction or Barth syndrome, *Circulation* 103, 1256-1263.

Ingles, J., Doolan, A., Chiu, C., Seidman, J., Seidman, C., and Semsarian, C. (2005) Compound and double mutations in patients with hypertrophic cardiomyopathy: implications for genetic testing and counselling, *J Med Genet* 42, e59.

Iorga, B., Blaudeck, N., Solzin, J., Neulen, A., Stehle, I., Lopez Davila, A. J., Pfitzer, G., and Stehle, R. (2008) Lys184 deletion in troponin I impairs relaxation kinetics and induces hypercontractility in murine cardiac myofibrils, *Cardiovasc Res* 77, 676-686.

Ishii, Y., and Lehrer, S. S. (1990) Excimer fluorescence of pyrenyliodoacetamide-labeled tropomyosin: a probe of the state of tropomyosin in reconstituted muscle thin filaments, *Biochemistry* 29, 1160-1166.

James, J., Zhang, Y., Osinska, H., Sanbe, A., Klevitsky, R., Hewett, T. E., and Robbins, J. (2000) Transgenic modeling of a cardiac troponin I mutation linked to familial hypertrophic cardiomyopathy, *Circ Res* 87, 805-811.

Johnson, J. D., Collins, J. H., Robertson, S. P., and Potter, J. D. (1980) A fluorescent probe study of Ca²⁺ binding to the Ca²⁺-specific sites of cardiac troponin and troponin C, *J Biol Chem* 255, 9635-9640.

- Kabsch, W., and Holmes, K. C. (1995) The actin fold, *FASEB J* 9, 167-174.
- Kabsch, W., Mannherz, H. G., Suck, D., Pai, E. F., and Holmes, K. C. (1990) Atomic structure of the actin:DNase I complex, *Nature* 347, 37-44.
- Kamisago, M., Sharma, S. D., DePalma, S. R., Solomon, S., Sharma, P., McDonough, B., Smoot, L., Mullen, M. P., Woolf, P. K., Wigle, E. D., Seidman, J. G., and Seidman, C. E. (2000) Mutations in sarcomere protein genes as a cause of dilated cardiomyopathy, *N Engl J Med* 343, 1688-1696.
- Kazmierczak, K., Xu, Y., Jones, M., Guzman, G., Hernandez, O. M., Kerrick, W. G., and Szczesna-Cordary, D. (2009) The role of the N-terminus of the myosin essential light chain in cardiac muscle contraction, *J Mol Biol* 387, 706-725.
- Kimura, A., Harada, H., Park, J. E., Nishi, H., Satoh, M., Takahashi, M., Hiroi, S., Sasaoka, T., Ohbuchi, N., Nakamura, T., Koyanagi, T., Hwang, T. H., Choo, J. A., Chung, K. S., Hasegawa, A., Nagai, R., Okazaki, O., Nakamura, H., Matsuzaki, M., Sakamoto, T., Toshima, H., Koga, Y., Imaizumi, T., and Sasazuki, T. (1997) Mutations in the cardiac troponin I gene associated with hypertrophic cardiomyopathy, *Nat Genet* 16, 379-382.
- Kobayashi, T., Dong, W. J., Burkart, E. M., Cheung, H. C., and Solaro, R. J. (2004) Effects of protein kinase C dependent phosphorylation and a familial hypertrophic cardiomyopathy-related mutation of cardiac troponin I on structural transition of troponin C and myofilament activation, *Biochemistry* 43, 5996-6004.
- Kobayashi, T., Jin, L., and de Tombe, P. P. (2008) Cardiac thin filament regulation, *Pflugers Arch* 457, 37-46.
- Kobayashi, T., and Solaro, R. J. (2006) Increased Ca²⁺ affinity of cardiac thin filaments reconstituted with cardiomyopathy-related mutant cardiac troponin I, *J Biol Chem* 281, 13471-13477.
- Kohler, J., Chen, Y., Brenner, B., Gordon, A. M., Kraft, T., Martyn, D. A., Regnier, M., Rivera, A. J., Wang, C. K., and Chase, P. B. (2003) Familial hypertrophic cardiomyopathy mutations in troponin I (K183D, G203S, K206Q) enhance filament sliding, *Physiol Genomics* 14, 117-128.
- Kokado, H., Shimizu, M., Yoshio, H., Ino, H., Okeie, K., Emoto, Y., Matsuyama, T., Yamaguchi, M., Yasuda, T., Fujino, N., Ito, H., and Mabuchi, H. (2000) Clinical features of hypertrophic cardiomyopathy caused by a Lys183 deletion mutation in the cardiac troponin I gene, *Circulation* 102, 663-669.

Konno, T., Shimizu, M., Ino, H., Fujino, N., Hayashi, K., Uchiyama, K., Kaneda, T., Inoue, M., Masuda, E., and Mabuchi, H. (2005) Phenotypic differences between electrocardiographic and echocardiographic determination of hypertrophic cardiomyopathy in genetically affected subjects, *J Intern Med* 258, 216-224.

Kouyama, T., and Mihashi, K. (1981) Fluorimetry study of N-(1-pyrenyl)iodoacetamide-labelled F-actin. Local structural change of actin protomer both on polymerization and on binding of heavy meromyosin, *Eur J Biochem* 114, 33-38.

Kruger, M., Zittrich, S., Redwood, C., Blaudeck, N., James, J., Robbins, J., Pfitzer, G., and Stehle, R. (2005) Effects of the mutation R145G in human cardiac troponin I on the kinetics of the contraction-relaxation cycle in isolated cardiac myofibrils, *J Physiol* 564, 347-357.

Lam, L., Tsoutsman, T., Arthur, J., and Semsarian, C. Differential protein expression profiling of myocardial tissue in a mouse model of hypertrophic cardiomyopathy, *J Mol Cell Cardiol* 48, 1014-1022.

Lang, R., Gomes, A. V., Zhao, J., Housmans, P. R., Miller, T., and Potter, J. D. (2002) Functional analysis of a troponin I (R145G) mutation associated with familial hypertrophic cardiomyopathy, *J Biol Chem* 277, 11670-11678.

Lehman, W., Galinska-Rakoczy, A., Hatch, V., Tobacman, L. S., and Craig, R. (2009) Structural basis for the activation of muscle contraction by troponin and tropomyosin, *J Mol Biol* 388, 673-681.

Lehman, W., Hatch, V., Korman, V., Rosol, M., Thomas, L., Maytum, R., Geeves, M. A., Van Eyk, J. E., Tobacman, L. S., and Craig, R. (2000) Tropomyosin and actin isoforms modulate the localization of tropomyosin strands on actin filaments, *J Mol Biol* 302, 593-606.

Lehrer, S. S. (1994) The regulatory switch of the muscle thin filament: Ca²⁺ or myosin heads?, *J Muscle Res Cell Motil* 15, 232-236.

Lehrer, S. S., and Geeves, M. A. (1998) The muscle thin filament as a classical cooperative/allosteric regulatory system, *J Mol Biol* 277, 1081-1089.

Lehrer, S. S., Golitsina, N. L., and Geeves, M. A. (1997) Actin-tropomyosin activation of myosin subfragment 1 ATPase and thin filament cooperativity. The role of tropomyosin flexibility and end-to-end interactions, *Biochemistry* 36, 13449-13454.

Lehrer, S. S., and Morris, E. P. (1982) Dual effects of tropomyosin and troponin-tropomyosin on actomyosin subfragment 1 ATPase, *J Biol Chem* 257, 8073-8080.

Levick, J. R. (2003) *An introduction to cardiovascular physiology*. Fourth edition. ARNOLD. ISBN 0340809213.

Li, D., Czernuszewicz, G. Z., Gonzalez, O., Tapscott, T., Karibe, A., Durand, J. B., Brugada, R., Hill, R., Gregoritch, J. M., Anderson, J. L., Quinones, M., Bachinski, L. L., and Roberts, R. (2001) Novel cardiac troponin T mutation as a cause of familial dilated cardiomyopathy, *Circulation* 104, 2188-2193.

Li, M. X., Spyropoulos, L., and Sykes, B. D. (1999) Binding of cardiac troponin-I147-163 induces a structural opening in human cardiac troponin-C, *Biochemistry* 38, 8289-8298.

Li, M. X., Wang, X., and Sykes, B. D. (2004) Structural based insights into the role of troponin in cardiac muscle pathophysiology, *J Muscle Res Cell Motil* 25, 559-579.

Li, X. E., Lehman, W., Fischer, S., and Holmes, K. C. Curvature variation along the tropomyosin molecule, *J Struct Biol* 170, 307-312.

Li, Y., Mui, S., Brown, J. H., Strand, J., Reshetnikova, L., Tobacman, L. S., and Cohen, C. (2002) The crystal structure of the C-terminal fragment of striated-muscle alpha-tropomyosin reveals a key troponin T recognition site, *Proc Natl Acad Sci U S A* 99, 7378-7383.

Lindhout, D. A., Boyko, R. F., Corson, D. C., Li, M. X., and Sykes, B. D. (2005) The role of electrostatics in the interaction of the inhibitory region of troponin I with troponin C, *Biochemistry* 44, 14750-14759.

Lindhout, D. A., Li, M. X., Schieve, D., and Sykes, B. D. (2002) Effects of T142 phosphorylation and mutation R145G on the interaction of the inhibitory region of human cardiac troponin I with the C-domain of human cardiac troponin C, *Biochemistry* 41, 7267-7274.

Lindhout, D. A., and Sykes, B. D. (2003) Structure and dynamics of the C-domain of human cardiac troponin C in complex with the inhibitory region of human cardiac troponin I, *J Biol Chem* 278, 27024-27034.

Lohmann, K., Westerdorf, B., Maytum, R., Geeves, M. A., and Jaquet, K. (2001) Overexpression of human cardiac troponin in *Escherichia coli*: its purification and characterization, *Protein Expr Purif* 21, 49-59.

Lounes, K. C., Demeler, B., Anderson, D. E., Gomes, A. W., Potter, J. D., Nassar, R., and Anderson, P. A. (2008) Cardiac troponin T forms a tetramer in vitro, *Biochemistry* 47, 1970-1976.

Lowry, O. H., Rosebrough, N. J., Farr, A. L., and Randall, R. J. (1951) Protein measurement with the Folin phenol reagent, *J Biol Chem* 193, 265-275.

Lymn, R. W., and Taylor, E. W. (1971) Mechanism of adenosine triphosphate hydrolysis by actomyosin, *Biochemistry* 10, 4617-4624.

MacIntosh, B. R. (2003) Role of calcium sensitivity modulation in skeletal muscle performance, *News Physiol Sci* 18, 222-225.

Margossian, S. S., and Lowey, S. (1982) Preparation of myosin and its subfragments from rabbit skeletal muscle, *Methods Enzymol* 85, 55-71.

Martin, S. R., Maune, J. F., Beckingham, K., and Bayley, P. M. (1992) Stopped-flow studies of calcium dissociation from calcium-binding-site mutants of *Drosophila melanogaster* calmodulin, *Eur J Biochem* 205, 1107-1114.

Masood, S., and Yang, G. (2001) Macroscopic structure and physiology of the normal and diseased Heart.

Maytum, R., Lehrer, S. S., and Geeves, M. A. (1999) Cooperativity and switching within the three-state model of muscle regulation, *Biochemistry* 38, 1102-1110.

Maytum, R., Westerdorf, B., Jaquet, K., and Geeves, M. A. (2003) Differential regulation of the actomyosin interaction by skeletal and cardiac troponin isoforms, *J Biol Chem* 278, 6696-6701.

McKenna, W. J., and Camm, A. J. (1989) Sudden death in hypertrophic cardiomyopathy. Assessment of patients at high risk, *Circulation* 80, 1489-1492.

McKillop, D. F., and Geeves, M. A. (1993) Regulation of the interaction between actin and myosin subfragment 1: evidence for three states of the thin filament, *Biophys J* 65, 693-701.

Mestroni, L., Rocco, C., Gregori, D., Sinagra, G., Di Lenarda, A., Miocic, S., Vatta, M., Pinamonti, B., Muntoni, F., Caforio, A. L., McKenna, W. J., Falaschi, A., Giacca, M., and Camerini. (1999) Familial dilated cardiomyopathy: evidence for genetic and phenotypic heterogeneity. Heart Muscle Disease Study Group, *J Am Coll Cardiol* 34, 181-190.

Metzger, J. M., and Westfall, M. V. (2004) Covalent and noncovalent modification of thin filament action: the essential role of troponin in cardiac muscle regulation, *Circ Res* 94, 146-158.

Miles, A. J., and Wallace, B. A. (2006) Synchrotron radiation circular dichroism spectroscopy of proteins and applications in structural and functional genomics, *Chem Soc Rev* 35, 39-51.

Mirza, M., Robinson, P., Kremneva, E., Copeland, O., Nikolaeva, O., Watkins, H., Levitsky, D., Redwood, C., El-Mezgueldi, M., and Marston, S. (2007) The effect of mutations in alpha-tropomyosin (E40K and E54K) that cause familial dilated cardiomyopathy on the regulatory mechanism of cardiac muscle thin filaments, *J Biol Chem* 282, 13487-13497.

Mogensen, J., Klausen, I. C., Pedersen, A. K., Egeblad, H., Bross, P., Kruse, T. A., Gregersen, N., Hansen, P. S., Baandrup, U., and Borglum, A. D. (1999) Alpha-cardiac actin is a novel disease gene in familial hypertrophic cardiomyopathy, *J Clin Invest* 103, R39-43.

Mogensen, J., Murphy, R. T., Shaw, T., Bahl, A., Redwood, C., Watkins, H., Burke, M., Elliott, P. M., and McKenna, W. J. (2004) Severe disease expression of cardiac troponin C and T mutations in patients with idiopathic dilated cardiomyopathy, *J Am Coll Cardiol* 44, 2033-2040.

Moolman, J. C., Corfield, V. A., Posen, B., Ngumbela, K., Seidman, C., Brink, P. A., and Watkins, H. (1997) Sudden death due to troponin T mutations, *J Am Coll Cardiol* 29, 549-555.

Morner, S., Richard, P., Kazzam, E., Hainque, B., Schwartz, K., and Waldenstrom, A. (2000) Deletion in the cardiac troponin I gene in a family from northern Sweden with hypertrophic cardiomyopathy, *J Mol Cell Cardiol* 32, 521-525.

Morner, S., Richard, P., Kazzam, E., Hellman, U., Hainque, B., Schwartz, K., and Waldenstrom, A. (2003) Identification of the genotypes causing hypertrophic cardiomyopathy in northern Sweden, *J Mol Cell Cardiol* 35, 841-849.

Morris, E. P., and Lehrer, S. S. (1984) Troponin-tropomyosin interactions. Fluorescence studies of the binding of troponin, troponin T, and chymotryptic troponin T fragments to specifically labeled tropomyosin, *Biochemistry* 23, 2214-2220.

Moss, R. L. (1992) Ca²⁺ regulation of mechanical properties of striated muscle. Mechanistic studies using extraction and replacement of regulatory proteins, *Circ Res* 70, 865-884.

Moss, R. L., and Fitzsimons, D. P. Regulation of contraction in mammalian striated muscles--the plot thick-ens, *J Gen Physiol* 136, 21-27.

Moss, R. L., Razumova, M., and Fitzsimons, D. P. (2004) Myosin crossbridge activation of cardiac thin filaments: implications for myocardial function in health and disease, *Circ Res* 94, 1290-1300.

Murakami, K., Stewart, M., Nozawa, K., Tomii, K., Kudou, N., Igarashi, N., Shirakihara, Y., Wakatsuki, S., Yasunaga, T., and Wakabayashi, T. (2008) Structural basis for tropomyosin overlap in thin (actin) filaments and the generation of a molecular swivel by troponin-T, *Proc Natl Acad Sci U S A* 105, 7200-7205.

Murakami, K., Yumoto, F., Ohki, S. Y., Yasunaga, T., Tanokura, M., and Wakabayashi, T. (2007) Structural basis for calcium-regulated relaxation of striated muscles at interaction sites of troponin with actin and tropomyosin, *Adv Exp Med Biol* 592, 71-86.

Murphy, R. T., Mogensen, J., Shaw, A., Kubo, T., Hughes, S., and McKenna, W. J. (2004) Novel mutation in cardiac troponin I in recessive idiopathic dilated cardiomyopathy, *Lancet* 363, 371-372.

Murray, D., Fleiszer, D., McArdle, A. H., and Brown, R. A. (1980) Effect of dietary fiber on intestinal mucosal sodium-potassium-activated ATPase, *J Surg Res* 29, 135-140.

Nguyen, L., Chung, J., Lam, L., Tsoutsman, T., and Semsarian, C. (2007) Abnormal cardiac response to exercise in a murine model of familial hypertrophic cardiomyopathy, *Int J Cardiol* 119, 245-248.

Niimura, H., Patton, K. K., McKenna, W. J., Soultis, J., Maron, B. J., Seidman, J. G., and Seidman, C. E. (2002) Sarcomere protein gene mutations in hypertrophic cardiomyopathy of the elderly, *Circulation* 105, 446-451.

Oberst, L., Zhao, G., Park, J. T., Brugada, R., Michael, L. H., Entman, M. L., Roberts, R., and Marian, A. J. (1998) Dominant-negative effect of a mutant cardiac troponin T on cardiac structure and function in transgenic mice, *J Clin Invest* 102, 1498-1505.

Ohtsuki, I., and Morimoto, S. (2008) Troponin: regulatory function and disorders, *Biochem Biophys Res Commun* 369, 62-73.

Oleszczuk, M., Robertson, I. M., Li, M. X., and Sykes, B. D. Solution structure of the regulatory domain of human cardiac troponin C in complex with the switch region of cardiac troponin I and W7: the basis of W7 as an inhibitor of cardiac muscle contraction, *J Mol Cell Cardiol* 48, 925-933.

Olson, T. M., Kishimoto, N. Y., Whitby, F. G., and Michels, V. V. (2001) Mutations that alter the surface charge of alpha-tropomyosin are associated with dilated cardiomyopathy, *J Mol Cell Cardiol* 33, 723-732.

Olson, T. M., Michels, V. V., Thibodeau, S. N., Tai, Y. S., and Keating, M. T. (1998) Actin mutations in dilated cardiomyopathy, a heritable form of heart failure, *Science* 280, 750-752.

Opie, L. H., Commerford, P. J., Gersh, B. J., and Pfeffer, M. A. (2006) Controversies in ventricular remodelling, *Lancet* 367, 356-367.

Pan, B. S., and Solaro, R. J. (1987) Calcium-binding properties of troponin C in detergent-skinned heart muscle fibers, *J Biol Chem* 262, 7839-7849.

Pardee, J. D., and Spudich, J. A. (1982) Purification of muscle actin, *Methods Cell Biol* 24, 271-289.

Parry, D. A., and Squire, J. M. (1973) Structural role of tropomyosin in muscle regulation: analysis of the x-ray diffraction patterns from relaxed and contracting muscles, *J Mol Biol* 75, 33-55.

Perrin, B. J., and Ervasti, J. M. The actin gene family: function follows isoform, *Cytoskeleton (Hoboken)* 67, 630-634.

Perry, S. V. (1998) Troponin T: genetics, properties and function, *J Muscle Res Cell Motil* 19, 575-602.

Perry, S. V. (2001) Vertebrate tropomyosin: distribution, properties and function, *J Muscle Res Cell Motil* 22, 5-49.

Pinto, J. R., Parvatiyar, M. S., Jones, M. A., Liang, J., Ackerman, M. J., and Potter, J. D. (2009) A functional and structural study of troponin C mutations related to hypertrophic cardiomyopathy, *J Biol Chem* 284, 19090-19100.

Poetter, K., Jiang, H., Hassanzadeh, S., Master, S. R., Chang, A., Dalakas, M. C., Rayment, I., Sellers, J. R., Fananapazir, L., and Epstein, N. D. (1996) Mutations in either the essential or regulatory light chains of myosin are associated with a rare myopathy in human heart and skeletal muscle, *Nat Genet* 13, 63-69.

Potter, J. D. (1982) Preparation of troponin and its subunits, *Methods Enzymol* 85 Pt B, 241-263.

Rayment, I., Rypniewski, W. R., Schmidt-Base, K., Smith, R., Tomchick, D. R., Benning, M. M., Winkelmann, D. A., Wesenberg, G., and Holden, H. M. (1993) Three-dimensional structure of myosin subfragment-1: a molecular motor, *Science* 261, 50-58.

Redwood, C., Lohmann, K., Bing, W., Esposito, G. M., Elliott, K., Abdulrazzak, H., Knott, A., Purcell, I., Marston, S., and Watkins, H. (2000) Investigation of a truncated cardiac troponin T that causes familial hypertrophic cardiomyopathy: Ca²⁺ regulatory properties of reconstituted thin filaments depend on the ratio of mutant to wild-type protein, *Circ Res* 86, 1146-1152.

Redwood, C. S., Moolman-Smook, J. C., and Watkins, H. (1999) Properties of mutant contractile proteins that cause hypertrophic cardiomyopathy, *Cardiovasc Res* 44, 20-36.

Reiffert, S., Maytum, R., Geeves, M., Lohmann, K., Greis, T., Bluggel, M., Meyer, H. E., Heilmeyer, L. M., and Jaquet, K. (1999) Characterization of the cardiac holotroponin complex reconstituted from native cardiac troponin T and recombinant I and C, *Eur J Biochem* 261, 40-47.

Reiffert, S. U., Jaquet, K., Heilmeyer, L. M., Jr., Ritchie, M. D., and Geeves, M. A. (1996) Bisphosphorylation of cardiac troponin I modulates the Ca²⁺-dependent binding of myosin subfragment S1 to reconstituted thin filaments, *FEBS Lett* 384, 43-47.

Richard, P., Charron, P., Carrier, L., Ledeuil, C., Cheav, T., Pichereau, C., Benaiche, A., Isnard, R., Dubourg, O., Burban, M., Gueffet, J. P., Millaire, A., Desnos, M., Schwartz, K., Hainque, B., and Komajda, M. (2003) Hypertrophic cardiomyopathy: distribution of disease genes, spectrum of mutations, and implications for a molecular diagnosis strategy, *Circulation* 107, 2227-2232.

Robinson, J. M., Dong, W. J., Xing, J., and Cheung, H. C. (2004) Switching of troponin I: Ca(2+) and myosin-induced activation of heart muscle, *J Mol Biol* 340, 295-305.

Robinson, P., Griffiths, P. J., Watkins, H., and Redwood, C. S. (2007) Dilated and hypertrophic cardiomyopathy mutations in troponin and alpha-tropomyosin have opposing effects on the calcium affinity of cardiac thin filaments, *Circ Res* 101, 1266-1273.

Rosenfeld, S. S., and Taylor, E. W. (1985) Kinetic studies of calcium binding to regulatory complexes from skeletal muscle, *J Biol Chem* 260, 252-261.

Ruppel, K. M., and Spudich, J. A. (1996) Structure-function analysis of the motor domain of myosin, *Annu Rev Cell Dev Biol* 12, 543-573.

Sadayappan, S., Finley, N., Howarth, J. W., Osinska, H., Klevitsky, R., Lorenz, J. N., Rosevear, P. R., and Robbins, J. (2008) Role of the acidic N' region of cardiac troponin I in regulating myocardial function, *FASEB J* 22, 1246-1257.

Sanbe, A., James, J., Tuzcu, V., Nas, S., Martin, L., Gulick, J., Osinska, H., Sakthivel, S., Klevitsky, R., Ginsburg, K. S., Bers, D. M., Zinman, B., Lakatta, E. G., and Robbins, J. (2005) Transgenic rabbit model for human troponin I-based hypertrophic cardiomyopathy, *Circulation* 111, 2330-2338.

Satoh, M., Takahashi, M., Sakamoto, T., Hiroe, M., Marumo, F., and Kimura, A. (1999) Structural analysis of the titin gene in hypertrophic cardiomyopathy: identification of a novel disease gene, *Biochem Biophys Res Commun* 262, 411-417.

Schaertl, S., Lehrer, S. S., and Geeves, M. A. (1995) Separation and characterization of the two functional regions of troponin involved in muscle thin filament regulation, *Biochemistry* 34, 15890-15894.

Seidman, J. G., and Seidman, C. (2001) The genetic basis for cardiomyopathy: from mutation identification to mechanistic paradigms, *Cell* 104, 557-567.

Sellers, J. R., and Knight, P. J. (2007) Folding and regulation in myosins II and V, *J Muscle Res Cell Motil* 28, 363-370.

Sheng, Z., Pan, B. S., Miller, T. E., and Potter, J. D. (1992) Isolation, expression, and mutation of a rabbit skeletal muscle cDNA clone for troponin I. The role of the NH2 terminus of fast skeletal muscle troponin I in its biological activity, *J Biol Chem* 267, 25407-25413.

Shimizu, M., Ino, H., Yasuda, T., Fujino, N., Uchiyama, K., Mabuchi, T., Konno, T., Kaneda, T., Fujita, T., Masuta, E., Katoh, M., Funada, A., and Mabuchi, H. (2005) Gene mutations in adult Japanese patients with dilated cardiomyopathy, *Circ J* 69, 150-153.

Siemankowski, R. F., and White, H. D. (1984) Kinetics of the interaction between actin, ADP, and cardiac myosin-S1, *J Biol Chem* 259, 5045-5053.

Siemankowski, R. F., Wiseman, M. O., and White, H. D. (1985) *Proc. Natl. Acad. Sci. U.S.A.* 82, 658-662

Slupsky, C. M., and Sykes, B. D. (1995) NMR solution structure of calcium-saturated skeletal muscle troponin C, *Biochemistry* 34, 15953-15964.

Solaro, R. J., Montgomery, D. M., Wang, L., Burkart, E. M., Ke, Y., Vahebi, S., and Buttrick, P. (2002) Integration of pathways that signal cardiac growth with modulation of myofilament activity, *J Nucl Cardiol* 9, 523-533.

Solaro, R. J., Rosevear, P., and Kobayashi, T. (2008) The unique functions of cardiac troponin I in the control of cardiac muscle contraction and relaxation, *Biochem Biophys Res Commun* 369, 82-87.

Spudich, J. A., and Watt, S. (1971) The regulation of rabbit skeletal muscle contraction. I. Biochemical studies of the interaction of the tropomyosin-troponin complex with actin and the proteolytic fragments of myosin, *J Biol Chem* 246, 4866-4871.

Squire, J. M., and Morris, E. P. (1998) A new look at thin filament regulation in vertebrate skeletal muscle, *FASEB J* 12, 761-771.

Stehle, R., Iorga, B., and Pfitzer, G. (2007) Calcium regulation of troponin and its role in the dynamics of contraction and relaxation, *Am J Physiol Regul Integr Comp Physiol* 292, R1125-1128.

- Stehle, R., Solzin, J., Iorga, B., and Poggesi, C. (2009) Insights into the kinetics of Ca²⁺-regulated contraction and relaxation from myofibril studies, *Pflugers Arch* 458, 337-357.
- Stewart, M. (2001) Structural basis for bending tropomyosin around actin in muscle thin filaments, *Proc Natl Acad Sci U S A* 98, 8165-8166.
- Straub, F. B. *Actin. Stud Szeged* 2: 3-15, 1942.
- Studier, F. W., Rosenberg, A. H., Dunn, J. J., and Dubendorff, J. W. (1990) Use of T7 RNA polymerase to direct expression of cloned genes, *Methods Enzymol* 185, 60-89.
- Sugiura, S. (1999) Actin-myosin interaction, *Cardiovasc Res* 44, 266-273.
- Sun, Y. B., and Irving, M. The molecular basis of the steep force-calcium relation in heart muscle, *J Mol Cell Cardiol* 48, 859-865.
- Sun, Y. B., Lou, F., and Irving, M. (2009) Calcium- and myosin-dependent changes in troponin structure during activation of heart muscle, *J Physiol* 587, 155-163.
- Suomalainen, A., Paetau, A., Leinonen, H., Majander, A., Peltonen, L., and Somer, H. (1992) Inherited idiopathic dilated cardiomyopathy with multiple deletions of mitochondrial DNA, *Lancet* 340, 1319-1320.
- Szczesna, D., Zhang, R., Zhao, J., Jones, M., Guzman, G., and Potter, J. D. (2000) Altered regulation of cardiac muscle contraction by troponin T mutations that cause familial hypertrophic cardiomyopathy, *J Biol Chem* 275, 624-630.
- Takahashi-Yanaga, F., Morimoto, S., Harada, K., Minakami, R., Shiraishi, F., Ohta, M., Lu, Q. W., Sasaguri, T., and Ohtsuki, I. (2001) Functional consequences of the mutations in human cardiac troponin I gene found in familial hypertrophic cardiomyopathy, *J Mol Cell Cardiol* 33, 2095-2107.
- Takahashi-Yanaga, F., Morimoto, S., and Ohtsuki, I. (2000) Effect of Arg145Gly mutation in human cardiac troponin I on the ATPase activity of cardiac myofibrils, *J Biochem* 127, 355-357.
- Takeda, S., Yamashita, A., Maeda, K., and Maeda, Y. (2003) Structure of the core domain of human cardiac troponin in the Ca²⁺-saturated form, *Nature* 424, 35-41.

Tardiff, J. C. (2005) Sarcomeric proteins and familial hypertrophic cardiomyopathy: linking mutations in structural proteins to complex cardiovascular phenotypes, *Heart Fail Rev* 10, 237-248.

Tausky, H. H., and Shorr, E. (1953) A microcolorimetric method for the determination of inorganic phosphorus, *J Biol Chem* 202, 675-685.

Teare, D. (1958) Asymmetrical hypertrophy of the heart in young adults, *Br Heart J* 20, 1-8.

Thierfelder, L., Watkins, H., MacRae, C., Lamas, R., McKenna, W., Vosberg, H. P., Seidman, J. G., and Seidman, C. E. (1994) Alpha-tropomyosin and cardiac troponin T mutations cause familial hypertrophic cardiomyopathy: a disease of the sarcomere, *Cell* 77, 701-712.

Tobacman, L. S. (1996) Thin filament-mediated regulation of cardiac contraction, *Annu Rev Physiol* 58, 447-481.

Tobacman, L. S., and Adelstein, R. S. (1986) Mechanism of regulation of cardiac actin-myosin subfragment 1 by troponin-tropomyosin, *Biochemistry* 25, 798-802.

Towbin, J. A., and Bowles, N. E. (2002) The failing heart, *Nature* 415, 227-233.

Tsien, R. Y. (1983) Intracellular measurements of ion activities, *Annu Rev Biophys Bioeng* 12, 91-116.

Tsoutsman, T., Chung, J., Doolan, A., Nguyen, L., Williams, I. A., Tu, E., Lam, L., Bailey, C. G., Rasko, J. E., Allen, D. G., and Semsarian, C. (2006) Molecular insights from a novel cardiac troponin I mouse model of familial hypertrophic cardiomyopathy, *J Mol Cell Cardiol* 41, 623-632.

Tung, C. S., Wall, M. E., Gallagher, S. C., and Trewhella, J. (2000) A model of troponin-I in complex with troponin-C using hybrid experimental data: the inhibitory region is a beta-hairpin, *Protein Sci* 9, 1312-1326.

Tyska, M. J., and Warshaw, D. M. (2002) The myosin power stroke, *Cell Motil Cytoskeleton* 51, 1-15.

Van Driest, S. L., Ellsworth, E. G., Ommen, S. R., Tajik, A. J., Gersh, B. J., and Ackerman, M. J. (2003) Prevalence and spectrum of thin filament mutations in an outpatient referral population with hypertrophic cardiomyopathy, *Circulation* 108, 445-451.

Van Driest, S. L., Vasile, V. C., Ommen, S. R., Will, M. L., Tajik, A. J., Gersh, B. J., and Ackerman, M. J. (2004) Myosin binding protein C mutations and compound heterozygosity in hypertrophic cardiomyopathy, *J Am Coll Cardiol* 44, 1903-1910.

Vikstrom, K. L., Factor, S. M., and Leinwand, L. A. (1996) Mice expressing mutant myosin heavy chains are a model for familial hypertrophic cardiomyopathy, *Mol Med* 2, 556-567.

Vikstrom, K. L., and Leinwand, L. A. (1996) Contractile protein mutations and heart disease, *Curr Opin Cell Biol* 8, 97-105.

Vinogradova, M. V., Stone, D. B., Malanina, G. G., Karatzaferi, C., Cooke, R., Mendelson, R. A., and Fletterick, R. J. (2005) Ca²⁺-regulated structural changes in troponin, *Proc Natl Acad Sci U S A* 102, 5038-5043.

Ward, D. G., Brewer, S. M., Gallon, C. E., Gao, Y., Levine, B. A., and Trayer, I. P. (2004) NMR and mutagenesis studies on the phosphorylation region of human cardiac troponin I, *Biochemistry* 43, 5772-5781.

Watkins, H., Conner, D., Thierfelder, L., Jarcho, J. A., MacRae, C., McKenna, W. J., Maron, B. J., Seidman, J. G., and Seidman, C. E. (1995) Mutations in the cardiac myosin binding protein-C gene on chromosome 11 cause familial hypertrophic cardiomyopathy, *Nat Genet* 11, 434-437.

Watkins, H., McKenna, W. J., Thierfelder, L., Suk, H. J., Anan, R., O'Donoghue, A., Spirito, P., Matsumori, A., Moravec, C. S., Seidman, J. G., and et al. (1995) Mutations in the genes for cardiac troponin T and alpha-tropomyosin in hypertrophic cardiomyopathy, *N Engl J Med* 332, 1058-1064.

Watkins, H., Seidman, C. E., Seidman, J. G., Feng, H. S., and Sweeney, H. L. (1996) Expression and functional assessment of a truncated cardiac troponin T that causes hypertrophic cardiomyopathy. Evidence for a dominant negative action, *J Clin Invest* 98, 2456-2461.

Weeds, A. G., and Taylor, R. S. (1975) Separation of subfragment-1 isoenzymes from rabbit skeletal muscle myosin, *Nature* 257, 54-56.

Wei, B., and Jin, J. P. (2010) Troponin T isoforms and posttranscriptional modifications: Evolution, regulation and function, *Arch Biochem Biophys* 505, 144-154.

Westfall, M. V., Borton, A. R., Albayya, F. P., and Metzger, J. M. (2002) Myofilament calcium sensitivity and cardiac disease: insights from troponin I isoforms and mutants, *Circ Res* 91, 525-531.

Whitby, F. G., and Phillips, G. N., Jr. (2000) Crystal structure of tropomyosin at 7 Angstroms resolution, *Proteins* 38, 49-59.

White, H. D., Belknap, B., and Webb, M. R. (1997) Kinetics of nucleoside triphosphate cleavage and phosphate release steps by associated rabbit skeletal actomyosin, measured using a novel fluorescent probe for phosphate, *Biochemistry* 36, 11828-11836.

White, S. P., Cohen, C., and Phillips, G. N., Jr. (1987) Structure of co-crystals of tropomyosin and troponin, *Nature* 325, 826-828.

Wolska, B. M., Keller, R. S., Evans, C. C., Palmiter, K. A., Phillips, R. M., Muthuchamy, M., Oehlenschläger, J., Wieczorek, D. F., de Tombe, P. P., and Solaro, R. J. (1999) Correlation between myofilament response to Ca²⁺ and altered dynamics of contraction and relaxation in transgenic cardiac cells that express beta-tropomyosin, *Circ Res* 84, 745-751.

Wolska, B. M., and Wieczorek, D. M. (2003) The role of tropomyosin in the regulation of myocardial contraction and relaxation, *Pflugers Arch* 446, 1-8.

Zhang, R., Zhao, J., and Potter, J. D. (1995) Phosphorylation of both serine residues in cardiac troponin I is required to decrease the Ca²⁺ affinity of cardiac troponin C, *J Biol Chem* 270, 30773-30780.

Zot, A. S., Potter, J. D., and Strauss, W. L. (1987) Isolation and sequence of a cDNA clone for rabbit fast skeletal muscle troponin C. Homology with calmodulin and parvalbumin, *J Biol Chem* 262, 15418-15421.